

## DECOMPRESSION THEORY

B.R. Wienke

Nuclear Weapons Technology/Simulation And Computing  
Applied And Computational Physics Division  
Los Alamos National Laboratory  
Los Alamos, N.M. 87545

### ABSTRACT

*Decompression theory and related topics are detailed in a Twelve Part series, with topics self contained and strategically developed in their relationship to diving. Topics span many disciplines and focus in a number of decompression arenas. Targeted audience is the commercial diver, instructor, hyperbaric technician, underwater researcher, and technical diver looking for greater detail, and especially the doctor, physiologist, physicist, chemist, mathematician, engineer, or biologist by training. Topics include energy and thermodynamics, pressure and density, flow mechanics and gas kinetics, free and dissolved phase transfer, nucleation and cavitation, bubbles and surfactants, mixed gases, maladies and drugs, statistics, risk and probability, binomial distributions, high performance computing and models, and altitude effects. References are included at the end of each Part, and a representative suite of Exercises (problems and solutions) is also provided for the fastidious reader. This version builds upon and extends material presented in the first edition of Basic Decompression Theory And Application. An extended Bibliography is also included.*

*Specifically, we cover a number of overlapping technical topics:*

- 1. perfusion and diffusion limited processes;*
- 2. inert gas transfer and isobaric counterdiffusion;*
- 3. critical tensions and phase volumes;*
- 4. nucleation and cavitation, persistence, and time scales;*
- 5. bubbles, equations of state, and phase mechanics;*
- 6. dive table and decometer algorithms;*
- 7. diving maladies, drugs, and physiological impacts;*
- 8. ideal gas laws and flow dynamics;*
- 9. energy, thermodynamics, and pressure mechanics;*
- 10. comparative profiles and diving practices;*
- 11. probability, statistical methods, and likelihood;*
- 12. validation and testing;*
- 13. mixed gases, oxygen dose, and decompression;*
- 14. modern computing, software, and diving applications;*
- 15. altitude similarity and procedures.*

*Pages - 182, Tables - 34, Figures - 40, References - 164, Examples - 99*

*TO LUZANNE AND HILLARY*

## AUTHOR SKETCH

Bruce Wienke is a Program Manager in the Nuclear Weapons Technology/ Simulation And Computing Office at the Los Alamos National Laboratory (LANL), with interests in computational decompression and models, gas transport, and phase mechanics. He contributes to underwater symposia, educational publications, technical periodicals and decompression workshops, having authored seven monographs (*Technical Diving In Depth, Decompression Theory, Physics, Physiology And Decompression Theory For The Technical And Commercial Diver, High Altitude Diving, Basic Diving Physics And Application, Diving Above Sea Level, Basic Decompression Theory And Application*) and some 200 technical journal articles. Diving environs include the Caribbean, South Pacific, Asia, inland and coastal United States, Hawaii, and polar Arctic and Antarctic for sundry technical, scientific, military, and recreational activities. He functions on the LANL Nuclear Emergency Strategy Team (NEST), in exercises often involving Special Warfare Units, above and below water. He heads Southwest Enterprises, a consulting company for research and applications in overlapping areas of applied science and simulation, functions as an Expert Witness in diving litigation, and SEAL

Wienke is an Instructor Trainer/Technical Diving Instructor with the National Association Of Underwater Instructors (NAUI), has served on the Board Of Directors (Vice Chairman for Technical Diving, Technical and Decompression Review Board Member), is a Master Instructor with the Professional Association Of Diving Instructors (PADI) in various capacities (Instructor Review Committee), is an Institute Director with the YMCA, and is an Instructor Trainer/Technical Diving Instructor with Scuba Diving International/Technical Diving International (SDI/TDI). Wintertime he hobbies skiing, coaching, and teaching as a Racing Coach and Instructor, certified United States Ski Coaches Association (USSCA) and Professional Ski Instructors of America (PSIA), and races in the United States Ski Association (USSA) Masters Series Competition, holding a 8 NASTAR racing handicap. Other interests include tennis, windsurfing, and mountain biking. He quarterbacked the 63 Northern Michigan Wildcats to an NCAA II Championship (Hickory Bowl).

Wienke received a BS in physics and mathematics from Northern Michigan University, MS in nuclear physics from Marquette University, and PhD in particle physics from Northwestern University. He belongs to the American Physical Society (APS), American Nuclear Society (ANS), Society Of Industrial And Applied Mathematics (SIAM), South Pacific Underwater Medical Society (SPUMS), Undersea And Hyperbaric Medical Society (UHMS), and American Academy Of Underwater Sciences (AAUS). He is a Fellow of the American Physical Society, and a Technical Committee Member of the American Nuclear Society.

Wienke, a former dive shop owner in Santa Fe, presently serves as a Consultant for decompression algorithms in the Industry. He has worked with DAN on applications of high performance computing and communications to diving, and is a Regional Data Coordinator for Project Dive Exploration. Scubapro, Suunto, Abysmal Diving, and Atomic engage him (or have) as Consultant for meter algorithms. He is the developer of the Reduced Gradient Bubble Model (RGBM), a dual phase approach to staging diver ascents over an extended range of diving applications (altitude, nonstop, decompression, multiday, repetitive, multilevel, mixed gas, and saturation). The Suunto VYPER dive computer incorporates the RGBM into staging regimens, particularly for recreational diving (including nitrox). ABYSS, a commercial software product, features some of the RGBM dynamical diving algorithms developed by him for Internet users and technical divers. He is also Associate Editor for the International Journal Of Aquatic Research And Education, and is a former Contributing Editor of *Sources*, the NAUI Training Publication. NAUI Technical Training has adopted the RGBM for technical diving, and employs RGBM trimix, heliair, EANx, and air tables.

## TABLE OF CONTENTS

### PROLOGUE

## CONVENTIONS AND UNITS

## DIVING HISTORY

## ACKNOWLEDGMENTS

1. GAS, FLUID, AND PHASE KINETICS / Ideal Gases / Real Gases / Collisional Phenomena / State Variables And Energy Balance / High Pressure Equipment And Flows / Steady Flow / Dissolved Phase Transfer / Perfusion Controlled Transport / Diffusion Controlled Transport / Free Phase Transfer
2. CRITICAL TENSIONS AND PHASE VOLUMES / Critical Tensions And Decompression / Controlling Tissues / Time Remaining / Saturation Curve And Separated Phase / Critical Phase Volumes / Ascent Staging
3. ALTITUDE SIMILARITY AND PROCEDURES / Reduced Atmospheric Pressure / Critical Extrapolations / Altitude Procedures / Altitude Delay Time / Equivalent Decompression Ratios / Extended Haldane Staging / Equipment And Consumption Rate Effects
4. MIXED GASES AND DECOMPRESSION / Mixtures And Biological Reactivities / Comparative Properties / Nitrox / Heliox / Trimix / Hydrox / Haldane Decompression Procedures / Equivalent Air Depth / Oxygen Rebreathing / Isobaric Countertransport / Oxygen Dose
5. DECOMPRESSION TABLES, METERS, AND MODELS / Protocols / Tables / Meters / Model History / Bulk Diffusion Model / Multitissue Model / Thermodynamic Model / Varying Permeability Model / Reduced Gradient Bubble Model / Tissue Bubble Diffusion Model
6. COMPARATIVE PROFILES AND OPERATIONAL DIVING / Haldane Profiles / Empirical Practices / Phase Versus Haldane Profiles / RGBM Validation And Testing / Reverse Profiles
7. DECOMPRESSION RISK AND STATISTICS / Systematics And Issues / Binomial Distribution / Normal Distribution / Poisson Distribution / Probabilistic Decompression / Maximum Likelihood / Saturation Bends Probability / Table And Profile Risks
8. COMPUTING AND DECOMPRESSION ALGORITHMS / Computing Advances / Supercomputers / Networks / Storage / Grand Challenge Applications / Multilevel Dive Profile Analysis / Computational Models And Algorithms
9. DIVING MALADIES AND DRUGS / Maladies / Bends / High Pressure Nervous Syndrome / Inert Gas Narcosis / Hyperoxia And Hypoxia / Hypercapnia And Hypocapnia / Barotrauma / Altitude Sickness / Pulmonary Edema / Hypothermia And Hyperthermia / Dysbaric Osteonecrosis / Drugs
10. BUBBLES AND BIOSYSTEMS / Doppler Effect / Moving Bubbles / Operational Protocols / Pulmonary And Circulatory Networks / Inherent Unsaturation / Surface Tension / Adsorption / Surfactants / Micronuclei / Free Phases / Nucleation / Cavitation / Bubble And Seed Pressure Response
11. NUCLEATION PROCESSES AND STATISTICAL MECHANICS / Quiescent Nucleation / Cavitation / Triobnucleation / Gas Turbulent Nucleation / Chemical Nucleation / Microscopic Mechanisms / Ensemble Theory
12. EQUATIONS OF STATE AND SEED PERSISTENCE / Gases / Solids / Structured Fluids / Unstructured Fluids / Ensemble Averaging / Time Scales

## EPILOGUE

## EXERCISES AND SOLUTIONS

## BIBLIOGRAPHY

## PROLOGUE

This exposition attempts to walk a line between a discussion of decompression theory with equations and corresponding dialogue using extended prose. Both theory and diving application are, at times, more an artform than exact science. Some physiologists take the view that deterministic modeling can only be fortuitous. Technological advance, elucidation of competing mechanisms, and resolution of model issues over the past 80 years has not been rapid. Model applications tend to be *ad hoc*, tied to data fits, and difficult to quantify on just first principles. Almost any description of decompression processes in tissue and blood can be disputed, and possibly turned around on itself. The fact that decompression sickness occurs in metabolic and perfused matter makes it difficult to design and analyze experiments outside living matter. Yet, for application to safe diving, we need models to build tables and meters. And deterministic models, not discounting shortcomings, are the real subject of this monograph.

The reader will notice an emphasis on free gas phases (bubbles, nuclei, and whatever else is not dissolved), and comments about free phase models versus (just) dissolved phase models, the present basis for most decompression analysis. Most comments are based on recent experiments coupled to basic physics. While we do not know all the facts yet, the author takes the view that phase models correlated with available data, linked to underlying physical principles, and which recover dissolved gas models in appropriate limits, are the types of models which should be extended, refined, and used in table and meter algorithms. The alternative to model algorithms is statistical analyses of decompression risk data, folded into meaningful and useful table and meter format, an area under active study.

The intent here is to present a working view of decompression in diving, mostly focusing on theory with application, including equations. The discussion is neither a medical nor physiological synthesis. Such aspects are simplified, and for some certainly oversimplified. Nonetheless, it is directed toward the diver and reader with some rudimentary understanding of decompression. Background in the physical or life sciences is helpful, but certainly not requisite. Basically, the mechanistic of tissue gas exchange, bubbles and nucleation, supersaturation, perfusion and diffusion, and related mechanisms are discussed.

The physics, biology, engineering, physiology, medicine, and chemistry of diving center on pressure, and pressure changes. The average individual is subjected to atmospheric pressure swings of 3% at sea level, as much as 20% a mile in elevation, more at higher altitudes, and all usually over time spans of hours to days. Divers and their equipment can experience compressions and decompressions orders of magnitude greater, and within considerably shorter time scales. While the effects of pressure change are readily quantified in physics, chemistry, and engineering applications, the physiology, medicine, and biology of pressure changes in living systems are much more complicated. Caution is needed in transposing biological principles from one pressure range to another. Incomplete knowledge and mathematical complexities often prevent extensions of even simple causal relationships in biological science. Causal relationships between observables are, of course, the pervue of physics, and that difficult process in living systems is biophysics. Other source material and further development can be found in the References at the end of the monograph. For the interested and hard core analyst, a suite of applied and theoretical diving (and otherwise) problems follows each Part. Details broach fundamental to advanced material presented.

Material detailed builds upon and extends topics presented in *Physics, Physiology, And Decompression Theory For The Technical And Commercial Diver, Basic Diving Physics And Application, Diving Above Sea Level, High Altitude Diving, Basic Decompression Theory And Application (first edition)*, detailed in the References. Each Part suggests related developments. Hopefully, this updated version will further broaden your understanding and working knowledge of decompression theory and application to diving.

Good reading, and have fun with the Exercises at the end of each Part.

## CONVENTIONS AND UNITS

Standard (SI) and English units are employed. By convention, by usage, or for ease, some nonstandard units are employed. Pressure and depth are both measured in feet of sea water (*fsw*) and meters of sea water (*msw*), with  $1 \text{ atm} = 33 \text{ fsw} = 10 \text{ msw}$  to good approximation. Specific densities,  $\eta$  (dimensionless), in pressure relationships are normalized to sea water density.

Table 1. Equivalence And Unit Conversion Table.

Time	
$1 \text{ megahertz} = 10^6 \text{ hertz} = 10^6 \text{ sec}^{-1}$	
Length	
$1 \text{ m} = 3.28 \text{ ft} = 1.09 \text{ yd} = 39.37 \text{ in}$	
$1 \mu\text{m} = 10^4 \text{ angstrom} = 10^3 \text{ nm} = 10^{-6} \text{ m}$	
$1 \text{ km} = .62 \text{ mile}$	
$1 \text{ fathom} = 6 \text{ ft}$	
$1 \text{ nautical mile} = 6,080 \text{ ft} = 1.15 \text{ mile} = 1.85 \text{ km}$	
$1 \text{ light year} = 9.46 \times 10^{12} \text{ km} = 5.88 \times 10^{12} \text{ mile}$	
Speed	
$1 \text{ km/hr} = 27.77 \text{ cm/sec}$	
$1 \text{ mi/hr} = 5280 \text{ ft/sec}$	
$1 \text{ knot} = 1.15 \text{ mi/hr} = 51.48 \text{ cm/sec}$	
Volume	
$1 \text{ cm}^3 = .06 \text{ in}^3$	
$1 \text{ m}^3 = 35.32 \text{ ft}^3 = 1.31 \text{ yd}^3$	
$1 \text{ l} = 10^3 \text{ cm}^3 = .04 \text{ ft}^3 = .91 \text{ qt}$	
Mass and Density	
$1 \text{ g} = .04 \text{ oz}$	
$1 \text{ kg} = 32.27 \text{ oz} = 2.20 \text{ lb}$	
$1 \text{ g/cm}^3 = .57 \text{ oz/in}^3$	
$1 \text{ kg/m}^3 = .06 \text{ lb/ft}^3$	
Force and Pressure	
$1 \text{ newton} = 10^5 \text{ dyne} = .22 \text{ lb}$	
$1 \text{ g/cm}^2 = .23 \text{ oz/in}^2$	
$1 \text{ kg/m}^2 = .20 \text{ lb/ft}^2$	
$1 \text{ atm} = 33 \text{ fsw} = 10 \text{ msw} = 1.03 \text{ kg/cm}^2 = 14.69 \text{ lbs/in}^2$	
Energy and Power	
$1 \text{ cal} = 4.19 \text{ joule} = 3.96 \times 10^{-3} \text{ btu} = 3.09 \text{ ft lb}$	
$1 \text{ joule} = 10^7 \text{ ergs} = .74 \text{ ft lb}$	
$1 \text{ keV} = 10^3 \text{ eV} = 1.60 \times 10^{-16} \text{ joule}$	
$1 \text{ amu} = 931.1 \text{ MeV}$	
$1 \text{ watt} = 3.41 \text{ btu/hr} = 1.34 \times 10^{-3} \text{ hp}$	
Electricity and Magnetism	
$1 \text{ coul} = 2.99 \times 10^9 \text{ esu}$	
$1 \text{ amp} = 1 \text{ coul/sec} = 1 \text{ volt/ohm}$	
$1 \text{ volt} = 1 \text{ newton coul m} = 1 \text{ joule/coul}$	
$1 \text{ gauss} = 10^{-4} \text{ weber/m}^2 = 10^{-4} \text{ newton/amp m}$	
$1 \text{ f} = 1 \text{ coul/volt}$	

Standard mathematical and physical conventions are followed. Bold face quantities are vectors, while roman face quantities are scalars. Fundamental constants are tabulated below in Table 2. Full discussion of constants and impacts can be found in the References, particularly the physics and chemistry entries.

Table 2. Fundamental Constants.

$$\begin{aligned}
 g_0 &= 9.80 \text{ m/sec}^2 && (\text{Sea Level Acceleration Of Gravity}) \\
 G_0 &= 6.67 \times 10^{-11} \text{ newton m}^2/\text{kg}^2 && (\text{Gravitational Constant}) \\
 M_0 &= 5.98 \times 10^{24} \text{ kg} && (\text{Earth Mass}) \\
 \Gamma_0 &= 1.98 \text{ cal/min cm}^2 && (\text{Solar Constant}) \\
 c &= 2.998 \times 10^8 \text{ m/sec} && (\text{Speed Of Light}) \\
 h &= 6.625 \times 10^{-34} \text{ joule sec} && (\text{Planck Constant}) \\
 R &= 8.317 \text{ joule/gmole K}^\circ && (\text{Universal Gas Constant}) \\
 k &= 1.38 \times 10^{-23} \text{ joule/gmole K}^\circ && (\text{Boltzmann Constant}) \\
 N_0 &= 6.025 \times 10^{23} \text{ atoms/gmole} && (\text{Avogadro Number}) \\
 m_0 &= 9.108 \times 10^{-31} \text{ kg} && (\text{Electron Mass}) \\
 e_0 &= 1.609 \times 10^{-19} \text{ coulomb} && (\text{Electron Charge}) \\
 r_0 &= .528 \text{ angstrom} && (\text{First Bohr Orbit}) \\
 \epsilon_0 &= (4\pi)^{-1} \times 1.11 \times 10^{-10} \text{ f/m} && (\text{Vacuum Permittivity}) \\
 \mu_0 &= 4\pi \times 10^{-7} \text{ h/m} && (\text{Vacuum Permeability}) \\
 \kappa_0 &= (4\pi\epsilon_0)^{-1} = 8.91 \times 10^9 \text{ m/f} && (\text{Coulomb Constant}) \\
 \alpha_0 &= \mu_0/4\pi = 1 \times 10^{-7} \text{ h/m} && (\text{Ampere Constant}) \\
 \sigma_0 &= 5.67 \times 10^{-8} \text{ watt/m}^2 \text{ K}^{o4} && (\text{Stefan - Boltzmann Constant})
 \end{aligned}$$

Metrology is the science of measurement, and broadly construed, encompasses the bulk of experimental science. In the more restricted sense, metrology refers to the maintenance and dissemination of a consistent set of units, support for enforcement of equity in trade by weights and measure laws, and process control for manufacturing.

A measurement is a series of manipulations of physical objects or systems according to experimental protocols producing a number. The objects or systems involved are test objects, measuring devices, or computational operations. The objects and devices exist in and are influenced by some environment. The number relates to the some unique feature of the object, such as the magnitude, or the intensity, or the weight, or time duration. The number is acquired to form the basis of decisions effecting some human feature or goal depending on the test object.

In order to attain the goal of useful decision, metrology requires that the number obtained is functionally identical whenever and wherever the measurement process is performed. Such a universally reproducible measurement is called a *proper measurement* and leads to describing *proper quantities*. The equivalences in Table 1 relate *proper quantities* and the fundamental constants in Table 2 permit closure of physical laws. Unit conversion follows from Table 2, via the chain rule, So, for example, consider the following reductions and conversions, where the identities in Table 1 define equivalence ratios that work like simple arithmetic fractions as far as unit conversions are concerned. Units cancel just like numbers.

#### Exercises

1. How many nautical miles to a kilometer?
2. How many electrostatic units (esu) to a coulomb?
3. How many light years to a mile?
4. Convert depth,  $d = 38 \text{ fsw}$ , to ft in fresh water?

5. Convert ascent rate,  $r = 60 \text{ fsw/min}$ , to  $\text{msw/sec}$ ?
6. Convert volume,  $V = 6.2 \text{ m}^3$ , to  $\text{ft}^3$ ?
7. Convert pressure,  $P = 5.3 \text{ kg/m}^2$ , to  $\text{lb/in}^2$ ?
8. Convert density,  $\rho = .06 \text{ lb/ft}^3$ , to  $\text{kg/m}^3$ ?
9. Convert acceleration,  $g = 32 \text{ ft/sec}^2$ , to  $\text{m/sec}^2$ ?

#### Related Reading

1. Beckwith B., 1969, *Mechanical Measurements, Reading: Addison Wesley.*
2. Defant A., 1961, *Physical Oceanography, New York: Doubleday.*
3. Feynman R.P., Leighton R.B., and Sands M., 1975, *The Feynman Lectures On Physics, I, II, III, Reading: Addison Wesley.*
4. Fleagle R.G. and Businger J.A., 1963, *An Introduction To Atmospheric Physics, New York: Academic Press.*
5. Kahaner D., Moler C., and Nash S., 1989, *Numerical Methods And Software, Englewood Cliffs: Prentice Hall.*
6. Wienke B.R., 1994, *Basic Diving Physics And Application, Flagstaff: Best.*

## DIVING HISTORY

Man has probably practised breathhold diving in some form across all stages of development, first becoming adept at swimming and then recovering food from lakes and oceans. Now, breathhold diving and snorkeling are popular sports. Breathhold and inverted bell diving reach back over many centuries, like fifty or so. Written records of Cretan sponge divers (3000 *BC*) and Chinese pearl divers (2000 *BC*) exist today. Detailed military accounts link to Xerxes who employed combat divers to recover treasure from sunken ships (519 *BC*), as chronicled by the Greek historian, Herodotus. Alexander the Great (356 *BC*) also deployed breathhold divers in the siege for Tyre. Depths rarely exceeded 60 *fsw* in these exploits. According to Pliny (77 *AD*), reed breathing tubes were employed by Roman Legions, hiding or waiting in ambush. Aristotle (384 *BC*), pupil of Plato, and tutor of Alexander, writes of diving bells used to recover treasure. These inverted receptacles, utilizing trapped compressed air as breathing mixture, gained renown in Europe in the 1600s. Ancient Assyrians and Persians also carried air in goatskins underwater. Some Korean and Japanese breathhold divers (*armaghs*) still gather pearls and sponges with lung power, but most of the fishing, pearling, and sponging divers of the world today have gone over to SCUBA. Terrorists in Southeast Asia avoided capture by lying beneath swamp surfaces and breathing through hollow reeds. SEALs adopted similar assault tactics in the Mekong Delta of Vietnam.

Halley patented a large diving bell in 1690, refurbished with surface air for periods beyond an hour. In 1770, Le Havre developed a manual air compressor. Surface supplied air and demand regulators were employed in hard hat diving by the 1800s, with the first demand regulator, patented by Rouquayrol in 1866, supplied by hand bellows. The first case of nitrogen narcosis was reported by Junod in 1835. Full diving suits, in which air escapes through a one way exhaust valve, were invented by Siebe in 1840, and a few are still around. Quietly, the revolutionary *aqua lung* of Cousteau, a refinement of the Rouquayrol surface supplied demand regulator, ushered the modern era of SCUBA in wartime Europe in 1943. Diving would never be the same afterward. In the US Navy, elite SRs,

NCDUs, UDTs, and SEALs honed their skills above and below the surface, extending the meaning of combat utility. Freed from surface umbilical, open and closed circuit units enhanced the mobility and range of tactical operations for sure, but the impact on nonmilitary diving was orders of magnitude greater. Coupled to high pressure compressed air in tanks, SCUBA offered the means to explore the underwater world for fun and profit.

Commercial availability of the demand regulator in 1947 initiated sport diving and a fledgling equipment industry. Serious diver training and certification Agencies, such as the National Association of Underwater Instructors, YMCA, and Professional Association of Diving Instructors, still online, organized in the late 1950s and 1960s. In the mid 1950s, the Royal Navy released their bulk diffusion decompression tables, while a little later, in 1958, the US Navy compiled their modified Haldane tables with six perfusion limited compartments. Both would acquire biblical status over the next 25 years, or so. In the mid to late 1950s, Fredrickson in the USA and Alinari in Italy designed and released the first analog decompression meters, or computers, emulating tissue gas uptake and elimination with pressure gauges, porous plugs, and distensible gas bags. The first digital computers, designed by DCIEM in Canada, appeared in the mid 1950s. Employed by the Canadian Navy, they were based on a four compartment analog model of Kidd and Stubbs. Following introduction of a twelve compartment Haldanian device, linked to Doppler technology, by Barshinger and Huggins in 1983, decompression computers reached a point of maturation and acceptance. Flexible, more reliable to use, and able to emulate almost any mathematical model, digital computers rapidly replaced pneumatic devices in the 1980s. Their timely functionality and widespread use heralded the present era of high tech diving, with requirements for comprehensive decompression models across a full spectrum of activity. Computer usage statistics, gathered in the 1990s, suggest an enviable track record of diver safety, with an underlying decompression sickness (DCS) incidence below 0.05

Diver mobility concerns ultimately fostered development of the modern SCUBA unit, and the quest to go deeper led to exotic gas breathing mixtures. High pressure cylinders and compressors similarly expedited deeper diving and prolonged exposure time. The world record dives of Keller to 1,000 *fsw* in 1960 not only popularized multiple gas mixtures, but also witnessed the first real use of computers to generate decompression schedules. Saturation diving and underwater habitats followed soon after, spurred by a world thirst for oil. Both multiple gas mixtures and saturation diving became a way of life for some commercial divers by the 1970s, particularly after the oil embargo. Oil concerns still drive the commercial diving industry today.

Cochrane in England invented the high pressure caisson in 1830. Shortly afterward, the first use of a caisson in 1841 in France by Triger also precipitated the first case of decompression sickness, aptly termed the bends because of the position assumed by victims to alleviate the pain. Some fifty years later, in 1889, the first medical lock was employed by Moir to treat bends during construction of the Hudson River Tunnel. Since that time many divers and caisson workers have been treated in hyperbaric chambers. Indeed, the operational requirements of diving over the years have provided the incentives to study hyperbaric physiology and its relationship to decompression sickness, and impetus for describing fundamental biophysics. Similarly, limitations of nitrogen mixtures at depth, because of narcotic reactivity, prompted recent study and use of helium, nitrogen, hydrogen, and oxygen breathing mixtures at depth, especially in the commercial and (now) *hard core* technical diving sectors.

Increases in pressure with increasing depth underwater impose many of the limitations in diving, applying equally well to the design of equipment used in this environment. Early divers relied on their breathholding ability, while later divers used diving bells. Surface supplied air and SCUBA are rather recent innovations. With increasing depth and exposure time, divers encountered a number of physiological and medical problems constraining activity, with decompression sickness perhaps the most restrictive. By the 1800s, bubbles were noted in animals subject to pressure reduction. In the 1900s, they were postulated as the cause of decompression sickness in caisson workers and divers. Within that postulate, and driven by a need to both optimize diver safety and time underwater, de-

compression modeling has consolidated early rudimentary schedules into present more sophisticated tables and meters. As knowledge and understanding of decompression sickness increase, so should the validity, reliability, and range of applicability of models.

A consensus of opinions, and for a variety of reasons, suggests that modern diving began in the early 1960s. Technological achievements, laboratory programs, military priorities, safety concerns, commercial diving requirements, and international business spurred diving activity and scope of operation. Diving bells, hot water heating, mixed gases, saturation, deep diving, expanded wet testing, computers, and efficient decompression algorithms signaled the modern diving era. Equipment advances in open and closed circuit breathing devices, wet and dry suits, gear weight, mask and fin design, high pressure compressors, flotation and buoyancy control vests, communications links, gauges and meters, lights, underwater tools (cutting, welding, drilling, explosives), surface supplied air, and photographic systems paced technological advances. Training and certification requirements for divers, in military, commercial, sport, and scientific sectors, took definition with growing concern for underwater safety and well being.

In the conquest and exploration of the oceans, saturation diving gained prominence in the 1960s, thereby permitting exploitation of the continental shelf impossible within exposure times permitted by conventional regimens. Spurred by both industrial and military interests in the ability of men to work underwater for long periods of time, notable *habitat* experiments, such as Sealab, Conshelf, Man In Sea, Gulf Task, and Tektite established the feasibility of living and working underwater for extended periods. These efforts followed proof of principle validation, by Bond and coworkers (USN) in 1958, of saturation diving. Saturation tests have been conducted from 35 *fsw* down to 2,000 *fsw*.

The development and use of underwater support platforms, such as habitats, bell diving systems, lockout and free flooded submersibles, and diver propulsion units also accelerated in the 1960s and 1970s, for reasons of science and economics. Support platforms extended both diver usefulness and bottom time, by permitting him to live underwater, reducing descent and ascent time, expanding mobility, and lessing physical activity. Today, operating from underwater platforms themselves, remotely operated vehicles (ROVs) scan the ocean depths at 6,000 *fsw* for minerals and oil.

Around 1972, strategies for diving in excess of 1,000 *fsw* received serious scrutiny, driven by a commercial quest for oil and petroleum products, and the needs of the commercial diving industry to service that quest. Questions concerning pharmacological additives, absolute pressure limits, thermal exchange, therapy, compression-decompression procedures, effective combinations of mixed breathing gases, and equipment functionality addressed many fundamental issues, unknown or only partially understood. By the early 1980s, it became clear that open sea water work in the 1,000 to 2,000 *fsw* range was entirely practical, and many of the problems, at least from an operational point of view, could be solved. Today, the need for continued deep diving remains, with demands that cannot be answered with remote, or 1 *atm*, diver systems. Heliox and trimix have become standards for deep excursion breathing gases, with heliox the choice for shallower exposures, and trimix a choice for deeper exposures in the field.

Yet, despite tremendous advances in deep diving technology, most of the ocean floor is outside human reach. Breathing mixtures that are compressible are limiting. Breathing mixtures that are not compressible offer interesting alternatives. In the 1960s, serious attention was given to liquid breathing mixtures, physiological saline solutions. Acting as inert respiratory gas diluents, oxygenated fluids have been used as breathing mixtures, thereby eliminating decompression requirements. Some synthetic fluids, such as fluorocarbon (*FX<sub>80</sub>*), exhibit enormous oxygen dissolution properties.

## ACKNOWLEDGMENTS

Many thanks go to my colleagues here at Los Alamos National Laboratory, to collaborators in the industrial, military, and academic sectors, and to investigators and teachers over the years who asked many interesting diving questions. Affiliations with the American Physical Society, American Nuclear Society, American Academy Of Underwater Sciences, Undersea And Hyperbaric Medical Society, South Pacific Underwater Medicine Society, and Society Of Industrial And Applied Mathematics are also gratefully acknowledged. Thanks to the diver training agencies, NAUI, PADI, and YMCA for providing additional support and stimulus for this undertaking, as well as the technical training agencies, TDI, IANTD, and ANDI. And collegial thanks to Ari Nikkola and Jarmo Luukkanen of Suunto, Doug Toth of Scubapro and Atomics, Chris Parrett of Abysmal Diving, Tim O'Leary and Jan Neal of NAUI Technical Diving, Charlie Lehner and Ed Lanphier of the University of Wisconsin, Dick Vann of Duke University, David Yount of the University of Hawaii, Wayne Gerth of NEDU, Jim Bram of NAUI, the Decompression List at *deco@decompression.org*, NAUI Instructors everywhere, Tom Kunkle of Los Alamos National Laboratory, and Lee Somers of the University of Michigan.

On a personal note, warm thanks to Luzanne Rippentrop for being a spectacular woman in all ways, and to Hillary Froemel for being a constant reminder that adults have much to learn from children. Both of you bring out the best in others.

Collectively, thanks to all of you who stacked a pile of queries on my LANL desk here. Hopefully this monograph builds and extends upon all of its predecessors, and all of your queries.

Bruce Wienke  
Los Alamos National Laboratory  
Applied And Computational Physics Division  
LANL, X-7  
MS-D413  
(505) 667-1358 (office)  
(505) 992-8725 (home)

brw@lanl.gov  
<http://www-xdiv.lanl.gov/brw/wienke.html>  
10/1/00

PART 1: DECOMPRESSION THEORY  
GAS, FLUID, AND PHASE KINETICS

Ideal Gases

Air is a mixture of inert and metabolic gases, composed of hydrogen and oxygen mainly, with variable amounts of carbon dioxide, water vapor, ozone, sulfur dioxide, and nitrogen dioxide, and fixed trace amounts of xenon, helium, krypton, argon, methane, nitrous oxide, hydrogen, and neon. By volume, air is 78.1% nitrogen, 20.9% oxygen, and 1% everything else. Over nominal pressure and temperature ranges encountered in the Earth's atmosphere, air can be treated as an *ideal*, or dilute, gas.

Ideal gas molecules occupy no space, do not interact, scatter elastically from each other, and cannot be distorted upon collision, in short, act as vanishingly small, perfectly elastic, hard spheres in constant random motion from collisions. Real gases, in the limit of very large confining volumes, all behave like ideal gases, as well as over select ranges of pressure, temperature, and density. Simple monatomic (one atom molecules) and diatomic (two atom molecules) gases and mixtures, such as air, at room temperatures and atmospheric pressures are considered ideal, and satisfy an equation of state (EOS) linking pressure  $P$ , volume,  $V$ , and and temperature,  $T$ , of the form,

$$PV = nRT \quad (1)$$

with  $n$  the number of moles of gas, and  $R$  the universal gas constant ( $8.317 \text{ joule/mole} - K^\circ$ ). Temperature is measured in absolute, or Kelvin ( $K^\circ$ ), units. In conservative processes,  $n$  is constant and changes in the state variables,  $P$ ,  $V$ , and  $T$ , are linked to each other by the  $P-V-T$  relationship. If each variable is alternatively held fixed, we get three, well known, ideal gas law corollaries,

$$PV = \gamma_T \quad (\text{Boyle's law}) \quad , \quad (2)$$

$$\frac{P}{T} = \gamma_V \quad (\text{Amonton's law}) \quad , \quad (3)$$

$$\frac{V}{T} = \gamma_P \quad (\text{Charles' law}) \quad , \quad (4)$$

with  $\gamma_T = nRT$ ,  $\gamma_V = nR/V$ , and  $\gamma_P = nR/P$  all constant. The relationships connect any number of arbitrary changes of state for constant temperature, volume, or pressure, respectively. In a mixture of ideal gases, the total pressure is the sum of component gas partial pressures, intuitively obvious, but also known as Dalton's law. Denoting gas partial pressures,  $p$ , the total pressure,  $P$ , is given by,

$$P = \sum_{j=1}^J p_j \quad , \quad (5)$$

with  $p_j$  the partial pressure of the  $j^{\text{th}}$  gas species in a  $J$  component mixture.

Temperatures, which really measure average kinetic energy of gas molecules in the ensemble, are measured in Centigrade ( $C^\circ$ ), Fahrenheit ( $F^\circ$ ), Kelvin ( $K^\circ$ ), and Rankine ( $R^\circ$ ) degree units, related by,

$$F^\circ = \frac{9}{5}C^\circ + 32 \quad , \quad (6)$$

$$K^\circ = C^\circ + 273 \quad , \quad (7)$$

$$R^\circ = F^\circ + 460 \quad . \quad (8)$$

## Real Gases

All gas molecules occupy space, exert short ranged forces on each other, scatter inelastically at times, and possibly distort with collision, in short, act as nonideal gas molecules. Then equations-of-state need include such effects, particularly in appropriate pressure, temperature, and density regimes. The most general form of the equation of state can be cast in *virial* form, in terms of the molal specific volume,  $v$ ,

$$v = \frac{V}{n} \quad (9)$$

for  $n$  the number of moles,

$$Pv = RT \left[ 1 + \frac{a}{v} + \frac{b}{v^2} + \frac{c}{v^3} + \dots \right] , \quad (10)$$

with  $a, b, c$  functions mostly of temperature, possibly specific volume. For ideal gases,  $a = b = c = 0$ , but in general these virial constants are nonzero. Certainly as the specific volume,  $v$ , or real volume,  $V$ , gets large, the virial expansion collapses to the ideal case. The virial expansion and coefficients can be fitted to sets of experimental data for gases. Such fits to even very complicated gas behavior all have one feature in common. The quantity,  $pv/T$ , always approaches the universal gas constant,  $R$ , as temperature,  $T$ , approaches absolute zero ( $-273\text{ }C^\circ$  or  $-460\text{ }F^\circ$ ).

Clausius suggested that the volume,  $V$ , available to a single gas molecule be reduced by the actual volume occupied by all other molecules in the assembly, as shown in Figure 1. Accordingly, a correction factor,  $b$ , enters the ideal gas law through the simple relationship,

$$P(v - b) = RT \quad (11)$$

yielding the Clausius equation of state. Van der Waals, in 1873, suggested a second correction term, accounting for forces between molecules,  $a$ , be added to the ideal equation of state,

$$(P + a/v^2)(v - b) = RT \quad (12)$$

giving the van der Waals relationship. Both  $a$  and  $b$  are functions of temperature,  $T$ , and not simple constants. As  $a, b \rightarrow 0$ , the van der Waals and Clausius equations go over to the ideal gas limit.

The van der Waals equation can be put in virial form by first rewriting,

$$Pv = RT \left[ 1 - \frac{b}{v} \right]^{-1} - \frac{a}{v} \quad (13)$$

and then using the binomial expansion,

$$\left[ 1 - \frac{b}{v} \right]^{-1} \approx 1 + \frac{b}{v} + \frac{b^2}{v^2} + \dots \quad (14)$$

so that,

$$Pv = RT + \frac{RTb - a}{v} + \frac{RTb^2}{v^2} + \dots \quad (15)$$

The Beattie-Bridgman equation is a modified virial equation which fits the experimental data over a wide range of pressure, volume, and temperature,

$$Pv = \frac{RT(1 - \delta/vT^3)}{v} (v + \beta) - \frac{\alpha}{v} \quad (16)$$

for  $\alpha, \beta$ , and  $\delta$  slowly varying (temperature) constants. The van der Waals gas law permits two degrees of freedom ( $a, b$ ), while the Beattie-Bridgman equation is more flexible, admitting three degrees of freedom ( $\alpha, \beta, \delta$ ), in fitting experimental data.

### Collisional Phenomena

The properties of matter in bulk are predicted from kinetic, or dynamic, theory through application of the laws of mechanics to the individual molecules of the system, and from these laws, deriving expressions for the pressure of a gas, internal energy, and specific heat. Statistical mechanics, more broadly, ignores detailed considerations of molecules as individuals, and applies considerations of probability to the very large ensemble of molecules comprising matter. Both were developed on the assumption that the laws of mechanics, deduced from the behavior of matter in bulk, could be applied to molecules, atoms, and electrons. In gases, particles are in continuous collisional mode.

If we imagine that at a certain instance in time all the molecules of a gas, except one, are frozen in position, while the remaining single molecule continues to move among the others with ensemble average speed,  $\bar{v}$ , and that all molecules are perfectly elastic spheres, we can define a collision cross section,  $\sigma$ , as the area swept out by their total radial separation,  $2r$ , with  $r$  the molecular radius,

$$\sigma = 4\pi r^2 \quad . \quad (17)$$

For gases, molecular radii are on the order of *angstroms* ( $10^{-10} m$ ). In a time interval,  $dt$ , if there are  $N$  molecules in volume,  $V$ , the number,  $dN$ , with centers in the cylinder swept out by the molecule moving with velocity,  $\bar{v}$ , is,

$$dN = \sigma \frac{N}{V} \bar{v} dt \quad , \quad (18)$$

also representing the number of collisions in that time interval. The collisional frequency,  $f$ , is the number of collisions per unit time interval,

$$f = \frac{dN}{dt} = \sigma \frac{N}{V} \bar{v} \quad . \quad (19)$$

Collisional frequencies are on the order of  $10^{10} sec^{-1}$ . The average distance between collisions,  $\Lambda$ , or the mean free path, equals distance covered,  $\bar{v}dt$ , divided by number of collisions,  $dN$ , that is,

$$\Lambda = \frac{V}{\sigma N} \quad . \quad (20)$$

Typical values for  $\Lambda$  are near  $10^{-7} cm$  for gases. Every collision removes a molecule from  $N$ , and the corresponding change,  $dN$ , in distance,  $dx$ , depends on  $N$ , and collision probability,  $\chi$ ,

$$dN = -\chi N dx \quad , \quad (21)$$

with, in the simplest case of solid spheres,

$$\chi = \frac{1}{\Lambda} \quad . \quad (22)$$

The standard survival equation follows upon integration of the above, with  $N = N_0$  at  $x = 0$ ,

$$N = N_0 \exp(-x/\Lambda) \quad . \quad (23)$$

The viscosity,  $X$ , thermal conductivity,  $K$ , and diffusivity,  $D$ , in the kinetic picture depend on particle transport of momentum, energy, and mass by collisions. Considerations of the momentum, energy, and mass transfer across any imagined surface by molecular collisions yields,

$$X = \frac{1}{3} \frac{N}{V} m \bar{v} \Lambda \quad , \quad (24)$$

$$K = \frac{1}{2} \frac{N}{V} \bar{v} k \Lambda \quad , \quad (25)$$

$$D = \frac{1}{3} \bar{v} \Lambda \quad , \quad (26)$$

with  $m$  the molecular mass, and  $k$  Boltzmann's constant. Obviously the density,  $\rho$ , is given by,

$$\rho = \frac{N}{V} m \quad , \quad (27)$$

so that,

$$D = \frac{X}{\rho} \quad , \quad (28)$$

$$H = \frac{3}{2} \frac{X}{\rho} k \quad . \quad (29)$$

Table 1 lists transport coefficients for a number of gases, that is, mean free path, molecular radius, viscosity, thermal conductivity, and diffusivity, at room temperature.

Table 1. Kinetic Transport Coefficients.

gas	$\Lambda$ ( $\mu m$ )	$r$ ( $nm$ )	$X$ ( $dyne \ sec/m^2$ )	$K$ ( $joule/cm \ sec \ K^\circ$ )	$D$ ( $cm^2/sec$ )
<i>He</i>	.186	.109	1.94	.144	.124
<i>Ne</i>	.132	.132	3.12	.046	.358
<i>N<sub>2</sub></i>	.063	.188	1.73	.023	.072
<i>O<sub>2</sub></i>	.068	.179	2.01	.024	.073
<i>NH<sub>3</sub></i>	.045	.222	.97	.021	.014
<i>CO<sub>2</sub></i>	.042	.232	1.45	.030	.009

### State Variables And Energy Balance

Pressure, density, and temperature are intuitive, fundamental concepts, elucidated and measured at early times in our scientific history by the Greeks, Romans, Babylonians, Egyptians, and probably others, well before atomic hypotheses. And the quthetitative relationship linking them is the equation of state.

#### 1. Pressure

Pressure,  $P$ , is simply the force,  $F$ , per unit area,  $A$ , that is,

$$P = \frac{F}{A} \quad (30)$$

and is equal in all directions (scalar quantity, while force itself is formally a vector quantity). As seen, pressure in gases results from molecular collisions with surroundings. Pressure from extended matter results from the collective forces applied across boundaries of fluids and solids.

#### 2. Density

Density  $\rho$ , similarly is mass,  $m$ , per unit volume,  $V$ ,

$$\rho = \frac{m}{V} \quad (31)$$

and suggests how tightly packed matter can exist. Weight density is weight per unit mass, differing from mass density by the acceleration of gravity,  $g$ . Both are used interchangeably in applications. Objects denser than a fluid will sink in that fluid, and objects less dense than a fluid will float. Sinking objects have negative buoyancy, while floating objects have positive buoyancy. Objects with the same density as the fluid are neutrally buoyant, and can be moved about without sinking or rising. Relative buoyancy obviously depends on fluid and object densities. Table 2 list densities of known, naturally occurring, elements as function of atomic number,  $Z$ , and atomic mass,  $A$ .

Table 2. Densities Of Elements.

element	$Z$	$A$	$\rho$ ( $g/cm^3$ )	element	$Z$	$A$	$\rho$ ( $g/cm^3$ )
<i>H</i>	1	1.008	.0009	<i>Cd</i>	48	112.41	8.65
<i>He</i>	2	4.003	.0017	<i>In</i>	49	114.82	7.28
<i>Li</i>	3	6.940	.53	<i>Sn</i>	50	118.70	6.52
<i>Be</i>	4	9.013	1.85	<i>Sb</i>	51	121.76	6.69
<i>B</i>	5	10.82	2.45	<i>Te</i>	52	127.61	6.24
<i>C</i>	6	12.01	1.62	<i>I</i>	53	126.91	4.93
<i>N</i>	7	14.08	.0013	<i>Xe</i>	54	131.30	.0059
<i>O</i>	8	16.00	.0014	<i>Cs</i>	55	132.91	1.87
<i>F</i>	9	19.00	.0017	<i>Ba</i>	56	137.36	5.52
<i>Ne</i>	10	20.18	.0009	<i>La</i>	57	138.92	6.19
<i>Na</i>	11	22.99	.971	<i>Ce</i>	58	140.13	6.78
<i>Mg</i>	12	24.32	1.74	<i>Pr</i>	59	140.92	6.78
<i>Al</i>	13	26.98	2.70	<i>Nd</i>	60	144.27	6.95
<i>Si</i>	14	28.09	2.42	<i>Pm</i>	61	145.01	7.23
<i>P</i>	15	30.98	1.82	<i>Sm</i>	62	150.35	7.70
<i>S</i>	16	32.06	2.07	<i>Eu</i>	63	152.08	5.22
<i>Cl</i>	17	35.46	.0032	<i>Gd</i>	64	157.26	7.95
<i>Ar</i>	18	39.94	.0018	<i>Tb</i>	65	158.93	8.33
<i>K</i>	19	39.10	.87	<i>Dy</i>	66	162.51	8.56
<i>Ca</i>	20	40.08	1.55	<i>Ho</i>	67	164.94	8.76
<i>Sc</i>	21	44.96	2.52	<i>Er</i>	68	167.27	9.16
<i>Ti</i>	22	47.90	4.58	<i>Tm</i>	69	168.94	9.35
<i>V</i>	23	50.95	5.96	<i>Yb</i>	70	173.04	7.01
<i>Cr</i>	24	52.01	7.10	<i>Lu</i>	71	174.99	9.74
<i>Mn</i>	25	54.94	7.22	<i>Hf</i>	72	178.53	13.32
<i>Fe</i>	26	55.85	7.86	<i>Ta</i>	73	180.95	16.62
<i>Co</i>	27	58.94	8.91	<i>W</i>	74	183.86	19.28
<i>Ni</i>	28	58.71	8.86	<i>Re</i>	75	186.22	20.53
<i>Cu</i>	29	63.54	8.94	<i>Os</i>	76	190.24	22.48
<i>Zn</i>	30	65.38	7.14	<i>Ir</i>	77	192.18	22.42
<i>Ga</i>	31	69.72	5.91	<i>Pt</i>	78	195.09	21.37
<i>Ge</i>	32	72.60	5.36	<i>Au</i>	79	197.02	19.39
<i>As</i>	33	74.91	5.73	<i>Hg</i>	80	200.61	13.55
<i>Se</i>	34	78.96	4.79	<i>Tl</i>	81	204.39	11.85
<i>Br</i>	35	79.92	3.12	<i>Pb</i>	82	207.21	11.35
<i>Kr</i>	36	83.82	.0037	<i>Bi</i>	83	209.03	9.75
<i>Rb</i>	37	85.48	1.53	<i>Po</i>	84	210.06	9.24
<i>Sr</i>	38	87.63	2.54	<i>At</i>	85	211.12	10.24
<i>Y</i>	39	88.92	5.52	<i>Rn</i>	86	222.13	.0010
<i>Zr</i>	40	91.22	6.43	<i>Fr</i>	87	223.09	
<i>Nb</i>	41	92.91	6.45	<i>Ra</i>	88	226.05	5.04
<i>Mo</i>	42	95.95	10.21	<i>Ac</i>	89	227.13	
<i>Tc</i>	43	98.02		<i>Th</i>	90	232.09	11.32
<i>Ru</i>	44	101.12	12.23	<i>Pa</i>	91	231.12	15.43
<i>Rh</i>	45	102.91	12.53	<i>U</i>	92	238.07	18.91
<i>Pd</i>	46	106.42	12.22	<i>Np</i>	93	237.52	
<i>Ag</i>	47	107.88	10.52	<i>Pu</i>	94	239.12	19.73

The range in densities, gas to solid, for the naturally occurring elements is a factor of  $20 \times 10^4$  roughly.

Specific densities,  $\eta$ , are just the ratios of densities of two substances. Specific densities of substances with respect to sea water are often useful in diving applications, fresh water to sea water conversions in quantitative gauge and meter calibrations, and depth equivalences.

Solids and fluids possess essentially fixed density under nominal pressure changes, but gases, and flexible objects containing gases, change density rapidly under pressure change. Relative buoyancy also changes rapidly as object density varies. For contained gases, density and buoyancy changes result from changes in volume. The body itself, and equipment specifically worn by divers, contain air spaces that can expand and contract under pressure changes. The lungs, wet and dry suit, and buoyancy compensator (BC), for instance, respond readily to pressure change, inducing commensurate buoyancy change. Since salt water is denser than freshwater, it exerts a greater buoyant force than fresh water. Buoyancy changes in fresh and salt water thus differ as object density changes.

Buoyancy changes occur when divers descend and ascend, move between fresh and salt water and/or different elevations. Buoyancy is lost relative to the surface when wet suit divers descend. Since fresh water is less dense than salt water, buoyancy is lost in fresh water relative to salt water. Similarly, since ambient pressure at altitude is less than at sea level, wet suits expand at elevation, increasing buoyancy. Effects can be quantified by Archimedes' and Boyle's laws. In all cases, effects ultimately relate to the densities of constituent fluid media.

### 3. Archimedes' Principle

According to Archimedes many centuries ago, any object displacing a volume,  $V$ , of fluid of density,  $\rho$ , is buoyed upward by a force,  $B$ , equal to the weight of the displaced fluid. From what we know about pressure in a fluid, this fact can be deduced easily.

Imagine a uniform block, of height,  $h$ , and cross sectional surface area,  $A$ , so that its volume,  $V$ , is

$$V = Ah \quad . \quad (32)$$

Submerging the block in a fluid of density,  $\rho$ , in an upright position, we can add up all the pressures on the block to determine the buoyant upward force,  $B$ . The sum total of all pressures on faces is zero, since every force on every face is balanced by an equal force on the opposite face. At the top of the block, a downward force,  $F_d$ , is exerted by the

$$F_d = \rho g Ad \quad , \quad (33)$$

with  $d$  the depth of the submerged top face of the block. At the bottom of the block, an upward force,  $F_u$ , is exerted by the fluid,

$$F_u = \rho g A(h + d) \quad . \quad (34)$$

The difference of the two forces,  $B$ , is the buoyant (upward) force,

$$B = F_u - F_d = \rho g Ah = \rho g V \quad , \quad (35)$$

or Archimedes' principle.

The weight of a column of air, or water, of height,  $d$ , density,  $\rho$ , and cross sectional area,  $A$ , is obviously,

$$W = \rho g Ad \quad (36)$$

and so the pressure,  $P$ , of (just) that same column, is,

$$P = \frac{W}{A} = \rho g d \quad (37)$$

An atmosphere of air (some 80 *miles* high) exerts roughly the same pressure as a column of sea water 33 *fsw* deep.

#### 4. Temperature

Temperature is a measure of hotness or coldness. But more particularly, temperature is a measure of the average kinetic energy of the molecular ensemble comprising the object, also called the internal energy. For an ideal gas, the mean molal kinetic energy,  $\bar{\epsilon}$ , satisfies the Boltzmann relationship,

$$\bar{\epsilon} = \frac{3}{2} kT \quad , \quad (38)$$

with  $k$  Boltzmann's constant ( $1.38 \times 10^{-23} \text{ j/gmole } K^\circ$ ), and  $T$  the absolute temperature. The first temperature measuring devices, employing displaced air volumes to define hotness or coldness according to the pronouncements of the instrument maker, were called thermometers in the 1600s. The liquid sealed in glass thermometers, based on thermal expansion and contraction, appeared in the latter half of the 1600s.

Use of temperature as a measurement of hotness or coldness is based on two requirements, that is, a universal agreement on calibration and scale, and technology sufficient to produce reliable instruments giving identical readings under the same conditions. Wide adoption of the Fahrenheit scale,  $F^\circ$ , was promoted by the trusty mercury (in glass) thermometers constructed in Danzig, by Fahrenheit, in the early 1700s. The scale was based on two fixed points, namely, the melting point of ice and the temperature of a healthy human body (later replaced by the boiling point of water). Celsius, at Uppsala, around the mid 1700s, introduced the Celsius (Centigrade) scale,  $C^\circ$ , on which the degree was 1/100 of the interval between the freezing and boiling points of water. Later, in the 1800s, Kelvin introduced the absolute scale,  $K^\circ$ , based on the second law of thermodynamics and entropy, ultimately linked by statistical mechanics to an absolute zero, that is, a temperature at which random molecular motion ceases. By 1887, the international community adopted the constant volume hydrogen gas thermometer as defining measurements on the Kelvin scale.

Kelvin ( $K^\circ$ ), Centigrade ( $C^\circ$ ), Rankine ( $R^\circ$ ), and Fahrenheit ( $F^\circ$ ) temperatures are linearly scaled, and are easily related,

$$F^\circ = \frac{9}{5} C^\circ + 32 \quad , \quad (39)$$

$$K^\circ = C^\circ + 273 \quad , \quad (40)$$

$$R^\circ = F^\circ + 460 \quad . \quad (41)$$

Kelvin and Rankine temperatures are employed in the gas laws.

#### 5. First And Second Laws

The first law of thermodynamics is really a statement of conservation of energy in any system. Denoting the internal energy of the system,  $U$ , the net heat flow into the system,  $Q$ , and the work,  $W$ , done on the system, the first law requires that infinitesimal changes  $dQ$ ,  $dU$ , and  $dW$  satisfy,

$$dU = dQ - dW \quad . \quad (42)$$

The internal energy of an ideal gas is only dependent on temperature, and that is a good approximation in most other real gases near standard temperature and pressure. ( $32 F^\circ$ , and  $1 \text{ atm}$ ). Denoting the number of molecules of the gas,  $N$ , and the number of moles,  $n$ , with  $R$  the gas constant and  $k$  Boltzmann's constant, we have

$$dU = N\bar{\epsilon}dT = \frac{3}{2} NkdT = \frac{3}{2} nRdT \quad , \quad (43)$$

as a measure of the internal energy change,  $dU$ , for temperature change,  $dT$ . Heat flow,  $dQ$ , into or out of the system occurs through conduction, convection, or radiation. Mechanical work,  $dW$ , performed on, or by, the system is associated with volume change,  $dV$ , under pressure,  $P$ ,

$$dW = P dV \quad , \quad (44)$$

so that,

$$dU = dQ - P dV \quad , \quad (45)$$

in a mechanical system. We do not live in a reversible world, that is to say, processes usually proceed in only one direction. Collectively, the directionality ascribed to physical processes is termed *entropy*.

From experience, we know that some processes satisfying the first law (conservation of energy) never occur. For instance, a piece of rock resting on the floor will never cool itself down and jump up to the ceiling, thereby converting heat energy into potential energy. The second law defines a state *directional* variable,  $S$ , called the entropy, so that for any process, the heat transferred,  $dQ$ , is given by,

$$dQ = T dS \quad (46)$$

$$dS \geq 0 \quad . \quad (47)$$

The requirement that the entropy change,  $dS$ , associated with the process must be greater than or equal to zero imparts directionality to the process, or the process is forbidden. Put another way by Kelvin, there exist no thermodynamic processes, nor transformations, that extract heat from a reservoir and convert it entirely into work. Dissipative mechanisms, such as friction and viscosity, prevent a reduction in system entropy for any process. Processes for which the entropy change is zero,

$$dS = 0 \quad , \quad (48)$$

are termed reversible, or *isentropic*, represent an idealization of physical reality. Processes in which no heat is exchanged by the system are called *adiabatic*, that is,

$$dQ = 0 \quad . \quad (49)$$

Combining the first and second laws, and considering only mechanical work,

$$dW = P dV \quad , \quad (50)$$

we see that,

$$dU = T dS - P dV \quad (51)$$

A useful quantity in engineering applications is the enthalpy change,  $dH$ , given by,

$$dH = P dV + V dP + dU \quad (52)$$

because enthalpy is often conserved ( $dH = 0$ ) in thermodynamic transitions.

Simple energy considerations applied to the steady flow of a fluid (gas or liquid) in system able to exchange heat and do external work, such as a steam engine, refrigerator, turbine, compressor, and scuba regulator, provide a simple means to relate temperature, internal energy, kinetic and potential energy, and pressure changes to external work and heat. The simple, yet powerful, relationships detailed above can be applied to air and fluid flows in diving systems, such as regulators, compressors, tanks, hoses, and gauges to yield rough estimates of pressures, temperatures, heat, and work. Actual flow patterns can be extremely complicated, requiring numerical solution on high speed computers, especially high pressure flows.

## High Pressure Equipment And Flows

Under compression-decompression, breathing gases very nearly approximate ideal gas behavior under nominal temperature and flow regimes. Much of the foregoing applies directly to the gases in high pressure cylinders and the flow through regulators and rebreathers. Consider tanks first.

### 1. Tanks

High pressure cylinders are mostly made from steel and aluminum, although prototypes of stainless steel and fiber wound composites have appeared. Carbon steel, used in early tanks, has been replaced with chrome molybdenum steel. Aluminum is alloyed with other metals, such as magnesium and titanium. Steel tanks were introduced in the late 1940s, and aluminum tanks became popular in the 1970s, though the first were imported from France in 1950. Cylinders carry compressed gases for underwater breathing, and are rated according to maximum working pressure, and the corresponding volume occupied by the breathing gas at 1 *atm*. Table 3 summarizes tank characteristics for a number of rated steel and aluminum cylinders. Steel tanks are generally heavier and exhibit negative buoyancy when filled with air. Aluminum tanks are lighter and tend to exhibit positive buoyancy before all tank air is depleted. To recover the buoyancy characteristics of steel tanks, aluminum tanks of the same size must have thicker walls, thus increasing their weight, but not their displacement.

Table 3. Cylinder Specifications.

material	volume ( <i>ft</i> <sup>3</sup> )	pressure ( <i>lbs/in</i> <sup>2</sup> )	length ( <i>in</i> )	diameter ( <i>in</i> )	weight ( <i>lbs</i> )	buoyancy ( <i>lbs</i> )
steel	15	3300	13.80	4.00	7.5	-1.30
aluminum	14	2015	16.60	4.40	5.4	3.22
aluminum	50	3000	19.00	6.90	21.5	2.25
steel	50	1980	22.50	6.80	20.8	2.43
steel	72	2475	25.00	6.80	29.5	3.48
aluminum	72	3000	26.00	6.90	28.5	3.60
aluminum	80	3000	26.40	7.25	33.3	4.00
aluminum	80	3000	27.00	7.25	34.5	4.12
steel	95	3300	25.00	7.00	39.1	-6.11

Pressures in a tank cylinder increase as temperature increases, decrease as temperature decreases. Denoting the initial pressure and temperature,  $P_0$  and  $T_0$ , and the final pressure and temperature,  $P$  and  $T$ , we have, assuming an ideal gas,

$$\frac{P_0}{T_0} = \frac{P}{T} \quad , \quad (53)$$

or,

$$P = \frac{T}{T_0} P_0 \quad , \quad (54)$$

Put another way, the change in pressure,  $\Delta P$ , satisfies,

$$\Delta P = P - P_0 = P_0 \left[ \frac{T}{T_0} - 1 \right] \quad . \quad (55)$$

The pressure change depends linearly on the temperature ratio,  $T/T_0$ , increasing or decreasing as  $T$  increases or decreases.

## 2. Regulators

Regulators, rebreathers, and compressors move gases from one reservoir to another at different pressure, and often, temperature. Regulators and rebreathers simply reduce gases at high pressure to low pressure, and compressors elevate gases at low pressure to high pressure. In both cases, gas flows involve high pressures and turbulent flows, for which steady state dynamics are a low order approximation, particularly as time scales decrease. The essence of regulator, rebreather, and compressor flow dynamics can be extracted from a simple high pressure flow model, namely, a fixed reservoir with connecting flow, treating the air as an ideal gas. In zero order, for adiabatic flow, and in the absence of shaft work and elevation changes, the flow temperature change,  $dT$ , and velocity change,  $dv$ , are related,

$$\frac{dv}{dT} = \frac{1}{v} \frac{\gamma R}{1 - \gamma} \quad , \quad (56)$$

with universal gas constant,  $R$ , and  $\gamma = 5/3$ . With this approximation for laminar flow, the volume flow rate,  $J$ , in a hose of length,  $dl$ , with cross sectional radius,  $r$ , is given by,

$$J = \frac{\pi r^4}{8\eta} \frac{dP}{dl} \quad (57)$$

for  $dP$  the pressure drop in  $dl$ , and  $\eta$  the viscosity of the fluid (gas).

## 3. Rebreathers

Crucial to the operation of rebreathers is a constant and continuous mass flow of breathing gas, subject to oxygen metabolic requirements and depth. Mass balance simply requires that the flow into the breathing bag equals the amount used by the body plus that exhaled into the breathing bag or exhalation bag. Denoting the breathing gas flow rate,  $F$ , the metabolic oxygen (consumption) rate,  $m$ , the source oxygen fraction,  $f_{O_2}$ , and inspired (breathing bag) oxygen fraction,  $i_{O_2}$ , mass balance is written,

$$f_{O_2}F = i_{O_2}F + (1 - i_{O_2})m \quad (58)$$

The source flow rate,  $F$ , and oxygen fraction,  $f_{O_2}$ , depend on nozzle and mixture. The metabolic rate,  $m$ , depends on workload, and the inspired fraction,  $i_{O_2}$ , is uniquely determined with the other three specified. Or, for requisite inspired fraction,  $i_{O_2}$ , and metabolic rate,  $m$ , the source rate,  $F$ , and oxygen source fraction,  $f_{O_2}$ , can be fixed within limits. Workload rates,  $m$ , range, 0.5 - 20.5 *l/min*, while source flows,  $F$ , depend on depth, cylinder and nozzle, with typical values, 5 - 16 *l/min*. As seen, the source oxygen fraction,  $f_{O_2}$ , is uniquely determined by the maximum depth,  $d_{max}$ , and maximum oxygen pressure (typically 1.6 - 1.4 *atm*). Always, inspired oxygen partial pressures are kept between hyperoxic and hypoxic limits, roughly, 0.16 - 1.6 *atm*. At depth,  $d$ , the source flow rate,  $F$ , decreases according to,

$$F = \frac{F_0}{1 + d/33} \quad (59)$$

for  $F_0$  the surface rate, unless the flow is depth compensated.

## Steady Flow

The most general statement about mass flow continuity takes the form,

$$\frac{\partial \rho}{\partial t} + \nabla \cdot (\rho \mathbf{v}) = 0 \quad (60)$$

for mass density,  $\rho$ , and velocity,  $\mathbf{v}$ . Certainly, within this conservation statement, a variety of turbulent and nonturbulent flow regimes are possible. Most often flows are turbulent (as seen above). For incompressible flow without circulation, the velocity field (vector),  $\mathbf{v}$ , satisfies two additional constraint equations,

$$\nabla \cdot \mathbf{v} = 0 \quad (61)$$

$$\nabla \times \mathbf{v} = 0 \quad (62)$$

the so called steady state condition. The above (with some mathematical finesse), lead to streamline results for pressure,  $p$ , density,  $\rho$ , elevation,  $z$ , and velocity,  $v$ ,

$$p + \frac{1}{2}\rho v^2 + \rho g z = \gamma \quad (63)$$

with  $g$  the acceleration of gravity, and  $\gamma$  a flow constant.

Yet, to a lower order (nonturbulent) in flow regimes, a steady state approximation to fluid flow dynamics can be stated very simply in terms of energy balances. Denoting initial and final states of a flowing fluid (gas or liquid),  $i$  and  $f$ , in a system capable of doing external work,  $W$ , and exchanging heat,  $Q$ , application of the first law yields for the differential increase of total energy,  $U$ , of the system,

$$U = Q - (W + p_f V_f - p_i V_i) \quad (64)$$

for  $p$  pressures and  $V$  volumes. Assuming that the total energy,  $U$ , of the flowing system consists of internal energy of the fluid,  $mu$ , kinetic energy,  $1/2mv^2$ , and potential energy,  $mgz$ , the balance takes the simple form,

$$Q - (W + p_f V_f - p_i V_i) = m(u_f - u_i) + \frac{1}{2}m(v_f^2 - v_i^2) + mg(z_f - z_i) \quad (65)$$

where  $z$  is the position,  $v$  is the flow speed, and  $u$  is the specific internal energy of the fluid. The representation above is also known as Bernoulli's generalized law. Its importance is well established in that it is the governing relationship for flight, that is, a pressure reduction on the top side of a wing or airfoil, relative to the pressure on the bottom side, results in hydrodynamical lift (then flight). It is also the basic governing relationship for blood flow in the arterial and venous circulation of the body.

Another example is flow through a nozzle, discussed earlier. If the work,  $W$ , and heat exchanged,  $Q$ , are zero (certainly an idealization), as in air exhausting from the valve of a scuba tank, the initial and final (exiting) flow velocities depend only on initial and final enthalpies,  $h$ , with

$$h = mu + pV \quad (66)$$

so that,

$$mv_f^2 = mv_i^2 + 2(h_i - h_f) \quad (67)$$

at the same elevation,  $z$ . More generally, the work,  $W$ , and heat exchanged,  $Q$ , are not zero, and so we see,

$$mv_f^2 = mv_i^2 + 2(h_i - h_f) + 2(Q - W) \quad (68)$$

which takes into account cooling or heating of a tank exhausting or filling a breathing mixture. Both cases assume laminar flow. In perspective, we also recall for incompressible and adiabatic fluid flow with no shaft work,

$$p_i + \frac{1}{2}\rho v_i^2 + \rho g z_i = p_f + \frac{1}{2}\rho v_f^2 + \rho g z_f = \gamma \quad (69)$$

for  $\gamma$  the *streamline* constant in phase space, and,

$$\rho = \rho_i = \rho_f \quad (70)$$

because the fluid is incompressible. Historically, such is Bernoulli's law, and follows easily from the above mass-energy conservation laws.

### Dissolved Phase Transfer

All gases dissolve in all liquids, but actual solubilities range over many orders of magnitude. Considering inert gases at room temperature, for illustration, the solubility of xenon in *n*-octane, a hydrocarbon liquid, is 470 times that of helium in water. Gas solubilities can vary much more for complex solutes and solvents. The solubility of the anesthetic gas halothane in olive oil is more than  $10^6$  times the solubility of common gases in liquid mercury. Inert gases such as helium and nitrogen are readily soluble in tissue and blood, and their solubility can fuel bubble growth with reduction in ambient pressure, a concern for decompressing divers.

Denoting the ambient partial pressure of a gas,  $p$ , and its solubility,  $S$ , in a liquid, the relative concentration of the dissolved gas component,  $c$ , is given by Henry's law,

$$c = Sp. \quad (71)$$

The corresponding *tension*, or dissolved gas partial pressure, is also  $p$  at equilibrium. By convention, partial pressures usually refer to the free gas phase, while tensions refer to the dissolved gas phase, though some folks use them interchangeably. When there exist differences, or *gradients*, between gas partial pressures and/or tensions across regions of varying concentration or solubility, gases will diffuse until partial pressures are equal, in short, move from regions of higher partial pressures to regions of lower partial pressures, regardless of the phases (free or dissolved) of the components. This movement is the crux of the decompression problem in divers and aviators, and modeling this movement is central to the formulation of decompression tables and dive computer algorithms.

Gas is driven across the tissue-blood interface by the gradient, but the rate at which bulk tissue transfers gas also depends on the blood flow rate and the degree of vascularity. Then both blood perfusion rate and gas diffusion rate contribute to the overall transfer process.

### Perfusion Controlled Transport

Exchange of dissolved tissue and blood gas, controlled by blood flow rates across regions of varying concentration or solubility, is driven by the local tissue-blood gradient, that is, the difference between the arterial blood tension,  $p_a$ , and the instantaneous tissue tension,  $p$ , assuming that blood flow rates are considerably slower than gas diffusion rates across the regions. Such behavior is modeled in time,  $t$ , by simple classes of exponential response functions, bounded by  $p_a$  and the initial value of  $p$ , denoted  $p_i$ . These multitissue functions satisfy a differential *perfusion* rate equation,

$$\frac{\partial p}{\partial t} = -\lambda (p - p_a) , \quad (72)$$

and take the form, tracking both dissolved gas buildup and elimination symmetrically,

$$p - p_a = (p_i - p_a) \exp(-\lambda t) , \quad (73)$$

$$\lambda = \frac{.6931}{\tau} , \quad (74)$$

with perfusion constant,  $\lambda$ , defined by the tissue half-time,  $\tau$ . Compartments with 2, 5, 10, 20, 40, 80, 120, 180, 240, 360, 480, and 720 minute half-times,  $\tau$ , are employed, and half-times are independent of pressure.

In a series of dives or multiple stages,  $p_i$  and  $p_a$  represent extremes for each stage, or more precisely, the initial tension and the arterial tension at the beginning of the next stage. Stages are treated sequentially, with finishing tensions at one step representing initial tensions for the next step, and so on. Exposures are controlled through critical tensions,  $M$ , such that, throughout the dive (Part 2),

$$p \leq M . \quad (75)$$

### Diffusion Controlled Transport

Exchange of dissolved tissue and blood gas, controlled by diffusion across regions of varying concentration or solubility, is also driven by the local tissue-blood gradient, but solutions to the diffusion equation control transport. In simple planar geometry, the diffusion equation can be cast,

$$D \frac{\partial^2 p}{\partial^2 x} = \frac{\partial p}{\partial t} , \quad (76)$$

with  $D$  the diffusion coefficient. As in the perfusion case, solutions depend on initial values, and also on boundary conditions. Tissue is separated into intravascular and extravascular regions for application of boundary conditions, with the tissue tension,  $p$ , equal to the arterial tension,  $p_a$ , at the tissue-blood interface. Solving and applying initial and boundary conditions, and then averaging the solutions over the spatial region, of thickness,  $l$ , there obtains,

$$p - p_a = (p_i - p_a) \frac{8}{\pi^2} \sum_{n=1}^{\infty} \frac{1}{(2n-1)^2} \exp(-\alpha_{2n-1}^2 Dt) , \quad (77)$$

with,

$$\alpha_{2n-1} = \frac{(2n-1)\pi}{l} . \quad (78)$$

A decay constant,  $\kappa$ , fitted to exposure data, is related to the diffusion coefficient,  $D$ ,

$$\kappa = \frac{\pi^2 D}{l^2} = .007928 \text{ min}^{-1} , \quad (79)$$

in the exponential expansion, and plays a similar role to  $\lambda$  in the perfusion controlled case. The diffusion expansion looks like a weighted sum of multitissue perfusion functions with decay constants,  $(2n-1)^2 \kappa$ . A diffusion equivalent halftime,  $\omega$ , is simply defined,

$$\omega = \frac{.6931}{\kappa} = 87.4 \text{ min} , \quad (80)$$

so that halftimes,  $\omega_{2n-1}$ , in the weighted expansion, are given by,

$$\omega_{2n-1} = \frac{\omega}{(2n-1)^2} . \quad (81)$$

As before,  $p_i$  and  $p_a$  represent extremes for each stage. Critical gradients,  $G$ , control diving through the constraint (Part 2),

$$p - p_a \leq G , \quad (82)$$

### Free Phase Transfer

To satisfy thermodynamic laws, bubbles in blood and tissue assume spherical shapes in the absence of external or mechanical (distortion) pressures. Bubbles entrain free gases because of a thin film, exerting surface tension pressure on the gas, of magnitude,  $2\gamma/r$ , with  $\gamma$  the Laplacian surface tension and  $r$  the bubble radius. Hydrostatic pressure balance requires that the pressure inside the bubble,  $P_t$ ,

$$P_t = \sum_{j=1}^J P_j , \quad (83)$$

with  $P_j$  bubble partial pressures of component (free) gases, exceed ambient pressure,  $P$ , by the surface tension pressure,  $2\gamma/r$ ,

$$P_t = P + \frac{2\gamma}{r} , \quad (84)$$

as seen in Figure 2. At small radii, surface tension pressure is greatest, and at large radii, surface tension pressure is least.

Gases will also diffuse into or out of a bubble according to differences in gas partial pressures inside and outside the bubble, whether in free or dissolved phases outside the bubble. In the former case, the gradient is termed *free – free*, while in the latter case, the gradient is termed *free – dissolved*. Unless the surface tension,  $\gamma$ , is identically zero, there is always a gradient tending to force gas out of the bubble, thus making the bubble collapse on itself because of surface tension pressure. If surrounding external pressures on bubbles change in time, however, bubbles may grow or contract. The flow regime is depicted in Figure 3.

Bubbles grow or contract according to the strength of the free-free or free-dissolved gradient, and it is the latter case which concerns divers under decompression. The radial rate at which bubbles grow or contract is roughly given by,

$$\frac{\partial r}{\partial t} = \frac{DS}{r}(p_t - P_t) \quad , \quad (85)$$

with  $D$  and  $S$  tissue diffusivity and solubility, and total tissue tension,  $p_t$ , the sum of component dissolved gas tensions,

$$p_t = \sum_{j=1}^J p_j \quad , \quad (86)$$

as before. A critical radius,  $r_c$ , separating growing from contracting bubbles is given by,

$$r_c = \frac{2\gamma}{p_t - P} \quad , \quad (87)$$

and bubbles with radius  $r > r_c$  will grow, while bubbles with radius  $r < r_c$  will contract. Limiting bubble growth and impact upon nerves and circulation are issues when decompressing divers and aviators. The interplay between tissue tension and bubble growth is further complicated with ascent, since ambient pressure changes in time (depending on ascent rate). Figure 4 shows the effects of bubble growth in fast and slow tissue compartments for varying ascent rate.

### *Exercises*

1. A tank initially at standard temperature and pressure,  $P_i = 1 \text{ atm}$ , and,  $T_i = 273 \text{ K}^\circ$ , is heated to  $313 \text{ K}^\circ$  by the sun. What is the pressure,  $P$ , in the tank (Part 1)?
2. The air in a dry suit at ambient sea level pressure,  $P_0 = 33 \text{ fsw}$ , occupies volume,  $V_0 = .3 \text{ ft}^3$ , at temperature,  $T = 300 \text{ K}^\circ$ . What is volume,  $V$ , occupied at depth,  $P = 50 \text{ fsw}$ , and temperature,  $T = 280 \text{ K}^\circ$  (Part 1)?
3. What volume,  $V$ , does a gmole of an ideal gas occupy at standard temperature and pressure (Part 1)?
4. Convert  $37 \text{ C}^\circ$  to Fahrenheit ( $F^\circ$ ), and then to Rankine ( $R^\circ$ ) temperatures (Part 1)? Convert  $80 \text{ F}^\circ$  to Centigrade ( $C^\circ$ ), and then to Kelvin ( $K^\circ$ ) temperatures (Part 1)?
5. A skin diver with lung volume of  $6 \text{ qt}$  descends to a depth,  $d = 85 \text{ fsw}$ . Assuming his lung tissues are  $40\%$  air space, what is his compressed lung volume,  $V$  (Part 1)?
6. Compute the specific density,  $\eta$ , of mercury ( $Hg$ ) with respect to seawater (Part 1)?
7. What is the mass,  $m$ , of  $1500 \text{ cm}^3$  of iron ( $Fe$ ) (Part 1, Table 2)? What volume,  $V$ , does  $600 \text{ g}$  of calcium ( $Ca$ ) occupy (Part 1, Table 2)? What is the gram molecular weight,  $G$ , of osmium ( $Os$ ), and density,  $\rho_{Os}$ , (Part 1, Table 2)?

8. What is the pressure of a column of seawater,  $d = 33$  fsw, now assuming density,  $\rho = 64$  lbs/ft<sup>3</sup> (Part 1)? What is the pressure of the same column of fresh water, assuming density,  $\rho = 62.4$  lbs/ft<sup>3</sup> (Part 1)?
9. A diver inflates his BC at depth,  $d = 10$  msw, to approximately .015 m<sup>3</sup>. How much work,  $dW$ , does the diver do (Part 1)?
10. A 448 lb winch gear, displacing a volume,  $V = 2$  ft<sup>3</sup>, rests on a hard sea bottom at 99 fsw. What surface volume of air,  $V_{sur}$ , is needed to inflate lift bags to bring the gear to the surface (Parts 1, 3)?
11. A buoy weighing 48 lbs occupies,  $V = 3$  ft<sup>3</sup>. What fraction,  $\xi$ , of its volume will float above water (Parts 1, 3)?
12. What is the temperature,  $T$ , of a kgmole van der Waals gas at pressure,  $P = 500$  nt/m<sup>2</sup>, and a specific volume,  $v = 2$  m<sup>3</sup>/kgmole, taking the virial coefficients,  $a = 100$  nt m/kgmole, and  $b = .03$  m<sup>3</sup>/kgmole (Part 1)?
13. What is the relative buoyancy,  $\Delta B$ , of an empty 95 ft<sup>3</sup> steel tank, rated at 3300 lbs/in<sup>2</sup> (Part 1, Table 3)? What is the approximate tank volume,  $V$  (Part 1, Table 3)? What does the tank weigh,  $w$ ?
14. A mole of air in a tank at 300 K° is released to the atmosphere and registers an average temperature drop of 30 K°. What is the mean square speed change,  $vdv$ , of the exiting gas (Part 1)? If the mean square speed change is roughly half the velocity squared of the exiting gas, what is the average velocity,  $v$  (Part 1)?
15. What is the inspired oxygen fraction,  $i_{O_2}$ , for a rebreather delivering 7.6 l/min of 50/50 nitrox to a Navy SEAL needing 1 l/min oxygen for metabolic consumption off the coast of Kuwait (Part 1)? If ambient pressure doubles, what is the nozzle flow,  $F_d$ , and inspired oxygen fraction,  $i_{O_2}$  (Part 1)?
16. What is the total pressure,  $P_t$ , inside a bubble lodged in an arteriole of diameter,  $2r = 10$  μm, if ambient pressure,  $P = 45$  fsw, and assuming a watery surface tension,  $\gamma = 50$  dyne/cm (Part 1)? For ambient pressure,  $P = 28$  fsw, what is the watery critical bubble radius,  $r_c$ , at total tissue tension,  $p_t = 20$  nt/cm<sup>2</sup> (Part 1)?
17. After 6 halftimes,  $t = 6\tau$ , what is the ratio,  $\omega$ , of tissue saturation gradient,  $(p - p_a)$ , to initial tissue saturation gradient,  $(p - p_i)$  (Part 1)?

#### Related Reading

1. Bennett P.B. and Elliot D.H., 1996, *The Physiology And Medicine Of Diving And Compressed Air Work*, London: Bailliere Tindall And Cassell.
2. Bert P., 1878, *La Pression Barometrique*, Paris: Masson.
3. Buhlmann A.A., 1984, *Decompression/Decompression Sickness*, Berlin: Springer Verlag.
4. Case K.M. and Zweifel P.F., 1977, *Linear Transport Theory*, Reading: Addison Wesley.
5. Feynman R.P., Leighton R.B., and Sands M., 1975, *The Feynman Lectures On Physics I, II, III*, Reading: Addison Wesley.
6. Guillen M., 1995, *Five Equations That Changed The World*, New York: Hyperion.

7. Hills B.A., 1977, *Decompression Sickness*, New York: John Wiley And Sons.
8. Hirschfelder J.O., Curtiss C.F., and Bird R.B., 1964, *Molecular Theory Of Gases And Liquids*, New York: John Wiley And Sons.
9. Huang K., 1973, *Statistical Mechanics*, New York: John Wiley And Sons.
10. Sears F.W., 1969, *Thermodynamics*, Reading: Addison Wesley.
11. Wienke B.R., 1998, *Physics, Physiology, And Decompression Theory For The Technical And Commercial Diver*, National Association Of Underwater Instructors Publication, Tampa.
12. Wienke B.R., 1994, *Basic Diving Physics And Application*, Flagstaff: Best.

PART 2: DECOMPRESSION THEORY  
CRITICAL TENSIONS AND PHASE VOLUMES

Critical Tensions And Decompression

Bubbles can form in tissue and blood when ambient pressure drops below tissue tensions, according to the rules of established phase mechanics. Trying to track free and dissolved gas buildup and elimination in tissue and blood, especially their interplay, is extremely complex, beyond the capabilities of even supercomputers. But safe computational prescriptions are necessary in the formulation of dive tables and digital meter algorithms. The simplest way to stage decompression, following extended exposures to high pressure with commensurate dissolved gas buildup, is to limit tissue tensions. Historically, Haldane first employed that approach, and it persists today.

To maximize the rate of uptake or elimination of dissolved gases, the *gradient*, simply the difference between  $p_i$  and  $p_a$ , is maximized by pulling the diver as close to the surface as possible. Exposures are limited by requiring that the perfusion-dominated tissue tensions,  $p$ , never exceed criticality,  $M$ , for instance, written for each tissue compartment in the US Navy approach employing 5, 10, 20, 40, 80, and 120 *minute* tissue halftimes,  $\tau$ ,

$$M = M_0 + \Delta M d \quad , \quad (1)$$

with,

$$M_0 = 152.7\tau^{-1/4} \quad , \quad (2)$$

$$\Delta M = 3.25\tau^{-1/4} \quad , \quad (3)$$

as a function of depth,  $d$ , for  $\Delta M$  the change per unit depth. Figure 1 plots the US Navy critical tensions.

Surfacing values,  $M_0$ , are principal concerns in nonstop diving, while values at depth,  $\Delta M d$ , concern decompression diving. In both cases, the staging regimen tries to pull the diver as close to the surface as possible, in as short a time as possible. By contrast, free phase (bubble) elimination gradients, as seen, *increase* with depth, directly opposite to dissolved gas elimination gradients which *decrease* with depth. In actuality, decompression is a playoff between dissolved gas buildup and free phase growth, tempered by body ability to eliminate both. But dissolved gas models cannot handle both, so there are problems when extrapolating outside tested ranges.

In absolute pressure units, the corresponding critical gradient,  $G$ , is given by,

$$G = \frac{M}{.79} - P = 1.27 M - P \quad , \quad (4)$$

with  $P$  ambient pressure, and  $M$  critical nitrogen pressure. In bubble theories, supersaturation is limited by the critical gradient,  $G$ . In decompressed gel experiments, Strauss suggested that  $G \approx 20$  *fsw* at ambient pressures less than a few atmospheres. Other studies suggest,  $14 \leq G \leq 30$  *fsw*, as a range of critical gradients ( $G$ -values).

In diffusion-dominated approaches, the tissue tension is often limited by a single, depth-dependent criterion, such as,

$$M = \frac{709 P}{P + 404} \quad , \quad (5)$$

a continuous parameterization lying between fixed gradient and multitissue schemes. The corresponding critical gradient,  $G$ , is shown in Figure 2.

Controlling Tissues

Blood rich, well perfused, aqueous tissues are usually thought to be *fast* (small  $\tau$ ), while blood poorer, scarcely-perfused, lipid tissues are thought to be *slow* (large  $\tau$ ), though the spectrum of halftimes is not correlated with actual perfusion rates in critical tissues. As reflected in relationship

above, critical parameters are obviously larger for faster tissues. The range of variation with compartment and depth is not insignificant. Fast compartments control short deep exposures, while slow compartments control long shallow, decompression, and saturation exposures.

As is well known, bounce exposures are often limited by a depth-time law of the form,

$$d t_n^{1/2} \leq C \quad , \quad (6)$$

with  $t_n$  the nonstop time limit, and  $400 \leq C \leq 500 \text{ fsw min}^{1/2}$ . For  $C = 465 \text{ fsw min}^{1/2}$ , Figure 3 depicts the depth-time relationship. One can obtain the corresponding tissue constant,  $\lambda$ , controlling the exposure at depth  $d$ , for nonstop time  $t_n$ , by differentiating the tissue equation with respect to depth,  $d$ , and setting the result to zero. With  $p_a = 0.79 (d + 33)$  at sea level, there results,

$$1 - \exp(-\lambda t_n) (1 + 2 \lambda t_n) = 0 \quad . \quad (7)$$

Corresponding critical tensions,  $M$ , are then easily obtained from the tissue equation using  $d$ ,  $\lambda$ , and  $t_n$ . In the above case, the transcendental equation is satisfied when,

$$\lambda t_n = 1.25 \quad , \quad (8)$$

thus providing a means to estimate controlling tissue half-time at depth for corresponding nonstop time limits.

#### Time Remaining

Time remaining before a stop or surfacing, time at a stop, or surface interval before flying can all be obtained by inverting the tissue equation. Taking the perfusion equation, and denoting the limiting critical tension at some desired stage (lower ambient pressure),  $M$ , the initial tension,  $p_i$ , and the instantaneous tension at that particular time,  $p$ , at stage,  $p_a$ , the limiting time,  $t$ , follows from,

$$t = \frac{1}{\lambda} \ln \left[ \frac{p_i - p_a}{p - p_a} \right] \quad (9)$$

as the inversion of the tissue equation in time.

The nonstop time limit,  $t_n$ , follows by replacing the instantaneous tension,  $p$ , with the (limiting) critical tension,  $M$ , that is,

$$t_n = \frac{1}{\lambda} \ln \left[ \frac{p_i - p_a}{M - p_a} \right] \quad (10)$$

while time remaining,  $t_r$ , at level,  $p_a$ , before ascension to new level with limiting critical tension,  $M$ , is given by,

$$t_r = \frac{1}{\lambda} \ln \left[ \frac{p - p_a}{M - p_a} \right] \quad , \quad (11)$$

with  $p$  the instantaneous tension now the initial tension. These hold for each compartment,  $\lambda$ . Across all compartments, the smallest  $t_n$  limits time at the present level when ascent is permitted, while the largest  $t_r$  prescribes wait time at the present level when ascent is not permitted. Table 1 lists compartment time limits using the critical tensions,  $M_0$ , from Figure 1 (USN) for the six compartments,  $\tau = 5, 10, 20, 40, 80,$  and  $120 \text{ min}$ , that is,  $M_0 = 104, 88, 72, 58, 52, 51 \text{ fsw}$ . Note the blank entries in the Table correspond to depths less than the critical tension, so tissue loading to that critical tension is not possible.

Table 1. Compartment Time Limits At Depth.

$\tau$ ( <i>min</i> )	5	10	20	40	80	120
$M_0$ ( <i>fsw</i> )	104	88	72	58	52	51
$d$ ( <i>fsw</i> )						
40					198	269
50				95	123	173
60			100	65	91	129
70			51	50	73	103
80		56	37	41	61	87
90		30	30	34	52	75
100	31	22	25	30	46	66
110	16	18	22	26	41	59
120	12	15	19	24	37	53
130	10	13	17	21	34	48
140	9	12	16	20	31	44
150	8	11	14	18	29	41
160	7	10	13	17	27	38
170	6	9	12	16	25	35
180	6	8	11	15	23	33
190	5	8	11	14	22	31
200	5	7	10	13	21	30

Generally, the  $t_n$  are monotonically decreasing functions of depth, while  $t_r$  are monotonically increasing functions of depth, for fixed  $M$ .

#### Saturation Curve And Separated Phase

In elegant experiments, using both animals and humans, subjects were first saturated at various pressures,  $Q$ , then decompressed to lower absolute pressures,  $P$ , and closely checked for bends development. Various values of  $Q$  and  $P$  can be determined in a controlled *titration*, that is, by holding one variable fixed and changing the other very slightly over times spans of a day, or more. In analyzing this saturation data, it is possible to draw a linear relationship, in the hyperbaric regime, separating bends from no bends for ranges of  $P$  and  $Q$ . For instance, Figure 4 portrays the linear relationship for air, the saturation curve. The line takes the form, in *fsw*,

$$Q = \zeta P + \xi \quad , \quad (12)$$

with an approximate spread over different studies, depending on statistics,

$$1.20 \leq \zeta \leq 1.40 \quad (13)$$

$$7.5 \text{ fsw} \leq \xi \leq 15.3 \text{ fsw} \quad , \quad (14)$$

and a range of ambient pressures,  $P$ ,

$$33 \text{ fsw} \leq P \leq 300 \text{ fsw} \quad . \quad (15)$$

In the hypobaric regime,  $P < 33 \text{ fsw}$ , recent studies suggest that the air saturation curve passes through the origin as ambient pressure drops, behavior predicted within phase models and discussed at length following.

Hennessy and Hempleman, and later Yount and Hoffman, established a linear titration curve for the data assuming that the same critical volume of released gas provokes mild attacks of decompression sickness. Such analyses also offer explanations for changes in signs and symptoms which follow changes in the nature of the exposure to pressure. Findings press dissolved gas approaches.

While the above titration expression is compatible with broad trends, it is clear that dissolved gas limiters, such as tensions, are often not the best critical flags. Indicators such as the volume fraction of separated gas are not only more natural, but seem to correlate more strongly with experiment. Computational algorithms, coupling phase equilibration or observed numbers of bubbles to critical volumes, offer more rational physical alternatives to the matrix of critical tensions. The critical volume hypothesis is an important development in decompression modeling, and certainly extends to breathing mixtures other than air.

#### Critical Phase Volumes

The rate at which gas inflates in tissue depends upon both excess bubble number,  $\Delta n$ , and supersaturation gradient,  $G$ . The critical volume hypothesis requires that the integral of the product of the two must always remain less than some limit point,  $\alpha V$ , with  $\alpha$  a proportionality constant. Accordingly this requires,

$$\int_0^\infty \Delta n G dt \leq \alpha V \quad , \quad (16)$$

for bubble number excess,  $\Delta n$ , an approximately linear function of excitation seed radius (difference) on compression-decompression,  $\Delta P$ ,

$$\Delta n = N\beta(r_i - r) \quad (17)$$

with  $N$ ,  $\beta$  seed constants,  $r_i$ ,  $r$  seed sizes (Part 10, Table 1), and  $V$  the limiting gas volume. Assuming that tissue gas gradients are constant during compression-decompression,  $t_d$ , while decaying exponentially to zero afterwards, and taking limiting condition of the equal sign, yields for a bounce dive,

$$\Delta n G(t_d + \lambda^{-1}) = \alpha V \quad . \quad (18)$$

For compression-decompression,  $\Delta P$ , the excitation radius,  $r$ , follows from micronuclei growth experiments in gels and tissue,

$$\frac{1}{r} = \frac{1}{r_i} + \frac{\Delta P}{\zeta} \quad (19)$$

where  $r_i$  are excitation radii at initial pressure,  $P_i$ , (Part 10, Table 1), for final pressure,  $P_f$ , so that,  $\Delta P = P_f - P_i$ , and with,  $\zeta = 158 \mu m fsw$ . At sea level, consistent fits to exposure data suggest that,  $r_i = .80 \text{ microns}$ . From the above,  $r \leq r_i$ , as,  $P_f \geq P_i$ , that is, smaller seeds grow on decompression. With all exposures, the integral must be evaluated iteratively over component decompression stages, maximizing each  $G$  while satisfying the constraint equation. In the latter case,  $t_d$  is the sum of individual stage times plus interstage ascent times, assuming the same interstage ascent speed,  $v$ . Employing the above iteratively, and one more constant,  $\delta$ , defined by,

$$\delta = \frac{\gamma_c \alpha V}{\gamma \beta r_i N} = 7500 \text{ fsw min} \quad , \quad (20)$$

we have,

$$\left[ 1 - \frac{r}{r_i} \right] G(t_d + \lambda^{-1}) = \delta \frac{\gamma}{\gamma_c} = 522.3 \text{ fsw min} \quad , \quad (21)$$

from the Spencer bounce and Tektite saturation data. A set of critical phase volume gradients,  $G$ , appears in Table 2 below, and the gradient representation,  $G$ , is of the usual form,

$$G = G_0 + \Delta G d \quad (22)$$

at depth,  $d$ .

Table 2. Critical Phase Volume Gradients.

halftime $\tau$ ( <i>min</i> )	threshold depth $\delta$ ( <i>fsw</i> )	surface gradient $G_0$ ( <i>fsw</i> )	gradient change $\Delta G$
2	190	151.0	.518
5	135	95.0	.515
10	95	67.0	.511
20	65	49.0	.506
40	40	36.0	.468
80	30	27.0	.417
120	28	24.0	.379
240	16	23.0	.329
480	12	22.0	.312

For repetitive diving, the gradients,  $G$ , above are replaced with a reduced set,  $\bar{G}$ , with the property,

$$\bar{G} \leq G \quad . \quad (23)$$

tending to reduce bottom time for repetitive activities and exposures. Because of this constraint, the approach is termed a reduced gradient bubble model. The terms,  $\Delta n G$  and  $\Delta n \bar{G}$ , differ by effective bubble elimination during the previous surface interval. To maintain the phase volume constraint during multiding, the elimination rate must be downscaled by a set of bubble growth, regeneration, and excitation factors, cumulatively designated,  $\xi$ , such that,

$$\bar{G} = \xi G \quad . \quad (24)$$

A conservative set of bounce gradients,  $G$ , can be employed for multiday and repetitive diving, provided they are reduced by  $\xi$ . Three bubble factors,  $\eta$ , reduce the driving gradients to maintain the phase volume constraint. The first bubble factor,  $\eta^{reg}$ , reduces  $G$  to account for creation of new stabilized micronuclei over time scales,  $\omega^{-1}$ , of days,

$$\eta^{reg} = \exp(-\omega t_{cum}) \quad , \quad (25)$$

$$7 \leq \omega^{-1} \leq 21 \text{ days} \quad , \quad (26)$$

for  $t_{cum}$  the cumulative (multiday) dive time. The second bubble factor,  $\eta^{exc}$ , accounts for additional micronuclei excitation on reverse profile dives,

$$\eta^{exc} = \frac{(\Delta n)_{prev}}{(\Delta n)_{pres}} = \frac{(rd)_{prev}}{(rd)_{pres}} \quad , \quad (27)$$

for excitation radius,  $r$ , at depth,  $d$ , and the subscripts referencing the *previous* and *present* dives. Obviously,  $\eta^{exc}$  remains one until a deeper point than on the previous dive is reached. The third factor,  $\eta^{rep}$ , accounts for bubble growth over repetitive exposures on time scales,  $\chi^{-1}$ , of hours,

$$\eta^{rep} = 1 - \left[ 1 - \frac{G^{bub}}{G_0 \exp(-\omega t_{cum})} \right] \exp(-\chi t_{sur}) \quad , \quad (28)$$

$$10 \leq \chi^{-1} \leq 120 \text{ minutes} \quad , \quad (29)$$

$$0.05 \leq \frac{G^{bub}}{G_0} \leq 0.90 \quad , \quad (30)$$

according to the tissue compartment, with  $t_{sur}$  the repetitive surface interval.

In terms of individual bubble factors,  $\eta$ , the multidiving fraction,  $\xi$ , is defined at the start of each segment, and deepest point of dive,

$$\xi = \eta^{reg} \eta^{rep} \eta^{exc} \quad (31)$$

with surface and cumulative surface intervals appropriate to the preceding dive segment. Since  $\eta$  are bounded by zero and one,  $\xi$  are similarly bounded by zero and one. Corresponding critical tensions,  $M$ , can be computed from the above,

$$M = \xi G + P \quad , \quad (32)$$

with  $G$  listed in Table 2 above. Both  $G$  and  $\xi$  are lower bounded by the shallow saturation data,

$$G \geq G^{bd} = .303 P + 11 \quad , \quad (33)$$

for  $P$  ambient pressure, and similarly,

$$\xi \geq \xi^{bd} = \frac{.12 + .18 \exp(-480\lambda_{bd})}{.12 + .18 \exp(-\tau\lambda_{bd})} \quad , \quad (34)$$

$$\lambda_{bd} = .0559 \text{ min}^{-1} \quad . \quad (35)$$

A set of repetitive, multiday, and excitation factors,  $\eta^{rep}$ ,  $\eta^{reg}$ , and  $\eta^{exc}$ , are drawn in Figures 5, 6, and 7, using conservative parameter values,  $\chi^{-1} = 80 \text{ min}$  and  $\omega^{-1} = 7 \text{ days}$ . Clearly, the repetitive factors,  $\eta^{rep}$ , relax to one after about 2 hours, while the multiday factors,  $\eta^{reg}$ , continue to decrease with increasing repetitive activity, though at very slow rate. Increases in  $\chi^{-1}$  (bubble elimination halftime) and  $\omega^{-1}$  (nuclei regeneration halftime) will tend to decrease  $\eta^{rep}$  and increase  $\eta^{reg}$ . Figure 5 plots  $\eta^{rep}$  as a function of surface interval in minutes for the 2, 10, 40, 120, and 720 minute tissue compartments, while Figure 6 depicts  $\eta^{reg}$  as a function of cumulative exposure in days for  $\omega^{-1} = 7, 14, \text{ and } 21 \text{ days}$ . The repetitive fractions,  $\eta^{rep}$ , restrict back to back repetitive activity considerably for short surface intervals. The multiday fractions get small as multiday activities increase continuously beyond 2 weeks. Excitation factors,  $\eta^{exc}$ , are collected in Figure 7 for exposures in the range 40-200 fsw. Deeper-than-previous excursions incur the greatest reductions in permissible gradients (smallest  $\eta^{exc}$ ) as the depth of the exposure exceeds previous maximum depth. Figure 7 depicts  $\eta^{exc}$  for various combinations of depths, using 40, 80, 120, 160, and 200 fsw as the depth of the first dive.

Considering interpolating behavior, a checklist of the properties of  $\eta$  correlating with diving practices can be drawn:

1.  $\eta$  equal one for bounce diving, remaining less than one for repetitive diving within characteristic time scales of hours;
2.  $\eta$  decrease with increasing exposure time;
3.  $\eta$  increase with increasing surface interval time;
4.  $\eta$  scale the faster tissue compartments the most;
5.  $\eta$  decrease with depths of dive segments;
6.  $\eta$  scale short surface interval repetitive and deeper than previous dives the most;
7.  $\eta$  relate to the regeneration time scales for microbubble formation, the permissible bubble excess, and a time constant characteristic of bubble inflation rate.

In repetitive applications, the set  $\eta$  impose restrictions to model parameters directly:

1. reduce permissible bubble numbers, and hence, repetitive bottom time;

2. reduce permissible gradients, and hence multiexposure time;
3. penalize deeper than previous dives;
4. impact the fastest tissues the most, and hence, deeper diving.

#### Ascent Staging

Clearly, from all of the foregoing, the dominant modes for staging diver ascents depend upon the preponderance of separated or dissolved phases in the tissues and blood, their coupling, and their relative time scales for elimination. This is (and will always be) the central consideration in staging hyperbaric or hypobaric excursions to lower ambient pressure environments. The dynamics of elimination are directly opposite, as depicted in Figure 8. To eliminate dissolved gases (the central tenet of Haldane decompression theory), the diver is brought as close as possible to the surface. To eliminate free phases (the coupled tenet of bubble decompression theory), the diver is maintained at depth to both crush bubbles and squeeze gas out by diffusion across the bubble film surface. Since both phases must be eliminated, the problem is a playoff in staging. In mathematical terms, staging is a minimax problem, and one that requires full blown dual phase models, exposure data, and some consensus of what is an acceptable level of DCI incidence.

Another transfer pathway that needs highlighting is seen in Figure 9. Many competing transfer pathways exist between tissues and blood (dissolved and free gas phases in both). The central problem of the table and meter designer is to stage ascents so that both free and dissolved phases are removed from tissues by the capillary system in optimal fashion. This is equally as difficult since we know little about the composition and susceptibility of tissue sites, blood perfusion rates, and geometries for modeling gas transfer. And even if we did, the complexity of the model and the computing power of our largest and fastest supercomputers would mitigate solutions. As seen graphically in Figure 4 (Part 1), the complexity of ascent rates, tissue tensions, and ambient pressures on bubble growth, especially with tensions and ambient pressures varying widely on ascent, is not a simply tracked quantity in diving exposures even when we know all the variables.

Attempts to track free phases within patently dissolved phase models may not optimize, but still can be mocked up for consistency with phase dynamics. One approach is to slow ascent rates and/or introduce safety stops strategically. As far as net gas exchange is concerned, most combinations of stops and rates can be equivalenced to almost any other set at given pressure, so there is always some leeway. Growth minimization and free phase elimination favor slow ascents. Figure 4 (Part 1) plots surfacing radius of an initially small bubble ( $r = .36 \text{ microns}$ ), held in both fast and slow tissue compartments, as a function of ascent rate. The results are typical for classes of bounce and repetitive diving, and underscore growth minimization with slow ascent rate due to increased ambient pressure on the average.

Based on suggestions at an American Academy Of Underwater Sciences ascent workshop, recorded by Lang and Egstrom, discretionary safety stops for 2-4 *min* in the 10-20 *fsw* zone are recommended. Calculations reported by Wienke and Lewis and summarized in Tables 3 and 4, underscore the bases of the suggestions for a number of reasons. Relative changes in three computed trigger points, tissue tension, separated phase volume, and bubble radius, are listed for six compartments following a nominal bounce dive to 120 *fsw* for 12 *min*, with and without a safety stop at 15 *fsw* for 3 *min*. Stop procedures markedly restrict bubble and phase volume growth, while permitting insignificant levels of dissolved gas buildup in the slow tissues. The reduction in growth parameters far outstrips any dissolved gas buildup in slow compartments, and faster compartments naturally eliminate dissolved gases during the stop, important for deeper diving.

Table 3. Relative Changes In Critical Parameters After Safety Stop

$\tau$ ( <i>min</i> ) halftimes	tissue tension relative change	critical volume relative change	bubble radius relative change
5	-21%	-34%	-68%
10	-11%	-24%	-39%
20	-6%	-11%	-24%
40	-2%	-8%	-18%
80	1%	3%	-2%
120	2%	4%	1%

Safety stop time can be added to bottom time for additional conservatism, but the effect of neglecting stop time is also small, as seen in Table 4. A stop at 15 *fsw* for 2 *min* is roughly equivalent to more than halving the standard ascent rate at depths in excess of 120 *fsw*. Procedures such as this, as well as reduced nonstop time limits, appear beneficial in multiday, multilevel, and repetitive diving. A safety stop near 15 *fsw* is easier than 10 *fsw* in adverse water conditions, such as surge and surface disturbances. Slower ascent rates afford additional advantages, but safety stops in the 2-4 *min* range are easier and more efficient.

Table 4. Comparative Surfacing Tissue Tensions

$\tau$ ( <i>min</i> ) halftimes	surfacing tension ( <i>fsw</i> ) 120 <i>fsw</i> /15 <i>min</i>	surfacing tension ( <i>fsw</i> ) 120 <i>fsw</i> /12 <i>min</i> 15 <i>fsw</i> /3 <i>min</i>	surfacing tension ( <i>fsw</i> ) 120 <i>fsw</i> /15 <i>min</i> 15 <i>fsw</i> /3 <i>min</i>
5	101.5	77.0	79.7
10	87.5	73.0	78.1
20	66.9	59.0	64.0
40	49.9	45.7	49.2
80	39.0	36.9	38.9
120	34.9	33.5	34.8

At altitude the same procedures can be employed, with depths, ascent rates, and stops conservatively scaled by the altitude correction factors (ratio of sea level pressure to ambient pressure at altitude) when using tables for which critical tensions need extrapolation at reduced ambient pressure. Tables with critical tensions fitted to altitude data have their own rules, as do meters.

Generally, bubble growth and excitation are compounded at altitude because of reduced pressure. Recent modeling work and experiments underscore this fact, indicating why critical tension models often fall short in hypobaric applications. Bubbles grow faster as they get bigger, and as pressure drops. With decreased pressure, bubbles will also expand by Boyle's law. Bigger bubbles are not as constricted by Laplacian film tension, while reduced pressure supports a faster rate of tissue gas diffusion into the bubble itself. Lanphier and Lehner performed extensive aerial decompression studies with goats, concluding that aerial decompression sickness strongly resembles underwater decompression sickness following saturation exposure. For ranging profiles followed by decompression to reduced ambient pressure, a high incidence of chokes was noted. Chokes is thought to result from microemboli interfering with pulmonary function. It is easy to speculate that rapid decompression to reduced pressure contributes to the buildup and growth of pulmonary emboli for the same reasons. Lanphier also concluded that slow tissue ( $\tau \geq 80$  *min*) compartments do not correlate with chokes, suggesting that pulmonary microemboli are linked to fast compartments. Clearly, such an assertion also points out differences between types of decompression sickness, inferred critical tissue halftimes, and bubble formation time scales. Chokes and limb bends result from different critical insults, at different places, and over possibly different time scales.

The point to be made here in all cases is simple. Increased offgassing pressures reduce bubble growth rates dramatically in shallow zones, while impacting dissolved gas buildup in the slowest compartments minimally. Fast compartments also offload gas during safety stops, important for repetitive diving. Stops and slow ascent rates are always advisable, but particularly following multiexposures.

### Exercises

1. What is the USN critical tension,  $M$ , in the 80 min tissue compartment at a depth,  $d = 80$  fsw (Part 2, Figure 1)? What is the critical ratio,  $R$  (Parts 2, 5)? What is the critical gradient,  $G$  (Parts 2, 5)?
2. What is the critical tension,  $M$ , at depth,  $d = 34$  fsw, for the nitrogen tissue compartment,  $\tau = 7.56$  min (Part 2)?
3. What is the instantaneous nitrogen pressure,  $p$ , in the 15 min tissue compartment of a Maine scallop diver at 67 fsw for 38 min, assuming initial sea level equilibration (Parts 2, 1)? What is the tension in the 240 min compartment (Parts 2, 1)?
4. What is the critical tension,  $M$ , at a nominal depth of 10 fsw for the 15 min tissue compartment (Parts 2, 5)? What is the corresponding critical ratio,  $R$ , (Parts 2, 5)?
5. How long does it take for the 80 min tissue compartment to approach its critical surfacing tension,  $M = M_0 = 52$  fsw, at a depth of 140 fsw, assuming initial nitrogen tension of 45 fsw (Parts 2, 1)? What is the nonstop limit,  $t_n$ , for the 80 min tissue at this depth (Parts 2, 1)?
6. If the nonstop time limit at depth,  $d = 90$  fsw, is,  $t_n = 22$  min, what is the surfacing critical tension,  $M_0$ , assuming that the 5 min compartment controls the exposure (has largest computed tissue tension at this depth) (Parts 2, 1)?
7. An oil rig diver is saturated at a depth of 300 fsw in the North Sea on heliox. For critical helium gradient (absolute),  $G = M - P = 40$  fsw, what is the minimum depth (ceiling),  $d$ , accessible to the platform diver (Parts 2, 5)?
8. For a compression-decompression,  $\Delta P = 120$  fsw, at an ambient pressure,  $P = 13$  fsw, what is the seed excitation radius,  $r$  (Part 2, Part 10, Table 1)?
9. What is the reduction factor,  $\xi$ , for a repetitive dive, after 40 min surface interval, to a depth of 80 fsw, if a first dive was to 40 fsw following 6 consecutive days of diving, using the multiday regeneration timescale of 21 days for the compartment,  $\tau = 40$  min (Part 2, Figures 5, 6, 7)? What is the bounding reduction factor,  $\xi^{bd}$ , for this compartment and exposure (Part 2)? At depth,  $d = 80$  fsw, what is the critical gradient,  $\bar{G}$ , same exposure and tissue compartment (Part 2, Table 2)?
10. Which tissues are affected most by slow ascent rates and safety stops (Part 2, Tables 3, 4)?

### Related Reading

1. Bennett P.B. and Elliot D.H., 1996, *The Physiology And Medicine Of Diving And Compressed Air Work*, London: Bailliere Tindall And Cassell.
2. Buhlmann A.A., 1984, *Decompression/Decompression Sickness*, Berlin: Springer Verlag.

3. *Hamilton R.W., 1975, Development Of Decompression Procedures For Depths In Excess Of 400 Feet, Undersea And Hyperbaric Medical Society Report, WS: 2-28-76, Bethesda.*
4. *Hills B.A., 1977, Decompression Sickness, New York: John Wiley And Sons.*
5. *Hirschfelder J.O., Curtiss C.F., and Bird R.B., 1964, Molecular Theory Of Gases And Liquids, New York: John Wiley And Sons.*
6. *Lang M.A. and Egstrom G.H., 1990, Proceedings Of The American Academy Of Underwater Sciences Biomechanics Of Safe Ascents Workshop, American Academy Of Underwater Sciences Diving Safety Publication, AAUSDSP-BSA-01-90, Costa Mesa.*
7. *Schreiner H.R. and Hamilton R.W., 1987, Validation Of Decompression Tables, Undersea And Hyperbaric Medical Society Publication 74 (VAL), Bethesda.*
8. *Sears F.W., 1969, Thermodynamics, Reading: Addison Wesley.*
9. *Wienke B.R., 1998, Physics, Physiology, And Decompression Theory For The Technical And Commercial Diver, National Association Of Underwater Instructors Publication, Tampa.*
10. *Wienke B.R., 1994, Basic Diving Physics And Application, Flagstaff: Best.*
11. *Wienke B.R., 1993, Diving Above Sea Level, Flagstaff: Best.*
12. *Wienke B.R., 1991, Basic Decompression Theory And Application, Flagstaff: Best.*

### PART 3: DECOMPRESSION THEORY ALTITUDE SIMILARITY AND PROCEDURES

#### Reduced Atmospheric Pressure

Decompression at reduced ambient pressure,  $P < 33 \text{ fsw}$ , has been a study in itself, as reported by many researchers over the years. Recall that ambient pressure,  $P_h$ , at elevation,  $h$ , in multiples of 1,000  $ft$ , is written

$$P_h = 33 \exp(-0.038h) \quad (1)$$

Studies developed separately above and below sea level, referenced as aerial and underwater decompression, also by the adjectives, hypobaric and hyperbaric. Aerial decompression differs from routine underwater decompression because the blood and tissues are equilibrated (saturated) with nitrogen ambient pressure before ascent. Breathing pure oxygen before ascent helps to protect against decompression sickness by washing out nitrogen. Up to about 18,000  $ft$ , such procedure offers a considerable degree of protection. Beyond that, silent bubbles may retard nitrogen elimination. Simple bubble mechanics suggest that bubble excitation and growth are enhanced as ambient pressure decreases, and so decompression problems are theoretically exacerbated by altitude. Nucleation theory also suggests that critical radii increase with decreasing pressure, offering larger, less stable gas seeds for possible excitation and growth into bubbles. Larger bubbles possess smaller constricting surface tensions, and will thus grow faster in conducive situations. Such facts have been verified in the laboratory, and follow from simple bubble theory. Certainly the same considerations confront the diver at altitude, and are compounded with increasing nitrogen tension upon surfacing at reduced atmospheric pressure.

#### Critical Extrapolations

Lower ambient pressures at elevation, as depicted in Figure 1, and the lesser density of fresh water in smaller degree, affect gas uptake and elimination rates in tissues and blood. If critical tensions are employed to limit exposures, an immediate question centers upon their extrapolation and testing at altitude. Looking at Figure 1 (Part 2), a linear extrapolation of the critical tensions seems obvious, indeed just such an extrapolation of the US Navy critical tensions was proposed and tested by Bell and Borgwardt. Buhlmann, employing a different set of halftimes and critical tensions, also extended the Haldane algorithm to altitudes near 10,000  $ft$ . Along with reduced critical tensions at altitude, reduced nonstop time limits, compared to sea level, are a natural consequence.

Another approach reduces critical tensions exponentially with decreasing ambient pressure. Such an extrapolation turns the curves in Figure 1 (Part 2) down through the origin at zero ambient pressure. Intuitively, an exponential extrapolation of critical tensions through the origin is more conservative than the linear extrapolation, since corresponding critical tensions for given ambient pressure are smaller, also noted by others. If the extrapolation of critical tensions is allowed to follow the same exponential decrease of ambient pressure with altitude, then the ratio of the critical tension over ambient pressure,  $R$ , remains constant. Nonstop time limits in the exponential scheme are also smaller than corresponding time limits in the linear scheme. As seen in Table 1, atmospheric pressure falls off approximately 1  $fsw$  for every 1,000  $ft$  of elevation. Exponential extrapolations of critical tensions have been tested, and serve as the operational basis of altitude procedures suggested by many others. Correlations of altitude chokes data for goats with constant ratio,  $R$ , trigger points have also been established, along with similar suggestions for the nitrogen washout data in aviators.

#### Altitude Procedures

Tables and meters designed for sea level need be conservatively modified at altitude if possible, otherwise, not employed. Decomputer and table use are best left to manufacturer and designer discretions, but in any case, modification of critical tensions is central to any Haldane altitude algorithm. We detail the similarity method, using, for example, the US Navy Tables.

Present diving schedules are based to large extent on the Haldane model discussed in the previously, constraining activities so that  $M$  or  $R$  are never compromised. An approach to altitude diving that is roughly as conservative as the tested schemes of original researchers, holds the ratios,  $R$ , constant at altitude, forcing altitude exposures to be *similar* to sea level exposures. Such similarity will force  $M$  to decrease exponentially with increasing altitude, keeping  $R$  constant with commensurate exponential reduction in the ambient pressure,  $P$ . Constant  $R$  extrapolations of this sort should be confined to nominal diving activities, certainly not heavy repetitive, decompression, nor saturation exposures.

The sought ratio constancy,  $R$ , at altitude induces a necessary scaling of actual depth to *equivalent sea level depth* (ESLD) for table entry, while all times remain unchanged. Actual depths at altitude are multiplied by factors,  $\alpha$ , called altitude correction factors, which are just the ratios of sea level atmospheric pressure to altitude atmospheric pressure, multiplied by the specific density of fresh water (0.975). Neglect of the specific density scaling is a conservative convenience, and one of minimal impact on these factors. Today, wrist altimeters facilitate rapid, precise estimation of  $\alpha$  on site. They can also be estimated from the *barometer* equation and are always greater than one. Table 1 lists correction factors at various altitudes,  $z$ , ranging to 10,000 *ft*. Up to about 7,000 *ft* elevation,  $\alpha \approx 1 + .038 h$ , with  $h$  measured in multiples of 1,000 *ft*, that is,  $z = 1000 h$ . The higher one ascends to dive, the deeper is his relative exposure in terms of equivalent sea level depth. Figure 2 contrasts correction factors scaled by the specific density of fresh water for elevations up to 18,000 *ft*. Relative increases in correction factors hasten rapidly above 10,000 *ft*. As described and seen in Table 1,  $P$  and  $\alpha$  are reciprocally related, inverses actually. Again, time is measured directly, that is, correction factors are only applied to underwater depths, ascent rates, and stops.

Table 1. Altitude Correction Factors And US Navy Altitude Groups.

altitude, or change $z$ ( <i>ft</i> )	atmospheric pressure $P_h$ ( <i>fsw</i> )	correction factor $\alpha$	penalty group on arrival at altitude	permissible group for ascension to altitude
0	33.00	1.00		
1,000	31.9	1.04	A	L
2,000	30.8	1.07	B	K
3,000	29.7	1.11	B	J
4,000	28.5	1.16	C	I
5,000	27.5	1.20	D	H
6,000	26.5	1.24	E	G
7,000	25.4	1.29	E	F
8,000	24.5	1.34	F	E
9,000	23.6	1.39	G	D
10,000	22.7	1.45	H	C

The similarity rule for altitude table modification and applying correction factors to calculations is straightforward. Convert depths at altitude to sea level equivalent depths through multiplication by  $\alpha$ . Convert all table sea level stops and ascent rates back to actual altitude through division by  $\alpha$ . Ascent rates are always less than 60 *fsw/min*, while stops are always less than at sea level. Thus, a diver at 60 *fsw* at an elevation of 5,000 *ft* uses a depth correction of 72 *fsw*, taking  $\alpha = 1.2$ . Corresponding ascent rate is 50 *fsw/min*, and a stop at 10 *fsw* at sea level translates to 8 *fsw*. A capillary gauge at altitude performs these depth calculations automatically, and on the fly, as described below. Here the 3% density difference between salt and fresh water is neglected. Neglecting the 3% density correction is conservative, because the correction decreases equivalent depth by 3%. The effect on ascent rate or stop level is not on the conservative side, but is so small that it can be neglected in calculations anyway.

If a diver has equilibrated with ambient pressure at any elevation, than any reduction in ambient pressure will put the diver in a repetitive group, merely because tissue tensions exceed ambient pressure. If the original and new pressures are specified, it is possible to estimate tissue saturation and, hence, repetitive group for the excursion. Similar comments apply to pressure reductions following any diving activity, with sea level diving the usual bill of fare. These considerations are treated as follows.

At sea level, each repetitive group represents an increment of tissue pressure over ambient ( $P_0 = 33 \text{ fsw}$ ). For the US Navy tables, this increment is  $2 \text{ fsw}$  (absolute). If we compute the difference between sea level pressure and altitude pressure, and then scale the difference by the ratio of sea level atmospheric pressure to that altitude atmospheric pressure (correction factor  $\alpha$ ), we can estimate the repetitive group in which a sea level diver finds himself following immediate ascent to altitude. These group specifications are listed in column 4 of Table 1, and represent penalty time for the excursion to altitude, Entries were computed using sea level as the baseline, but are also appropriate (conservative) for any excursion between differing elevations.

In similar fashion, excursions to higher altitude following diving are limited by tissue critical tensions, and minimal repetitive group designators can be attached to any planned excursion. For the 120 minute compartment, the surfacing critical tension (sea level) is  $51 \text{ fsw}$ . On the safer side, we take  $44 \text{ fsw}$  as the limiting tension, convert it to an absolute tension of  $60 \text{ fsw}$  ( $44/.79$ ), and then inversely scale it to altitude by the ratio of sea level pressure to altitude pressure, that is,  $\alpha$ . The resulting limiting tensions at altitude can then be converted to standard US Navy groups which are tabulated in column 5 of Table 1. Entries represent maximum permissible groups for immediate altitude excursions, and do not account for any travel time. Thus a diver would have to wait some length of time after a dive, until he dropped into the permissible group category, before ascending. The *D - group* rule for flying after diving is seen as a subcase for an altitude excursion to  $9,000 \text{ ft}$  (maximum cabin pressure). The question of altitude delay is an interesting one, a subject of recent discussions.

#### Altitude Delay Time

Time delays before altitude ascension, implicit to the permissible groups listed in the last column of Table 1, ultimately depend on the tissue compartment controlling the surface interval. In the US Navy tables, the 120 *minute* compartment controls surface intervals, and indeed Table 1 can be routinely applied to the US Navy Surface Interval Table to ascertain delay. With a 120 *minute* controlling compartment, corresponding time delays are compatible with a 12 hour rule for flying after diving. If a faster compartment is used to control surface intervals, a less conservative flying after diving rule would result, and similarly, if a slower compartment were employed, a more conservative rule would ensue.

Today, the 24 hour rule for flying after nominal diving is popular. Such a rule is more compatible with the 635 *minute* controlling compartment in Swiss tables (Buhlmann) than the 120 *minute* compartment in the US Navy tables (Workman). However, using a 635 *minute* compartment, we can still compute time delays for altitude excursions with the help of Table 1.

The calculation of permissible time for an altitude excursion following a dive, or flying after diving, amounts to determining the permissible altitude group from Table 1, the repetitive group following the dive, the standard (US Navy) surface interval to drop into the permissible altitude group, and multiplication of that surface interval by roughly 5.4. The factor of 5.4 results from replacement of the US Navy 120 *minute* compartment by the 635 *minute* compartment in the Surface Interval Table, so that intervals times are increased by roughly  $635/120$  plus rounding calculations at group boundaries. For given repetitive group and altitude excursion (change in elevation), Table 2 list minimum delay times for altitude excursions as a function of altitude and repetitive dive group. Entries are consistent with a 635 *minute* compartment controlling offgassing, and  $44 \text{ fsw}$  limiting dissolved gas buildup in that compartment.

Table 2. Altitude Delay Chart For The 24 Hour Rule.

altitude change $z$ ( $ft$ )	group								
	D	E	F	G	H	I	J	K	L
2,000	0:00	0:00	0:00	0:00	0:00	0:00	0:00	0:00	2:26
3,000	0:00	0:00	0:00	0:00	0:00	0:00	0:00	2:37	4:08
4,000	0:00	0:00	0:00	0:00	0:00	0:00	2:53	4:30	5:51
5,000	0:00	0:00	0:00	0:00	0:00	3:04	4:57	6:29	7:44
6,000	0:00	0:00	0:00	0:00	3:20	5:24	7:12	8:38	9:54
7,000	0:00	0:00	0:00	3:41	6:02	8:06	9:43	11:10	12:36
8,000	0:00	0:00	4:08	6:50	9:11	11:04	12:41	14:19	15:40
9,000	0:00	4:50	8:06	10:48	12:58	14:51	16:39	18:11	23:09
10,000	6:18	10:37	13:25	15:56	18:05	20:10	21:18	23:24	24:50

Note, in Table 2, that some 24 *hours* must elapse before the L-group diver can ascend to an altitude of 10,000 *ft*, reflecting the current 24 hour delay recommended before flying after diving.

#### Equivalent Decompression Ratios

At altitude, the formal mathematical equivalence with diving at sea level can be established through the similarity method, by first noting that the ambient pressure,  $P$ , at depth,  $d$ , is less than at sea level,

$$P = P_h + d \quad (2)$$

with atmospheric pressure,  $P_h$ , at altitude,  $h$ , depicted in Figure 1 and given by (*fsw*),

$$P_h = 33 \exp(-0.0381h) = \frac{33}{\alpha} \quad (3)$$

$$\alpha = \exp(0.0381 h) \quad (4)$$

for  $h$  in multiples of 1,000 *ft*, and then requiring that dives at altitude be equivalent to dives at sea level as far as decompression ratios,  $R$ , are concerned. Extrapolations of critical tensions, below  $P = 33$  *fsw*, must then fall off more rapidly than in the linear case, since surfacing ambient pressures decreases exponentially.

The similarity (exponential) extrapolation holds the ratio,  $R = M/P$ , constant at altitude. Denoting a *sea level equivalent depth*,  $\delta$ , at altitude,  $h$ , one has for an excursion to actual depth,  $d$ ,

$$\frac{M(d)}{d + 33\beta^{-1}} = \frac{M(\delta)}{\delta + 33} \quad (5)$$

$$\beta = \eta\alpha \quad (6)$$

so that the equality is satisfied when,

$$\delta = \beta d \quad (7)$$

$$M(\delta) = \beta M(d) \quad (8)$$

As a limit point, the similarity extrapolation should be confined to elevations below 10,000 *ft*, and neither for decompression nor heavy repetitive diving. Again, the exponential factor,  $\alpha$ , is the altitude correction factor and is plotted in Figure 2. Consequently at altitude,  $h$ , the previously defined fitted critical tensions,  $M(d)$ , are then written,

$$M_h(d) = \beta^{-1} M(\delta) = \beta^{-1} M_0 + \beta^{-1} \Delta M \delta = \beta^{-1} M_0 + \Delta M d \quad (9)$$

preserving the altitude similarity ratios as required above.

### Extended Haldane Staging

Operational consistency of Haldane table and meter algorithms is also of interest here, and part of the reason is reflected in Table 3, which contrasts surfacing critical tensions,  $M_0$ , for a number of meter algorithms. Entries were estimated (computed) from quoted meter nonstop time limits,  $t_n$ , using the 5, 10, 20, 40, 80, and 120 *min* compartments for convenience of illustration, that is to say that arbitrary  $\tau$  and  $M_0$  can be fitted to any set of nonstop time limits. Ascent and descent rates of 60 *fsw/min* were also employed in calculations. The Workman, Buhlmann, and Spencer critical surfacing tensions are fixed, while the equivalent Wienke-Yount surfacing critical tensions vary, depending on repetitive exposure. Entries are also representative of critical tensions employed in related tables.

Table 3. Table And Meter Surfacing Critical Tensions ( $M_0$ ).

halftime $\tau$ ( <i>min</i> )	Workman $M_0$ ( <i>fsw</i> )	Spencer $M_0$ ( <i>fsw</i> )	Buhlmann $M_0$ ( <i>fsw</i> )	Wienke-Yount $M_0$ ( <i>fsw</i> )
5	104	100	102	100-70
10	88	84	82	81-60
20	72	68	65	67-57
40	58	53	56	57-49
80	52	51	50	51-46
120	51	49	48	48-45

A glance at Table 3 underscores the operational consistency of classes of Haldane meter algorithms, with the Wienke-Yount approach effectively reducing critical tensions in multidiving applications as the simplest meter implementation of a dual phase model. The variation in  $M_0$  within the same compartments is relatively small. Table 4 collates the corresponding nonstop time limits,  $t_n$ , for completeness.

Table 4. Table And Meter Nonstop Time Limits ( $t_n$ ).

depth $d$ ( <i>fsw</i> )	Workman $t_n$ ( <i>min</i> )	Spencer $t_n$ ( <i>min</i> )	Buhlmann $t_n$ ( <i>min</i> )	Wienke-Yount $t_n$ ( <i>min</i> )
30		225	290	250
40	200	135	125	130
50	100	75	75	73
60	60	50	54	52
70	50	40	38	39
80	40	30	26	27
90	30	25	22	22
100	25	20	20	18
110	20	15	17	15
120	15	10	15	12
130	10	5	11	9

Variation in the nonstop limits is greater than in the critical tensions, with the US Navy set the most liberal. Using the equivalent depth approach within the similarity method, the nonstop limits in Table 4 can be extrapolated to altitude with correction factors. Figure 3 plots the Wienke-Yount nonstop time limits at various altitudes directly, using a bubble model constraint on the separated phase volume (Table 1, Part 2). Correction factors, depicted in Figure 2, are routinely employed to scale (multiply) actual depths at altitude for direct table entry. Scaled depths for table entry at altitude are always greater than actual dive depths, as discussed earlier. If correction factors are

applied to the Wienke-Yount critical tensions in Table 3, virtually the same set of nonstop limits at altitude result. This is no real surprise, since phase volume models recover Haldane predictions for short (nonstop) exposures.

Table 5 encapsulates calculations of altitude modifications using the above, gauge and meter corrections described in the following, and a set of modified US Navy Tables (Figure 1, Part 5). The exercise pulls together a number of altitude considerations for operational diving.

#### Equipment And Consumption Rate Effects

Altitude impacts diver buoyancy because of both reduced ambient pressure and density difference between salt and fresh water. Effective activities and air consumption rates, hookah and compressor output, and oxygen supply are also affected by elevation. Consider the buoyancy changes first.

Wetsuits expand and compress, while fresh water is less dense than salt water. Both affect diver and equipment buoyancy because of Archimedes' principle and Boyle's law.

#### 1. Wetsuits

Gas bubbles in wetsuits are subject to Boyle's law as external pressure changes, though the response is something less than 50% of the volume change predicted by the gas law. To estimate the buoyancy increase due to wetsuit expansion at elevation, one computes the effect using Archimedes' principle and Boyle's law directly, and then scales the result by the factor 0.50, as a figure of merit. Denoting the volume of the wetsuit on the surface at sea level,  $v_0$ , and the corresponding volume at altitude,  $v_h$ , we have by the gas law,

$$33 v_0 = P_h v_h \quad , \quad (10)$$

with  $P_h$  surface pressure at altitude. The theoretical buoyancy change (gain),  $\Delta B_{alt}$ , at altitude is given by,

$$\Delta B_{alt} = \rho(v_h - v_0) \quad , \quad (11)$$

with  $\rho$  the actual water density. Using the above gas law, it follows that,

$$\Delta B_{alt} = \rho v_0 \left[ \frac{33}{P_h} - 1 \right] \quad . \quad (12)$$

Making the assumption that the wetsuit offsets the weight belt, somewhere near 10% of diver body weight,  $w$ ,

$$\rho v_0 = .10 w \quad , \quad (13)$$

and that the expansion of the wetsuit is some 50% of maximum, we obtain,

$$\Delta B_{alt} = .050 w \left[ \frac{33}{P_h} - 1 \right] \quad . \quad (14)$$

Approximating ambient pressure at altitude,

$$P_h = \frac{33}{\alpha} \approx 33 (1 - .0381h) \quad , \quad (15)$$

$$\alpha = \exp(0.0381h) \quad , \quad (16)$$

with  $h$  the elevation in multiples of 1,000 *ft*, we find,

$$\Delta B_{alt} \approx .0017 wh \quad , \quad (17)$$

as the approximate buoyancy gain, good to few percent up to 7,000 *ft*. Figure 4 plots buoyancy increase against altitude.

## 2. Fresh And Salt Water

Application of Archimedes' principle directly to a diver submerged in fresh and salt water at sea level yields the fresh water buoyancy loss,  $\Delta B_{sea}$ . Denoting total diver plus gear weight,  $W$ , and the corresponding volume of water displaced at sea level in salt water,  $v$ , we have for neutral buoyancy,

$$W = \rho v \quad , \quad (18)$$

with  $\rho$  sea water density. The difference in buoyant forces acting upon an object of displaced volume,  $v$ , in fresh water and salt water is the buoyancy change (loss),

$$\Delta B_{sea} = \rho v(\eta - 1) = W(\eta - 1) \quad , \quad (19)$$

with  $\eta$  the fresh water *specific* density (ratio of fresh water to salt water density). Taking  $\eta = .975$ , there results,

$$\Delta B_{sea} = -.025W \quad , \quad (20)$$

with the minus sign denoting a buoyancy loss. The buoyancy loss for given diver weight is shown in Figure 5.

Capillary gauges employ pressure ratios to register depths, using a sea level ratio calibration point, while bourdon and oil filled gauges measure direct pressure and subtract off sea level atmospheric pressure to register depths. Submersible tank gauges also measure pressure directly, and subtract off atmospheric pressure. Mechanics are straightforward, as follows, taking the capillary gauge first.

### 1. Capillary Gauges

In any fluid, capillary gauge readings are dependent on the volume of compressed air in the tube. Out of the fluid, at atmospheric pressure,  $P_h$ , the volume of the tube occupied by air,  $v_{max}$ , is maximum. At actual depth,  $d$ , the volume of the tube,  $v$ , occupied by air is less (because of compression). At depth,  $d$ , the total pressure,  $P$ , is simply,

$$P = P_h + \eta d \quad , \quad (21)$$

with  $\eta$  the fluid specific density. By Boyle's law, the volumes are related,

$$(P_h + \eta d)v = P_h v_{max} \quad , \quad (22)$$

for any specific density,  $\eta$ , and any surface pressure,  $P_h$ . Capillary gauges are calibrated for sea level atmospheric pressure,  $P_0 = 33 \text{ fsw}$ , and in salt water,  $\eta = 1$ , at some depth,  $\delta$ , so that the volume ratio reduces,

$$\frac{v_{max}}{v} = \left[ \frac{33 + \delta}{33} \right] \quad . \quad (23)$$

In any other fluid, at actual depth,  $d$ , the corresponding gauge reading,  $\delta$ , can be obtained by substituting the calibration relationship into the above, and simplifying, with the result,

$$\delta = \left[ \frac{33}{P_h} \right] \eta d \quad . \quad (24)$$

For fresh water,  $\eta = .975$ , as noted, and atmospheric pressure,  $P_h$ , at elevation,  $h$ , decreases exponentially. Capillary gauge readings versus depth are plotted in Figure 6 for various altitudes.

## 2. Bourdon And Oil Filled Gauges

Other gauges measure absolute ambient pressure and mechanically subtract off surface pressure to give a reading. Thus, at depth,  $d$ , a bourdon or oil filled gauge in fluid of specific density,  $\eta$ , senses ambient pressure,  $P$ , subtracts off a constant,  $X$ , and registers a mechanical response,  $Y$ ,

$$Y = \eta d + P_h - X \quad , \quad (25)$$

If calibrated at depth,  $\delta$ , in salt water,  $\eta = 1$ , for sea level atmospheric pressure,  $P_0 = 33 \text{ fsw}$ , then,

$$Y = \delta + 33 - X \quad (26)$$

Substituting equations yields the gauge reading,  $\delta$ , in any fluid,  $\eta$ , at actual depth,  $d$ , for any surface pressure,  $P_h$ ,

$$\delta = \eta d + P_h - 33 \quad , \quad (27)$$

in analogy to a capillary gauge. Bourdon and oil filled gauge readings at elevation are plotted against actual depth in Figure 7. Mechanically, submersible pressure (tank) gauges work the same way.

## 3. Submersible Tank Gauges

Submersible gauges read tank pressure directly. Knowing the rated tank pressure,  $P_r$ , and rated gas volume,  $V_r$ , permits rapid estimation of air remaining in the tank for breathing. The rated tank pressure is the maximum recommended pressure for the tank upon filling. The rated tank volume is the amount of gas, initially at standard temperature and pressure, compressed to the rated tank pressure. For instance, the standard steel 72  $ft^3$  tank, is rated at 2475  $lbs/in^2$ , meaning that,  $V_r = 72 \text{ ft}^3$ , and that,  $P_r = 2475 \text{ lbs/in}^2$ .

From Boyle's law, we can write for any tank pressure,  $P$ , and remaining breathing volume,  $V$ , denoting the actual tank volume,  $V_t$ , and standard pressure,  $P_0$ , usually 1  $atm$ ,

$$PV_t = P_0 V \quad , \quad (28)$$

and we also know at rated pressure,  $P_r$ , and volume,  $V_r$ ,

$$P_r V_t = P_0 V_r \quad . \quad (29)$$

Dividing the above two equations yields the ratio,

$$\frac{P}{P_r} = \frac{V}{V_r} \quad , \quad (30)$$

which permits direct estimation of remaining air volume,  $V$ , for submersible gauge reading,  $P$ , and specified  $P_r$  and  $V_r$ . The ratio,  $P_r/V_r$  is called the *tank constant*, using any convenient set of units.

Regulator function exploits air compressibility to deliver air to the lungs at any ambient pressure. Filled with compressed air at ambient pressure, the lungs can function underwater in the same manner as on the surface, inflating and deflating normally. However, underwater, assuming the same metabolic consumption rate for given activity, the diver uses more air to fill the lungs than on the surface, because the air is compressed. At sea level, we consume air at a rate,  $\chi_0$ . Relative to  $\chi_0$ , the underwater rate is greater. At elevation, the surface consumption is less than  $\chi_0$ .

### 1. Activities Rate

Variation in consumption rate with ambient pressure is a gas density effect (regulator function), while variation in rate with activity is a metabolic effect (oxygen requirement). Figure 8 graphs

surface consumption rates at altitude for corresponding sea level consumption rates. Table 5 lists nominal consumption rates at sea level for various activities, in water and on land. Certainly these activities rates vary with individual, temperature, physical condition, body morphology, lung capacity, drag, mental state, metabolism, and so on.

Table 5. Activities Air Consumption Rates At Sea Level.

Land/Water Activity	Sea Level Consumption Rate $\chi_0$ ( $ft^3/min$ )
Reclining/Floating Horizontally	.6
Standing/Floating Vertically	.8
Walking/Light Treading	1.0
Jogging/Slow Swimming	1.3
Running/Moderate Swimming	1.6
Sprinting/Cold Arduous Diving	2.0

## 2. Consumption Rate

Compared to the sea level surface consumption rate, the altitude surface consumption rate is reduced by the ratio of ambient pressure to sea level pressure,  $\alpha$ . Quite obviously the surface rate at altitude, decreases inversely with elevation. Underwater rates, of course, continue to increase with pressure. Thus at depth, reductions in surface pressures at altitude have increasingly lesser effect on consumption rates, an effect also seen in wetsuit bouyancy with increasing pressure.

Denoting the altitude surface consumption rate,  $\chi_h$ , the consumption rate,  $\chi$ , at depth,  $d$ , and implied elevation,  $\alpha$ , scales directly with the pressure, that is, neglecting the 3% density difference between salt and fresh water for simplicity,

$$\chi = \chi_h \left[ 1 + \frac{d\alpha}{33} \right] . \quad (31)$$

The total pressure,  $P$ , satisfies a similar relationship in terms of surface pressure,  $P_h$ ,

$$P = P_h + d = \frac{33}{\alpha} + d = \frac{33}{\alpha} \left[ 1 + \frac{\alpha d}{33} \right] . \quad (32)$$

At any altitude, consumption rates increase rapidly with depth, offsetting reduced surface rates. The surface rate at altitude,  $\chi_h$ , is related to the surface rate at sea level,  $\chi_0$ , by the relationship,

$$\chi_h = \frac{\chi_0}{\alpha} \approx \chi_0 (1 - .038h) , \quad (33)$$

for  $h$  the usual elevation in multiples of 1,000  $ft$ . The above set of rate equations apply equally well to the output of compressors and hookah units. The result is simple, namely, altitude decreases their useful output.

### Exercises

1. What is ambient pressure,  $P_h$ , at an elevation of 6,500  $ft$  (Part 3)? What is the altitude scaling factor,  $\alpha$ , for depth, and what is the equivalent sea level depth,  $\delta$ , for actual depth,  $d = 78$   $ft$  (Part 3)?
2. If a decompression stop is required at 20  $fsw$  according to the USN Tables, what is the actual depth,  $d$ , of the stop at 6,500  $ft$  elevation (Part 3)?

3. Construct a set of critical surfacing ratios,  $R_7$ , at 7,000 ft elevation using the standard USN set,  $R_0$ , at sea level, and altitude similarity (downscaling) through the correction factor,  $\alpha$  (Parts 3, 7)?
4. At an altitude,  $z = 10,000$  ft, what is the approximate nonstop limit,  $t_n$ , for an exposure at 60 fsw (Part 3, Figure 3)? Using the similarity method, what is the nonstop time limit (Part 3, Part 7, Figure 1)?
5. A 75 kg diver journeys to a mountain lake at 1,830 m. What is the surface wetsuit buoyancy,  $\Delta w$ , increase (Part 3)?
6. What is the salt water to fresh water buoyancy loss,  $\Delta W$ , for a salvage diver plus gear of mass,  $m = 90$  kg (Part 3)?
7. A fully inflated BC displaces,  $V = .78$  ft<sup>3</sup>, of sea water. What is the lift,  $B$ , provided by the BC (Parts 3, 2)?
8. A pearl diver displaces,  $V = 3.5$  ft<sup>3</sup>, of fresh water. What is the buoyant force,  $B$ , on diver and gear (Parts 3, 2)? If diver plus gear weigh,  $W = 200$  lb, how much additional weight,  $\Delta W$ , must be added to the belt for neutral buoyancy (Parts 3, 2)?
9. The air pressure in a scuba tank drops from 2475 lbs/in<sup>2</sup> to 1500 lbs/in<sup>2</sup> in 8 min. What is the air consumption rate,  $\chi$  (Part 3)? If the tank is rated at 72 ft<sup>3</sup>, what is the consumption rate,  $\chi$ , in ft<sup>3</sup>/min (Part 3)?
10. How long,  $t$ , will a tank containing,  $V = 34$  ft<sup>3</sup>, of air last at 33 fsw for an EOD specialist swimming against a 6 knot very cold current in the ocean (Part 3, Table 5)?
11. What is the air consumption rate,  $\chi$ , at depth,  $d = 46$  ft, and elevation,  $z = 6,500$  ft, for sea level surface consumption rate,  $\chi_0 = .95$  ft<sup>3</sup>/min, in fresh water (Part 3)?
12. If a hookah unit pumps a surface rate,  $\chi_0 = 5$  ft<sup>3</sup>/min, of air ,
13. What fill rate at 9,000 ft elevation will a high speed compressor deliver if its rated output is 10 ft<sup>3</sup>/min at sea level (Part 3)?
14. At an altitude,  $z = 1,300$  m, what reading,  $\delta$ , will a capillary gauge register at actual depth,  $d = 18$  m, in fresh water (Part 3)? What does a bourdon (oil filled) gauge read,  $\delta$  (Part 3)?
15. A tank rated 80 ft<sup>3</sup> at 3000 lb/in<sup>2</sup>, registers a pressure,  $P = 1420$  lb/in<sup>2</sup> on a sub gauge. What is the remaining air volume,  $V$  (Part 3)? What is the tank constant,  $\kappa$  (Part 3)?

#### Related Reading

1. Buhlmann A.A., 1984, *Decompression/Decompression Sickness*, Berlin: Springer Verlag.
2. Hamilton R.W., 1975, *Development Of Decompression Procedures For Depths In Excess Of 400 Feet*, Undersea And Hyperbaric Medical Society Report, WS: 2-28-76, Bethesda.
3. Hills B.A., 1977, *Decompression Sickness*, New York: John Wiley And Sons.
4. Schreiner H.R. and Hamilton R.W., 1987, *Validation Of Decompression Tables*, Undersea And Hyperbaric Medical Society Publication 74 (VAL), Bethesda.
5. Sheffield P.J., 1990, *Flying After Diving*, Undersea And Hyperbaric Medical Society Publication 77 (FLYDIV), Bethesda.

6. *Smith C.L., 1975, Altitude Procedures For The Ocean Diver, National Association Of Underwater Instructors Technical Publication 5, Colton.*
7. *Somers L.H., 1991, The University Of Michigan Diving Manual, Ann Arbor: University Of Michigan Press.*
8. *Wallace D., 1975, NOAA Diving Manual, Washington DC: US Government Printing Office.*
9. *Wienke B.R., 1993, Diving Above Sea Level, Flagstaff: Best.*

Table 5. Altitude Worksheet

This Worksheet traces altitude corrections for an ocean diver journeying to higher elevation to make two dives. Embarkation altitude is 980 *ft*, and destination altitude is 4895 *ft*. The diver weighs 174 *lbs*, gear is an additional 46 *lbs*. On site, 2 *hrs* are spent preparing for the dives. With capillary gauge, the first dive is 51 *ft* for 25 *min*, followed by 3 *hrs* and 35 *min* on the surface, and the second dive to 27 *ft* for 65 *min*. After diving, the destination altitude is 10,755 *ft*.

PART 4: DECOMPRESSION THEORY  
MIXED GASES AND DECOMPRESSION

Mixtures And Biological Reactivities

Mixed breathing gases, across a spectrum of underwater activities, have been utilized successfully, mostly mixtures of nitrogen, helium, and oxygen, differing from pure air, and lately those with higher oxygen content than air (*enriched*), which can be employed efficiently in shallow diving. Non-enriched mixtures of nitrogen/oxygen (nitrox), helium/oxygen (heliox), and helium/nitrogen/oxygen (trimix), of course, have long been employed commercially in deep and saturation diving. Recently, mixtures of hydrogen/oxygen (hydrox) have also been tested. A closer look at these inert gases in a range of diving applications is illuminating, particularly gas properties, advantages and disadvantages, and interplay.

Low pressure oxygen toxicity can occur if a gas mixture with 60% oxygen is breathed at 1 *atm* for 12 *hours* or more. Pulmonary damage, irritation, and coughing are manifestations (pulmonary toxicity). High pressure oxygen toxicity can occur when breathing pure oxygen at pressures greater than 1 *atm* for periods of minutes to hours, the lower the oxygen pressure the longer the time for symptoms to develop, and vice versa, as seen in Table 1 below. Twitching, convulsions, and dizziness are the symptoms (nervous system toxicity). On the other hand, if oxygen pressures fall below .16 *atm*, unconsciousness may result. Low levels of oxygen inhibit tissue cell metabolic function (hypoxia). Confusion and difficulty in maintaining coordination are milder symptoms. Severe hypoxia requires medical attention.

Table 1. Oxygen Depth-Time Limits ( $t_x$ ).

oxygen depth $d$ ( <i>fsw</i> )	air depth $d$ ( <i>fsw</i> )	time limit $t_x$ ( <i>min</i> )
10	50	240
15	75	150
20	100	110
25	125	75
30	150	45
35	175	25
40	200	10

Clearly a constraint in mixed gas diving is the oxygen partial pressure. Inspired partial pressures of oxygen must remain below 1.6 *atm* (52.8 *fsw*) to prevent central nervous system (CNS) toxicity, and above .16 *atm* (5.3 *fsw*) to prevent hypoxia. This window, so to speak, is confining, some 1.44 *atm* (47.5 *fsw*). Denoting the mole fraction of oxygen,  $f_{O_2}$ , the upper and lower limits of this window,  $d_{max}$  and  $d_{min}$ , can be written (*fsw*),

$$\eta d_{max} = \frac{52.8}{f_{O_2}} - P_h \quad , \quad (1)$$

$$\eta d_{min} = \frac{5.3}{f_{O_2}} - P_h \quad , \quad (2)$$

$$\eta d_{max} - \eta d_{min} = \frac{47.5}{f_{O_2}} \quad , \quad (3)$$

with  $\eta$  the specific density (with respect to sea water) and with working depths,  $d$ , limited by  $d_{max}$  and  $d_{min}$ ,

$$d_{min} \leq d \leq d_{max} \quad . \quad (4)$$

For fresh water,  $\eta = .975$ , and for sea water,  $\eta = 1.000$ . Certainly up to about 7,000 *ft* elevation, the lower limit,  $d_{min}$ , is no real constraint, with the surface accessible as the limit.

Another factor inhibiting performance underwater is inert gas narcosis, particularly at increasing ambient pressure. Although the common gases nitrogen and helium associated with diving are physiologically inert under normal atmospheric conditions, they both exhibit anesthetic properties as their partial pressures increase. The mechanism is not completely understood, but impaired carbon dioxide diffusion in the lungs, increased oxygen tension, fear, and related chemical reactions have all been implicated in the past. With 80/20 mixtures, symptom onset for nitrogen is near 100 *fsw*, and very much deeper for helium, in the 1,000 *fsw* range. Symptoms range from light headedness to unconsciousness at the extreme.

Nitrogen is limited as an inert gas for diving. Increased pressures of nitrogen beyond 200 *fsw* lead to excessive euphoria, and reduced mental and physical functional ability, while beyond 600 *fsw* loss of consciousness results. Individual tolerances vary widely, often depending on activity. Symptoms can be marked at the beginning of a deep dive, gradually decreasing with time. Flow resistance and the onset of turbulence in the airways of the body increase with higher breathing gas pressure, considerably reducing ventilation with nitrogen-rich breathing mixtures during deep diving. Oxygen is also limited at depth for the usual toxicity reasons. Dives beyond 300 *fsw* requiring bottom times of hours need employ lighter, more weakly reacting, and less narcotic gases than nitrogen, and all coupled to reduced oxygen partial pressures.

#### Comparative Properties

A number of inert gas replacements have been tested, such as hydrogen, neon, argon, and helium, with only helium and hydrogen performing satisfactorily on all counts. Because it is the lightest, hydrogen has elimination speed advantages over helium, but, because of the high explosive risk in mixing hydrogen, helium has emerged as the best all-around inert gas for deep and saturation diving. Helium can be breathed for months without tissue damage. Argon is highly soluble and heavier than nitrogen, and thus a very poor choice. Neon is not much lighter than nitrogen, but is only slightly more soluble than helium. Of the five, helium is the least and argon the most narcotic inert gas under pressure.

Saturation and desaturation speeds of inert gases are inversely proportional to the square root of their atomic masses. Hydrogen will saturate and desaturate approximately 3.7 times faster than nitrogen, and helium will saturate and desaturate some 2.7 times faster than nitrogen. Differences between neon, argon, and nitrogen are not significant for diving. Comparative properties for hydrogen, helium, neon, nitrogen, argon, and oxygen are listed in Table 2. Solubilities,  $S$ , are quoted in  $atm^{-1}$ , weights,  $A$ , in *atomic mass units (amu)*, and relative narcotic potencies,  $\nu$ , are dimensionless (referenced to nitrogen in observed effect). The least potent gases have the highest index,  $\nu$ .

Table 2. Inert Gas And Oxygen Molecular Weights, Solubilities, and Narcotic Potency.

	$H_2$	$He$	$Ne$	$N_2$	$Ar$	$O_2$
$A$ ( <i>amu</i> )	2.02	4.00	20.18	28.02	39.44	32.00
$S$ ( $atm^{-1}$ )						
blood	.0149	.0087	.0093	.0122	.0260	.0241
oil	.0502	.0150	.0199	.0670	.1480	.1220
$\nu$	1.83	4.26	3.58	1.00	0.43	

The size of bubbles formed with various inert gases depends upon the amount of gas dissolved, and hence the solubilities. Higher gas solubilities promote bigger bubbles. Thus, helium is preferable to hydrogen as a light gas, while nitrogen is preferable to argon as a heavy gas. Neon solubility

roughly equals nitrogen solubility. Narcotic potency correlates with lipid (fatty tissue) solubility, with the least narcotic gases the least soluble. Different uptake and elimination speeds suggest optimal means for reducing decompression time using helium and nitrogen mixtures. Following deep dives beyond 300 *fsw* breathing helium, switching to nitrogen is without risk, while helium elimination is accelerated because the helium tissue-blood gradient is increased when breathing an air mixture. By gradually increasing the oxygen content after substituting nitrogen for helium, the nitrogen uptake can also be kept low. Workable combinations of gas switching depend upon the exposure and the tissue compartment controlling the ascent.

Mixed gas diving dates back to the mid 1940s, but proof of principle diving experiments were carried out in the late 50s. In 1945, Zetterstrom dove to 500 *fsw* using hydrox and nitrox as a travel mix, but died of hypoxia and DCI when a tender hoisted him to the surface too soon. In 1959, Keller and Buhlmann devised a heliox schedule to 730 *fsw* with only 45 *min* of decompression. Then, in 1962, Keller and Small bounced to 1,000 *fsw*, but lost consciousness on the way up due to platform support errors. Small and another support diver, Whittaker, died as a result. In 1965, Workman published decompression tables for nitrox and heliox, with the nitrox version evolving into USN Tables. At Duke University Medical Center, the 3 man team of Atlantis III made a record chamber dive to 2250 *fsw* on heliox, and Bennett found that 10% nitrogen added to the heliox eliminated high pressure nervous syndrome (HPNS). In deep saturation diving, *normoxic* breathing mixtures of gases are often advantageously employed to address oxygen concerns. A normoxic breathing mixture, helium or nitrogen, reduces the oxygen percentage so that the partial pressure of oxygen at the working depth is the same as at sea level, the obvious concerns, again, hypoxia and toxicity. Critical tensions can be employed in helium saturation diving in much the same fashion as nitrogen diving. A critical tension, recall, is the maximum permissible value of inert gas tension ( $M$ -value) for a hypothetical tissue compartment with specified halftime. An approach to helium exchange in tissue compartments employs the usual nitrogen set with halftimes reduced by 2.7, that is, the helium halftimes are extracted from the nitrogen halftimes following division by 2.7, and the same critical tension is assumed for both gas compartments. Researchers have tested schedules based on just such an approach. Tissue tensions scale as the relative proportion of inert gas in any mixture. More so than in air diving, computational methods for mixed gas diving and decompression are often proprietary information in the commercial sector.

Helium (normal 80/20 mixture) nonstop time limits are shorter than nitrogen, but follow a  $t^{1/2}$  law similar to nitrogen, that is, depth times the square root of the nonstop time limit is approximately constant. Using standard techniques of extracting critical tensions from the nonstop time limits, fast compartment critical tensions can be assigned for applications. Modern bubble models, such as the varying permeability model, have also been used strategically in helium diving.

Today, the three helium and nitrogen mixtures (nitrox, heliox, trimix) are employed for deep and saturation diving, with a tendency towards usage of enriched oxygen mixtures in shallow (recreational) diving. The use of enriched oxygen mixtures by recreational divers is the subject of controversy, aptly a concern over diver safety. Breathing mixture purity, accurate assessment of component gas ratios, oxygen toxicity, and appropriate decompression procedures are valid concerns for the mixed gas diver. Care, in the use of breathing mixtures, is to be underscored. Too little, or too much, oxygen can be disastrous. The fourth hydrogen mixture (hydrox) is much less commonplace.

#### Nitrox

Mixtures of oxygen and nitrogen with less oxygen than 21% (pure air) offer protection from oxygen toxicity in moderately deep and saturation diving. Moderately deep here means no more than a few hundred feet. Hypoxia is a concern with mixtures containing as much as 15% oxygen in this range. Saturation diving on oxygen-scarce nitrox mixtures is a carefully planned exposure. The narcotic effects of nitrogen in the 100 *fsw* to 200 *fsw* depth range mitigate against nitrox for deep diving.

Diving on enriched air mixtures need be carefully planned exposures, but for opposite reason, that

is, oxygen toxicity. Mixtures of 30% more of oxygen significantly reduce partial pressures of nitrogen to the point of down loading tissue tensions compared to air diving. If standard air decompression procedures are employed, nitrox affords a diving safety margin. However, because of elevated oxygen partial pressures, a maximum permissible depth (floor) needs be assigned to any enriched oxygen mixture. Taking 1.6 *atm* (52.8 *fsw*) as the oxygen partial pressure limit, the floor for any mixture is easily computed. Enriched nitrox with 32% oxygen is floored at a depth of 130 *fsw* for diving, also called the oxygen limit point. Higher enrichments raise that floor proportionately.

Decompression requirements on nitrox are less stringent than air, simply because the nitrogen content is reduced below 79%. Many equivalent means to schedule nitrox diving exist, based on the standard Haldane critical tension approach. Air critical tensions can be employed with exponential buildup and elimination equations tracking the (reduced) nitrogen tissue gas exchange, or equivalent air depths (always less than the actual depths on nitrox) can be used with air tables. The latter procedure ultimately relates inspired nitrogen pressure on a nitrox mixture to that of air at shallower depth (equivalent air depth). For instance, a 74/26 nitrox mixture at a depth of 140 *fsw* has an equivalent air depth of 130 *fsw* for table entry. Closed breathing circuit divers have employed the equivalent air depth approach (discussed shortly) for many years.

### Heliox

The narcotic effects of nitrogen in the several hundred feet range prompted researchers to find a less reactive breathing gas for deeper diving. Tests, correlating narcotic effects and lipid solubility, affirm helium as the least narcotic of breathing gases, some 4 times less narcotic than nitrogen according to Bennett, and as summarized in Table 2. Deep saturation and extended habitat diving, conducted at depths of 1,000 *ft* or more on helium/oxygen mixtures by the US Navy, ultimately ushered in the era of heliox diving. For very deep and saturation diving above 700 *fsw* or so, heliox remains a popular, though expensive, breathing mixture.

Helium uptake and elimination can also be tracked with the standard Haldane exponential expressions employed for nitrogen, but with a notable exception. Corresponding helium halftimes are some 2.7 times faster than nitrogen for the same hypothetical tissue compartment. Thus, at saturation, a 180 *minute* helium compartment behaves like a 480 *minute* nitrogen compartment. All the computational machinery in place for nitrogen diving can be ported over to helium nicely, with the 2.7 scaling of halftimes expedient in fitting most helium data.

When diving on heliox, particularly for deep and long exposures, it is advantageous to switch to nitrox on ascent to optimize decompression time, as discussed earlier. The higher the helium saturation in the slow tissue compartments, the later the change to a nitrogen breathing environment. Progressive increases of nitrogen partial pressure enhance helium washout, but also minimize nitrogen absorption in those same compartments. Similarly, progressive increases in oxygen partial pressures aid washout of all inert gases, while also addressing concerns of hypoxia.

An amusing problem in helium breathing environments is the high-pitched voice change, often requiring electronic voice encoding to facilitate diver communication. Helium is also very penetrating, often damaging vacuum tubes, gauges, and electronic components not usually affected by nitrogen. Though helium remains a choice for deep diving, some nitrogen facilitates decompression, ameliorates the voice problem, and helps to keep the diver warm. Pure helium, however, can be an asphyxiant.

### Trimix

Diving much below 1400 *fsw* on heliox is not only impractical, but also marginally hazardous. High pressure nervous syndrome (HPNS) is a major problem on descent in very deep diving, and is quite complex. The addition of nitrogen to helium breathing mixtures (trimix), is beneficial in ameliorating HPNS. Trimix is a useful breathing mixture at depths ranging from 500 *fsw* to 2,000 *fsw*, with nitrogen percentages usually below 10% in operational diving, because of narcotic effect.

Decompression concerns on trimix can be addressed with traditional techniques. Uptake and elimination of both helium and nitrogen can be limited by critical tensions. Using a basic set of nitrogen halftimes and critical tensions, and a corresponding set of helium halftimes approximately

3 times faster for the same nitrogen compartment, total inert gas uptake and elimination can be assumed to be the sum of fractional nitrogen and helium in the trimix breathing medium, using the usual exponential expressions for each inert gas component. Such approaches to trimix decompression were tested by researchers years ago, and many others after them.

#### Hydrox

Since hydrogen is the lightest of gases, it is reasonably expected to offer the lowest breathing resistance in a smooth flow system, promoting rapid transfer of oxygen and carbon dioxide within the lungs at depth. Considering solubility and diffusivity, nitrogen uptake and elimination rates in blood and tissue should be more rapid than nitrogen, and even helium. In actuality, the performance of hydrogen falls between nitrogen and helium as an inert breathing gas for diving.

Despite any potential advantages of hydrogen/oxygen breathing mixtures, users have been discouraged from experimenting with hydrox because of the explosive and flammable nature of most mixtures. Work in the early 1950s by the Bureau of Mines, however, established that oxygen percentages below the 3%-4% level provide a safety margin against explosive and flammability risks. A 97/3 mixture of hydrogen and oxygen could be utilized at depths as shallow as 200 *fsw*, where oxygen partial pressure equals sea level partial pressure. Experiments with mice also indicate that the narcotic potency of hydrogen is less than nitrogen, but greater than helium. Unlike helium, hydrogen is also relatively plentiful, and inexpensive.

#### Haldane Decompression Procedures

In the case of mixtures of gases (nitrogen, helium, hydrogen), the Haldane decompression procedures (Parts 1 and 2) can be generalized in a straightforward manner, using a set of nitrogen critical tensions,  $M$ , and halftimes,  $\tau$ , as the bases. Denoting gas species,  $j = N_2, He, H_2$ , atomic masses,  $A_j$ , and partial pressures,  $p_j$ , each component satisfies a Haldane tissue equation, with rate modified coefficient,  $\lambda_j$ , given by,

$$p_j - p_{aj} = (p_{ij} - p_{aj}) \exp(-\lambda_j t) \quad , \quad (5)$$

for  $p_{aj}$  and  $p_{ij}$  ambient and initial partial pressures of the  $j^{th}$  species, and with decay constant,  $\lambda_j$ , related by Graham's law to the nitrogen coefficient,  $\lambda_{N_2} = \lambda$ , by,

$$\lambda_j = \left[ \frac{A_{N_2}}{A_j} \right]^{1/2} \lambda \quad . \quad (6)$$

Thus, for instance, one has,

$$\lambda_{He} = 2.7 \lambda \quad , \quad (7)$$

$$\lambda_{H_2} = 3.7 \lambda \quad . \quad (8)$$

In a mixture, the total tension,  $\Pi$ , is the sum of all  $J$  partial tensions,  $p_j$ ,

$$\Pi = \sum_{j=1}^J [ p_{aj} + (p_{ij} - p_{aj}) \exp(-\lambda_j t) ] \quad (9)$$

and the decompression requirement is simply,

$$\Pi = \sum_{j=1}^J p_j \leq M \quad , \quad (10)$$

for all exposures. Denoting ambient partial pressures,  $p_{aj}$ , as a fraction,  $f_j$ , of total pressure,  $P$ , that is,

$$p_{aj} = f_j P \quad , \quad (11)$$

it follows that,

$$f_{O_2} + \sum_{j=1}^J f_j = 1 \quad (12)$$

neglecting any carbon dioxide or water vapor in the mixture, of course. For 75/25 (enriched) nitrox,  $f_{N_2} = .75$ , for 90/10 heliox,  $f_{He} = .90$ , for 75/10/15 trimix,  $f_{He} = .75$ ,  $f_{N_2} = .10$ , while for 95/5 hydrox,  $f_{H_2} = .95$ . For pure air obviously  $f_{N_2} = 0.79$ , as the common case. Clearly the treatment of breathing mixtures assumes a single critical tension,  $M$ , for each compartment,  $\tau$ , in this case, extracted from the nitrogen data.

With nitrox ( $f_{N_2} < .79$ ), it is clear that the nitrogen decompression requirements are reduced when using the same set of  $M$ , that is, the air set of  $M$  are assumed to apply equally to both air and other nitrogen mixtures. The procedure has been applied to heliox, trimix, and hydrox mixtures in similar vein. One important constraint in any mixture is the oxygen content. Partial pressures of oxygen must be kept below 52.8 *fsw* (1.6 *atm*) to prevent toxicity, and above 5.3 *fsw* (.16 *atm*) to prevent hypoxia. Balancing diver mobility within this window at increasing depth is a delicate procedure at times.

#### Equivalent Air Depth

In extending air tables to other breathing mixtures, an extrapolation based on critical tensions is the crux of the *equivalent air depth* (EAD) method. The equivalent air depth method for table use derives from the imposed equality of mixture and inert gas partial pressures, and is very similar to the altitude equivalent depth method, but is not the same. For instance, with nitrox mixtures, the usual case, the equivalent air depth,  $\delta$ , is related to the effective depth,  $d$ , by requiring equality of nitrogen partial pressures for air and nitrogen mixture with mole fraction  $f_{N_2}$ ,

$$\delta = \frac{f_{N_2}}{.79}(P_h + d) - P_h. \quad (13)$$

At altitude, the effective depth,  $d$ , is the equivalent sea level depth described earlier. At sea level, the actual depth and effective depth are the same.

With enriched mixtures ( $f_{N_2} < .79$ ), it is clear that the equivalent air depth,  $\delta$ , is less than the effective depth,  $d$ , so that nitrogen decompression requirements are reduced when using  $\delta$  to enter any set of air tables. Obviously, the same set of  $M$  are assumed to apply equally to both air and other mixture in the approach. At sea level, the above reduces to the form,

$$\delta = \frac{f_{N_2}}{.79}(33 + d) - 33 \text{ fsw}, \quad (14)$$

with  $d$  the actual depth, and has been utilized extensively in ocean diving.

The same procedure can be applied to arbitrary heliox, trimix, and hydrox mixtures in theory, basically an extrapolation from a reference (standard) table with the same gas components (helium, nitrogen, or hydrogen with oxygen). Denoting gas molar fractions in the standard (table) mixture,  $f_{s,k}$ , with  $k = N_2, He, H_2, O_2$ , and molar fractions in the arbitrary mixture,  $f_k$ , we have for a  $K$  component mixture,

$$\delta = \frac{(1 - f_{O_2})}{(1 - f_{s,O_2})}(P_h + d) - P_h \quad (15)$$

using mixture balance,

$$\sum_{k=1}^K f_k = 1 - f_{O_2} \quad (16)$$

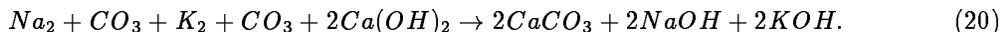
$$\sum_{k=1}^K f_{s,k} = 1 - f_{s,O_2} \quad (17)$$

This approach yields the *equivalent mixture depth* (EMD). Both EAD and EMD are applied at altitude after the ESLD correction.

### Oxygen Rebreathing

As early as 1880, Fleuss developed and tested the first closed circuit, oxygen rebreathing system. At that time, of course, oxygen toxicity was not completely understood, though the effects of breathing pure oxygen were coupled to excitability and fever. In ensuing years, the apparatus was refined considerably, and was used by underwater combatants in World War II. During the 1950s, recreational divers used oxygen rebreathers. However, by the late 1950s, recreational divers switched to the popular open circuit device developed by Cousteau and Gagnan, thereby trading oxygen toxicity and caustic carbon dioxide concerns for decompression sickness and nitrogen narcosis. Today, rebreathers are witnessing a rebirth among technical divers. And, US Navy Underwater Demolition (UDT) and Sea Air Land (SEAL) Teams have continuously employed rebreathers for tactical operations.

In closed circuit systems, exhaled gas is kept in the apparatus, scrubbed of carbon dioxide by chemical absorbents, and then returned to the diver. No gas is released into the water (no bubbles). Gas consumption is related only to the physiological consumption of oxygen. Only a small amount of oxygen is required for extended exposures. Oxygen is taken directly from a breathing bag, and exhaled gas passes separately through an alkaline, absorbent material, where it is scrubbed of carbon dioxide. A typical reduction process involves water vapor, sodium and potassium hydroxide, and carbon dioxide in the reaction chain,



Rebreathers today last about 3 *hr*, using approximately 6 *m*<sup>3</sup> of oxygen and 4 *lbs* of absorbent. Because of oxygen toxicity, depth is a limitation for oxygen rebreathing. Depth limitation for pure oxygen rebreathing is near 20 *fsw*. Today, closed circuit mixed gas rebreathers blend inert gases with oxygen (lowering oxygen partial pressure) to extend depth limitations. Two cylinders, one oxygen and the other inert gas (or a premixed cylinder), are employed, and the mixture is scrubbed of carbon dioxide before return to the breathing bag.

Closed circuit oxygen scuba takes advantage of gas conservation, but is limited in dive depth and duration by oxygen toxicity effects. Open circuit scuba offers greater depth flexibility, but is limited in depth and duration by the inefficiency of gas utilization. To bridge this gap, semi-closed circuit mixed gas rebreathers were developed. The semi-closed circuit rebreather operates much like the closed circuit rebreather, but requires a continuous, or frequent, purge to prevent toxic inert gas buildup. Two cylinders of oxygen and inert gas (or one premixed), are charged with safe levels of both, usually corresponding to safe oxygen partial pressure at the maximum operating depth. Gas flow from the high pressure cylinders the breathing circuit is controlled by a regulator and nozzle, admitting a continuous and constant mass flow of gas determined by oxygen consumption requirements. The diver inhales the mixture from the breathing bag and exhales it into the exhalation bag. Pressure in the exhalation bag forces the gas mixture through the carbon dioxide scrubber, and from the scrubber back into the breathing bag for diver consumption. When gas pressure in the breathing circuit reaches a preset limit, a relief valve opens in the exhalation bag, purging excess gas into the water.

Oxygen rebreathing at high partial pressures can lead to central nervous system (or pulmonary) oxygen poisoning. It is thought that high pressure oxygen increases the production of oxygen free radicals disrupting cell function. The US Navy conducted research into safe depths and durations for oxygen diving, and concluded that there is very little risk of central nervous system oxygen toxicity

when partial pressures of oxygen are maintained below 1.6 *atm*. Additionally, risk only increases slightly when oxygen partial pressures are maintained below 1.8 *atm*.

#### Isobaric Countertransport

Isobaric countertransport simply denotes isobaric diffusion of two gases in opposite directions. Perhaps a better descriptor is countercurrent diffusion. Historically, both terms have been used, with the former mostly employed in the decompression arena. Countertransport processes are a concern in mixed gas diving, when differing gas solubilities and diffusion coefficients provide a means for multiple inert gases to move in opposite directions under facilitating gradients. While ambient pressure remains constant, such counterdiffusion currents can temporarily induce high tissue gas supersaturation levels, and greater susceptibility to bubble formation and DCI. In general, problems can be avoided when diving by employing light to heavy (breathing) gas mixture switches, and by using more slowly diffusing gases than the breathing mixture inside enclosure suits (drysuits). Such procedure promotes *isobaric desaturation*, as termed in the lore. The opposite, switching from heavy to light gas mixtures and using more rapidly diffusing gases than the breathing mixture inside exposure suits, promotes *isobaric saturation* and enhanced susceptibility to bubble formation. More simply, the former procedure reduces gas loading, while the latter increases gas loading. The effects of gas switching can be dramatic, as is well known. For instance, a dive to 130 *fsw* for 120 *min* on 80/20 heliox with a switch to 80/20 nitrox at 60 *fws* requires 15 *min* of decompression time, while 210 *min* is required without the switch (Keller and Buhlmann in famous mixed gas tests in 1965). Yet, skin lesions and vestibular dysfunctionality have developed in divers breathing nitrogen while immersed in helium (test chambers and exposure suits). And nitrogen-to-helium breathing mixture switches are seldom recommended for diving. A closer look at the isobaric countertransport phenomenon is interesting.

In the perfusion case, for a mixture of  $J$  gases, the total tissue tension,  $\Pi$ , at time,  $t$ , for ambient partial pressure,  $p_{aj}$ , and initial partial pressure,  $p_{ij}$ , with  $j$  denoting the gas species, can be written,

$$\Pi = \sum_{j=1}^J [ p_{aj} + (p_{ij} - p_{aj}) \exp(-\lambda_j t) ] \quad (21)$$

for, as usual,

$$\lambda_j = \frac{.693}{\tau_j} \quad (22)$$

and  $\tau_j$  the tissue half-time. In the diffusion case, we similarly find

$$\Pi = \sum_{j=1}^J \left[ p_{aj} + (p_{ij} - p_{aj}) \frac{8}{\pi^2} \sum_{n=1}^{\infty} \frac{1}{(2n-1)^2} \exp(-\alpha_{2n-1}^2 D_j t) \right] \quad (23)$$

with,

$$\alpha_{2n-1} = \frac{(2n-1)\pi}{l} \quad (24)$$

for  $l$  a characteristic tissue scale parameter, and  $D_j$  the tissue diffusivity. These two expressions accommodate a multiplicity of initial conditions, gas switches, and provide a platform to discuss isobaric counterprocesses.

The form of the perfusion and diffusion total tensions,  $\Pi$ , is very similar. In fact, if we assume that the first term in the diffusion case dominates, we can write in general,

$$\Pi = \sum_{j=1}^J [ p_{aj} + (p_{ij} - p_{aj}) \exp(-\kappa_j t) ] \quad (25)$$

with, in the perfusion limit,

$$\kappa_j = \lambda_j \quad (26)$$

and, in the diffusion limit, taking just the first term ( $n = 1$ ),

$$\kappa_j = \alpha_1^2 D_j = \frac{\pi^2 D_j}{l^2} \quad (27)$$

Simplifying matters by taking the case for two gases,  $J = 2$ , we have,

$$\Pi = (p_{a1} + p_{a2}) + (p_{i1} - p_{a1}) \exp(-\kappa_1 t) + (p_{i2} - p_{a2}) \exp(-\kappa_2 t) \quad (28)$$

for total tension,  $\Pi$ , as a function of individual gas initial tensions, time, and ambient partial pressures.

A local maxima or minima occurs in the total tension,  $\Pi$ , whenever,

$$\frac{\partial \Pi}{\partial t} = -\kappa_1 (p_{i1} - p_{a1}) \exp(-\kappa_1 t) - \kappa_2 (p_{i2} - p_{a2}) \exp(-\kappa_2 t) = 0 \quad (29)$$

for constant ambient partial pressures,  $p_a$ . Or, equivalently written,

$$\frac{(p_{i1} - p_{a1})}{(p_{a2} - p_{i2})} = \frac{\kappa_2}{\kappa_1} \exp[(\kappa_1 - \kappa_2)t] \quad (30)$$

The equation is satisfied at a time,  $t_m$ , such that,

$$t_m = \frac{1}{(\kappa_1 - \kappa_2)} \ln \left[ \frac{\kappa_2 (p_{i2} - p_{a2})}{\kappa_1 (p_{i1} - p_{a1})} \right] \quad (31)$$

and represents a local maxima in total tension,  $\Pi$ , if (after some algebra),

$$\left[ \frac{\partial^2 \Pi}{\partial t^2} \right]_{t=t_m} < 0 \quad (32)$$

or, a local minima, if,

$$\left[ \frac{\partial^2 \Pi}{\partial t^2} \right]_{t=t_m} > 0 \quad (33)$$

Some interesting features of isobaric counterdiffusion are imbedded in the above relationships, such as flow directionality, time scales, effects of switching, light versus heavy gases, and isobaric supersaturation or desaturation.

With positive time,  $t_m > 0$ , only two conditions are permissible:

$$\frac{\kappa_1 (p_{i1} - p_{a1})}{\kappa_2 (p_{a2} - p_{i2})} > 1 \quad , \quad \kappa_1 > \kappa_2 \quad (34)$$

or,

$$\frac{\kappa_1 (p_{i1} - p_{a1})}{\kappa_2 (p_{a2} - p_{i2})} < 1 \quad , \quad \kappa_1 < \kappa_2 \quad (35)$$

and the argument of the log function must be greater than zero always. The above relationships are complex functions of diffusivities, initial tensions, and ambient tensions before and after gas switching. The former case,  $\kappa_1 > \kappa_2$ , represents light-to-heavy gas switching (helium-to-nitrogen, for instance, where  $\kappa_{He} = 2.7\kappa_{N_2}$ ), facilitating rapid desaturation of the lighter gas before heavier gas buildup. The latter case,  $\kappa_1 < \kappa_2$ , enhances supersaturation, as the lighter gas builds up rapidly before the heavier gas is eliminated.

Figure 1 tracks gas supersaturation following nitrogen-to-helium switching due to the isobaric counterdiffusion of both gases. For helium-to-nitrogen switching (usual case for technical and commercial divers), a state of gas desaturation would ensue due to isobaric counterdiffusion.

## Oxygen Dose

Decompression sickness could be avoided by breathing just pure oxygen. And the usage of higher concentrations of oxygen in breathing mixtures not only facilitates metabolic function, but also aids in the washout of inert gases such as nitrogen and helium. Despite the beneficial effects of breathing oxygen at higher concentrations, oxygen proves to be toxic in excessive amounts, and over cumulative time intervals. Too little oxygen is equally detrimental to the diver. As discussed, limits to oxygen partial pressures in breathing mixtures range,  $0.16 \text{ atm}$  to  $1.6 \text{ atm}$ , roughly, but symptoms of hypoxia and hyperoxia are dose dependent. Or, in other words, symptom occurrences depend on oxygen partial pressures and exposure times, just like inert gas decompression sickness. The mixed gas diver needs to pay attention not only to helium and nitrogen in staged decompression, but also cumulative oxygen exposure over the dive, and possible underexposure on oxygen depleted breathing mixtures.

The neurotoxic actions of high pressure oxygen are thought to relate directly to biochemical oxidation of enzymes, either those linked to membrane permeability or metabolic pathways. The list below is not exhaustive, but includes the following mechanisms:

1. the inability of blood to remove carbon dioxide from tissue when hemoglobin is oxygen saturated;
2. inhibition of enzymes and coenzymes by lipid peroxides;
3. increased concentration of chemical free radicals which attack cells:
4. oxidation of membranes and structural deterioration reducing electrical permeability for neuron activation:
5. direct oxygen attack on smooth muscle fibres;
6. oxygen induced vasoconstriction in arterioles;
7. elevation of brain temperature due to lack of replacement of oxygen by carbon dioxide in hemoglobin;
8. and, simple chemical kinetic redistribution of cellular carbon dioxide and oxygen with high surrounding oxygen tensions.

Fortunately for the diver, there are ways to avoid complications of hyperoxia. Careful attention to dose (depth-time) limitations for oxygen exposures is needed.

Despite the multiplicity and complexity of the above, limits for safe oxygen exposure are reasonably defined. Table 3 below lists NOAA oxygen exposure time limits,  $t_x$ , for corresponding oxygen partial pressures,  $p_{O_2}$ . Below  $0.5 \text{ atm}$ , oxygen toxicity is not really a problem.

Table 3. Oxygen Dose-Time Limits

oxygen partial pressure $p_{O_2}$ ( <i>atm</i> )	oxygen time limit $t_x$ ( <i>min</i> )	oxygen tolerance (OTU) $\Upsilon$ ( <i>min</i> )
1.6	45	87
1.5	120	213
1.4	150	244
1.3	180	266
1.2	210	278
1.1	240	279
1.0	300	300
0.9	360	299
0.8	450	295
0.7	570	266
0.6	720	189

The data in Table 3 is easily fitted to a dose time curve, using least squares, yielding,

$$t_x = \exp \left[ \frac{3.0 - p_{O_2}}{.36} \right] = 4160 \exp (-2.77p_{O_2}) \quad (36)$$

or, equivalently,

$$p_{O_2} = 3.0 - .36 \ln (t_x) \quad (37)$$

in the same units, that is  $p_{O_2}$  and  $t_x$  in *atm* and *min* respectively. The last column tabulates an exposure dose,  $\Upsilon$ , for divers, called the oxygen tolerance unit (OTU), developed by Lambertsen and coworkers at the University of Pennsylvania. Formally, the oxygen tolerance,  $\Upsilon$ , is given by,

$$\Upsilon = \left[ \frac{p_{O_2} - 0.5}{0.5} \right]^{0.83} t$$

and can be cumulatively applied to diving exposures according to the following prescriptions:

1. maintain single dive OTUs below 750 *min* on the liberal side, or allow for 550 *min* of that as possible full DCI recompression treatment on the conservative side;
2. maintain repetitive total dive OTUs below 300 *min*.

The expression is applied to each and all segments of a dive, and summed accordingly for total OTUs, and then benchmarked against the 750 *min* or 300 *min* rough rule. The 750 *min* and 300 *min* OTU rules are not cast in stone in the diving community, and 10% to 25% variations are common, in both conservative and liberal directions. Formally, if  $\Upsilon_n$  is the oxygen tolerance for the  $n^{th}$  segment of a dive, with segment time,  $t_n$ , and oxygen partial pressure,  $p_{nO_2}$ , the total OTU accumulated,  $\Upsilon$ , is,

$$\Upsilon = \sum_{n=1}^N \Upsilon_n = \sum_{n=1}^N \left[ \frac{p_{nO_2} - 0.5}{0.5} \right]^{0.83} t_n \quad (39)$$

with  $N$  the total number of dive segments (multilevel, deco, repetitive). Originally, Lambertsen defined a unit pulmonary toxicity dose (UPTD),  $\Phi$ , given by,

$$\Phi = \left[ \frac{p_{O_2} - 0.5}{0.5} \right]^{1.2} t \quad (40)$$

weighing oxygen partial pressure more than the OTU, but the definitions share the same basis, though slightly different fits to oxygen dose data. In the diving community, both representations have their proponents, favoring the oxygen partial pressure or time in oxygen dose estimations.

For exceptional and multiple exposures, the USN and University of Pennsylvania suggest the limits summarized in Table 4, where for multiple exposures,  $N$ , and segment times,  $t_{x_n}$ ,

$$T_x = \sum_{n=1}^N t_{x_n} \quad (41)$$

Table 4. Oxygen Exceptional Exposure Time Limits

oxygen partial pressure $p_{O_2}$ ( <i>atm</i> )	single exposure $t_x$ ( <i>min</i> )	multiple exposures $T_x$ ( <i>min</i> )
2.0	30	
1.9	45	
1.8	60	
1.7	75	
1.6	120	15
1.5	150	180
1.4	180	180
1.3	240	210
1.2	270	240
1.1	300	270
0.9	360	360
0.8	450	450
0.7	570	570
0.6	720	720

Note the severe reduction in multiple oxygen exposure time at 1.6 *atm* in Table 4. For this reason, technical divers generally restrict mixed gas diving exposures to  $p_{O_2} \leq 1.6$  *atm* throughout any sequence of dives.

There are many ways to measure oxygen, with devices called oxygen analyzers. They are employed in chemical plants and refineries, hyperbaric chambers, intensive care units, and nurseries. The paramagnetic analyzer is very accurate, and relies on oxygen molecular response to a magnetic field in displacing inert gases from collection chambers. Thermal conductivity analyzers differentiate oxygen and nitrogen conduction properties in tracking temperatures in thermistors, with difference in temperatures proportional to the oxygen concentration. Magnetic wind analyzers combine properties of paramagnetic and thermal analyzers. Polarographic analyzers measure oxygen concentration by resistance changes across permeable oxygen membranes. Galvanic cell analyzers are microfuel cells, consuming oxygen on touch and generating a small current proportional to the amount of oxygen consumed. In all cases, analyzer response is linear in oxygen concentration.

Although it is tempting to avoid problems of oxygen toxicity by maintaining oxygen partial pressures,  $p_{O_2}$ , far below toxic limits, this is not beneficial to inert gas elimination (free or dissolved state). Higher levels of inspired oxygen, thus correspondingly lower levels of inert gases, are advantageous in minimizing inert gas buildup and maximizing inert gas washout. Coupled to narcotic potency of helium and nitrogen, and molecular diffusion rates, balancing and optimizing breathing mixtures with decompression requirements is truly a complex and careful technical diving exercise.

### Exercises

1. At elevation,  $z = 3,800$  m, what are the working depths,  $d_{max}$  and  $d_{min}$ , for a 74/26 nitrox mixture, assuming 1.6 atm and .16 atm as the upper and lower oxygen partial pressure limits (Parts 4, 3)?
2. What is the equivalent air depth,  $\delta$ , at ocean depth,  $d = 98$  fsw, for enriched 74/26 nitrox (Part 4)?
3. What is the nitrogen fraction,  $f_{N_2}$ , for an equivalent air depth,  $\delta = 110$  fsw, at ocean depth,  $d = 125$  fsw (Part 4)? What is the corresponding oxygen floor,  $d_{max}$  (Part 4)?
4. What is the relative concentration,  $c$ , of neon dissolved in oil at a partial pressure  $p = 9.8$  atm (Part 4, Table 2)? What is the ratio,  $\zeta$ , of relative solubilities of neon in water and oil (Part 4, Table 2)? How much more,  $\zeta$ , is nitrogen soluble in oil versus water (Part 4, Table 2)?
5. According to Graham, what roughly is the ratio,  $\psi$ , of molecular diffusion speeds of hydrogen to oxygen (Part 4)?
6. A commercial diving operation is constructing a set of helium proprietary tables using the popular DCIEM nitrogen tables as a basis before testing. If the spectrum of tissues,  $\tau$ , in the DCIEM nitrogen tables is ( 2.5, 5, 10, 20, 40, 80, 160, 320 min), what are the corresponding set for the helium tables, assuming the same critical tensions,  $M$ , as the nitrogen tables (Parts 4, 7)?
7. What is the ratio,  $\zeta$ , of narcotic potency of helium to argon (Part 4, Table 2)? Which is the least potent (Part 4, Table 2)?
8. What is the surface oxygen partial pressure,  $p_0$ , for a normoxic breathing mixture at 450 fsw (Part 4)? What can you say about such a mixture at the surface (Parts 4, 11)?
9. Assuming surface equilibration on air, what is the total tissue tension,  $\Pi$ , in the,  $\tau = 20$  min, compartment after 10 min at depth,  $d = 90$  fsw, of a salvage diver breathing 60/25/15 trimix ( $f_{He} = .60$ ,  $f_{N_2} = .25$ ,  $f_{O_2} = .15$ ) (Parts 4, 1)? What is the critical surfacing tension,  $M_0$ , for the 20 min compartment (Part 2)? Should this diver ascend to the surface on his trimix?
10. What is the critical tension,  $M$ , at depth,  $d = 34$  fsw, in the helium tissue compartment,  $\tau = 15$  min, using the air fit to critical tensions (Parts 4, 2)?
11. If an oil rig diver on 80/20 heliox saturated at  $P_i = 6$  atm, switches to 80/20 nitrox at  $P_a = 4$  atm on ascent, how long after the switch,  $t_m$ , does isobaric counterdiffusion produce a minima in total gas tension,  $\Pi$ , in the  $\tau_{N_2} = 54$  min compartment (Part 4)? If the gas switch is 80/20 nitrox to 80/20 heliox, how long after the switch (all else the same),  $t_m$ , does isobaric counterdiffusion produce a maxima in total gas tension,  $\Pi$ , in the same compartment (Part 4)?
12. How many OTUs does a 14/50 trimix (14% oxygen, 50% helium) diver register at 230 fsw for 45 min (Part 4)? What is the toxic limit,  $t_x$ , on this mixture at this depth (Part 14)?

### *Related Reading*

1. Bennett P.B. and Elliot D.H., 1996, *The Physiology And Medicine Of Diving And Compressed Air Work*, London: Bailliere Tindall And Cassell.
2. Buhlmann A.A., 1984, *Decompression/Decompression Sickness*, Berlin: Springer Verlag.
3. Gilliam B., Webb D. and von Maier R., 1995, *Deep Diving*, San Diego: Watersports.
4. Hamilton R.W., 1975, *Development Of Decompression Procedures For Depths In Excess Of 400 Feet*, Undersea And Hyperbaric Medical Society Report, WS: 2-28-76, Bethesda.
5. Hills B.A., 1977, *Decompression Sickness*, New York: John Wiley And Sons.
6. Lambertsen C.J. and Bornmann R.C., 1977, *Isobaric Inert Gas Counterdiffusion*, Undersea And Hyperbaric Medical Society Publication 54WS(IC)1-11-82, Bethesda.
7. Mount T. and Gilliam B., 1991, *Mixed Gas Diving*, San Diego: Watersport.
8. Neal J.G., O'Leary T.R. and Wienke B.R., 1999, *Trimix Diving*, Fort Lauderdale: Underwater Dynamics Incorporated.
9. Rutkowski D., 1989, *Nitrox Manual*, San Diego: International Association of Nitrox Divers (IAND).
10. Schreiner H.R. and Hamilton R.W., 1987, *Validation Of Decompression Tables*, Undersea And Hyperbaric Medical Society Publication 74 (VAL), Bethesda.
11. Somers L.H., 1991, *The University Of Michigan Diving Manual*, Ann Arbor: University Of Michigan Press.
12. Wallace D., 1975, *NOAA Diving Manual*, Washington DC: US Government Printing Office.
13. Wienke B.R., 1998, *Physics, Physiology, And Decompression Theory For The Technical And Commercial Diver*, National Association Of Underwater Instructors Publication, Tampa.
14. Wienke B.R., 1994, *Basic Diving Physics And Application*, Flagstaff: Best.

## PART 5: DECOMPRESSION THEORY DECOMPRESSION TABLES, METERS, AND MODELS

### Protocols

Operational diving requires arbitrary numbers of dives to various depths over periods of hours, and often days. Once a standard set of decompression tables has been constructed, with bounce diving the simple case of nonstop decompression, a repetitive dive procedure is a necessity. After any air dive, variable amounts of dissolved and free residual nitrogen remain in body tissues for periods of 24 *hr*, and more. Similarly, elevated tissue tensions can promote, or sustain, bubble growth over the same time scales. This residual gas buildup (dissolved and free) will shorten the exposure time for subsequent repetitive dives. The longer and deeper the first dive, the greater the amount of residual tissue nitrogen affecting decompression on subsequent dives. Nonstop depth-time allowances for repetitive dives are reduced in such circumstance. Within bubble models, residual free gas phases are also included in procedures, imposing additional constraints on repetitive diving. The many possibilities are easily tracked in continuous time mode by computers, as mentioned, but tables face a more difficult task.

### Tables

Considering only dissolved gases, one standard table approach, developed by Workman, groups combinations of depth and exposure times according to the surfacing tension in the slowest compartment. Then it is possible to account for desaturation during any arbitrary surface interval. The remaining excess nitrogen at the start of the next dive can always be converted into equivalent time spent at the deepest point of the dive. So called penalty time is then added to actual dive time to updated appropriate tissue tensions. Surfacing tensions in excess of 33 *fsw* (absolute) in the slowest compartment are assigned letter designations (groups), A to O, for each 2 *fsw* over 33 *fsw*. Any, and all, exposures can be treated in this manner. To credit outgassing, a Surface Interval Table, accounting for 2 *fsw* incremental drops in tensions in the slowest compartment, is also constructed. Such procedures are bases for the US Navy Air Decompression and Repetitive Surface Interval Tables, with the 120 *min* compartment (the slowest) controlling repetitive activity. Standard US Navy Tables provide safe procedures for dives up to 190 *fsw* for 60 *min*. Dives between 200 and 300 *fsw* were tested and reported in the exceptional exposure US Navy tables, including a 240 *min* compartment. The Swiss tables, compiled by Buhlmann, incorporate the same basic procedures, but with a notable exception. While the US Navy tables were constructed for sea level usage, requiring some safe extrapolation procedure to altitude, the Swiss tables are formulated and tested over a range of reduced ambient pressure. The controlling repetitive tissue in the Buhlmann compilation is the 635 *min* compartment. Similar approaches focusing on deep and saturation diving have resulted in decompression tables for helium-oxygen (heliox), helium-oxygen-nitrogen (trimix), and recent mixtures with some hydrogen (hydrox). Clearly, the USN and Swiss Repetitive Tables can be easily converted to other (longer or shorter) controlling tissues by arithmetic scaling of the 120 *min* or 635 *min* compartment to the desired controlling tissue halftime (simple ratio). To scale the USN Tables to 720 *min*, for instance, the repetitive intervals need only be multiplied by  $720/120 = 6$ .

While it is true that the table procedures just described are quite easily encoded in digital meters, and indeed such devices exist, digital meters are capable of much more than table recitations. Pulsing depth and pressure at short intervals, digital meters can monitor diving almost continuously, providing rapid estimates of any model parameter. When employing the exact same algorithms as tables, meters provide additional means to control and safety beyond table lookup. When model equations can be inverted in time, meters can easily compute time remaining before decompression, time at a stop, surface interval before flying, and optimal ascent procedure. Profiles can be stored for later analysis, and the resulting data bank used to tune and improve models and procedures. Considering utility and functionality, meter usage should increase in diving, supported by technolog-

ical advance in computing power, algorithmic sophistication, and general acceptance, though it will probably be some time though before tables are supplanted.

A set of (modified) USN Tables is given in Figure 1. The set has reduced nonstop time limits, consistent with present safety margins associated with lower Doppler scores (Spencer reduction).

### Meters

On the heels of growing interest in underwater science and exploration following World War II, monitoring devices have been constructed to control diver exposure and decompression procedures. Devices, with records of varying success, include mechanical and electrical analogs, and within the past 15 years, microprocessor based digital computers. With inexpensive microprocessor technology, recent years have witnessed explosive growth in compact digital meters usage. All use the simple dissolved tissue gas model proposed by Haldane some 80 years ago, but given the sophistication of these devices, many feel that broader models can be incorporated into meter function today, increasing their range and flexibility. Although the biophysics of bubble formation, free and dissolved phase buildup and elimination is formidable, and not fully understood yet, contemporary models treating both dissolved and free phases, correlated with existing data, and consistent with diving protocols might extend the utility of diving computers. An approach treating bubble nucleation, excitation, and growth in tissue and blood is needed. In the industry, such new models are termed bubble mechanical, because they focus on bubbles and their interactions with dissolved gas in tissue and blood.

Decompression computers are sophisticated items these days. Basically a decompression meter is a microprocessor computer consisting of a power source, pressure transducer, analog to digital signal converter, internal clock, microprocessor chip with RAM (random access memory) and ROM (read only memory), and pixel display screen. Pressure readings from the transducer are converted to digital format by the converter, and sent to memory with the elapsed clock time for model calculations, usually every 1 - 3 *sec*. Results are displayed on the screen, including time remaining, time at a stop, tissue gas buildup, time to flying, and other model flag points, usually Haldanean (perfusion) tissue control variables. Some 3 - 9 volts is sufficient power to drive the computer for a couple of years, assuming about 100 dives per year. The ROM contains the model program (step application of model equations), all constants, and queries the transducer and clock. The RAM maintains storage registers for all dive calculations ultimately sent to the display screen. Dive computers can be worn on the wrist, incorporated in consoles, or even integrated into *heads - up* displays in masks. A typical dive computer is schematized in Figure 2.

Statistics point to an enviable track record of decompression meter usage in nominal diving activities, as well as an expanding user community. When coupled to slow ascent rates and safety stops, computer usage has witnessed a very low incidence rate of decompression sickness, below 0.01% according to some reports. Computers for nitrox are presently online today, with heliox and trimix units a rather simple modification of any nitrox unit, using existing decompression algorithms.

### Model History

Tables and schedules for diving at sea level can be traced to a model proposed in 1908 by the eminent English physiologist, John Scott Haldane. He observed that goats, saturated to depths of 165 feet of sea water (*fsw*), did not develop decompression sickness (DCS) if subsequent decompression was limited limited to half the ambient pressure. Extrapolating to humans, researchers reckoned that tissues tolerate elevated dissolved gas pressures (tensions), greater than ambient by factors of two, before the onset of symptoms. Haldane then constructed schedules which limited the critical supersaturation ratio to two in hypothetical tissue compartments. Tissue compartments were characterized by their halftime,  $\tau$ . Halftime is also termed *halflife* when linked to exponential processes, such as radioactive decay. Five compartments (5, 10, 20, 40, 75 *min*) were employed in decompression calculations and staged procedures for fifty years.

Some years following, in performing deep diving and expanding existing table ranges in the 1930s, US Navy investigators assigned separate limiting tensions (*M*-values) to each tissue compartment.

Later in the 1950s and early 1960s, other US Navy investigators, in addressing repetitive exposures for the first time, advocated the use of six tissues (5, 10, 20, 40, 80, 120 *min*) in constructing decompression schedules, with each tissue compartment again possessing its own limiting tension. Temporal uptake and elimination of inert gas was based on mechanics addressing only the macroscopic aspects of gas exchange between blood and tissue. Exact bubble production mechanisms, interplay of free and dissolved gas phases, and related transport phenomena were not quantified, since they were neither known nor understood. Today, we know more about dissolved and free phase dynamics, bubbles, and transport mechanisms, but still rely heavily on the Haldane model. Inertia and simplicity tend to sustain its popularity and use, and it has been a workhorse.

#### Bulk Diffusion Model

Diffusion limited gas exchange is modeled in time by a sum of exponential response functions, bounded by arterial and initial tissue tensions. However, instead of many tissue compartments, a single bulk tissue is assumed for calculations, characterized by a gas diffusion constant,  $D$ . Tissue is separated into intravascular (blood) and extravascular (cells) regions. Blood containing dissolved inert and metabolic gases passes through the intravascular zone, providing initial and boundary conditions for subsequent gas diffusion into the extravascular zone. Diffusion is driven by the difference between arterial and tissue tensions, according to the strength of a single diffusion coefficient,  $D$ , appropriate to the media. Diffusion solutions, averaged over the tissue domain, resemble a weighted sum over effective tissue compartments with time constants,  $\lambda_{2n-1} = \alpha_{2n-1}^2 D$ , determined by diffusivity and boundary conditions, with  $\alpha_{2n-1} = (2n-1)\pi/l$  for tissue thickness,  $l$ .

Applications fit the time constant,  $\kappa = \pi^2 D/l^2$ , to exposure data, with a typical value employed by the Royal Navy given by,  $\kappa = 0.007928 \text{ min}^{-1}$ , approximating the US Navy 120 *min* compartment used to control saturation, decompression, and repetitive diving. Corresponding critical tensions in the bulk model,

$$M = \frac{709P}{P + 404}, \quad (1)$$

fall somewhere between fixed gradient and multitissue values. At the surface,  $M = 53 \text{ fsw}$ , while at 200 *fsw*,  $M = 259 \text{ fsw}$ . A critical gradient,

$$G = \frac{P(493 - P)}{(P + 404)}, \quad (2)$$

also derives from the above. Originally, a critical gradient,  $G$ , near 30 *fsw* was used to limit exposures. Such value is too conservative for deep and bounce exposures, and not conservative enough for shallow exposures. Hempleman introduced the above relationship, providing the means to parameterize bounce and saturation diving.

Bulk diffusion models (BDM) are attractive because they permit the whole dive profile to be modeled with one equation, and because they predict a  $t^{1/2}$  behavior of gas uptake and elimination. Nonstop time limits,  $t_n$ , are related to depth,  $d$ , by the bulk diffusion relationship, seen in Figure 3,

$$dt_n^{1/2} = C, \quad (3)$$

with approximate range,  $400 \leq C \leq 500 \text{ fsw min}^{1/2}$ , linking nonstop time and depth simply through the value of  $C$ . For the US Navy nonstop limits,  $C \approx 500 \text{ fsw min}^{1/2}$ , while for the Spencer reduced limits,  $C \approx 465 \text{ fsw min}^{1/2}$ . In the Wienke-Yount model,  $C \approx 400 \text{ fsw min}^{1/2}$ .

#### Multitissue Model

Multitissue models (MTM), variations of the original Haldane model, assume that dissolved gas exchange, controlled by blood flow across regions of varying concentration, is driven by the local gradient, that is, the difference between the arterial blood tension and the instantaneous tissue tension. Tissue response is modeled by exponential functions, bounded by arterial and initial tensions, and

perfusion constants,  $\lambda$ , linked to the tissue halftimes,  $\tau$ , for instance, 1, 2, 5, 10, 20, 40, 80, 120, 180, 240, 360, 480, and 720 *min* compartments assumed to be independent of pressure.

In a series of dives or multiple stages, initial and arterial tensions represent extremes for each stage, or more precisely, the initial tension and the arterial tension at the beginning of the next stage. Stages are treated sequentially, with finishing tensions at one step representing initial tensions for the next step, and so on. To maximize the rate of uptake or elimination of dissolved gases the gradient, simply the difference between arterial and tissue tensions is maximized by pulling the diver as close to the surface as possible. Exposures are limited by requiring that the tissue tensions never exceed

$$M = M_0 + \Delta M d, \tag{4}$$

as a function of depth,  $d$ , for  $\Delta M$  the change per unit depth. A set of  $M_0$  and  $\Delta M$  are listed in Table 1.

Table 1. Classical US Navy Surfacing Ratios And Critical Tensions.

halftime $\tau$ ( <i>min</i> )	critical ratio $R_0$	critical tension $M_0$ ( <i>fsw</i> )	tension change $\Delta M$
5	3.15	104	2.27
10	2.67	88	2.01
20	2.18	72	1.67
40	1.76	58	1.34
80	1.58	52	1.26
120	1.55	51	1.19

At altitude (Part 3), some critical tensions have been correlated with actual testing, in which case, an effective depth,  $d$ , is referenced to the absolute pressure,  $P$  (in *fsw*),

$$d = P - 33 \tag{5}$$

with surface pressure,  $P_h$ , at elevation,  $h$ ,

$$P_h = 33 \exp(-0.0381h) \tag{6}$$

for  $h$  in multiples of 1,000 *ft*. However, in those cases where critical tensions have not been tested, nor extended, to altitude, an exponentially decreasing extrapolation scheme, called similarity, has been employed. Extrapolations of critical tensions, below  $P = 33$  *fsw*, then fall off more rapidly than in the linear case. A similarity extrapolation holds the ratio,  $R = M/P$ , constant at altitude. Estimating minimum surface tension pressure of bubbles near 10 *fsw*, as a limit point, the similarity extrapolation might be limited to 10,000 *ft* in elevation, and neither for decompression nor heavy repetitive diving.

Models of dissolved gas transport and coupled bubble formation are not complete, and all need correlation with experiment and wet testing. Extensions of basic (perfusion and diffusion) models can redress some of the difficulties and deficiencies, both in theory and application. Concerns about microbubbles in the blood impacting gas elimination, geometry of the tissue region with respect to gas exchange, penetration depths for gas diffusion, nerve deformation trigger points for pain, gas uptake and elimination asymmetry, effective gas exchange with flowing blood, and perfusion versus diffusion limited gas exchange, to name a few, motivate a number of extensions of dissolved gas models.

The multitissue model addresses dissolved gas transport with saturation gradients driving the elimination. In the presence of free phases, free-dissolved and free-blood elimination gradients can compete with dissolved-blood gradients. One suggestion is that the gradient be split into two

weighted parts, the free-blood and dissolved-blood gradients, with the weighting fraction proportional to the amount of separated gas per unit tissue volume. Use of a split gradient is consistent with multiphase flow partitioning, and implies that only a portion of tissue gas has separated, with the remainder dissolved. Such a split representation can replace any of the gradient terms in tissue response functions.

If gas nuclei are entrained in the circulatory system, blood perfusion rates are effectively lowered, an impairment with impact on all gas exchange processes. This suggests a possible lengthening of tissue halftimes for elimination over those for uptake, for instance, a 10 *min* compartment for uptake becomes a 12 *min* compartment on elimination. Such lengthening procedure and the split elimination gradient obviously render gas uptake and elimination processes asymmetric. Instead of both exponential uptake and elimination, exponential uptake and linear elimination response functions can be used. Such modifications can again be employed in any perfusion model easily, and tuned to the data.

#### Thermodynamic Model

The thermodynamic model (TM) suggested by Hills, and extended by others, is more comprehensive than earlier models, addressing a number of issues simultaneously, such as tissue gas exchange, phase separation, and phase volume trigger points. This model is based on phase equilibration of dissolved and separated gas phases, with temporal uptake and elimination of inert gas controlled by perfusion and diffusion. From a boundary (vascular) thin zone, gases diffuse into the cellular region. Radial, one dimensional, cylindrical geometry is assumed as a starting point, though the extension to higher dimensionality is straightforward. As with all dissolved gas transfer, diffusion is controlled by the difference between the instantaneous tissue tension and the venous tension, and perfusion is controlled by the difference between the arterial and venous tension. A mass balance for gas flow at the vascular cellular interface, enforces the perfusion limit when appropriate, linking the diffusion and perfusion equations directly. Blood and tissue tensions are joined in a complex feedback loop. The trigger point in the thermodynamic model is the separated phase volume, related to a set of mechanical pain thresholds for fluid injected into connective tissue.

The full thermodynamic model is complex, though Hills has performed massive computations correlating with the data, underscoring basic model validity. One of its more significant features can be seen in Figure 4. Considerations of free phase dynamics (phase volume trigger point) require deeper decompression staging formats, compared to considerations of critical tensions, and are characteristic of phase models. Full blown bubble models require the same, simply to minimize bubble excitation and growth.

#### Varying Permeability Model

The varying permeability model (VPM) treats both dissolved and free phase transfer mechanisms, postulating the existence of gas seeds (micronuclei) with permeable skins of surface active molecules, small enough to remain in solution and strong enough to resist collapse. The model is based upon laboratory studies of bubble growth and nucleation.

Inert gas exchange is driven by the local gradient, the difference between the arterial blood tension and the instantaneous tissue tension. Compartments with 1, 2, 5, 10, 20, 40, 80, 120, 240, 480, and 720 halftimes,  $\tau$ , are again employed. While, classical (Haldane) models limit exposures by requiring that the tissue tensions never exceed the critical tensions, fitted to the US Navy nonstop limits, for example, the varying permeability model, however, limits the supersaturation gradient, through the phase volume constraint (Part 2). An exponential distribution of bubble seeds, falling off with increasing bubble size is assumed to be excited into growth by compression-decompression. A critical radius,  $r_c$ , separates growing from contracting micronuclei for given ambient pressure,  $P_c$ . At sea level,  $P_c = 33 \text{ fsw}$ ,  $r_c = .8 \text{ microns}$ . Deeper decompressions excite smaller, more stable, nuclei.

Within the phase volume constraint, a set of nonstop limits,  $t_n$ , at depth,  $d$ , satisfy a modified law,  $dt_n^{1/2} = 400 \text{ fsw min}^{1/2}$ , with gradient,  $G$ , extracted for each compartment,  $\tau$ , using the

nonstop limits and excitation radius, at generalized depth,  $d = P - 33 \text{ fsw}$ . Tables 2 and 1 (Part 2) summarize  $t_n$ ,  $G_0$ ,  $\Delta G$ , and  $\delta$ , the depth at which the compartment begins to control exposures.

Table 2. Critical Phase Volume Time Limits.

depth $d \text{ (fsw)}$	nonstop limit $t_n \text{ (min)}$	depth $d \text{ (fsw)}$	nonstop limit $t_n \text{ (min)}$
30	250.	130	9.0
40	130.	140	8.0
50	73.	150	7.0
60	52.	160	6.5
70	39.	170	5.8
80	27.	180	5.3
90	22.	190	4.6
100	18.	200	4.1
110	15.	210	3.7
120	12.	220	3.1

Gas filled crevices can also facilitate nucleation by cavitation. The mechanism is responsible for bubble formation occurring on solid surfaces and container walls. In gel experiments, though, solid particles and ragged surfaces were seldom seen, suggesting other nucleation mechanisms. The existence of stable gas nuclei is paradoxical. Gas bubbles larger than  $1 \mu\text{m}$  should float to the surface of a standing liquid or gel, while smaller ones should dissolve in a few *sec*. In a liquid supersaturated with gas, only bubbles at the critical radius,  $r_c$ , would be in equilibrium (and very unstable equilibrium at best). Bubbles larger than the critical radius should grow larger, and bubbles smaller than the critical radius should collapse. Yet, the Yount gel experiments confirm the existence of *stable* gas phases, so no matter what the mechanism, effective surface tension must be zero. Although the actual size distribution of gas nuclei in humans is unknown, these experiments in gels have been correlated with a decaying exponential (radial) distribution function. For a stabilized distribution accommodated by the body at fixed pressure,  $P_c$ , the excess number of nuclei excited by compression-decompression must be removed from the body. The rate at which gas inflates in tissue depends upon both the excess bubble number, and the supersaturation gradient,  $G$ . The critical volume hypothesis requires that the integral of the product of the two must always remain less than some volume limit point,  $\alpha V$ , with  $\alpha$  a proportionality constant.

#### Reduced Gradient Bubble Model

The reduced gradient bubble model (RGBM) extends the earlier VPM naturally. The full blown RGBM treats coupled perfusion-diffusion transport as a two step flow process, with blood flow (perfusion) serving as a boundary condition for tissue gas penetration by diffusion. Depending on time scales and rate coefficients, one or another (or both) processes dominate the exchange. However, for most meter implementations, perfusion is assumed to dominate, simplifying matters and permitting online calculations. Additionally, tissues and blood are naturally undersaturated with respect to ambient pressure at equilibration through the mechanism of biological inherent unsaturation (oxygen window), and the model includes this debt in calculations.

The RGBM assumes that a size distribution of seeds (potential bubbles) is always present, and that a certain number is excited into growth by compression-decompression. An iterative process for ascent staging is employed to control the inflation rate of these growing bubbles so that their collective volume never exceeds a phase volume limit point. Gas mixtures of helium, nitrogen, and oxygen contain bubble distributions of different sizes, but possess the same phase volume limit point.

The RGBM postulates bubble seeds with varying permeability. Bubble skins are assumed permeable down to  $10 \text{ atm}$  crushing pressure. The size of seeds excited into growth is inversely proportional

to the supersaturation gradient. Beyond 10 *atm*, bubble seeds permit gas diffusion at a slower rate. The model assumes bubble skins are stabilized by surfactants over unknown time scales, but that the seeds are persistent in the body. Bubble skins are probably molecularly activated, complex, biosubstances found throughout the body. Whatever the formation process, the model assumes the size distribution is exponentially decreasing in size, that is, more smaller seeds than larger seeds in exponential proportions.

The model incorporates a spectrum of tissue compartments, ranging from 1 *min* to 720 *min*, depending on gas mixture (helium, nitrogen, oxygen). Phase separation and bubble growth in slower compartments is a central focus in calculations, and the model uses nonstop time limits tuned to recent Doppler measurements, conservatively reducing them along the lines originally suggested by Spencer (and others), but within the phase volume constraint.

The RGBM reduces the phase volume limit in multiding by considering free phase elimination and buildup during surface intervals, depending on altitude, time, and depth of previous profiles. Repetitive, multiday, and reverse profile exposures are tracked and impacted by critical phase volume reductions over appropriate time scales. The model generates replacement bubble seed distributions on time scales of days, adding new bubbles to existing bubbles in calculations. Phase volume limit points are also reduced by the added effects of new bubbles.

The reduced gradient bubble model extends the varying permeability model to repetitive diving, by conservatively reducing the gradients,  $G$ . A conservative set of bounce gradients,  $G$ , can always be used for multiday and repetitive diving, provided they are multiplicatively reduced by a set of bubble factors, all less than one (Part 2). Three bubble factors reduce the driving gradients to maintain the phases volume constraint. The first bubble factor reduces  $G$  to account for creation of new stabilized micronuclei over time scales of days. The second factor accounts for additional micronuclei excitation on reverse profile dives. The third bubble factor accounts for bubble growth over repetitive exposures on time scales of hours. Their behavior (in Part 2) is depicted in Figures 5, 6, and 7.

The RGBM and VPM are both diveware implementations, accessible on the Internet at various sites. Additionally, the RGBM has been encoded into a number of commercial decompression meter products. Specific comparisons between RGBM and Haldane predictions for staging are summarized (Part 6), with resultants generic for phase versus dissolved gas models.

#### Tissue Bubble Diffusion Model

The tissue bubble diffusion model (TBDM), according to Gernhardt and Vann, considers the diffusive growth of an extravascular bubble under arbitrary hyperbaric and hypobaric loadings. The approach incorporates inert gas diffusion across the tissue-bubble interface, tissue elasticity, gas solubility and diffusivity, bubble surface tension, and perfusion limited transport to the tissues. Tracking bubble growth over a range of exposures, the model can be extended to oxygen breathing and inert gas switching. As a starting point, the TBDM assumes that, through some process, stable gas nuclei form in the tissues during decompression, and subsequently tracks bubble growth with dynamical equations. Diffusion limited exchange is invoked at the tissue-bubble interface, and perfusion limited exchange is assumed between tissue and blood, very similar to the thermodynamic model, but with free phase mechanics. Across the extravascular region, gas exchange is driven by the pressure difference between dissolved gas in tissue and free gas in the bubble, treating the free gas as ideal. Initial nuclei in the TBDM have assumed radii near 3 *microns* at sea level, to be compared with .8 *microns* in the VPM and RGBM.

As in any free phase model, bubble volume changes become more significant at lower ambient pressure, suggesting a mechanism for enhancement of hypobaric bends, where constricting surface tension pressures are smaller than those encountered in hyperbaric cases. As seen in Figure 5, the model has been coupled to statistical likelihood, correlating bubble size with decompression risk, a topic discussed in a few chapters. For instance, a theoretical bubble dose of 5 *ml* correlates with a 20% risk of decompression sickness, while a 35 *ml* dose correlates with a 90% risk, with the bubble

dose representing an unnormalized measure of the separated phase volume. Coupling bubble volume to risk represents yet another extension of the phase volume hypothesis, a viable trigger point mechanism for bends incidence.

### *Exercises*

1. According to the Wienke-Yount bulk diffusion law, what is the nonstop time limit,  $t_n$ , at a depth of 155 fsw (Part 5)?
2. According to USN Tables (modified), what is the surfacing Group for a photographer at 67, fsw for 35 min, assuming the ascent rate is standard,  $r = 60$  fsw/min (Part 5, Figure 1)? If 68 min are spent on the surface, what is the new Group (Part 5, Figure 1)? On the next dive to 46 fsw, what is the penalty time,  $t$  (Part 5, Figure 1)? If bottom time at 46 fsw is 15 min, what is the new surfacing Group (Part 5, Figure 1)?
3. A Group F diver sustains what overpressure,  $\Delta P$ , in nitrogen loading (absolute) in the 120 min compartment (Part 5)? What is the nitrogen tension,  $p$ , in the 120 min compartment of that (surface) F diver after 160 min (Parts 5, 1)? Into what Group does the diver now fall (Parts 1, 7)?
4. A reef ecologist at depth,  $d = 35$  fsw, on a dive computer registers a spectrum of nitrogen tensions,  $p = (50, 48, 43, 41, 40, 42, 44)$  fsw, in tissues,  $\tau = (5, 10, 20, 40, 80, 120, 240)$  min. What are the corresponding tissue gradients,  $g = p - p_a$  (Parts 5, 1)? Since tissue gradients are inward (all negative), what is the implication for the present dive (Parts 5, 1)? What might higher tissue tensions in the two slowest compartments, relative to faster middle compartments, suggest (Parts 5, 1)?
5. If a Park Ranger lugs his dive gear to Lake Catherine above Santa Fe (New Mexico) at an elevation of 9,560 ft and plans a dive to 40 ft, what is the altitude correction factor,  $\beta$ , and what is the equivalent sea level depth,  $\delta$ , for the dive (Parts 5, 3)? If the ascent rate,  $r_0$ , in the Tables at sea level is 60 fsw/min, what is the altitude rate,  $r$  (Parts 5, 3)? If the excursion to Lake Catherine is launched from Sante Fe, elevation 6,860 ft, taking 15 min, what Group should the Ranger diver assign to the start of the dive (Part 3, Table 1)? If the dive lasts 20 min, in what group does the diver surface (Part 5, Figure 1)? As a Group G diver, what is the maximum change in altitude permitted (Part 3, Table 1)? How long before a mountain Group G diver drops into Group A (Part 5, Figure 1)? How long before a Group G diver can ascend 7,000 ft in elevation, according to the 24 hr rule (Part 3, Table 2)?
6. According to the USN Tables at sea level, the nonstop limit at 100 fsw is 22 min. What is the nonstop limit,  $t_n$ , at elevation of 5,600 ft, using the similarity method (Parts 5, 3 Figure 1)?
7. If the surfacing critical tension for the  $\tau = 90$  min compartment is,  $M_0 = 55$  fsw, what is the compartment limit,  $t_n$ , for 79/21 nitrox (air) at,  $d = 50$  fsw (Parts 5, 2, 4)?  $p_a = f_{N_2}(33 + 50)$  fsw =  $.79 \times 83$  fsw = 65.6 fsw What is the compartment limit,  $t_n$ , for 79/21 heliox at,  $d = 50$  fsw (Parts 5, 2, 4)?
8. Match model features to the BDM, MTM, TM, VPM, RGBM, and TBDM (Parts 5, 8)? Dissolved gas phase treatment only? Many perfusion tissue compartments? Single bulk tissue compartment? Exponential distributions of bubble seeds? Critical tension, ratio, or gradient limit points? Critical separated phase volume or dose limit points? Pain thresholds? Multidiving limitations? Commercial meter implementations? Seed regeneration? Dissolved and free gas phase treatment?

### *Related Reading*

1. *Buhlmann A.A., 1984, Decompression/Decompression Sickness, Berlin: Springer Verlag.*
2. *Hamilton R.W., 1975, Development Of Decompression Procedures For Depths In Excess Of 400 Feet, Undersea And Hyperbaric Medical Society Report, WS: 2-28-76, Bethesda.*
3. *Hills B.A., 1977, Decompression Sickness, New York: John Wiley And Sons.*
4. *Lang M.A. and Vann R.D., 1992, Proceedings Of The American Academy Of Underwater Sciences Repetitive Diving Workshop, AAUS Safety Publication AAUSDSP-RDW-02-92, Costa Mesa.*
5. *Lang M.A. and Egstrom G.H., 1990, Proceedings Of The American Academy Of Underwater Sciences Biomechanics Of Safe Ascents Workshop, American Academy Of Underwater Sciences Diving Safety Publication, AAUSDSP-BSA-01-90, Costa Mesa.*
6. *Lang M.A. and Hamilton R.W., 1989, Proceedings Of The American Academy Of Underwater Sciences Dive Computer Workshop, University Of Southern California Sea Grant Publication, USCSG-TR-01-89, Los Angeles.*
7. *Loyst K., Huggins K.E. and Steidley M., 1991, Dive Computers, San Diego: Watersports.*
8. *Schreiner H.R. and Hamilton R.W., 1987, Validation Of Decompression Tables, Undersea And Hyperbaric Medical Society Publication 74 (VAL), Bethesda.*
9. *Wienke B.R., 1998, Physics, Physiology, And Decompression Theory For The Technical And Commercial Diver, National Association Of Underwater Instructors Publication, Tampa.*
10. *Wienke B.R., 1994, Basic Diving Physics And Application, Flagstaff: Best.*
11. *Wienke B.R., 1993, Diving Above Sea Level, Flagstaff: Best.*
12. *Wienke B.R., 1991, High Altitude Diving, National Association Of Underwater Instructors Technical Publication, Montclair.*

PART 6: DECOMPRESSION THEORY  
COMPARATIVE PROFILES AND OPERATIONAL DIVING

Haldane Profiles

In applying models and equations, we are faced with either fitting data to situations using plausible bases, or synthesizing mathematical models based strategically on first principles. Present practice relies upon the former, and calculational methods target a limited range of conditions. With that understanding, we can launch into specific application of the Haldane model. In presenting gas buildup and elimination curves, square wave profiles, assuming maximum gas tension over any time interval of interest, will be employed for graphical simplicity, and without loss of generality.

In compressed air diving, nitrogen tensions are measured in weight fractions of ambient (absolute) pressure, with nitrogen fraction the usual 0.79. By conventions, both pressures and depths are measured in feet-of-sea-water (*fsw*). Degrees to which compartments tolerate supersaturation are limited by critical values,  $M$ , fitted to the historical data by straight lines, depicted in Figure 1 (Part 2), with  $\tau$ ,  $M_0$ , and  $\Delta M$  tabulated in Table 1 (Part 5). They are representative of multitissue sets employed in tables and meters. Ranges of variation are neither large, nor diverse in application. How they are employed, that is, their implementation across a spectrum of exposures, also does not vary theoretically from table to meter. Self consistency is somewhat a keynote, though claims about advantages of particular sets of tissue parameters can be made on bases of test ranges, statistics, and correlations.

Parameter sets and critical values derive from data fits, iterative repetitions, hindsight, possibly venous gas emboli correlations, and bootstrapping of earlier models. Ranges are bounded, as are permissible activities. If extended to altitude, the surfacing limits,  $M_0$ , decrease either exponentially (very rapidly) or linearly (more gradually). With notable parameter leeway in Table 1, additional leeway in permissible ascent and descent rates, and a set of non-stop time limits, a multiplicity of (safe) schedules are possible within the model framework. After testing, such schedules would then be fit for general diving consumption. Similar comments apply to the software driving any digital meter, effectively employing some equivalent version of Table 1 (Part 5), or Table 2 (Part 2).

Repetitive and decompression diving must contend with a greater fraction of separated gas. And this makes extrapolations of bounce diving fits more difficult. In the early days, slower tissue compartments were added to accommodate deeper, prolonged, and decompression exposures. Ostensibly, slower compartments might track a greater proportion of separated gas, possibly dumped from tissues into gas micronuclei. Laboratory studies in decompressed gels bear witness to typical growth and elimination patterns in gas nuclei and bubbles spanning hours. Of course, bubbles and nuclei in the body are both perfused and metabolic, adding to complexity. While not always optimal, tissue response functions with very slow compartments can be coupled to critical tensions for repetitive diving. The approach is more limited for repetitive diving than bounce diving, as possibly witnessed by higher bends incidence in divers embarking on multiday and repetitive activity, according to Vann and Dovenbarger. In such repetitive application, tables and meters which do not accommodate slower compartments, like  $\tau > 60$  minutes, appear further limited. For that very reason, the US Navy expanded the original set some fifty years ago, replacing the 70 minute compartment with an 80 minute compartment and adding the 120 minute compartment. Yet, the tendency today to add compartments in the several hundred minutes range, while well-intentioned, is probably not the best means for tracking separated phases. Very slow compartments, in the several hundred minute range, cannot really control multiday and heavy repetitive diving by tracking just dissolved phases. Present consensus thus cautions against 3 or more repetitive dives in any 24 hour period, especially in the deeper categories (beyond 100 *fsw*), and relaxation periods of at least a day following 3-4 days of repetitive activity.

### 1. Bounce Diving

In bounce diving, exposures at depth for any time are followed by immediate return to the surface. Accordingly, consider a bounce dive to 60 *fsw* for 40 *minutes*, an exposure in the nonstop category for tables and meters. Figure 1 depicts both gas uptake (solid line) in the 20 minute compartment as a function of time and corresponding  $M$  (dotted line) throughout the exposure, neglecting the time to surface from 60 *fsw*, and thus any outgassing during the interval. Note that at no time underwater nor at the surface, is  $M$  exceeded by the tissue tension, the case in all compartments for this exposure. Bounce diving within dissolved gas models is well parameterized.

But, suppose we lengthen the exposure to 70 *minutes*, certainly a decompression dive. Figure 2 contrasts nitrogen uptake against  $M$  for the 40 minute compartment, should the diver surface immediately after 70 *minutes*. While  $M$  is not exceeded at 60 *fsw*, the surfacing limit  $M_0$ , is exceeded. Clearly this diver would need to first decompress before surfacing. Here, only the 40 minute compartment is impacted. In general more than one compartment can be affected by exposures exceeding the nonstop time limits. If the diver, after 70 *minutes* at 60 *fsw*, makes a stop at 10 *fsw* for 2 *minutes*, he could safely ascend to the surface. The profile for the 40 minute compartment is depicted in Figure 3 in that case. Again, critical tensions are not exceeded.

### 2. Repetitive Diving

The Haldane approach to repetitive diving parallels that for bounce diving. Critical tensions again limit permissible degrees of compartment saturation. As an example of both repetitive application and diving idiom, *deepest dive first*, consider the profiles in Figures 4 and 5 for the 40 minute compartment. In the first case (Figure 4), an exposure to 70 *fsw* for 45 minutes is followed by a surface interval of 35 minutes, and then another dive to 50 *fsw* for 35 minutes. In the second case (Figure 5), the order is reversed, that is 50 *fsw* for 35 minutes, 35 minutes of surface interval, followed by 70 *fsw* for 45 minutes. Clearly, the first repetitive case is a nonstop exposure, while the second is not. In Figure 4, critical tensions are not exceeded, while in Figure 5, the critical tension,  $M_0$ , is compromised at the end of the dive.

Repetitive application of dissolved gas models does not enjoy the same success as bounce diving application. Free phases in the tissues have had some time to grow between dives, and the next dive then pumps in a fresh supply of dissolved gas, possibly feeding phase growth if elimination has not been effective.

### 3. Multilevel Diving

Multilevel diving presents additional challenges to the classical scheme, though most problems occur with table usage, and less so with digital devices. The reason is not too complicated. Tables generally rely on the slowest tissue compartment to dictate staging and repetitive formats. Repetitive intervals are chosen so that the faster compartments cannot control the exposure upon surfacing, with 10 minutes the usual limit. Tables cannot account for gas uptake or elimination in faster compartments for shorter time intervals, and thus request that shorter time intervals be added directly to exposure times. In multilevel table application, the 10 minute interval is neglected, and gas exchange in the faster compartments is not considered. At times, neglect of the faster compartments causes trouble, especially when their critical tensions are exceeded with the tables blind for some 10 minutes. Because meters continuously monitor activities in all compartments, these table concerns are minimized in multilevel excursions. While such a problem is more an implementation issue than fundamental issue, foregoing concerns in bounce, repetitive, and decompression exposures still carry over here.

As a comparison of multilevel table and meter diving, consider Figure 6. Tissue and critical tensions in the 10 minute compartment for a multilevel exposure are depicted. The exposure

consists of three segments, 120 *fsw* for 12 minutes, 90 *fsw* for 10 minutes, and 80 *fsw* for 2 minutes. According to the USN tables, the profile is marginally safe. But, according to Figure 6, the surfacing critical tension,  $M_0$ , is violated. A meter could arrest this problem before it occurred, while a table might exhibit marginal indifference (depending on user discretion).

Systematically deeper-to-shallow diving practices are optimal in all cases. Deeper-than-previous excursions have the potential to excite smaller, more stable, gas nuclei into growth. Deeper-spike and sawtooth diving profiles become more hazardous as repetitive frequency increases, likely due to the presence of growing bubbles and excitable gas nuclei in slower tissues and slingshot effect of higher tensions surrounding them.

#### 4. Saturation Diving

Like bounce diving, saturation diving, especially with mixed gases, has received considerable attention. Following exposures near 12 *hrs*, all compartments are essentially equilibrated with ambient pressure. Ascent is then controlled by the slowest compartment, the one with the smallest critical tension,  $M$ . Compartments with halftimes in the range,  $160 \leq \tau \leq 720$  *minutes*, are usually employed. In spite of compartment structure chosen, an interesting feature, consistent with Figure 4 (Part 2), arises in terms of critical tension in the slowest compartments.

From experiments, the saturation curve, relating permissible tissue tension to ambient pressure, has been well established for almost any gas mixture. In the case of air, Figure 4 depicts that relationship in absolute units, that is,  $Q = M/.79$  versus  $P$ . In terms of a linear,  $M$  the saturation air curve requires  $M_0 = 44$  *fsw*, while  $\Delta M = 1.06$ . While time scales for ascent vary according to the halftime of the slowest compartment, critical tensions for saturation staging vary slightly. Similar structure is seen in diffusion algorithms, employing a critical gradient,  $G$ . For example, in the Royal Navy tables, Rashbass first employed a fixed gradient,  $G = 30$  *fsw*, compared to  $(M_0/.79 - 33) = 23$  *fsw* in Figure 2 (Part 2). Later, Hempleman reduced the surfacing gradient,  $G = 20$  *fsw*. As seen, the equivalent tissue halftime for the diffusion algorithm is 87 *minutes*. In short, no matter what the table or model, saturation staging formats are usually consistent with the saturation curve, more particularly, the slope and intercept. In that sense, all models collapse to a slow, single tissue equivalent, as discussed by Hennessy and Hempleman. For bounce diving, of course, models vary in their tissue number, critical parameters, or trigger points.

#### Empirical Practices

Utilitarian procedures, entirely consistent with phase mechanics and bubble dissolution time scales, have been developed under duress, and with trauma, by Australian pearl divers and Hawaiian diving fishermen, for both deep and repetitive diving with possible in-water recompression for hits. While the science behind such procedures was not initially clear, the operational effectiveness was always noteworthy and could not be discounted easily. Later, the rationale, essentially recounted in the foregoing, became clearer.

Pearling fleets, operating in the deep tidal waters off northern Australia, employed Okinawan divers who regularly journeyed to depths of 300 *fsw* for as long as one hour, two times a day, six days per week, and ten months out of the year. Driven by economics, and not science, these divers developed optimized decompression schedules empirically. As reported by Le Messurier and Hills, deeper decompression stops, but shorter decompression times than required by Haldane theory, were characteristics of their profiles. Such protocols are entirely consistent with minimizing bubble growth and the excitation of nuclei through the application of increased pressure, as are shallow safety stops and slow ascent rates. With higher incidence of surface decompression sickness, as might be expected, the Australians devised a simple, but very effective, in-water recompression procedure. The stricken diver is taken back down to 30 *fsw* on oxygen for roughly 30 *minutes* in mild cases, or 60 *minutes* in severe cases. Increased pressures help to constrict bubbles, while breathing pure oxygen maximizes

inert gas washout (elimination). Recompression time scales are consistent with bubble dissolution experiments.

Similar schedules and procedures have evolved in Hawaii, among diving fishermen, according to Farm and Hayashi. Harvesting the oceans for food and profit, Hawaiian divers make between 8 and 12 dives a day to depths beyond 350 *fsw*. Profit incentives induce divers to take risks relative to bottom time in conventional tables. Three repetitive dives are usually necessary to net a school of fish. Consistent with bubble and nucleation theory, these divers make their deep dive first, followed by shallower excursions. A typical series might start with a dive to 220 *fsw*, followed by 2 dives to 120 *fsw*, and culminate in 3 or 4 more excursions to less than 60 *fsw*. Often, little or no surface intervals are clocked between dives. Such types of profiles literally clobber conventional tables, but, with proper reckoning of bubble and phase mechanics, acquire some credibility. With ascending profiles and suitable application of pressure, gas seed excitation and any bubble growth are constrained within the body's capacity to eliminate free and dissolved gas phases. In a broad sense, the final shallow dives have been tagged as prolonged safety stops, and the effectiveness of these procedures has been substantiated *in vivo* (dogs) by Kunkle and Beckman. In-water recompression procedures, similar to the Australian regimens, complement Hawaiian diving practices for all the same reasons.

While the above practices developed by trial-and-error, albeit with seeming principle, venous gas emboli measurements, performed off Catalina by Pilmanis on divers making shallow safety stops, fall into the more *scientific* category perhaps. Contrasting bubble counts following bounce exposures near 100 *fsw*, with and without zonal stops in the 10-20 *fsw* range, marked reductions (factors of 4 to 5) in venous gas emboli, as seen in Figure 6 (Part 2), were noted when stops were made. If, as some suggest, venous gas emboli in bounce diving correlate with bubbles in sites such as tendons and ligaments, then safety stops probably minimize bubble growth in such extravascular locations. In these tests, the sample population was small, so additional validation and testing is warranted.

Only a handful of hard and fast conclusions about DCI can be drawn from present knowledge. So elementary as to be innocuous, they are stated:

1. bubble inception or phase separation is the primary event triggering simple decompression sickness;
2. prevention of decompression sickness amounts to prevention (as a limit) of bubble inception or phase separation;
3. gradual pressure reductions prevent bubble formation.

As known by many, after the above attempts at consensus usually diverge. Modelers and table designers must then supply, or assume, gas exchange models, trigger points, and safe diving protocols which prevent or, at least, minimize phase inception and bubble growth.

Present notions of nucleation and cavitation suggest that decompression phase separation is random, yet highly probable, in body tissue. Once established, a gaseous phase will further grow by acquiring gas from adjacent saturated tissue, according to the strength of the free-dissolved gradient. Although exchange mechanisms are better understood, nucleation and stabilization mechanisms remain less so, and computationally elusive. Stochastic Monte Carlo bubble tracking methods are powerful, but only in supercomputer environments, due to the large number of events required for meaningful statistics over simulation time spans. Exchange models for entrained bubbles and coalescence dynamics are similarly complicated. In all cases, more knowledge about gas micronuclei and size distributions, tissue sites, thermodynamics properties, stabilization, and excitation mechanisms is necessary before computing power can be leveraged to decompression modeling.

But even with a paucity of knowledge, many feel that empirical practices and recent studies on bubbles and nuclei shed considerable light on growth and elimination processes, and time scales. Their consistency with underlying physical principles suggest directions for table and meter modeling,

beyond parameter fitting and extrapolation techniques. Recovering dissolved gas algorithms for short exposure times, phase models link to bubble mechanics and critical volume trigger points. Bubble and phase models support the efficacy of recently suggested safe diving practices, by simple virtue of dual phase mechanics:

1. reduced nonstop time limits;
2. safety stops (or shallow swimming ascents) in the 10-20 *fsw* zone, 1-2 *min* for dives in the 40-90 *fsw* range, 2-3 *min* for dives in the 90-240 *fsw* range;
3. ascent rates not exceeding 30 *fsw/min*;
4. restricted repetitive exposures, particularly beyond 100 *fsw*, based on reduction in permissible bubble excess over time;
5. restricted spike (shallow-to-deep) exposures based on excitation of additional micronuclei;
6. restricted multiday activity based on regeneration of micronuclei over longer time scales;
7. smooth coalescence of bounce and saturation limit points, consistent with bubble experiments;
8. consistent model treatment of altitude diving;

Bubble models also tend to be consistent with the utilitarian measures observed for diving practice. Conservatism may be downplayed in some meter implementations, yet medical authorities are becoming increasingly concerned about long term effects of breathing pressurized gases. On firmer principles, bubble models tend to corroborate safety measures in multiding, and thus one might reasonably expect to witness their further development. Said another way, bubble models have the right physical signatures for diving application.

#### Phase Versus Haldane Profiles

Both Suunto and Abysmal Diving have released products incorporating a modern phase algorithm, the above Reduced Gradient Bubble Model (RGBM), for diving. An iterative approach to staging diver ascents, the RGBM employs separated phase volumes as limit points, instead of the usual Haldane (maximum) critical tensions across tissue compartments. The model is inclusive (altitude, repetitive, mixed gas, decompression, saturation, nonstop exposures), treating both dissolved and free gas phase buildup and elimination. NAUI Technical Diving employed the RGBM to schedule nonstop and decompression training protocols on trimix, heliox, and nitrox while also testing gas switching alternatives for deep exposures. The RGBM has its roots in the earlier work of the Tiny Bubble Group at the University of Hawaii, drawing upon and extending the so-called Varying Permeability Model (VPM) to multiding, altitude, and mixed gas applications. While certainly not radical, the RGBM is both different and new on the diving scene. And not unexpectedly, the RGBM recovers the Haldane approach to decompression modeling in the limit of relatively safe (tolerably little) separated phase, with *tolerably little* a qualitative statement here.

The Suunto VYPER is an RGBM-based decometer for recreational diving (plus nitrox), while ABYSS/RGBM is a licensed Abysmal Diving software product. On the Internet, the sites [http : //www.suunto.fi/diving.index.html](http://www.suunto.fi/diving/index.html) and [http : //www.abysmal.com/index.html](http://www.abysmal.com/index.html) can be visited for information and description. Both are first-time-ever commercial products with realistic implementation of a diving phase algorithm across a wide spectrum of exposure extremes. And both accommodate user knobs for additional conservatism.

Here, our intent is to (just) look at the underpinnings of both meter and diveware implementations of the RGBM algorithm, one with extended range of applicability based on simple dual phase principles. Haldane approaches have dominated decompression algorithms for a very long time, and the RGBM has been long in coming on the commercial scene. With recent technical diving interest

in deep stop modeling, and concerns with repetitive diving in the recreational community, phase modeling is timely and pertinent. And, of course, since the RGBM extends the VPM, much of the following applies to the VPM directly.

Recent years have witnessed many changes and modifications to diving protocols and table procedures, such as shorter nonstop time limits, slower ascent rates, discretionary safety stops, ascending repetitive profiles, multilevel techniques, both faster and slower controlling repetitive tissues, smaller critical tensions (M-values), longer flying-after-diving surface intervals, and others. Stimulated by observation, Doppler technology, decompression meter development, theory, statistics, or safer diving consensus, these modifications affect a gamut of activity, spanning bounce to multiday diving. Of these changes, conservative nonstop time limits, no decompression safety stops, and slower ascent rates (around 30 *fsw/min*) are in vogue, and have been incorporated into many tables and meters. As you might expect, recent developments support them on operational, experimental, and theoretical grounds.

But there is certainly more to the story as far as table and meter implementations. To encompass such far reaching (and often diverse) changes in a unified framework requires more than the simple Haldane models we presently rely upon in 99% of our tables and dive computers. To model gas transfer dynamics, modelers and table designers need address both free and dissolved gas phases, their interplay, and their impact on diving protocols. Biophysical models of inert gas transport and bubble formation all try to prevent decompression sickness. Developed over years of diving application, they differ on a number of basic issues, still mostly unresolved today:

1. the rate limiting process for inert gas exchange, blood flow rate (perfusion) or gas transfer rate across tissue (diffusion);
2. composition and location of critical tissues (bends sites);
3. the mechanistics of phase inception and separation (bubble formation and growth);
4. the critical trigger point best delimiting the onset of symptoms (dissolved gas buildup in tissues, volume of separated gas, number of bubbles per unit tissue volume, bubble growth rate to name a few);
5. the nature of the critical insult causing bends (nerve deformation, arterial blockage or occlusion, blood chemistry or density changes).

Such issues confront every modeler and table designer, perplexing and ambiguous in their correlations with experiment and nagging in their persistence. And here comments are confined just to Type I (limb) and II (central nervous system) bends, to say nothing of other types and factors. These concerns translate into a number of what decompression modelers call dilemmas that limit or qualify their best efforts to describe decompression phenomena. Ultimately, such concerns work their way into table and meter algorithms, with the same caveats. The RGBM treats these issues in a natural way, gory details of which are found in the References.

The establishment and evolution of gas phases, and possible bubble trouble, involves a number of distinct, yet overlapping, steps:

1. nucleation and stabilization (free phase inception);
2. supersaturation (dissolved gas buildup);
3. excitation and growth (free-dissolved phase interaction);
4. coalescence (bubble aggregation);
5. deformation and occlusion (tissue damage and ischemia).

Over the years, much attention has focused on supersaturation. Recent studies have shed much light on nucleation, excitation and bubble growth, even though *in vitro*. Bubble aggregation, tissue damage, ischemia, and the whole question of decompression sickness trigger points are difficult to quantify in any model, and remain obscure. Complete elucidation of the interplay is presently asking too much. Yet, the development and implementation of better computational models is necessary to address problems raised in workshops, reports and publications as a means to safer diving.

The computational issues of bubble dynamics (formation, growth, and elimination) are mostly outside the traditional framework, but get folded into halftime specifications in a nontractable mode. The very slow tissue compartments (halftimes large, or diffusivities small) might be tracking both free and dissolved gas exchange in poorly perfused regions. Free and dissolved phases, however, do not behave the same way under decompression. Care must be exercised in applying model equations to each component. In the presence of increasing proportions of free phases, dissolved gas equations cannot track either species accurately. Computational algorithms tracking both dissolved and free phases offer broader perspectives and expeditious alternatives, but with some changes from classical schemes. Free and dissolved gas dynamics differ. The driving force (gradient) for free phase elimination increases with depth, directly opposite to the dissolved phase elimination gradient which decreases with depth. Then, changes in operational procedures become necessary for optimality. Considerations of excitation and growth invariably require deeper staging procedures than supersaturation methods. Though not as dramatic, similar constraints remain operative in multiexposures, that is, multilevel, repetitive, and multiday diving.

Other issues concerning time sequencing of symptoms impact computational algorithms. That bubble formation is a predisposing condition for decompression sickness is universally accepted. However, formation mechanisms and their ultimate physiological effect are two related, yet distinct, issues. On this point, most hypotheses makes little distinction between bubble formation and the onset of bends symptoms. Yet we know that silent bubbles have been detected in subjects not suffering from decompression sickness. So it would thus appear that bubble formation, per se, and bends symptoms do not map onto each other in a one-to-one manner. Other factors are truly operative, such as the amount of gas dumped from solution, the size of nucleation sites receiving the gas, permissible bubble growth rates, deformation of surrounding tissue medium, and coalescence mechanisms for small bubbles into large aggregates, to name a few. These issues are the pervue of bubble theories, but the complexity of mechanisms addressed does not lend itself easily to table, nor even meter, implementation. But implement and improve we must, so consider the RGBM (and VPM) issues and tacks taken in the VYPER and ABYSS implementations:

#### 1. Perfusion And Diffusion

Perfusion and diffusion are two mechanisms by which inert and metabolic gases exchange between tissue and blood. Perfusion denotes the blood flow rate in simplest terms, while diffusion refers to the gas penetration rate in tissue, or across tissue-blood boundaries. Each mechanism has a characteristic rate constant for the process. The smallest rate constant limits the gas exchange process. When diffusion rate constants are smaller than perfusion rate constants, diffusion dominates the tissue-blood gas exchange process, and vice-versa. In the body, both processes play a role in real exchange process, especially considering the diversity of tissues and their geometries. The usual Haldane tissue halftimes are the inverses of perfusion rates, while the diffusivity of water, thought to make up the bulk of tissue, is a measure of the diffusion rate.

Clearly in the past, model distinctions were made on the basis of perfusion or diffusion limited gas exchange. The distinction is somewhat artificial, especially in light of recent analyses of coupled perfusion-diffusion gas transport, recovering limiting features of the exchange process in appropriate limits. The distinction is still of interest today, however, since perfusion and diffusion limited algorithms are used in mutually exclusive fashion in diving. The obvious

mathematical rigors of a full blown perfusion-diffusion treatment of gas exchange mitigate against table and meter implementation, where model simplicity is a necessity. So one or another limiting models is adopted, with inertia and track record sustaining use. Certainly Haldane models fall into that categorization.

Inert gas transfer and coupled bubble growth are subtly influenced by metabolic oxygen consumption. Consumption of oxygen and production of carbon dioxide drops the tissue oxygen tension below its level in the lungs (alveoli), while carbon dioxide tension rises only slightly because carbon dioxide is 25 times more soluble than oxygen. Figure 3 (Part 10) compares the partial pressures of oxygen, nitrogen, water vapor, and carbon dioxide in dry air, alveolar air, arterial blood, venous blood, and tissue (cells).

Arterial and venous blood, and tissue, are clearly unsaturated with respect to dry air at 1 *atm*. Water vapor content is constant, and carbon dioxide variations are slight, though sufficient to establish an outgradient between tissue and blood. Oxygen tensions in tissue and blood are considerably below lung oxygen partial pressure, establishing the necessary ingradient for oxygenation and metabolism. Experiments also suggest that the degree of unsaturation increases linearly with pressure for constant composition breathing mixture, and decreases linearly with mole fraction of inert gas in the inspired mix.

Since the tissues are unsaturated with respect to ambient pressure at equilibrium, one might exploit this window in bringing divers to the surface. By scheduling the ascent strategically, so that nitrogen (or any other inert breathing gas) supersaturation just takes up this unsaturation, the total tissue tension can be kept equal to ambient pressure. This approach to staging is called the zero supersaturation ascent.

*The full blown RGBM treats coupled perfusion-diffusion transport as a two step flow process, with blood flow (perfusion) serving as a boundary condition for tissue gas penetration by diffusion. Depending on time scales and rate coefficients, one or another (or both) processes dominate the exchange. However, for both the VYPER and ABYSS implementations, perfusion is assumed to dominate, simplifying matters and permitting online calculations. Additionally, tissues and blood are naturally undersaturated with respect to ambient pressure at equilibration through the mechanism of biological inherent unsaturation (oxygen window), and the RGBM includes this debt in calculations.*

## 2. Bubbles

We do not really know where bubbles form nor lodge, their migration patterns, their birth and dissolution mechanisms, nor the exact chain of physico-chemical insults resulting in decompression sickness. Many possibilities exist, differing in the nature of the insult, the location, and the manifestation of symptoms. Bubbles might form directly (de novo) in supersaturated sites upon decompression, or possibly grow from preformed, existing seed nuclei excited by compression-decompression. Leaving their birth sites, bubbles may move to critical sites elsewhere. Or stuck at their birth sites, bubbles may grow locally to pain-provoking size. They might dissolve locally by gaseous diffusion to surrounding tissue or blood, or passing through screening filters, such as the lung complex, they might be broken down into smaller aggregates, or eliminated completely. Whatever the bubble history, it presently escapes complete elucidation. But whatever the process, the end result is very simple, both separated and dissolved gas must be treated in the transfer process.

Bubbles may hypothetically form in the blood (intravascular) or outside the blood (extravascular). Once formed, intravascularly or extravascularly, a number of critical insults are possible. Intravascular bubbles may stop in closed circulatory vessels and induce ischemia, blood sludging, chemistry degradations, or mechanical nerve deformation. Circulating gas emboli may occlude the arterial flow, clog the pulmonary filters, or leave the circulation to lodge in tissue

sites as extravascular bubbles. Extravascular bubbles may remain locally in tissue sites, assimilating gas by diffusion from adjacent supersaturated tissue and growing until a nerve ending is deformed beyond its pain threshold. Or, extravascular bubbles might enter the arterial or venous flows, at which point they become intravascular bubbles.

Spontaneous bubble formation in fluids usually requires large decompressions, like hundreds of atmospheres, somewhere near fluid tensile limits. Many feel that such circumstance precludes direct bubble formation in blood following decompression. Explosive, or very rapid decompression, of course is a different case. But, while many doubt that bubbles form in the blood directly, intravascular bubbles have been seen in both the arterial and venous circulation, with vastly greater numbers detected in venous flows (venous gas emboli). Ischemia resulting from bubbles caught in the arterial network has long been implied as a cause of decompression sickness. Since the lungs are effective filters of venous bubbles, arterial bubbles would then most likely originate in the arteries or adjacent tissue beds. The more numerous venous bubbles, however, are suspected to first form in lipid tissues draining the veins. Lipid tissue sites also possess very few nerve endings, possibly masking critical insults. Veins, thinner than arteries, appear more susceptible to extravascular gas penetration.

Extravascular bubbles may form in aqueous (watery) or lipid (fatty) tissues in principle. For all but extreme or explosive decompression, bubbles are seldom observed in heart, liver, and skeletal muscle. Most gas is seen in fatty tissue, not unusual considering the five-fold higher solubility of nitrogen in lipid tissue versus aqueous tissue. Since fatty tissue has few nerve endings, tissue deformation by bubbles is unlikely to cause pain locally. On the other hand, formations or large volumes of extravascular gas could induce vascular hemorrhage, depositing both fat and bubbles into the circulation as noted in animal experiments. If mechanical pressure on nerves is a prime candidate for critical insult, then tissues with high concentrations of nerve endings are candidate structures, whether tendon or spinal cord. While such tissues are usually aqueous, they are invested with lipid cells whose propensity reflects total body fat. High nerve density and some lipid content supporting bubble formation and growth would appear a conducive environment for a mechanical insult.

To satisfy thermodynamic laws, bubbles assume spherical shapes in the absence of external or mechanical (distortion) pressures. Bubbles entrain free gases because of a thin film, exerting surface tension pressure on the gas. Hydrostatic pressure balance requires that the pressure inside the bubble exceed ambient pressure by the amount of surface tension,  $\gamma$ . Figure 2 (Part 1) depicts the pressure balance in a spherical (air) bubble. At small radii, surface tension pressure is greatest, and at large radii, surface tension pressure is least.

Gases will also diffuse into or out of a bubble according to differences in gas partial pressures inside and outside the bubble, whether in free or dissolved phases outside the bubble. In the former case, the gradient is termed free-free, while in the latter case, the gradient is termed free-dissolved. Unless the surface tension is identically zero, there is always a gradient tending to force gas out of the bubble, thus making the bubble collapse on itself because of surface tension pressure. If surrounding external pressures on bubbles change in time, however, bubbles may grow or contract. Figure 3 (Part 1) sketches bubble gas diffusion under instantaneous hydrostatic equilibrium for an air bubble.

Bubbles grow or contract according to the strength of the free-free or free-dissolved gradient, and it is the latter case which concerns divers under decompression. The radial rate at which bubbles grow or contract depends directly on the diffusivity and solubility, and inversely on the bubble radius. A critical radius,  $r_c$ , separates growing from contracting bubbles. Bubbles with radius  $r > r_c$  will grow, while bubbles with radius  $r < r_c$  will contract. Limiting bubble growth and adverse impact upon nerves and circulation are issues when decompressing divers and aviators.

*The RGBM assumes that a size distribution of seeds (potential bubbles) is always present, and that a certain number is excited into growth by compression-decompression. An iterative process for ascent staging is employed to control the inflation rate of these growing bubbles so that their collective volume never exceeds a phase volume limit point. Gas mixtures of helium, nitrogen, and oxygen contain bubble distributions of different sizes, but possess the same phase volume limit point.*

### 3. Bubble Seeds

Bubbles, which are unstable, are thought to grow from micron size, gas nuclei which resist collapse due to elastic skins of surface activated molecules (surfactants), or possibly reduction in surface tension at tissue interfaces or crevices. If families of these micronuclei persist, they vary in size and surfactant content. Large pressures (somewhere near 10 atm) are necessary to crush them. Micronuclei are small enough to pass through the pulmonary filters, yet dense enough not to float to the surfaces of their environments, with which they are in both hydrostatic (pressure) and diffusion (gas flow) equilibrium. When nuclei are stabilized, and not activated to growth or contraction by external pressure changes, the skin (surfactant) tension offsets both the Laplacian (film) tension and any mechanical help from surrounding tissue. Then all pressures and gas tensions are equal. However, on decompression, the seed pockets are surrounded by dissolved gases at high tension and can subsequently grow (bubbles) as surrounding gas diffuses into them. The rate at which bubbles grow, or contract, depends directly on the difference between tissue tension and local ambient pressure, effectively the bubble pressure gradient. At some point in time, a critical volume of bubbles, or separated gas, is established and bends symptoms become statistically more probable. On compression, the micronuclei are crunched down to smaller sizes across families, apparently stabilizing at new reduced size. Bubbles are also crunched by increasing pressure because of Boyle's law, and then additionally shrink if gas diffuses out of them. As bubbles get smaller and smaller, they probably restabilize as micronuclei.

*The RGBM postulates bubble seeds with varying permeability. Bubble skins are assumed permeable down to 10 atm crushing pressure. The size of seeds excited into growth is inversely proportional to the supersaturation gradient. Beyond 10 atm, bubble seeds permit gas diffusion at a slower rate. The RGBM assumes bubble skins are stabilized by surfactants over unknown time scales, but that the seeds are persistent in the body. Bubble skins are probably molecularly activated, complex, biosubstances found throughout the body. Whatever the formation process, the RGBM assumes the size distribution is exponentially decreasing in size, that is, more smaller seeds than larger seeds in exponential proportions.*

### 4. Slow Tissue Compartments

Based on concerns in multiday and heavy repetitive diving, with the hope of controlling stair-casing gas buildup in exposures through critical tensions, slow tissue compartments (halftimes greater than 80 minutes) have been incorporated into some algorithms. Calculations, however, show that virtually impossible exposures are required of the diver before critical tensions are even approached, literally tens of hours of near continuous activity. As noted in many calculations, slow compartment cannot really control multiday diving through critical tensions, unless critical tensions are reduced to absurd levels, inconsistent with nonstop time limits for shallow exposures. That is a model limitation, not necessarily a physical reality. The physical reality is that bubbles in slow tissues are eliminated over time scales of days, and the model limitation is that the arbitrary parameter space does not accommodate such phenomena.

And that is no surprise either, when one considers that dissolved gas models are not suppose to track bubbles and free phases. Repetitive exposures do provide fresh dissolved gas for excited nuclei and growing free phases, but it is not the dissolved gas which is the problem just by itself.

When bubble growth is considered, the slow compartments appear very important, because, therein, growing free phases are mostly left undisturbed insofar as surrounding tissue tensions are concerned. Bubbles grow more gradually in slow compartments because the gradient there is typically small, yet grow over longer time scales. When coupled to free phase dynamics, slow compartments are necessary in multiding calculations.

*The RGBM incorporates a spectrum of tissue compartments, ranging from 1 min to 720 min, depending on gas mixture (helium, nitrogen, oxygen). Phase separation and bubble growth in slower compartments is a central focus in calculations.*

## 5. Venous Gas Emboli

While the numbers of venous gas emboli detected with ultrasound Doppler techniques can be correlated with nonstop limits, and the limits then used to fine tune the critical tension matrix for select exposure ranges, fundamental issues are not necessarily resolved by venous gas emboli measurements. First of all, venous gas emboli are probably not the direct cause of bends per se, unless they block the pulmonary circulation, or pass through the pulmonary traps and enter the arterial system to lodge in critical sites. Intravascular bubbles might first form at extravascular sites. According to studies, electron micrographs have highlighted bubbles breaking into capillary walls from adjacent lipid tissue beds in mice. Fatty tissue, draining the veins and possessing few nerve endings, is thought to be an extravascular site of venous gas emboli. Similarly, since blood constitutes no more than 8% of the total body capacity for dissolved gas, the bulk of circulating blood does not account for the amount of gas detected as venous gas emboli. Secondly, what has not been established is the link between venous gas emboli, possible micronuclei, and bubbles in critical tissues. Any such correlations of venous gas emboli with tissue micronuclei would unquestionably require considerable first-hand knowledge of nuclei size distributions, sites, and tissue thermodynamic properties. While some believe that venous gas emboli correlate with bubbles in extravascular sites, such as tendons and ligaments, and that venous gas emboli measurements can be reliably applied to bounce diving, the correlations with repetitive and saturation diving have not been made to work, nor important correlations with more severe forms of decompression sickness, such as chokes and central nervous system (CNS) hits.

Still, whatever the origin of venous gas emboli, procedures and protocols which reduce gas phases in the venous circulation deserve attention, for that matter, anywhere else in the body. The moving Doppler bubble may not be the bends bubble, but perhaps the difference may only be the present site. The propensity of venous gas emboli may reflect the state of critical tissues where decompression sickness does occur. Studies and tests based on Doppler detection of venous gas emboli are still the only viable means of monitoring free phases in the body.

*The RGBM uses nonstop time limits tuned to recent Doppler measurements, conservatively reducing them along the lines originally suggested by Spencer (and others), but within the phase volume constraint. The VYPER implementation penalizes ascent violations by requiring additional safety stop time dictated by risk analysis of the violation.*

## 6. Multidiving

Concerns with multidiving can be addressed through variable critical gradients, then tissue tensions in Haldane models. While variable gradients or tensions are difficult to codify in table frameworks, they are easy to implement in digital meters. Reductions in critical parameters also result from the phase volume constraint, a constraint employing the separated volume of gas in tissue as trigger point for the bends, not dissolved gas buildup alone in tissue compartments. The phase volume is proportional to the product of the dissolved-free gas gradient times a bubble number representing the number of gas nuclei excited into growth by the compression-decompression, replacing just slow tissue compartments in controlling multidiving.

In considering bubbles and free-dissolved gradients within critical phase hypotheses, repetitive criteria develop which require reductions in Haldane critical tensions or dissolved-free gas gradients. This reduction simply arises from lessened degree of bubble elimination over repetitive intervals, compared to long bounce intervals, and need to reduce bubble inflation rate through smaller driving gradients. Deep repetitive and spike exposures feel the greatest effects of gradient reduction, but shallower multiday activities are impacted. Bounce diving enjoys long surface intervals to eliminate bubbles while repetitive diving must contend with shorter intervals, and hypothetically reduced time for bubble elimination. Theoretically, a reduction in the bubble inflation driving term, namely, the tissue gradient or tension, holds the inflation rate down. Overall, concern is bubble excess driven by dissolved gas. And then both bubbles and dissolved gas are important. In such an approach, multiday exposures experience reduced permissible tensions through lessened free phase elimination over time spans of two days. Parameters are consistent with bubble experiments, and both slow and fast tissue compartments must be considered.

*The RGBM reduces the phase volume limit in multiday diving by considering free phase elimination and buildup during surface intervals, depending on altitude, time, and depth of previous profiles, Repetitive, multiday, and reverse profile exposures are tracked and impacted by critical phase volume reductions over appropriate time scales.*

## 7. Adaptation

Divers and caisson workers have long contended that tolerance to decompression sickness increases with daily diving, and decreases after a few weeks layoff, that in large groups of compressed air workers, new workers were at higher risk than those who were exposed to high pressure regularly. This acclimatization might result from either increased body tolerance to bubbles (physiological adaptation), or decreased number and volume of bubbles (physical adaptation). Test results are totally consistent with physical adaptation.

Yet, there is slight inconsistency here. Statistics point to slightly higher bends incidence in repetitive and multiday diving. Some hyperbaric specialists confirm the same, based on experience. The situation is not clear, but the resolution plausibly links to the kinds of first dives made and repetitive frequency in the sequence. If the first in a series of repetitive dives are kept short, deep, and conservative with respect to nonstop time limits, initial excitation and growth are minimized. Subsequent dives would witness minimal levels of initial phases. If surface intervals are also long enough to optimize both free and dissolved gas elimination, any nuclei excited into growth could be efficiently eliminated outside repetitive exposures, with adaptation occurring over day intervals as noted in experiments. But higher frequency, repetitive and multiday loading may not afford sufficient surface intervals to eliminate free phases excited by earlier exposures, with additional nuclei then possibly excited on top of existing phases. Physical adaptation seems less likely, and decompression sickness more likely, in the latter case. Daily regimens of a single bounce dive with slightly increasing exposure times are consistent with physical adaptation, and conservative practices. The regimens also require deepest dives first. In short, acclimatization is as much a question of eliminating any free phases formed as it is a question of crushing or reducing nuclei as potential bubbles in repetitive exposures. And then time scales on the order of a day might limit the adaptation process.

*The RGBM generates replacement bubble seed distributions on time scales of days, adding new bubbles to existing bubbles in calculations. Phase volume limit points are also reduced by the added effects of new bubbles.*

So, having waded through the foregoing, a next question is how does the RGBM compare with classical Haldane models as far as staging ascents, limiting multiexposures, and treating mixed gases? Generally, for short nonstop air diving, the RGBM reproduces the Spencer limits. For multiday diving in

spans shorter than 1-3 *hrs*, the RGBM reduces nonstop limits by 10% to 20% depending on surface interval, depth, altitude, and duration of present and previous dive, Multiday diving is impacted to lesser degree. Some comparisons appear in Table 1 for 3 days of repetitive air diving (120 *fsw*/10 *min* twice a day with 45 *min* surface interval). Computer choices are illustrative, not inductive.

Table 1. Nonstop Limits For VYPER/RGBM And Haldane Air Multidiving

Computer/Algorithm	Dive 1 ( <i>min</i> )	Dive 2 ( <i>min</i> )	Dive 3 ( <i>min</i> )	Dive 4 ( <i>min</i> )	Dive 5 ( <i>min</i> )	Dive 6 ( <i>min</i> )
VYPER/RGBM	10	6	9	5	9	5
SPYDER/Haldane	10	9	10	9	10	9
DATA PLUS/Haldane	12	6	12	6	12	6
DELPHI/Haldane	10	10	10	10	10	10
DC11/Haldane	6	6	6	6	6	6
DC12/Haldane	9	7	9	7	9	7
ALADIN/Haldane	8	8	8	8	8	8
ALADIN PRO/Haldane	10	7	10	7	10	7
SOURCE/Haldane	12	9	12	9	12	9

The VYPER/RGBM (first dive) nonstop limits (depth/time) are 150/6, 140/7, 130/9, 120/10, 110/13, 100/17, 90/22, 80/28, 70/36, 60/51, 50/69, and 40/120. In the mixed gas arena, Table 2 lists nonstop time limits for ranged trimix, that is, 13% to 17% helium, 61% to 53% nitrogen, and 26% to 30% oxygen, according to ABYSS/RGBM and ABYSS/ZHL (Buhlmann).

Table 2. Trimix Nonstop Limits For ABYSS/RGBM And ABYSS/ZHL (Haldane).

Depth ( <i>fsw</i> )	ABYSS/RGBM ( <i>min</i> )	ABYSS/ZHL ( <i>min</i> )
80	28	26
90	23	22
100	19	18
110	16	15
120	14	13
130	12	11
140	11	10
150	10	9

These limits are used by NAUI Technical Diving for training purposes. While both sets of nonstop time limits are different in Tables 3 and 4, the more dramatic effects of the RGBM show up for deep staging, as seen in Table 3. Comparative deep schedules for a trimix dive to 250 *fsw* for 30 *min* are contrasted, following a switch to air at 100 *fsw* and a switch to pure oxygen at 20 *fsw* on the way up. ABYSS/RGBM and ABYSS/ZHL are again employed, but with and without conservative safety knobs. In the case of ABYSS/ZHL, the outgassing tissue halftimes are increased by 1.5 in the conservative case, while for ABYSS/RGBM the bubble excitation radius is increased by 1.2 for comparison. Deeper stops are noticeably requisite in ABYSS/RGBM, but total decompression times are less than ABYSS/ZHL. The trimix is 33% helium, 51% nitrogen, and 16% oxygen.

Table 3. Deep Schedules According To ABYSS/RGBM And ABYSS/ZHL (Haldane)

Stop	Depth ( <i>fsw</i> )	ABYSS/ZHL ( <i>min</i> ) ( <i>standard</i> )	ABYSS/RGBM ( <i>min</i> ) ( <i>standard</i> )	ABYSS/ZHL ( <i>min</i> ) ( <i>safer</i> )	ABYSS/RGBM ( <i>min</i> ) ( <i>safer</i> )
1	180	0	0	0	1
2	170	0	1	0	1
3	160	0	1	0	1
4	150	0	1	0	1
5	140	0	1	0	2
6	130	0	2	0	2
7	120	0	2	0	2
8	110	0	2	1	2
9	100	0	2	2	2
10	90	2	2	3	3
11	80	2	2	4	3
12	70	2	3	5	4
13	60	5	5	8	6
14	50	7	6	12	7
15	40	12	9	18	19
16	30	18	12	28	13
17	20	16	10	28	11
18	10	28	16	48	18
		93	77	147	98

That in a nutshell is a comparison of major differences between phase and dissolved gas models. The phase models recover dissolved gas models for short and nominal exposures, but require deeper stops and shorter decompression times for longer and exceptional exposures. A rundown of the software configuration of the RGBM used in full blown simulations follows. The package is under constant refinement and updating.

1. Module: Three major routines (RGBMNX, RGBMHX, RGBMTMX) for nitrox, heliox, and trimix.
2. Source Code: 1640 Lines
3. Language/Compiler: FORTRAN 77/90, BASIC.
4. CRAY YMP Running Time: 1 sec for deep trimix profile with 5 gas switches on way up.
5. Input: altitude, bottom mixture, ascent/descent rate, switch levels and gas mixtures, pre-dive breathing gas, safety knobs, previous dive history.
6. Output: controlling tissue compartments, stop depth and times, supersaturation gradient, permissible supersaturation, effective bubble and gas parameters, critical phase volume, dive profile.
7. Cost: \$4500

Testing is central to diving, and much testing of bounce (single), nonstop diving has transpired. Repetitive and multiday exposures can neither claim, nor reap, the same benefits, and application

of any algorithm in the latter cases has witnessed higher bends statistics than in the former one. Reasons, impacting modeling, can be conjectured. Most tables and meters use dissolved gas models, and so long as the bulk of tissue gas remains in the dissolved state, the more correct and useful will prove such approaches. But as increasing proportion of free phases grow, by direct excitation of critical micronuclei or more gradual bubble coalescing transitions, the algorithm can lose predictive capability. Invariably, such conditions attend diving activity *extrapolated* outside model and test ranges, sometimes as a surprise.

Certainly any algorithm can be piecewise safe over tested ranges, but not always globally. Some implementations, as pointed out by Weathersby and Homer, may not be statistically rigorous, relying on much too small a set of exposure data to confidently predict outcome. Models not strongly correlated with tests can promulgate wide variation in predictive capability. Similarly, models can often *interpolate* within data, while failing to *extrapolate* outside the data. And then we must modify procedures to accommodate the extrapolation. A good point in question is the repetitive use of the USN tables. It is now clear that single, nonstop (bounce) dives, followed possibly by one more repetitive dive, form the test basis of the nonstop parts of the schedules. Yet, we observe that multiple repetitive dives permitted by the tables incur higher bends statistics, particularly in the deeper categories. This results from both model shortcomings and less reliable statistics. Adequate testing of any algorithm is always requisite, that is, descent rate, exposure profile, ascent rate, surface interval, and repetitive loading, as reiterated by Schreiner. And, because differences in diver response have been noted in hyperbaric chambers and open water, for the same schedules, questions of wet versus dry testing are valid. As discussed in the next Part, statistically significant testing, at the few percent level of decompression incidence, usually requires some 20-40 trials,

#### RGBM Validation And Testing

Models need validation and testing. Often, strict chamber tests are not possible, economically nor otherwise, and models employ a number of benchmarks and regimens to underscore viability. The following are some supporting the RGBM phase model and (released) nitrox, heliox, and trimix diving tables:

1. counterterror and countermeasures (LANL) exercises have used the RGBM (full up iterative deep stop version) for a number of years, logging some 327 dives on mixed gases (trimix, heliox, nitrox) without incidence of DCI – 35% were deco dives, and 25% were reps (no deco) with at least 2 hr SIs, and in the forward direction (deepest dives first);
2. NAUI Technical Diving has been diving the deep stop version for the past 2 yrs, some estimated 200 dives, on mixed gases down to 250 *fsw*, without a single DCI hit. Some 15 divers, late 1999, in France used the RGBM to make 2 mixed gas dives a day, without mishap, in cold water and rough seas;
3. modified RGBM recreational algorithms (Haldane imbedded with bubble reduction factors limiting reverse profile, repetitive, and multiday diving), as coded into SUUNTO, ABYSS, Cochrane decometers, lower an already low DCI incidence rate of approximately 1/10,000 or less. More RGBM decompression meters, including mixed gases, are in the works (3 not named at this time);
4. a cadre of divers and instructors in mountainous New Mexico, Utah, and Colorado have been diving the modified (Haldane imbedded again) RGBM at altitude, an estimated 350 dives, without peril. Again, not surprising since the altitude RGBM is slightly more conservative than the usual Cross correction used routinely up to about 8,000 ft elevation, and with estimated DCI incidence less than 1/10,000;
5. within decometer implementations of the RGBM, not a single DCI hit has been reported in nonstop and multiday categories, beyond 2,000 dives or more, up to now;

6. extreme chamber tests for mixed gas RGBM are in the works, and less stressful exposures will be addressed shortly – extreme here means 300 *fsw* and beyond;
7. probabilistic decompression analysis of some selected RGBM profiles, calibrated against similar calculations of the same profiles by Duke, help validate the RGBM on computational bases, suggesting the RGBM has no more theoretical risk than other bubble or dissolved gas models (Weathersby, Vann, Gerth methodology at USN and Duke).
8. all divers and instructors using RGBM decometers, tables, or NET software have been advised to report individual profiles to DAN Project Dive Exploration (Vann, Gerth, Denoble and many others at Duke).
9. ABYSS is a NET software package that offers the modified RGBM (folded over the Buhlmann ZHL) and soon the full up, deep stop version for any gas mixture, has a fairly large contingent of tech divers already using the RGBM and has not received any reports of DCI.
10. outside of proprietary (commercial) and RGBM Tables, mixed gas tables are a smorgasboard of no longer applicable Haldane dynamics and discretionary stop insertions, as witnessed by the collective comments of a very vocal and extremely competent, experienced technical diving community.

Because DCI is binomially distributed in incidence probability, many trials are often needed (or other close profiles) to fully validate any model at the 1% level. Additionally, full validation requires DCI incidences, the higher the number, the better, contrary to desired dive outcomes.

#### Reverse Profiles

Though the manifestations of DCI are statistically distributed, tables and meters use deterministic models to stage divers, with models broadly categorized as Haldane (dissolved phase) or bubble (combinations of dissolved and free phases). And model differences depend on profiles, exposures, and model assumptions. For diversity, we will focus on reverse diving profiles (RPs), wherein the second dive is deeper than the previous in any repetitive sequence. A summary of models, their underpinnings, correlations with data, and predictions for 100/60 and 60/100 RPs with variable surface intervals are first presented, and then for deeper and greater reverse profile increments.

Diving models address the coupled issues of gas uptake and elimination, bubbles, and pressure changes in different computational frameworks. Application of a computational model to staging divers, recall, is called a diving algorithm. Consider the foregoing computational models and staging regimens for the popular algorithms, namely, the perfusion limited, diffusion limited, thermodynamic, varying permeability, reduced gradient bubble, and tissue bubble diffusion algorithms. The first two are Haldane models (workhorse algorithms in most tables and meters), while the remaining four are bubble models in the generic sense (coming online in tables and meters, often driven by tech diving). The first two track just dissolved gas transfer, using *critical tissue tensions* as limit points, while the latter four treat both dissolved and free phase transfer, using *free phase volumes* as limit points.

#### 1. Comparative Model Reverse Profiles

Employing the above described algorithms, we consider model predictions for RPs, extract underlying features and tendencies, and draw comparisons. The code, *DECOMP*, containing a number of model kernels, is employed for calculations.

The RPs (100/60 and 60/100) are normalized to roughly the same NDLs so that the nonstop time limits at 100 *fsw* and 60 *fsw* are 15 *min* and 50 *min*, respectively. This normalization leans slightly toward the conservative side as far as NDLs are concerned. Table 4 encapsulates the results for the MTM, BDM, TM, VPM, RGBM, and TBDM. Typically, tracking bubble growth and dissolved gas buildup and elimination, phase models require slightly more decompression times for the RPs. The MTM and BDM are comparable, the TM, VPM, and TBDM

also track closely, and the RGBM is most conservative. These profiles are relatively shallow, and the RP increment is small ( $\Delta d = 40 \text{ fsw}$ ). Generally, bubble models affect deep and prolonged exposures the most, requiring deeper stops, but usually shorter overall decompression times. The effect is not seen here trendwise, but will reappear as the RP increments increase. Bubble and Haldane models overlap for short and shallow exposures, such as these RPs, and entries in Table 4 are no exception. The observation has often been made that not much free gas phase has been excited during short and shallow exposures, and then, bubble models should collapse to dissolved gas phase models in the limit.

When exposures are deeper and RP increments are greater than  $40 \text{ fsw}$ , model differentiations between dissolved gas and dual phase models appear in the staging regimens, as seen in Table 5, contrasting the MTM and RGBM only for 160/40 and 40/160 RPs. Clearly phase models (RGBM) require deeper staging but shorter times, as seen in Table 5 for the same surface intervals in Table 4. The bottom times are  $7 \text{ min}$  and  $100 \text{ min}$  at  $160 \text{ fsw}$  and  $40 \text{ fsw}$  respectively in Table 5.

## 2. NEST Reverse Profile Data

The Nuclear Emergency Strategy Team (NEST) is involved in counterterrorism and countermeasures related to nuclear and biological threats. Exercises and tests have yielded scattered data about RPs across a spectrum of breathing gas mixtures (nitrox, heliox, trimix). Recent activities have settled on trimix as the bottom and ascent gas, with pure oxygen breathed at  $20 \text{ fsw}$ . Mixtures range 13-40% helium, 44-64% nitrogen, and 16-30% oxygen. RP increments,  $\Delta d$ , vary from  $40 - 120 \text{ fsw}$ , and surface intervals are nominally greater than  $60 \text{ min}$ . The RGBM is the staging algorithm.

Table 6 tabulates results of NEST field activities, with nominal surface intervals of an hour or more. Maximum bottom depth is  $250 \text{ fsw}$ , and exposures are near trimix NDLs. Dives are grouped in RP categories of  $40 \text{ fsw}$ . The NDLs computed from the RGBM for trimix in the range down to  $250 \text{ fsw}$  are roughly:

$100 \text{ fsw}$	$8 - 10 \text{ min}$
$150 \text{ fsw}$	$5 - 7 \text{ min}$
$200 \text{ fsw}$	$4 - 6 \text{ min}$
$250 \text{ fsw}$	$2 - 3 \text{ min}$

similar in duration to Haldane trimix NDLs. The ascent profile is different under the RGBM, as compared to standard Haldane staging. And this is well known, especially in technical diving circles where mixed gas diving pushes the exposure envelope.

Table 4. Comparative RPs And Algorithms

Algorithm	Dive 1	Deco 1	Surface Interval	Dive 2	Deco 2
MTM	100/15	none	30	60/30	10/2
BDM		none			10/2
TM		none			10/1
VPM		none			10/2
RGBM		none			10/4
TBDM		none			10/3
MTM	60/30	none		100/15	10/2
BDM		none			10/2
TM		none			10/2
VPM		none			10/3
RGBM		none			10/5
TBDM		none			10/3
MTM	100/15	none	60	60/30	10/1
BDM		none			10/1
TM		none			10/1
VPM		none			10/2
RGBM		none			10/4
TBDM		none			10/2
MTM	60/30	none		100/15	10/1
BDM		none			10/1
TM		none			10/1
VPM		none			10/3
RGBM		none			10/6
TBDM		none			10/2
MTM	100/15	none	120	60/30	none
BDM		none			none
TM		none			10/1
VPM		none			10/1
RGBM		none			10/3
TBDM		none			10/1
MTM	60/30	none		100/15	10/1
BDM		none			10/1
TM		none			10/1
VPM		none			10/2
RGBM		none			10/4
TBDM		none			10/2
MTM	100/15	none	240	60/30	none
BDM		none			none
TM		none			none
VPM		none			none
RGBM		none			10/1
TBDM		none			10/1
MTM	60/30	none		100/15	none
BDM		none			none
TM		none			none
VPM		none			10/1
RGBM		none			10/2
TBDM		none			10/1

Table 5. Comparative MTM And RGBM (Deep) RPs

Algorithm	Dive 1	Deco 1	Surface Interval	Dive 2	Deco 2
MTM	160/7	10/3	30	40/100	none
RGBM		10/1			10/4
MTM	40/100	none		160/7	10/11
RGBM		none			30/1,20/1,10/2
MTM	160/7	10/3	60	40/100	none
RGBM		10/1			10/3
MTM	40/100	none		160/7	10/3
RGBM		none			20/1,10/2
MTM	160/7	10/3	120	40/100	none
RGBM		10/1			10/2
MTM	40/100	none		160/7	10/3
RGBM		none			20/1,10/1
MTM	160/7	10/3	240	40/100	none
RGBM		10/1			10/1
MTM	40/100	none		160/7	10/3
RGBM		none			20/1,10/1

The incidence rate,  $p$ , in Table 6 is 6.7%, with highest count in the 40 - 120 *fsw* increment range. There are many variables here, such as staging depth, gas mixture, exposure time, and surface interval not tabulated separately.

Table 6. NEST RP Risk Table

Dives	RP Increment ( <i>fsw</i> )	Probable Hits
36	0 - 40	0
18	40 - 80	2
6	80 - 120	2

Practices for the deeper increments may border the yo-yo category, though no prior history of repetitive diving existed. Exercises continue, and data will grow. Trends are apparent in the above Table 6, but further analysis is required.

### 3. Comparative NAUI Table Reverse Profiles

NAUI Training adopts a conservative view on RPs, contraindicated over many hour time intervals. Within the NAUI Tables (US Navy Tables with reduced NDLs), implications of this approach are discussed and quantified. NAUI Training has an admirable record of diving safety and surety, and statistics underscore this fact. And so do other Training Agencies (PADI, SSI, YMCA, NASDS, TDI).

The US Navy Tables with reduced NDLs and the NAUI modifications based on consideration of multilevel activity (ascending or descending profiles) were discussed. For reference and comparison, a set of NAUI (modified) US Navy Tables is given in Figure 1 (Part 5), exhibiting reduced nonstop time limits, consistent with present safety margins associated with lower Doppler scores (Spencer reduction). But there is much more to the NAUI modification of the basic US Navy Tables, based on multilevel considerations. And that modification, coupled to recommended 1 *hr* surface intervals (SI) for repetitive diving, also impacts RPs favorably, as will be shown.

For the modified Tables (Figure 1), multilevel dives that stay to the left of the nonstop time limits never violate critical tensions, and are (hypothetically) sanctioned. Dive computers, of course, perform the same exercise underwater, comparing instantaneous values of computed tissue tensions in all compartments, throughout the duration of the dive, against stored  $M$ -values to estimate time remaining and time at a stop.

The set of NAUI NDLs corresponds to a reduced set of critical tensions,  $M_0$ ,  $\Delta M$ , given by,

$$M_0 = 102, 86, 70, 57, 51, 50 \text{ fsw} \quad (1)$$

$$\Delta M = 2.27, 2.01, 1.67, 1.34, 1.26, 1.19 \quad (2)$$

in round numbers for the same set of tissue halftimes,  $\tau$ . With risk analysis performed by US Navy investigators (Part 8), the relative probability,  $p$ , of DCI in (always) diving to the NAUI NDLs limits is bounded by,

$$1\% < p < 5\% \quad (3)$$

yet remembering that divers never dive consistently to (any) Table limits. Interpolating between bounding NDLs, the estimated probability,  $p$ , is

$$p < 2.5\% \quad (4)$$

at the limit point of diving to NAUI NDLs. Simple difference weighting between bounding NDLs and NAUI NDLs was invoked for the estimate.

Consider the scripted RPs within the NAUI Table framework. In a rather simple sense, these RPs represent multilevel diving with nonzero surface intervals, at least when only dissolved gases are tracked. However, with bubble growth under decompression fueled by high tissue tensions, such extensions and analogies probably breakdown. Profiles are 100 *fsw* and 60 *fsw* for 15 *min* and 30 *min* as also contrasted in Table 4.

Table 7. NAUI Tables And RPs

Algorithm	Dive 1	Deco 1	Surface Interval	Dive 2	Deco 2
NAUI Tables	100/15	none	30	60/30	15/5
	60/30	none		100/15	15/15
	100/15	none	60	60/30	none
	60/30	none		100/15	15/15
	100/15	none	120	60/30	none
	60/30	none		100/15	15/5
	100/15	none	240	60/30	none
	60/30	none		100/15	none

Clearly the step nature of Table decompression formats is evident in Table 7. The decompression stops at 15 *fsw* do not smoothly decrease in time as surface interval time increases. NAUI, of course, requires all training to be nonstop diving, so such profiles would not occur routinely.

#### 4. NAUI Reverse Profile Statistics

In the 10 years since NAUI introduced these Tables, nearly 1,000,000 divers were certified at an entry level. This represents some 5,000,000 actual dives, mainly performed above 60 *fsw*, with surface intervals beyond 60 *min*, and no more than 2 dives per day. Reverse profiles are not suggested, and training regimens also mandate minimum 60 *min* surface intervals, depth floors at 60 *fsw*, and less than 3 dives per day. To build diver confidence, much activity occurs

at depths in the 20 - 30 *fsw* range. All recreational NAUI diving is limited to 130 *fsw*, as are the NAUI Tables. These limits and mandates restrict all diving, and certainly impact RPs favorably.

Accident reports gathered by NAUI in this time average 50 per year (required for insurance and liability coverage). Of these 50 reports, only 5 relate (average) to DCI afflictions. This suggests an incidence rate,  $p$ , on the order of  $1 \times 10^{-5}$ , certainly a very low annual rate. Other Training Agencies (PADI, SSI, YMCA, NASDS, TDI) should echo the same ballpark figure, since training regimens across recreational diving are roughly the same.

Thus, any RPs probably range 30 - 40 *fsw* as far as depth increment,  $\Delta d$ , in training maneuvers. This is small, as are actual training depths. Based on low DCI incidence rate, NAUI Table conservatism, small RP increment, and shallow staging depths, RPs appear to have not been a major problem for NAUI Training Operations. But as RP depths and increments increase, the situation becomes less clear and riskier.

### *Exercises*

1. Match the following problematic profiles to model issues addressed by the BDM, MTM, TM, VPM, RGBM, or TBDM (Parts 6,5)? Deepest dive not first? Yo, yo diving? Multiple inert gas switches during dive? Multilevel diving? Rapid ascents? Short interval repetitive diving? Multiday diving? Saturation exposures? Altitude diving?
2. Link the MTM, BDM, TM, VPM, RGBM, and TBDM to the 5 overlapping steps leading to bubble trouble (Parts 6,5)? Nucleation and stabilization? Supersaturation? Bubble excitation and growth? Coalescence? Tissue deformation and occlusion?

### *Related Reading*

1. Buhlmann A.A., 1984, *Decompression/Decompression Sickness*, Berlin: Springer Verlag.
2. Gilliam B., Webb D. and von Maier R., 1995, *Deep Diving*, San Diego: Watersports.
3. Hamilton R.W., 1975, *Development Of Decompression Procedures For Depths In Excess Of 400 Feet*, Undersea And Hyperbaric Medical Society Report, WS: 2-28-76, Bethesda.
4. Hills B.A., 1977, *Decompression Sickness*, New York: John Wiley And Sons.
5. Lang M.A. and Vann R.D., 1992, *Proceedings Of The American Academy Of Underwater Sciences Repetitive Diving Workshop*, AAUSDSP-RDW-02-92, Costa Mesa.
6. Lang M.A. and Egstrom G.H., 1990, *Proceedings Of The American Academy Of Underwater Sciences Biomechanics Of Safe Ascents Workshop*, American Academy Of Underwater Sciences Diving Safety Publication, AAUSDSP-BSA-01-90, Costa Mesa.
7. Lang M.A. and Hamilton R.W., 1989, *Proceedings Of The American Academy Of Underwater Sciences Dive Computer Workshop*, University Of Southern California Sea Grant Publication, USCSG-TR-01-89, Los Angeles.
8. Loyst K., Huggins K.E. and Steidley M., 1991, *Dive Computers*, San Diego: Watersports.
9. Mount T. and Gilliam B., 1991, *Mixed Gas Diving*, San Diego: Watersport.
10. Neal J.G., O'Leary T.R. and Wienke B.R., 1999, *Trimix Diving*, Fort Lauderdale: Underwater Dynamics Incorporated.

11. Rutkowski D., 1989, *Nitrox Manual*, San Diego: International Association of Nitrox Divers (IAND).
12. Schreiner H.R. and Hamilton R.W., 1987, *Validation Of Decompression Tables*, Undersea And Hyperbaric Medical Society Publication 74 (VAL), Bethesda.
13. Sheffield P.J., 1990, *Flying After Diving*, Undersea And Hyperbaric Medical Society Publication 77 (FLYDIV), Bethesda.
14. Wallace D., 1975, *NOAA Diving Manual*, Washington DC: US Government Printing Office.
15. Wienke B.R., 1998, *Physics, Physiology, And Decompression Theory For The Technical And Commercial Diver*, National Association Of Underwater Instructors Publication, Tampa.
16. Wienke B.R., 1994, *Basic Diving Physics And Application*, Flagstaff: Best.
17. Wienke B.R., 1991, *High Altitude Diving*, National Association Of Underwater Instructors Technical Publication, Montclair.

PART 7: DECOMPRESSION THEORY  
DECOMPRESSION RISK AND STATISTICS

Systematics And Issues

The systematics of gas exchange, nucleation, bubble growth and elimination, and decompression are so complicated that theories only reflect pieces of the puzzle. Computational algorithms, tables, and manned testing are requisite across a spectrum of activities. And the potential of electronic devices to process tables of information or detailed equations underwater is near maturity, with virtually any algorithm or model amenable to digital implementation. Pressures for even more sophisticated algorithms are expected to grow.

Still computational models enjoy varying degrees of success or failure. More complex models address a greater number of issues, but are harder to codify in decompression tables. Simpler models are easier to codify, but are less comprehensive. Some models are based on first principles, but many are not. Application of models can be subjective in the absence of definitive data, the acquisition of which is tedious, sometimes controversial, and often ambiguous. If deterministic models are abandoned, statistical analysis can address the variability of outcome inherent to random occurrences, but only in manner indifferent to specification of controlling mechanisms. The so called dose-reponse characteristics of statistical analysis are very attractive in the formulation of risk tables. Applied to decompression sickness incidence, tables of comparative risk offer a means of weighing contributing factors and exposure alternatives. At the basis of statistical and probabilistic analyses of decompression sickness is the binomial distribution. The binomial distribution is the fundamental frequency distribution governing random events.

Binomial Distribution

Decompression sickness is a hit, or no hit, situation. Statistics are binary, as in coin tossing. Probabilities of occurrence are determined from the binomial distribution, which measures the numbers of possibilities of occurrence and nonoccurrence in any number of events, given the incidence rate. Specifically, the probability,  $P$ , in a random sample of size,  $N$ , for  $n$  occurrences of decompression sickness and  $m$  nonoccurrences, takes the form,

$$P(n) = \frac{N!}{n! m!} p^n q^m , \quad (1)$$

with,

$$n + m = N , \quad (2)$$

$p$  the underlying incidence rate (average number of cases of decompression sickness), and  $q$ ,

$$q = 1 - p , \quad (3)$$

the underlying nonincidence. The discrete probability distributions,  $P$ , are the individual terms of the binomial expansion of  $(p + q)^N$ ,

$$(p + q)^N = \sum_{n=0}^N P(n) = 1 . \quad (4)$$

In risk analysis,  $p$  and  $q$  are also the failure and success rates, gleaned, for instance, from random or strategic sampling of arbitrary lot sizes. Obviously, the larger the sample size, the better are the estimates of  $p$  or  $q$ . Once  $p$  or  $q$  is determined, the binomial statistics and probabilities are also fixed. The statistical mean,  $M$ , and variance,  $s$ , are given by,

$$M = \sum_{n=1}^N nP(n) = pN , \quad (5)$$

$$s = \sum_{n=1}^N (n - M)^2 P(n) = pqN \quad , \quad (6)$$

the usual measures of a statistical distribution. The square root of the variance is the standard deviation. The cumulative probability for more than  $n$  cases of decompression sickness,  $P_{>}(n)$ , is written,

$$P_{>}(n) = \sum_{j=n+1}^N P(j) = 1 - \sum_{j=0}^n P(j) \quad , \quad (7)$$

and the probability of less than  $n$  cases,  $P_{<}(n)$ , is similarly,

$$P_{<}(n) = \sum_{j=0}^{n-1} P(j) = 1 - \sum_{j=n}^N P(j) \quad . \quad (8)$$

The probability of nonoccurrence in any set of  $N$  trials is simply,

$$P(0) = q^N \quad , \quad (9)$$

while the probability of total occurrence in the same number,  $N$ , of trials is given by,

$$P(N) = p^N \quad . \quad (10)$$

The binomial distribution is a special case of the multinomial distribution describing processes in which several results having fixed probabilities,  $p_l$ ,  $q_l$ , for  $l = 1, L$ , are possible. Separate probabilities are given by the individual terms in the general multinomial expansion,

$$(p_1 + q_1 + \dots + p_L + q_L)^N = \sum_{n_1, \dots, n_{L-1}=0}^N P(n_1, \dots, n_{L-1}) = 1 \quad , \quad (11)$$

as in the binomial case. The normal distribution is a special case of the binomial distribution when  $N$  is very large and variables are not necessarily confined to integer values. The Poisson distribution is another special case of the binomial distribution when the number of events,  $N$ , is also large, but the incidence,  $p$ , is small.

#### Normal Distribution

The normal distribution is an analytic approximation to the binomial distribution when  $N$  is very large, and  $n$ , the observed value (success or failure rate), is not confined to integer values, but ranges continuously,

$$-\infty \leq n \leq \infty \quad . \quad (12)$$

Normal distributions thus apply to continuous observables, while binomial and Poisson distributions apply to discontinuous observables. Statistical theories of errors are ordinarily based on normal distributions.

For the same mean,  $M = pN$ , and variance,  $s = pqN$ , the normal distribution,  $P$ , written as a continuously varying function of  $n$ ,

$$P(n) = \frac{1}{(2\pi s)^{1/2}} \exp[-(n - M)^2/2s] \quad , \quad (13)$$

is a good approximation to the binomial distribution in the range,

$$\frac{1}{N+1} < p < \frac{N}{N+1} \quad , \quad (14)$$

and within three standard deviations of the mean,

$$pN - 3 (pqN)^{1/2} \leq n \leq pN + 3 (pqN)^{1/2} . \quad (15)$$

The distribution is normalized to one over the real infinite interval,

$$\int_{-\infty}^{\infty} P dn = 1 . \quad (16)$$

The probability that a normally distributed variable,  $n$ , is less than or equal to  $b$  is,

$$P_{<}(b) = \int_{-\infty}^b P dn , \quad (17)$$

while the corresponding probability that  $n$  is greater than or equal to  $b$  is,

$$P_{>}(b) = \int_b^{\infty} P dn . \quad (18)$$

The normal distribution is extremely important in statistical theories of random variables. By the central limit theorem, the distribution of sample means of identically distributed random variables is approximately normal, regardless of the actual distribution of the individual variables.

#### Poisson Distribution

The Poisson distribution is a special case of the binomial distribution when  $N$  becomes large, and  $p$  is small, and certainly describes all discrete random processes whose probability of occurrence is small and constant. The Poisson distribution applies substantially to all observations made concerning the incidence of decompression sickness in diving, that is,  $p \ll 1$  as the desired norm. The reduction of the binomial distribution to the Poisson distribution follows from limiting forms of terms in the binomial expansion, that is,  $P(n)$ .

In the limit as  $N$  becomes large, and  $p$  is much smaller than one, we have,

$$\frac{N!}{(N-n)!} = N^n , \quad (19)$$

$$q^n = (1-p)^{N-n} = \exp(-pN) , \quad (20)$$

and therefore the binomial probability reduces to,

$$P(n) = \frac{N^n p^n}{n!} \exp(-pN) = \frac{M^n}{n!} \exp(-M) , \quad (21)$$

which is the discrete Poisson distribution. The mean,  $M$ , is given as before,

$$M = pN \quad (22)$$

and the variance,  $s$ , has the same value,

$$s = pN , \quad (23)$$

because  $q$  is approximately one. The cumulative probabilities,  $P_{>}(n)$  and  $P_{<}(n)$ , are the same as those defined in the binomial case, a summation over discrete variable,  $n$ . It is appropriate to employ the Poisson approximation when  $p \leq .10$ , and  $N \geq 10$  in trials. Certainly, from a numerical point of view, the Poisson distribution is easier to use than than binomial distribution. Computation of factorials is a lesser task, and bookkeeping is minimal for the Poisson case.

In addition to the incidence of decompression sickness, the Poisson distribution describes the statistical fluctuations in such random processes as the number of cavalry soldiers kicked and killed by horses, the disintegration of atomic nuclei, the emission of light quanta by excited atoms, and the appearance of cosmic ray bursts. It also applies to most rare diseases.

Probabilistic Decompression

Table 1 lists corresponding binomial decomposition probabilities,  $P(n)$ , for 1% and 10% underlying incidence (99% and 90% nonincidence), yielding 0, 1, and 2 or more cases of decompression sickness. The underlying incidence,  $p$ , is the (fractional) average of hits.

As the number of trials increases, the probability of 0 or 1 occurrences drops, while the probability of 2 or more occurrences increases. In the case of 5 dives, the probability might be as low as 5%, while in the case of 50 dives, the probability could be 39%, both for  $p = .01$ . Clearly, odds even percentages would require testing beyond 50 cases for an underlying incidence near 1%. Only by increasing the number of trials for fixed incidences can the probabilities be increased. Turning that around, a rejection procedure for 1 or more cases of decompression sickness at the 10% probability level requires many more than 50 dives. If we are willing to lower the confidence of the acceptance, or rejection, procedure, of course, the number of requisite trials drops. Table 1 also shows that the test practice of accepting an exposure schedule following 10 trials without incidence of decompression sickness is suspect, merely because the relative probability of nonincidence is high, near 35%.

Questions as to how safe are decompression schedules have almost never been answered satisfactorily. As seen, large numbers of binary events are required to reliably estimate the underlying incidence. One case of decompression sickness in 30 trials could result from an underlying incidence,  $p$ , bounded by .02 and .16 roughly. Tens more of trials are necessary to shrink those bounds.

Table 1. Probabilities Of Decompression Sickness For Underlying Incidences.

$N$ (dives)	$n$ (hits)	$P(n)$	
		$p = .01$ $q = .99$	$p = .10$ $q = .90$
5	0	.95	.59
	1	.04	.33
	2 or more	.01	.08
10	0	.90	.35
	1	.09	.39
	2 or more	.01	.26
20	0	.82	.12
	1	.16	.27
	2 or more	.02	.61
50	0	.61	.01
	1	.31	.03
	2 or more	.08	.96

Biological processes are highly variable in outcome. Formal correlations with outcome statistics are then generally requisite to validate models against data. Often, this correlation is difficult to firmly establish (couple of percent) with fewer than 1,000 trial observations, while ten percent correlations can be obtained with 30 trials, assuming binomial distributed probabilities. For decompression analysis, this works as a disadvantage, because often the trial space of dives is small. Not discounting the possibly small trial space, a probabilistic approach to the occurrence of decompression sickness is useful and necessary. One very successful approach, developed and tuned by Weathersby, and others for decompression sickness in diving, called maximum likelihood, applies theory or models to diving data and adjusts the parameters until theoretical prediction and experimental data are in as close agreement as possible.

Validation procedures require decisions about uncertainty. When a given decompression procedure is repeated with different subjects, or the same subjects on different occasions, the outcome is not constant. The uncertainty about the occurrence of decompression sickness can be quantified with statistical statements, though, suggesting limits to the validation procedure. For instance, after

analyzing decompression incidence statistics for a set of procedures, a table designer may report that the procedure will offer an incidence rate below 5%, with 90% confidence in the statement. Alternatively, the table designer can compute the probability of rejecting a procedure using any number of dive trials, with the rejection criteria any arbitrary number of incidences. As the number of trials increases, the probability of rejecting a procedure increases for fixed incidence criteria. In this way, relatively simple statistical procedures can provide vital information as to the number of trials necessary to validate a procedure with any level of acceptable risk, or the maximum risk associated with any number of incidences and trials.

One constraint usually facing the statistical table designer is a paucity of data, that is, number of trials of a procedure. Data on hundreds of repetitions of a dive profile are virtually nonexistent, excepting bounce diving perhaps. As seen, some 30-50 trials are requisite to ascertain procedure safety at the 10% level. But 30-50 trials is probably asking too much, is too expensive, or generally prohibitive. In that case, the designer may try to employ global statistical measures linked to models in a more complex trial space, rather than a single profile trial space. Integrals of risk parameters, such as bubble number, supersaturation, separated phase, etc., over exposures in time, can be defined as probability measures for incidence of decompression sickness, and the maximum likelihood method then used to extract appropriate constants.

#### Maximum Likelihood

We can never measure any physical variable exactly, that is, without error. Progressively more elaborate experimental or theoretical efforts only reduce the possible error in the determination. In extracting parameter estimates from data sets, it is necessary to also try to minimize the error (or data scatter) in the extraction process. A number of techniques are available to the analyst, including the well known maximum likelihood approach.

The measure of any random occurrence,  $p$ , can be a complicated function of many parameters,  $\mathbf{x} = (x_k, k = 1, K)$ , with the only constraint,

$$0 \leq p(\mathbf{x}) \leq 1 \quad , \quad (24)$$

for appropriate values of the set,  $\mathbf{x}$ . The measure of nonoccurrence,  $q$ , is then by conservation of probability,

$$q(\mathbf{x}) = 1 - p(\mathbf{x}) \quad , \quad (25)$$

over the same range,

$$0 \leq q(\mathbf{x}) \leq 1 \quad . \quad (26)$$

Multivalued functions,  $p(\mathbf{x})$ , are often constructed, with specific form dictated by theory or observation over many trials or tests. In decompression applications, the parameters,  $\mathbf{x}$ , may well be the bubble-nucleation rate, number of venous gas emboli, degree of supersaturation, amount of pressure reduction, volume of separated gas, ascent rate, or combinations thereof. Parameters may also be integrated in time in any sequence of events, as a global measure, though such measures are more difficult to analyze over arbitrary trial numbers.

The likelihood of any outcome,  $\Phi$ , of  $N$  trials is the product of individual measures of the form,

$$\Phi(n) = p^n q^m = p^n (1 - p)^m \quad , \quad (27)$$

given  $n$  cases of decompression sickness and  $m$  cases without decompression sickness, and,

$$n + m = N \quad . \quad (28)$$

The natural logarithm of the likelihood,  $\Psi$ , is easier to use in applications, and takes the form,

$$\Psi = \ln \Phi = n \ln p + m \ln (1 - p) \quad , \quad (29)$$

and is maximized when,

$$\frac{\partial \Psi}{\partial p} = 0 \quad . \quad (30)$$

In terms of the above, we then must have,

$$\frac{n}{p} - \frac{m}{1-p} = 0 \quad , \quad (31)$$

trivially requiring,

$$p = \frac{n}{n+m} = \frac{n}{N} \quad , \quad (32)$$

$$1-p = q = \frac{m}{n+m} = \frac{m}{N} \quad . \quad (33)$$

Thus, the likelihood function is maximized when  $p$  is the actual incidence rate, and  $q$  is the actual nonincidence rate. The multivalued probability functions,  $p(x)$ , generalize in the maximization process according to,

$$\frac{\partial \Psi}{\partial p} = \sum_{k=1}^K \frac{\partial \Psi}{\partial x_k} \frac{\partial x_k}{\partial p} = 0 \quad , \quad (34)$$

satisfied when,

$$\frac{\partial \Psi}{\partial x_k} = 0 \quad \text{for } k = 1, K \quad . \quad (35)$$

In application, such constraints are most easily solved on computers, with analytical or numerical methods.

In dealing with a large number of decompression procedures, spanning significant range in depth, time, and environmental factors, an integrated approach to maximum likelihood and risk is necessary. Integral measures,  $p(x, t)$  and  $q(x, t)$ , can be defined over assumed decompression risk,  $\zeta(x, t)$ ,

$$p(x, t) = 1 - \exp \left[ - \int_0^t \zeta(x, t') dt' \right] \quad , \quad (36)$$

$$q(x, t) = \exp \left[ - \int_0^t \zeta(x, t') dt' \right] \quad , \quad (37)$$

with  $t'$  any convenient time scale, and  $\zeta$  any assumed risk, such as bubble number, saturation, venous emboli count, etc. as mentioned. Employing  $p(x, t)$  and  $q(x, t)$  in the likelihood function, and then maximizing according to the data, permits maximum likelihood estimation of  $\zeta(x, t)$ . Such an approach can be employed in decompression table fabrication, yielding good statistical estimates on incidence rates as a function of exposure factors.

#### Saturation Bends Probability

Many factors contribute to bends susceptibility. Age, obesity, temperature, physical condition, alcohol, and cigarettes are a few. Whatever the contributing factors, the distribution of bends depths for saturation exposures has been characterized in terms of the saturation tension,  $Q$ , and ambient pressure,  $P$ . by Hills. This characterization is not only of academic interest, but is also useful in assigning formal risk to decompression formats.

The distribution of saturation bends depths,  $\chi$ , fits a Weibull function. This is true for all breathing mixtures, nitrox, heliox, trimix, etc. If cumulative fraction of air bends cases up to  $G$  is  $\chi$ , the survivor fraction,  $1 - \chi$ , satisfies,

$$\ln (1 - \chi) = - \left[ \frac{G - 14.3}{25.1} \right]^{4.73} \quad (38)$$

for cumulative bends probability,  $\chi$ , the usual integral over bends risk,  $\zeta$ , as a function of gradient,  $G$ ,

$$\chi = \int_0^G \zeta(G') dG' \quad (39)$$

with saturation bends gradient,  $G$ , measured in *fsw*,

$$G = Q - P \quad (40)$$

As the gradient grows, the survivor function approaches zero exponentially. The smallest bends gradient is 14.3 *fsw*, which can be contrasted with the average value of 26.5 *fsw*. The root mean square gradient is 27.5 *fsw*. At 27 *fsw*, the survivor fraction is 0.96, while 67% of survivors fall in the range,  $26.5 \pm 7.6$  *fsw*, with 7.6 *fsw* the standard deviation. For gas mixtures other than air, the general form is given by,

$$\ln(1 - \chi) = -\epsilon \left[ \frac{(P_f - 20.5)}{(P_i - 33.0)} - \frac{1}{f_i} \right]^\delta \quad (41)$$

where  $f_i$  is the total volume fraction of inert breathing gases, for  $G = P_f - P_i$ , and with  $\epsilon$ ,  $\delta$  constants.

The efficiency of the Weibull distribution in providing a good fit to the saturation data is not surprising. The Weibull distribution enjoys success in reliability studies involving multiplicities of fault factors. It obviously extends to any set of hyperbaric or hypobaric exposure data, using any of the many parameter risk variables described above.

#### Table And Profile Risks

A global statistical approach to table fabrication consists of following a risk measure, or factor  $p$ , throughout and after sets of exposures, tallying the incidence of DCI, and then applying maximum likelihood to the risk integral in time, extracting any set of risk constants optimally over all dives in the maximization procedure. In analyzing air and helium data, Weathersby assigned risk as the difference between tissue tension and ambient pressure divided by ambient pressure. One tissue was assumed, with time constant ultimately fixed by the data in ensuing maximum likelihood analysis. The measure of nonincidence,  $q$ , was taken to be the exponential of risk integrated over all exposure time,

$$q(\kappa, \tau) = \exp \left[ - \int_0^\infty \zeta(\kappa, \tau, t') dt' \right] , \quad (42)$$

$$\zeta(\kappa, \tau, t') = \kappa \frac{p(t') - p_a}{p_a} , \quad (43)$$

with  $\kappa$  a constant determined in the likelihood maximization,  $p_a$  ambient pressure, and  $p(t')$  the instantaneous Haldane tension for tissue with halftime,  $\tau$ , also determined in the maximization process, corresponding to arbitrary tissue compartments for the exposure data. Other more complex likelihood functions can also be employed, for instance, the separated phase volume according to the varying permeability and reduced gradient bubble models,

$$\zeta(\kappa, \xi, \tau, t') = \kappa \Lambda(t') G(t') , \quad (44)$$

$$\Lambda(t') = \left[ 1 - \frac{r(t')}{\xi} \right] , \quad (45)$$

with  $\Lambda$  the permissible bubble excess,  $r$  the bubble radius,  $G$  the bubble diffusion gradient (dissolved-free gas), and  $\kappa$  and  $\xi$  constants determined in the fit maximization of the data. Another risk possibility is the tissue ratio,

$$\zeta(\kappa, \tau, t') = \kappa \frac{p(t')}{p_a} , \quad (46)$$

a measure of interest in altitude diving applications.

Hundreds of air dives were analyzed using this procedure, permitting construction of decompression schedules with 95% and 99% confidence (5% and 1% bends probability). These tables were published by US Navy investigators, and Table 2 tabulates the corresponding nonstop time limits ( $p = 0.05, 0.01$ ), and also includes the standard US Navy (Workman) limits for comparison. Later re-evaluations of the standard set of nonstop time limits estimate a probability rate of 1.25% for the limits. In actual usage, the incidence rates are below 0.001%, because users do not dive to the limits generally.

Table 2. Nonstop Time Limits For 1% And 5% DCI Probability.

depth $d$ (fsw)	nonstop limit $t_n$ (min) $p = .05$	nonstop limit $t_n$ (min) $p = .01$	nonstop limit $t_n$ (min) US Navy
30	240	170	
40	170	100	200
50	120	70	100
60	80	40	60
70	80	25	50
80	60	15	40
90	50	10	30
100	50	8	25
110	40	5	20
120	40	5	15
130	30	5	10

For the past 10-15 years, this probabilistic approach to assessing risk in diving has been in vogue. Sometimes this can be confusing, or misleading, since definitions or terms, as presented, are often mixed. Also confusing are risk estimates varying by factors of 10 to 1,000, and distributions serving as basis for analysis, also varying in size by the same factors. So, before continuing with a risk analysis of recreational profiles, a few comments are germane.

Any set of statistical data can be analyzed directly, or sampled in smaller chunks. The smaller sets (samples) may or may not reflect the parent distribution, but if the analyst does his work correctly, samples reflecting the parent distribution can be extracted for study. In the case of dive profiles, risk probabilities extracted from sample profiles try to reflect the incidence rate,  $p$ , of the parent distribution ( $N$  profiles, and  $p$  underlying DCI rate). The incidence rate,  $p$ , is the most important metric, followed by the shape of the distribution in total as measured by the variance,  $s$ . For smaller sample of profile size,  $K < N$ , we have mean incidences,  $Q$ , for sample incidence rate,  $r$ ,

$$Q = rK \tag{47}$$

and variance,  $v$ ,

$$v = r(1 - r)K \tag{48}$$

By the central limit theorem, the distribution of sample means,  $Q$ , is normally distributed about parent (actual) mean,  $M$ , with variance,  $v = s/K$ . Actually, the distribution of sample means,  $Q$ , is normally distributed no matter what the distribution of samples. This important fact is the basis for error estimation with establishment of confidence intervals,  $\chi$ , for  $r$ , with estimates denoted,  $r_{\pm}$ ,

$$r_{\pm} = r \pm \chi \left[ \frac{s}{K} \right]^{1/2} \tag{49}$$

$$0 < \chi < 1 \tag{50}$$

The sample binomial probability,  $B(k)$ , is analogously,

$$B(k) = \frac{K!}{k! j!} r^k (1-r)^j \quad (51)$$

constrained,  $k + j = K$ , for  $k$  number of DCI hits, and normalized,

$$\sum_{k=1}^K B(k) = 1 \quad (52)$$

with important limiting property, if  $K \rightarrow \infty$ , then  $B(k) \rightarrow 0$ , when,  $r \ll 1$ .

For example, if 12 cases of DCI are reported in a parent set of 7,896 profiles, then,

$$N = 7896 \quad (53)$$

$$p = \frac{12}{7896} = .0015 \quad (54)$$

Smaller samples might be used to estimate risk, via sample incidence,  $r$ , with samples possibly chosen to reduce computer processing time, overestimate  $p$  for conservancy sake, focus on a smaller subregion of profiles, or any other reason. Thus, one might nest all 12 DCI incidence profiles in a smaller sample,  $K = 1,000$ , so that the sample risk,  $r = 12/1,000 = 0.012$ , is larger than  $p$ . Usually though the analyst wishes to mirror the parent distribution in the sample. If the parent is a set of benign, recreational, no decompression, no multiday dive profiles, and the sample mirrors the parent, then both risks,  $p$  and  $r$ , are reasonably true measures of actual risk associated with recreational diving. If sample distributions chosen are not representative of the class of diving performed, risk estimates are not trustworthy. For instance, if a high risk set of mixed gas decompression profiles were the background against which recreational dive profiles were compared, all estimates would be skewed and faulty (actually underestimated in relative risk, and overestimated in absolute risk). For this parent set,  $N$  is large,  $p$  is small, with mean,  $M = pN = 0.0015 \times 7896 = 12$ , and the applicable binomial statistics smoothly transition to Poisson representation, convenient for logarithmic and covariant numerical analysis (on a computer). Additionally, any parent set may be a large sample of a megaset, so that  $p$  is itself an estimate of risk in the megaset.

Turns out that our parent distribution above is just that, a subset of larger megaset, namely, the millions and millions of recreational dives performed and logged over the past 30 years, or so. The above set of profiles was collected in training and vacation diving scenarios. The set is recreational (no decompression, no multiday, light, benign) and representative, with all the distribution metrics as listed. For reference and perspective, sets of recreational profiles collected by others (Gilliam, NAUI, PADI, YMCA, DAN) are similar in context, but larger in size,  $N$ , and smaller in incidence rate,  $p$ . Data and studies reported by many sources quote,  $N > 1,000,000$ , with,  $p < 0.00001 = 0.001\%$ . Obviously our set has higher rate,  $p$ , though still nominally small, but the same shape. So our estimates will be liberal (overestimate risk).

To perform risk analysis, a risk estimator need be employed. For diving, dissolved gas and phase estimators are useful. Two, detailed earlier, are used here. First is the dissolved gas supersaturation ratio, historically coupled to Haldane models,  $\phi$ ,

$$\phi = \kappa \frac{p - \lambda p_a}{p_a} \quad (55)$$

and second,  $\psi$ , is the separated phase, invoked by phase models,

$$\psi = \gamma \left[ 1 - \frac{r}{\xi} \right] G \quad (56)$$

For simplicity, the asymptotic exposure limit is used in the likelihood integrals for both risk functions,

$$1 - r(\kappa, \lambda) = \exp \left[ - \int_0^\infty \phi(\kappa, \lambda, t) dt \right] \quad (57)$$

$$1 - r(\gamma, \xi) = \exp \left[ - \int_0^\infty \psi(\gamma, \xi, t) dt \right] \quad (58)$$

with *hit – no hit*, likelihood function,  $\Omega$ , of form,

$$\Omega = \prod_{k=1}^K \Omega_k \quad (59)$$

$$\Omega_k = r_k^{\delta_k} (1 - r_k)^{1 - \delta_k} \quad (60)$$

where,  $\delta_k = 0$  if DCI does not occur in profile,  $k$ , or,  $\delta_k = 1$  if DCI does occur in profile,  $k$ . To estimate  $\kappa$ ,  $\lambda$ ,  $\gamma$ , and  $\xi$  in maximum likelihood, a modified Levenberg-Marquardt algorithm is employed (*SNLSE*, Common Los Alamos Applied Mathematical Software Library), just a nonlinear least squares data fit to an arbitrary function (minimization of variance over  $K$  datapoints here), with  $L1$  error norm. Additionally, using a random number generator for profiles across 1,000 parallel SMP (Origin 2000) processors at LANL, we construct 1,000 subsets, with  $K = 2,000$  and  $r = 0.006$ , for separate likelihood regression analysis, averaging  $\kappa$ ,  $\lambda$ ,  $\gamma$ , and  $\xi$  by weighting the inverse variance.

For recreational diving, both estimators are roughly equivalent, because little dissolved gas has separated into free phases (bubbles). Analysis shows this true for all cases examined, in that estimated risks for both overlap at the 95% confidence level. The only case where dissolved gas and phase estimators differ (slightly here) is within repetitive diving profiles. The dissolved gas estimator cues on gas buildup in the slow tissue compartments (staircasing for repets within an hour or two), while the phase estimator cues on bubble gas diffusion in the fast compartments (dropping rapidly over hour time spans). This holding true within all recreational diving distributions, we proceed to the risk analysis.

Nonstop limits (NDLs), denoted  $t_n$  as before, from the US Navy, PADI, and NAUI Tables, and those employed by the Oceanic decometer provide a set for comparison of relative DCI risk. Listed below in Table 3 are the NDLs and corresponding risks (in parentheses) for the profile, assuming ascent and descent rates of 60 *fsw/min* (no safety stops). Haldane and RGBM estimates vary little for these cases, and only the phase estimates are included.

Table 3. Risk Estimates For Various NDLs.

$d$ ( <i>fsw</i> )	USN $t_n$ ( <i>min</i> )	PADI $t_n$ ( <i>min</i> )	NAUI $t_n$ ( <i>min</i> )	Oceanic $t_n$ ( <i>min</i> )
35	310 (4.3%)	205 (2.0%)		181 (1.3%)
40	200 (3.1%)	140 (1.5%)	130 (1.4%)	137 (1.5%)
50	100 (2.1%)	80 (1.1%)	80 (1.1%)	80 (1.1%)
60	60 (1.7%)	55 (1.4%)	55 (1.4%)	57 (1.5%)
70	50 (2.0%)	40 (1.2%)	45 (1.3%)	40 (1.2%)
80	40 (2.1%)	30 (1.3%)	35 (1.5%)	30 (1.3%)
90	30 (2.1%)	25 (1.5%)	25 (1.5%)	24 (1.4%)
100	25 (2.1%)	20 (1.3%)	22 (1.4%)	19 (1.2%)
110	20 (2.2%)	13 (1.1%)	15 (1.2%)	16 (1.3%)
120	15 (2.0%)	13 (1.3%)	12 (1.2%)	13 (1.3%)
130	10 (1.7%)	10 (1.7%)	8 (1.3%)	10 (1.7%)

Risks are internally consistent across NDLs at each depth, and agree with the US Navy assessments in Table 2. Greatest underlying and binomial risks occur in the USN shallow exposures. The PADI, NAUI, and Oceanic risks are all less than 2% for this set, thus binomial risks for single DCI incidence are less than 0.02%. PADI and NAUI have reported that field risks ( $p$ ) across all exposures are less than 0.001%, so considering their enviable track record of diving safety, our estimates are liberal. Oceanic risk estimates track as the PADI and NAUI risks, again, very safely.

Next, the analysis is extended to profiles with varying ascent and descent rates, safety stops, and repetitive sequence. Table 4 lists nominal profiles (recreational) for various depths, exposure and travel times, and safety stops at 5 *msw*. Mean DCI estimates,  $r$ , are tabulated for both dissolved gas supersaturation ratio (ZHL) and bubble number excess (RGBM) risk functions, with, employing maximum variance,  $r_{\pm} = r \pm .004$ .

Table 4. Dissolved And Separated Phase Risk Estimates For Nominal Profiles.

profile ( <i>depth/time</i> )	descent rate ( <i>msw/min</i> )	ascent rate ( <i>msw/min</i> )	safety stop ( <i>depth/time</i> )	risk $r_{RGBM}$	risk $r_{ZHL}$
14 <i>msw/38 min</i>	18	9	5 <i>msw/3 min</i>	.0034	.0062
19 <i>msw/38 min</i>	18	9	5 <i>msw/3 min</i>	.0095	.0110
28 <i>msw/32 min</i>	18	9		.0200	.0213
37 <i>msw/17 min</i>	18	9	5 <i>msw/3 min</i>	.0165	.0151
18 <i>msw/31 min</i>	18	9	5 <i>msw/3 min</i>	.0063	.0072
	18	9		.0088	.0084
	18	18		.0101	.0135
	18	18	5 <i>msw/3 min</i>	.0069	.0084
17 <i>msw/32 min</i> SI 176 <i>min</i>	18	9	5 <i>msw/3 min</i>		
13 <i>msw/37 min</i> SI 174 <i>min</i>	18	9	5 <i>msw/3 min</i>		
23 <i>msw/17 min</i>	18	18	5 <i>msw/3 min</i>	.0127	.0232

The ZHL (Buhlmann) NDLs and staging regimens are widespread across decompression meters presently, and are good representation for Haldane risk analysis. The RGBM is newer and more modern (and more physically correct), and is coming online in decometers and associated software. For recreational exposures, the RGBM collapses to a Haldane dissolved gas algorithm. This is reflected in the risk estimates above, where estimates for both models differ little.

Simple comments hold for the analyzed profile risks. The maximum relative risk is 0.0232 for the 3 dive repetitive sequence according to the Haldane dissolved risk estimator. This translates to 0.2% binomial risk, which is comparable to the maximum NDL risk for the PADI, NAUI, and Oceanic NDLs. Again, this type of dive profile is common, practiced daily on liveboards, and benign. According to Gilliam, the absolute incidence rate for this type of diving is less than 0.02%. Again, our analyses overestimate risk.

Effects of slower ascent rates and safety stops are noticeable at the 0.25% to 0.5% level in relative surfacing risk. Safety stops at 5 *m* for 3 *min* lower relative risk an average of 0.3%, while reducing the ascent rate from 18 *msw/min* to 9 *msw/min* reduces relative risk an average of 0.35%.

Staging, NDLs, and constraints imposed by decometer algorithms are consistent with acceptable and safe recreational diving protocols. Estimated absolute risk associated across all ZHL NDLs and staging regimens analyzed herein is less than 0.232%, probably much less in actual practice. That is, we use  $p = 0.006$ , and much evidence suggests  $p < 0.0001$ , some ten times safer.

Implicit in such formulations of risk tables are assumptions that given decompression stress is more likely to produce symptoms if it is sustained in time, and that large numbers of separate events may culminate in the same probability after time integration. Though individual schedule segments may not be replicated enough to offer total statistical validation, categories of predicted safety can always be grouped within subsets of corroborating data. Since the method is general, any model parameter or meaningful index, properly normalized, can be applied to decompression data, and the full power of statistical methods employed to quantify overall risk. While powerful, such statistical methods are neither deterministic nor mechanistic, and cannot predict on first principles. But as a means to table fabrication with quoted risk, such approaches offer attractive pathways for analysis.

Validation procedures for schedules and tables can be quantified by a set of procedures based on statistical decompression analysis:

1. select or construct a measure of decompression risk, or a probabilistic model;
2. evaluate as many dives as possible, and especially those dives similar in exposure time, depth, and environmental factors;
3. conduct limited testing if no data is available;
4. apply the model to the data using maximum likelihood;
5. construct appropriate schedules or tables using whatever incidence of decompression sickness is acceptable;
6. release and then collect profile statistics for final validation and tuning.

Questions of what risk is acceptable to the diver vary. Sport and research divers would probably opt for very small risk (0.01% or less), while military and commercial divers might live with higher risk (1%), considering the nearness of medical attention in general. Many factors influence these two populations, but fitness and acclimatization levels would probably differ considerably across them. While such factors are difficult to fold into any table exercise or analysis, the simple fact that human subjects in dive experiments exhibit higher incidences during testing phases certainly helps to lower the actual incidence rate in the field, noted by Bennett and Lanphier.

#### *Exercises*

1. What is the probability,  $P(3)$ , for 3 DCI cases in 100 dives, given an underlying incidence rate of 5% (Part 7)? What is the probability,  $Q(97)$ , for 97 cases for no DCI in the same sample (Part 7)?
2. What is the probability,  $P(1)$ , for one hit (DCI) in 20 dives with underlying incidence,  $p = .01$  (Part 7, Table 1)? What is the probability,  $P_{>}(2)$ , for two or more hits in 20 dives for the same underlying incidence (Part 7, Table 1)?
3. What is the survivor fraction,  $1 - \chi$ , for decompression of saturated air divers across,  $G = 35$  fsw (Part 7)? What is the cumulative DCI incidence rate,  $\chi$  (Part 7)?
4. What can you say about the DCI relative incidence,  $p$ , for a nonstop exposure at 80 fsw for 40 min (Part 8, Table 2)? What can you say about the (old) USN nonstop limit of 200 min at 40 fsw (Part 7, Table 2)?
5. A table modeler wants to use maximum likelihood in fitting the data to a DCI risk function,  $\phi$ , of the temporal form,  $\phi = \exp(-qt)$ . for 1000 trial dives with some 200 cases of DCI. What are the risk forms,  $\rho$  and  $\sigma$  (probabilities) (Part 7)? What are the asymptotic limits,  $\rho(\infty)$  and  $\sigma(\infty)$ ? What is the value of  $q$  for the asymptotic forms (Part 7)?

*Related Reading*

1. *Bowker A.H. and Lieberman G.J., 1964, Engineering Statistics, Engelwood Cliffs: Prentice-Hall.*
2. *Gradshteyn I.S. and Ryzhik I.M., 1965, Table Of Integrals, Series, And Products, New York: Academic Press.*
3. *Hills B.A., 1977, Decompression Sickness, New York: John Wiley And Sons.*
4. *Johnson L.W. and Riess R.D., 1962, Numerical Analysis, Reading: Addison Wesley.*
5. *Mathews J. and Walker R.L., 1975, Mathematical Methods Of Physics, New York: W.A. Benjamin.*
6. *Parzen E., 1970, Modern Probability Theory And Its Applications, New York: John Wiley And Sons. Reading: Addison Wesley.*
7. *Weathersby P.K., Survanshi S. and Homer L.D., 1985, Statistically Based Decompression Tables: Analysis Of Standard Air Dives, 1950-1970, Naval Medical Research Institute Report, NMRI 85-16, Bethesda.*
8. *Wienke B.R., 1998, Physics, Physiology, And Decompression Theory For The Technical And Commercial Diver, National Association Of Underwater Instructors Publication, Tampa.*

## PART 8: DECOMPRESSION THEORY COMPUTING AND DECOMPRESSION ALGORITHMS

### Computing Advances

Computing technology has made incredible progress in the past 50 years. In 1945, there were no stored program computers. Today, a few thousand dollars will purchase a desktop personal computer with more performance, more memory, and more disk storage than a million dollar computer in 1965. This rapid rate of improvement has come from advances in technology used to build the computer and from innovation in computer design. Performance increase is sketched in Figure 1, in terms of a nominal 1965 minicomputer. Performance growth rates for supercomputers, minicomputers, and mainframes are near 20% per year, while performance growth rate for microcomputers is closer to 35% per year. Supercomputers are the most expensive, ranging from one to tens of millions of dollars, and microprocessors are the least expensive, ranging from a few to tens of thousands of dollars. Supercomputers and mainframes are usually employed in high end, general purpose, compute intensive applications. Minicomputers and microprocessors address the same functionality, but often in more diverse roles and applications. The latter class of computers is usually more portable, because they are generally smaller in size. They are on your desktop.

### Supercomputers

The label *supercomputer* usually refers to the fastest, biggest, and most powerful computer in existence at any time. In the 1940s, supercomputers were employed in the design of nuclear weapons (as still today), In the 1950s, supercomputers were first used in weather forecasting, while in the 1960s, computational fluid dynamics problems in the aerospace industry were solved on supercomputers. In the 1970s, 1980s, and 1990s seismological data processing, oil reservoir simulation, structural analysis of buildings and vehicles, quantum field theory, circuit layout, econometric modeling, materials and drug design, brain tomography and imaging, molecular dynamics, global climate and ocean circulation modeling, and semiconductor fabrication joined the supercomputing revolution. Very few areas in science and engineering have not been impacted by supercomputers. Diving is still on the fringes of supercomputing, but applications are growing, particularly in the areas of dive profile analysis, statistics, data management, and biomodeling. Smaller and less powerful computers are now employed for monitoring, controlling, directing, and analyzing dives, divers, equipment, and environments. Wrist computers perform rudimentary decompression calculations and stage ascents with mostly Haldane models.

Operational supercomputers today process data and perform calculations at rates of  $10^9$  floating point operations per second (*gigaflops*), that is,  $10^9$  adds, subtracts, multiplies, or divides per second. At the edge today, and in the marketplace, are shared memory processors (SMPs) providing users with  $10^{12}$  floating point operations per second (*teraflops*), impressively opening yet another age in computational science. These machines are massively parallel processors (MPPs), involving thousands of computing nodes processing trillions of data points. To support these raw computing speeds, networks transmitting data at gigabits/sec, and fast storage exchanging terabytes of information over simulation times are also requisite. Ultrafast, high resolution, graphics servers, able to process voluminous amounts of information, offer an expeditious means to assess output data. Differences in raw processing speeds between various components in a high performance computing environment can degrade overall throughput, conditions termed *latencies*, or simply, manifest time delays in processing data. Latencies are parasitic to sustained computing performance. Latencies develop at the nodes connecting various computer, storage, network, terminal, and graphics devices, simply because of impedance mismatch in data handling capabilities.

Obviously, computers work on processing information, doing calculations, and fetching and storing data in steps. A set of operations, performed in sequential fashion by one processor, is termed *serial*. A set of operations performed in any fashion, by any number of processors, is roughly termed *parallel*. Serial computing architectures, once the standard, are now being replaced by parallel

computing architectures, with anywhere from tens to thousands of central processing units (CPUs). Processors themselves can be *scalar*, or *vector*, that is, operating on a single entity, or group of entities (numbers).

The architectural feature associated with supercomputers in the 1970s was vector processing. Vector processing allowed large groups of numbers, or vectors, to be processed in parallel, resulting in performance speedups by factors of ten or more (compared to generational improvements on the order of 2 or 3). In the early 1980s, parallel supercomputing was introduced, allowing multiple processors to work concurrently on a single problem. By the end of the century, significantly greater computing parallelism (combining tens of thousands of processing units perhaps), and architectures that integrate modalities, such as numeric and symbolic processing, may be possible. As in the past, software developments on future state of the art supercomputers will probably trail hardware advances, perhaps with increasing distance due to increasingly more complex superparallel systems.

#### Networks

Networks are the backbone of modern computer systems. Supercomputers without high speed communications links and network interfaces are degraded in application processing speed, limited by the slowest component in the computing platform. Gigaflop computers need gigabit/sec network transmission speeds to expedite the flow of information.

Data, voice, image, and full motion video can be digitally encoded, and sent across a variety of physical media, including wire, fiber optics, microwaves, and satellites. The assumption is that all information transmitted will be digital. The greater the number of systems, people, and processes that need to transmit information to one another, the greater the speeds and bandwidths required. Like water in a pipe, to get more information through a network, one can increase the rate of flow (*speed*), and/or increase the amount that can flow through cross sectional area (*bandwidth*). Applications under development today presage the needs to transfer data very quickly tomorrow. To perform as a utility, that is, usefully communicate anything, anytime, anywhere, a network must possess four attributes:

1. connectivity – ability to move information regardless of the diversity of the media;
2. interoperability – ability of diverse intelligent devices to communicate with one another;
3. manageability – ability to be monitored, and to change with applications and devices;
4. distributed applications and connective services – ability to provide easy access to tools, data, and resources across different computing platforms, or organizations.

Commercial telecommunications links (modem connections to the Internet) are extremely slow, in the vicinity of 10 kilobits/sec to 56 kilobits/sec. Even dedicated communications lines are low speed, that is, T1 and T3 links (1.4 megabits/sec and 43 megabits/sec respectively), and cannot feed supercomputers with information fast enough to support economical processing. The 4 terabytes from a seismic map of an oil field in the Gulf (8 square miles) would take about 3 - 4 days to transmit from one site to another for processing. The 1 million dive profiles projected in DAN Project Dive Safety stacks up to hundreds of gigabytes, depending on resolution.

Advances in massively parallel, large memory computers, and high speed networks have created computing platforms, depicted in Figure 2, which allow researchers to execute supercodes that generate enormous data files. The supercomputing environment depicted in Figure 2 can be found in large Universities, National and Regional Laboratories, dedicated Commercial Computing Centers, and various Governmental Agencies. The one in Figure 2 depicts the superplatform at the Los Alamos National Laboratory. These facilities are available to the commercial user, and computing costs range from \$100-\$300 per hour on vector supercomputers (YMP, T90, J90) to \$1 - \$4 per node per hour on massively parallel supercomputers (CM5, T3D, SP2 Cluster, Origin 2000 SMP).

## Storage

Supercodes generate enormous amounts of data, and a typical large application will generate from tens of gigabytes up to several terabytes of data. Such requirements are one to two orders of magnitude greater than the comfortable capacities of present generation storage devices. New high performance data systems (HPDS) are online to meet the very large data storage and handling. Systems consist of fast, large capacity storage devices that are directly connected to a high speed network, and managed by software distributed across workstations. Disk devices are used to meet high speed and fast access requirements, while tape devices are employed to meet high speed and high capacity requirements. Storage devices usually have a dedicated workstation for storage and device management, and to oversee data transfer. Put simply, computer systems use a hierarchy to manage information storage:

1. primary storage – fast, solid state memory contained in the processor;
2. direct access storage – magnetic or optical disks, connected to the processor, providing fast access;
3. sequential access storage – magnetic tape cassettes or microfilm, providing large capacity.

Transfer rates in fast HPDS systems are presently near 800 megabits/sec. Moving down the hierarchy, access time goes up, storage capacity increases, and costs decrease. Today, of all computing components, the cost of storage is decreasing the most rapidly. A few hundred dollars will buy gigabyte hard drives for your PC. Renting storage commercially is also cheap (\$20 gigabyte/month).

In supercomputing today, there has been a paradigm shift towards shared memory processors (SMPs), many fast CPUs (64 or more) sharing common memory within an SMP, and communicating with other SMPs across very fast interconnects (switches) using message passing. Since 1999, the technology for their platform development has seen enormous advance, as depicted in Figure 3. Such advancement is ushering in the era of many tens of teraflops raw computing power.

## Grand Challenge Applications

Grand Challenge problems are computational problems requiring the fastest computers, networks, and storage devices in existence, and problems whose solutions will have tremendous impact on the economic well being of the United States. Vortices in combustion engines, porous flow in oil bearing substrates, fluid turbulence, three dimensional seismic imaging, ductile and brittle fracture of materials under stress, materials by computer design, global convection of tectonic plates, geomagnetic field generation, ocean and atmospheric circulation, high impact deformation and flow, air and groundwater pollution, global climate modeling, elastic-plastic flow, brain tomography, HIV correlations, bubble generation and cavitating flow, and many others are just such problems. Statistical modeling coupled to maximum likelihood for millions of trials, as employed to estimate DCI incidence in DAN Project Dive Safety, borders and pushes the Grand Challenge computational problem category, particularly as the number of model fit parameters increases beyond 5.

The scale of computational effort for nominal Grand Challenge problems can be gleaned from Table 3, listing floating point operations, computer memory, and data storage requirements. As a reference point, the 6 million volumes in the Library Of Congress represent 24 terabytes of information. The simulations listed in Table 3 run for many hours on the CM5, the Thinking Machines Corporation (TMC) massively parallel supercomputer. The CM5 is a 1024 node (Sparc processors) MPP supercomputer, with 32 gigabytes of fast memory, access to 450 gigabytes of disk storage, and a peak operational speed of 128 gigaflops. On the next (teraflops) generation supercomputers, simulation times are expected to drop to many minutes.

Table 3. Grand Challenge Computing Requirements.

Problem	Description	Operations ( <i>number</i> )	Memory ( <i>terabytes</i> )	Storage ( <i>terabytes</i> )
probabilistic decompression	DCI maximum likelihood	$10^{14}$	.030	.450
porous media	3D immiscible flow	$10^{18}$	1	4
ductile material	3D molecular dynamics	$10^{18}$	.30	3
	3D material hydro	$10^{18}$	1	20
plasma physics	numerical tokamak	$10^{18}$	1	100
global ocean	century circulation	$10^{17}$	4	20
brain topology	3D rendering	$10^{15}$	.015	.001
quantum dynamics	lattice QCD	$10^{18}$	.008	.008

Scientific advance rests on the interplay between theory and experiment. Computation closes the loop between theory and experiment in quantitative measure. Theory provides the framework for understanding. Experiment and data provide the means to verify and delineate that understanding. Although many disciplines rely on observational data (astronomy, geology, and paleontology, for instance), the hallmark of scientific endeavor is experiment. Clearly, the power of experimental science is its ability to design the environment in which data is gathered. And it is in the design process that modern computers play an important role.

While many believe that good experimentation depends on the skill and imagination of the designer, this is not entirely true. Insight and experience are certainly desirable to determine and optimize measurable response and procedures, but once this has been determined, it is the mathematics that dictates experimental structure, as detailed by Fisher some 70 years ago in noting that the real world is:

1. noisy – repeating an experiment under identical conditions yields different results;
2. multivariate – many factors potentially affect phenomena under investigation;
3. interactive – the effect of one factor may depend on the level of involvement of other factors.

Computers permit extension and analysis of experimental design methodology to problems for which only crude prescriptions have been hitherto available. Computer software is now widely and economically available to automate the basic and most useful procedures. This allows the user without extensive statistical background to routinely employ methods to optimize design.

Certainly, performing numerical experiments on computers, that is, leveraging model predictions to gain insight into phenomena under study, can often provide results that give the best possible

estimate of overall experimental response and behavior. The approach here is to use the smallest possible subsets of inputs to run the simulation model, thereby narrowing the focus. In designing experiments, Monte Carlo simulations are used in high energy and accelerator physics, semiconductor fabrication, material damage, neutron and photon shielding, and biomedical dose. Large deterministic modules, in excess of 100,000 lines of code, on the other hand, have been applied to the design of laser fusion target experiments. Similarly, atomistic simulations with millions and, in the future, billions of test atoms provide the opportunity for both fundamental and technological advances in material science. Nonequilibrium molecular dynamics calculations address basic scientific issues, such as interaction potentials and plastic flow. The interaction potentials developed in the last decade for metals, alloys, and ceramics can be used to model prototypical hardness experiments, such as crystal indentation. The underlying mechanisms for plastic flow are microscopic crystal defect motions, and molecular dynamics calculations yield quantitative estimates for hardness experiments. Linkages between experiment and supercomputer modeling are growing in scope and number. Consider some specifics:

### 1. Monte Carlo Bubble Simulations

Monte Carlo calculations explicitly employ random variates, coupled to statistical sampling, to simulate physical processes and perform numerical integrations. In computational science, Monte Carlo methods play a special role because of their combination of immediacy, power, and breadth of application. The computational speed and memory capacity of supercomputers have expedited solutions of difficult physical and mathematical problems with Monte Carlo statistical trials. Although Monte Carlo is typically used to simulate a random process, it is frequently applied to problems without immediate probabilistic interpretation, thus serving as a useful computation tool in all areas of scientific endeavor. Applied to bubble formation and tissue-blood interactions, Monte Carlo methods are truly powerful supercomputing techniques.

The Monte Carlo method is different than other techniques in numerical analysis, because of the use of random sampling to obtain solutions to mathematical and physical problems. A stochastic model, which may or may not be immediately obvious, is constructed. By sampling from appropriate probability distributions, numerical solution estimates are obtained. Monte Carlo calculations simulate the physical processes at each point in an event sequence. All that is required for the simulation of the cumulative history is a probabilistic description of what happens at each point in the history. This generally includes a description of the geometrical boundaries of regions, a description of material composition within each region, and the relative probability (functional) for an *event*. With high speed computers, millions of events can be generated rapidly to provide simulation of the processes defined by the probability function. Statistically, the accuracy of the simulation increases with number of events generated.

The generation of cavitation nuclei in tissue can be effected with Monte Carlo techniques, using the Gibbs potential (bubble formation energy) across liquid-vapor interfaces as a probability function for bubble radius as the random variable. Surrounded by dissolved gas at higher tension for any ambient pressure, bubbles generated can be tracked through growth and collapse cycles in time, allowed to move with surrounding material, coalesced with each other, and removed at external boundaries. Cavitation simulations are applied to multiphase flow in nuclear reactor vessels, cavitation around ship propellers, bubbles in gels, cloud and ice condensation processes in the atmosphere, cosmic ray tracking in chambers, and boiling processes in general.

### 2. Two Phase Porous Flow

Numerical simulations of oil-water fluid flows are a challenging problem, due in part to the complexities of interfacial dynamics and also because of the complexities of geometry. Rather than testing in the field, many oil companies have turned their efforts to the numerical study

of pore spaces in oil bearing rock, with high resolution, three dimensional, X-ray scans. Traditional numerical methods have been applied to problems with simple boundaries, but none of the methods apply successfully to the arbitrary geometries found in porous media. Recent emergent numerical techniques on supercomputers, such as derivatives of cellular automata, have demonstrated such capability. Using such cellular methods, it is now possible to study the interactions between oil-water systems and porous rock media.

### 3. HIV Analysis

Research directed at either finding a cure or vaccine for AIDS is hampered by the extreme variability of the viral genome. Because of this variability, it is difficult to identify targets for drug and vaccine design. Exploiting the speed of modern supercomputers, methods have been developed to test for potentially distant regions in viral proteins that interact. Identifications of interacting sites can be used by experimentalists in finding a vaccine or drug preventing infection or death. Linked positions imply biological correlation of functionality, and are important sites within the virus. A map of interaction zones can be used by experimentalists trying to track and define function regions of the virus. Such maps can be generated rapidly, and in three dimensions, on modern computing platforms with graphics capabilities.

### 4. Groundwater Remediation

Groundwater contamination occurs commonly throughout the world. According to recent estimates, cleanup costs in the US alone are estimated at \$1 trillion. Hence, any information or analysis that provides even minor cost savings for a single site, can have significant impact overall if the the information is transferable to disparate sites. Computational experiments performed on modern supercomputers are useful for understanding the complex chemical migration and transformation processes that occur when hazardous substances are released into heterogeneous groundwater systems in a variety quiescent states. Simulations of this sort provide an alternative basis to study detailed behavior under natural and engineered conditions.

### 5. Combustion Vortex Interactions

Experiments have shown that inducing rotational motions (*vortices*) in the gases of internal combustion engines enhances both turbulence and combustion efficiency. Combustion efficiency is improved because the rotational kinetic energy breaks down into fluid turbulence when the piston approaches the cylinder head. Although a qualitative understanding of the dynamics of vortices has already been obtained, supercomputing power provides the precision and speed to determine when and where vortices develop in combustion engines, questions hitherto obscure to the engine designers.

### 6. Molecular Dynamics

Material phenomena, such as fracture, dislocation, plasticity, ablation, stress response, and spall are important to the development and manufacture of novel materials. Molecular dynamics simulations on supercomputers, providing resolution on the *micron* scale, employ millions of interacting molecules to represent states of matter. In such calculations, each molecule moves in the collective force field of all other molecules, and molecular motions of all particles are tracked. This is atomistic physics at the most basic level of interaction.

Supercomputers open up new realms for investigation and enable greater problem domains to be considered. Researchers can develop solutions that treat entire problems from first principles, building from the interactions at the atomic level, all the way up to the macroscopic. As the tool of researcher imagination, new insights and approaches to problem solving are unconstrained.

## 7. Probabilistic Decompression And Maximum Likelihood

Maximum likelihood is a statistical technique used to fit model equations to a sample with relative probabilities for occurrence and nonoccurrence given. We can never measure any physical variable exactly, that is, without error. Progressively more elaborate experiments or theoretical representation only reduce the error in the determination. In extracting parameter estimates from data sets, it is also necessary to minimize the error (data scatter) in the extraction process. Maximum likelihood is one such technique applied to probabilistic decompression modeling.

DCI is a hit, or (hopefully) no-hit situation, and statistics are binary, as in coin tossing. As a random variable, DCI incidence is a complicated function of many physical variables, such as inert gas buildup, VGE counts, pressure reduction on decompression, volume of separated gas, number of bubble seeds, gas solubility in tissue and blood, ascent rate, nucleation rate, distribution of growing bubble sizes, and combinations thereof. Any, and all of these, can be assigned as risk functions in probabilistic decompression modeling, and associated constants deduced in the maximum likelihood fit process.

Project Dive Safety is a DAN program to collect and analyze data on real dives in real time for profiles, behavioral, and health aspects associated with recreational diving. The study focuses on actual dives and profiles recorded by depth/time computers, and verifies the general condition of the diver up to 48 hours after exiting the water, regarding health problems. Upwards of a million dive profiles are anticipated for this study, mainly because DCI incidence is low probability and many trials are necessary for meaningful modeling, statistics, correlations, and estimates. Multivariate model equations are fitted to the dive profiles and observed DCI incidence rate using maximum likelihood, a technique which minimizes the variance in fitting equations to a recreational diving sample. The recreational data file sizes to hundreds of gigabytes, and requires gigaflop supercomputing resources for processing. A 10 parameter risk function fit to 1 million dive profiles would take about an hour on the 256 node CRI T3D, an MPP with 16 gigabytes of memory, 65 gigabytes of fast disk, and a peak speed near 38 gigaflops. Run times scale as the number of events times the number of risk function parameters squared.

### Multilevel Dive Profile Analysis

Schemes for multilevel diving are employed in the commercial, scientific, and sport sectors. In addition to validation, questions arise as to method consistency with the formulation of the US Navy Tables on critical tension principles. One approach employs back to back repetitive sequencing, assigning groups at the start of each multilevel dive segment based on the total bottom time (actual plus residual nitrogen) of the previous segment. At times, the method allows critical tensions, other than the controlling (repetitive) 120 minute compartment tension, to be exceeded upon surfacing. In the context of the US Navy Tables, such circumstance is to be avoided. But, by tightening the exposure window and accounting for ascent and descent rates, such a multilevel technique can be made consistent with the permissible tension formulation of the US Navy Tables.

To adequately evaluate multilevel diving within any set of Tables, it is necessary to account for ascent and descent rates. While ascent and descent rates have small effect on ingassing and outgassing in slow tissue compartments, ascent and descent rates considerably impact fast tissue compartments. Model impact is measured in nitrogen buildup and elimination in hypothetical compartments, whose halftimes denote time to double, or half, existing levels of nitrogen. Buildup and elimination of nitrogen is computed with Haldane tissue equations (exponential rate expressions), and critical tensions, are assigned to each compartment to control diving activity and exposure time. In multilevel diving, computed tissue tensions in any and all compartments must be maintained below their critical values. This is a more stringent constraint than just flooring the 120 *minute* compartment tension, the approach used in the US Navy Tables for repetitive diving.

In the context of the US Navy Tables, from which many Tables with reduced nonstop time limits derive, six compartments with 5, 10, 20, 40, 80, and 120 *minute* halftimes limit diving through

maximum tensions ( $M$ -values) of 104, 88, 72, 58, 52, and 51 *fsw*, respectively. The 5 and 10 *minute* compartments are fast, the 80 and 120 *minute* compartments are slow, and the others are often between, depending on exposure profile. Dive exposure times, depths, ascent, and descent rates, affecting slow and fast compartments in a complicated manner, are virtually infinite in number, thus suggesting the need for both a supercomputer and meaningful representation of the results. A CRAY YMP supercomputer addressed the first concern, while the US Navy Tables provided a simple vehicle for representation of results.

Calculations were performed in roughly 1 *minute* time intervals, and 10 *fsw* depth increments for all possible multilevel dives up to, and including, the standard US Navy nonstop time limits, and down to a maximum depth of 130 *fsw*. Ascent and descent rates of 60 *fsw/min* were employed. Tissue tensions in all six compartments were computed and compared against their  $M$ -values. Dives for which the  $M$ -values were not violated were stored until the end of the multilevel calculations, for further processing. Dives violating any  $M$ -value, at any point in the simulation, were terminated, and the next dive sequence was initiated. The extremes in times for permissible multilevel dives form the envelope of calculations at each depth. The envelope terms out to be very close to the NAUI nonstop limits for the US Navy Tables, that is, the Tables shown in Figure 1 (Part 5). Within a minute, on the conservative side, the envelope tracks the reduced nonstop limits. Approximately 16 million multilevel dives were analyzed on a CRAY YMP in about 8 *minutes* CPU time, including construction of the envelope, with 10 *fsw* and 1 *minute* resolution. The CRAY YMP has raw speed near 320 megaflops per CPU.

Adjunct to Figure 1 (Part 5), one can summarize with regard to YMP calculations:

1. the deeper the initial depth, the shorter the total multilevel dive time;
2. maximum permissible multilevel dive times (total) vary between 100 and 60 *minutes*, depending on initial depths;
3. minimum permissible multilevel increments vary from 30 *fsw* to 10 *fsw* as the depth decreases from 130 *fsw* to 40 *fsw*;
4. multilevel US Navy Table dives falling within the envelope never exceed critical values, below or at the surface, in all compartments;
5. the multilevel envelope is the set of reduced nonstop limits.

In terms of the modified Tables (Figure 1, Part 7), multilevel dives that stay to the left of the nonstop time limits never violate critical tensions, and are (hypothetically) sanctioned. Dive computers, of course, perform the same exercise underwater, comparing instantaneous values of computed tissue tensions in all compartments, throughout the duration of the dive, against stored  $M$ -values to estimate time remaining and time at a stop.

#### Computational Models And Algorithms

The models touched upon lightly (Part 5) address the coupled issues of gas uptake and elimination, bubbles, and pressure changes in different computational approaches. Application of a computational model to staging divers and aviators is often called a diving algorithm. Consider the computational model and staging regimen for 6 popular algorithms, namely, the perfusion limited, diffusion limited, thermodynamic, varying permeability, reduced gradient bubble, and tissue bubble diffusion algorithms:

##### 1. Perfusion Limited Algorithm

Exchange of inert gas, controlled by blood flow rates across regions of varying concentration, is driven by the gas gradient, that is, the difference between the arterial blood tension,  $p_a$ , and the instantaneous tissue tension,  $p$ . This behavior is modeled in time,  $t$ , by classes of

exponential response functions, bounded by  $p_a$  and the initial value of  $p$ , denoted  $p_i$ . These multitissue functions satisfy a differential perfusion rate equation,

$$\frac{\partial p}{\partial t} = -\lambda(p - p_a) \quad (1)$$

and take the form, tracking both dissolved gas buildup and elimination symmetrically,

$$p - p_a = (p_i - p_a) \exp(-\lambda t) \quad (2)$$

$$\lambda = \frac{.693}{\tau} \quad (3)$$

with perfusion constant,  $\lambda$ , linked to tissue half-time,  $\tau$ . Compartments with 1, 2.5, 5, 10, 20, 40, 80, 120, 180, 240, 360, 480, and 720 minute half-times,  $\tau$ , are employed, and half-times are independent of pressure.

In a series of dives or multiple stages,  $p_i$  and  $p_a$  represent extremes for each stage, or more precisely, the initial tension and the arterial tension at the beginning of the next stage. Stages are treated sequentially, with finishing tensions at one step representing initial tensions for the next step, and so on. To maximize the rate of uptake or elimination of dissolved gases the *gradient*, simply the difference between  $p_i$  and  $p_a$ , is maximized by pulling the diver as close to the surface as possible. Exposures are limited by requiring that the tissue tensions never exceed  $M$ , written,

$$M = M_0 + \Delta M d \quad (4)$$

as a function of depth,  $d$ , for  $\Delta M$  the change per unit depth. A set of  $M_0$  and  $\Delta M$  are listed in Table 1 (Part 5). In absolute units, the corresponding critical gradient,  $G$ , is given by,

$$G = \frac{M}{.79} - P \quad (5)$$

with  $P$  ambient pressure, and  $M$  critical nitrogen pressure. Similarly, the critical ratio,  $R$ , takes the form,

$$R = \frac{M}{P} \quad (6)$$

At altitude, some critical tensions have been correlated with actual testing, in which case, the depth,  $d$ , is defined in terms of the absolute pressure,

$$d = P - 33 \quad (7)$$

with absolute pressure,  $P$ , at altitude,  $z$ , given by (*fsw*),

$$P = 33 \exp(-0.0381z) = 33 \alpha^{-1} \quad (8)$$

$$\alpha = \exp(0.0381z) \quad (9)$$

and  $z$  in multiples of 1000 *feet*. However, in those cases where the critical tensions have not been tested nor extended to altitude, an exponentially decreasing extrapolation scheme, called *similarity*, has been employed. Extrapolations of critical tensions, below  $P = 33$  *fsw*, then fall off more rapidly than in the linear case. The similarity extrapolation holds the ratio,  $R = M/P$ , constant at altitude. Denoting an equivalent sea level depth,  $\delta$ , at altitude,  $z$ , one has for an excursion to depth  $d$ ,

$$\frac{M(d)}{d + 33\alpha^{-1}} = \frac{M(\delta)}{\delta + 33} \quad (10)$$

so that the equality is satisfied when,

$$\delta = \alpha d \quad (11)$$

$$M(\delta) = \alpha M(d). \quad (12)$$

Considering the minimum surface tension pressure of bubbles,  $G^{min}$  (near  $10 fsw$ ), as a limit point, the similarity extrapolation should be limited to 10,000 *feet* in elevation, and neither for decompression, nor heavy repetitive diving.

As described previously, depth-time exposures are often limited by a law of the form,

$$dt_n^{1/2} = H \quad (13)$$

with  $t_n$  the nonstop time limit, and  $400 \leq H \leq 500 fsw \text{ min}^{1/2}$ . One can obtain the corresponding tissue constant,  $\lambda$ , controlling the exposure at depth  $d$ , for nonstop time  $t_n$ , by differentiating the tissue equation with respect to depth,  $d$ , and setting the result to zero. With  $p_a = .79(d + 33)$  at sea level, there results,

$$1 - \exp(-\lambda t_n)(1 + 2 \lambda t_n) = 0. \quad (14)$$

Corresponding critical tensions,  $M$ , are then easily obtained using  $d$ ,  $\lambda$ , and  $t_n$ . In the above case, the transcendental equation is satisfied when,

$$\lambda t_n = 1.25 \quad (15)$$

Time remaining before a stop, time at a stop, or surface interval before flying can all be obtained by inverting the tissue equation. Denoting the appropriate critical tension at some desired stage,  $M$ , and the instantaneous tension at that time,  $p$ , at stage,  $p_a$ , the time remaining,  $t_r$ , follows from,

$$t_r = \frac{1}{\lambda} \ln \left[ \frac{p - p_a}{M - p_a} \right] \quad (16)$$

for each compartment,  $\lambda$ . Obviously, the smallest  $t_r$  controls the ascent.

## 2. Diffusion Limited Algorithm

Exchange of inert gas, controlled by diffusion across regions of varying concentration, is also driven by the local gradient. As before, denoting the arterial blood tension,  $p_a$ , and instantaneous tissue tension,  $p$ , the gas diffusion equation takes the form in one dimensional planar geometry,

$$D \frac{\partial^2 p}{\partial x^2} = \frac{\partial p}{\partial t} \quad (17)$$

with  $D$  a single diffusion coefficient appropriate to the media. Using standard techniques of separation of variables, with  $\omega^2$  the separation constant (eigenvalue), the solution is written,

$$p - p_a = (p_i - p_a) \sum_{n=1}^{\infty} W_n \sin(\omega_n x) \exp(-\omega_n^2 Dt) \quad (18)$$

assuming at the left tissue boundary,  $x = 0$ , we have  $p = p_a$ , and with  $W_n$  a set of constants obtained from the initial condition. First, requiring  $p = p_a$  at the right tissue boundary,  $x = l$ , yields,

$$\omega_n = \frac{n\pi}{l} \quad (19)$$

for all  $n$ . Then, taking  $p = p_i$  at  $t = 0$ , multiplying both sides of the diffusion solution by  $\sin(\omega_n x)$ , integrating over the tissue zone,  $l$ , and collecting terms gives,

$$W_{2n} = 0 \quad (20)$$

$$W_{2n-1} = \frac{4}{(2n-1)\pi} \quad (21)$$

Averaging the solution over the tissue domain eliminates spatial dependence, that is  $\sin(\omega_n x)$ , from the solution, giving a bulk response,

$$p - p_a = (p_i - p_a) \sum_{n=1}^{\infty} \frac{8}{(2n-1)^2 \pi^2} \exp(-\omega_{2n-1}^2 Dt). \quad (22)$$

The expansion resembles a weighted sum over *effective* tissue compartments with time constants,  $\omega_{2n-1}^2 D$ , determined by diffusivity and boundary conditions.

Diffusion models fit the time constant,  $K$ ,

$$\kappa = \pi^2 D l^2 \quad (23)$$

to exposure data, with a typical value employed by the Royal Navy given by,

$$\kappa = 0.007928 \text{ min}^{-1}. \quad (24)$$

The approach is aptly single tissue, with equivalent tissue halftime,  $\tau_D$ ,

$$\tau_D = \frac{.693}{\kappa} = 87.5 \text{ min} \quad (25)$$

close to the US Navy 120 *minute* compartment used to control saturation, decompression, and repetitive diving. Corresponding critical tensions in the bulk model, take the form,

$$M = \frac{709 P}{P + 404} \quad (26)$$

falling somewhere between fixed gradient and multitissue values. At the surface,  $M = 53 \text{ fsw}$ , while at 200 *fsw*,  $M = 259 \text{ fsw}$ . A critical gradient,  $G$ , satisfies,

$$G = \frac{M}{.79} - P = \frac{P(493 - P)}{(P + 404)}. \quad (27)$$

The limiting features of bulk diffusion can be gleaned from an extension of the above slab model in the limit of thick tissue region, that is,  $l \rightarrow \infty$ . Replacing the summation over  $n$  with an integral as  $l \rightarrow \infty$ , we find

$$p - p_a = (p_i - p_a) \bar{erf} [l/(4Dt)^{1/2}] \quad (28)$$

with  $\bar{erf}$  the average value of the *error-function* over  $l$ , having the limiting form (Abramowitz and Stegun),

$$\bar{erf} [l/(4Dt)^{1/2}] = 1 - (4Dt)^{1/2} l \pi^{1/2} \quad (29)$$

for short times, and

$$\bar{erf} [l/(4Dt)^{1/2}] = \frac{l}{(4\pi Dt)^{1/2}} \quad (30)$$

for long times.

Unlike the perfusion case, the diffusion solution, consisting of a sum of exponentials in time, cannot be formally inverted to yield time remaining, time at a stop, nor time before flying. Such information can only be obtained by solving the equation numerically, that is, with computer or hand calculator for given  $M$ ,  $p$ , and  $p_a$ .

If we wrap the above planar geometry around into a hollow cylinder of inner radius,  $a$ , and outer radius,  $b$ , we generate Krogh geometry. The hollow cylindrical model retains all the features of the planar model, and additionally includes curvature for small  $a$  and  $b$ , with  $l = b - a$  from before. Assigning the same boundary conditions at  $a$  and  $b$ , namely, the tissue tension,  $p$ , equals the arterial tension,  $p_a$ , writing the diffusion equation in radial cylindrical coordinates,

$$D \frac{\partial^2 p}{\partial r^2} + \frac{D}{r} \frac{\partial p}{\partial r} = \frac{\partial p}{\partial t} \quad (31)$$

and solving yields,

$$p - p_a = (p_i - p_a) \sum_{n=1}^{\infty} X_n U_0(\epsilon_n r) \exp(-\epsilon_n^2 Dt) \quad (32)$$

with  $X_n$  a constant satisfying initial conditions,  $U_0$  the cylinder functions (Abramowitz and Stegun), and  $\epsilon_n$  the eigenvalues satisfying,

$$U_0(\epsilon_n a) = \frac{\partial U_0(\epsilon_n b/2)}{\partial r} = 0 \quad (33)$$

Averaging over the tissue region,  $a \leq r \leq b$ , finally gives,

$$p - p_a = (p_i - p_a) \frac{4}{(b/2)^2 - a^2} \sum_{n=1}^{\infty} \frac{1}{\epsilon_n^2} \frac{J_1^2(\epsilon_n b/2)}{J_0^2(\epsilon_n a) - J_1^2(\epsilon_n b/2)} \exp(-\epsilon_n^2 Dt) \quad (34)$$

with  $J_1$  and  $J_0$  Bessel functions, order 1 and 0. Typical vascular parameters are bounded roughly by,

$$0 < a \leq 4 \text{ microns} \quad (35)$$

$$10 \leq b \leq 32 \text{ microns}. \quad (36)$$

### 3. Thermodynamic Algorithm

The thermodynamic model couples both the tissue diffusion and blood perfusion equations. Cylindrical symmetry is assumed in the model. From a boundary vascular zone of thickness,  $a$ , gas diffuses into the extended extravascular region, bounded by  $b$ . The radial diffusion equation is given by,

$$D \frac{\partial^2 p}{\partial r^2} + \frac{D}{r} \frac{\partial p}{\partial r} = \frac{\partial p}{\partial t} \quad (37)$$

with the tissue tensions,  $p$ , equal to the venous tensions,  $p_v$ , at the vascular interfaces,  $a$  and  $b$ . The solution to the tissue diffusion equation is given previously,

$$p - p_v = (p_i - p_v) \frac{4}{(b/2)^2 - a^2} \sum_{n=1}^{\infty} \frac{1}{\epsilon_n^2} \frac{J_1^2(\epsilon_n b/2)}{J_0^2(\epsilon_n a) - J_1^2(\epsilon_n b/2)} \exp(-\epsilon_n^2 Dt) \quad (38)$$

with  $\epsilon_n$  eigenvalue roots of the boundary conditions,

$$J_0(\epsilon_n a) Y_1(\epsilon_n b/2) - Y_0(\epsilon_n a) J_1(\epsilon_n b/2) = 0 \quad (39)$$

for  $J$  and  $Y$  Bessel and Neumann functions, order 1 and 0. Perfusion limiting is applied as a boundary condition through the venous tension,  $p_v$ , by enforcing a mass balance across both the vascular and cellular regions at  $a$ ,

$$\frac{\partial p_v}{\partial t} = -\kappa(p_v - p_a) - \frac{3}{a} S_p D \left[ \frac{\partial p}{\partial r} \right]_{r=a} \quad (40)$$

with  $S_p$  the ratio of cellular to blood gas solubilities,  $\kappa$  the perfusion constant, and  $p_a$  the arterial tension. The coupled set relate tension, gas flow, diffusion and perfusion, and solubility in a complex feedback loop.

The thermodynamic trigger point for decompression sickness is the volume fraction,  $\chi$ , of separated gas, coupled to mass balance. Denoting the separated gas partial pressure,  $P_{N_2}$ , under worse case conditions of zero gas elimination upon decompression, the separated gas fraction is estimated,

$$\chi P_{N_2} = S_c (p - P_{N_2}) \quad (41)$$

with  $S_c$  the cellular gas solubility. The separated nitrogen partial pressure,  $P_{N_2}$  is taken up by the inherent unsaturation, and given by (*fsw*),

$$P_{N_2} = P + 3.21 \quad (42)$$

in the original Hills formulation, but other estimates have been employed. Mechanical fluid injection pain, depending on the injection pressure,  $\delta$ , can be related to the separated gas fraction,  $\chi$ , through the tissue modulus,  $K$ ,

$$K\chi = \delta \quad (43)$$

so that a decompression criteria requires,

$$K\chi \leq \delta \quad (44)$$

with  $\delta$  in the range, for  $K = 3.7 \times 10^4 \text{ dyne cm}^{-2}$ ,

$$0.34 \leq \delta \leq 1.13 \text{ fsw}. \quad (45)$$

Identification of the separated phase volume as a critical indicator is a significant development in decompression theory.

#### 4. Varying Permeability Algorithm

The critical radius,  $r_i$ , at fixed pressure,  $P_0$ , represents the cutoff for growth upon decompression to lesser pressure. Nuclei larger than  $r_i$  will all grow upon decompression. Additionally, following an initial compression,  $\Delta P = P - P_0$ , a smaller class of micronuclei of critical radius,  $r$ , can be excited into growth with decompression. If  $r_i$  is the critical radius at  $P_0$ , then, the smaller family,  $r$ , excited by decompression from  $P$ , obeys,

$$\frac{1}{r} = \frac{1}{r_i} + \frac{\Delta P}{158} \quad (46)$$

with  $\Delta P$  measured in *fsw*, and  $r$  in *microns*. Table 1 (Part 10) lists critical radii,  $r$ , excited by sea level compressions ( $P_0 = 33 \text{ fsw}$ ), assuming  $r_i = .8 \text{ microns}$ . Entries also represent the equilibrium critical radius at pressure,  $P$ .

The permissible gradient,  $G$ , is written for each compartment,  $\tau$ , using the standard formalism,

$$G = G_0 + \Delta G d \quad (47)$$

at depth  $d = P - 33 \text{ fsw}$ . A nonstop bounce exposure, followed by direct return to the surface, thus allows  $G_0$  for that compartment. Both  $G_0$  and  $\Delta G$  are tabulated in Table 2 (Part 2), with  $\Delta G$  suggested by Buhlmann. The minimum excitation,  $G^{min}$ , initially probing  $r$ , and taking into account regeneration of nuclei over time scales  $\tau_r$ , is ( $fsw$ ),

$$G^{min} = \frac{2 \gamma (\gamma_c - \gamma)}{\gamma_c r(t)} = \frac{11.01}{r(t)} \quad (48)$$

with,

$$r(t) = r + (r_i - r) [1 - \exp(-\lambda_r t)] \quad (49)$$

$\gamma$ ,  $\gamma_c$  film, surfactant surface tensions, that is,  $\gamma = 17.9 \text{ dyne/cm}$ ,  $\gamma_c = 257 \text{ dyne/cm}$ , and  $\lambda_r$  the inverse of the regeneration time for stabilized gas micronuclei (many days). Prolonged exposure leads to saturation, and the largest permissible gradient,  $G^{sat}$ , takes the form ( $fsw$ ), in all compartments,

$$G^{sat} = \frac{58.6}{r} - 49.9 = .372 P + 11.01. \quad (50)$$

On the other hand,  $G^{min}$  is the excitation threshold, the amount by which the surrounding tension must exceed internal bubble pressure to just support growth.

Although the actual size distribution of gas nuclei in humans is unknown, experiments *in vitro* suggest that a decaying exponential is reasonable,

$$n = N \exp(-\beta r) \quad (51)$$

with  $\beta$  a constant, and  $N$  a convenient normalization factor across the distribution. For small values of the argument,  $\beta r$ ,

$$\exp(-\beta r) = 1 - \beta r \quad (52)$$

as a nice simplification. For a stabilized distribution,  $n_0$ , accommodated by the body at fixed pressure,  $P_0$ , the excess number of nuclei,  $\Delta n$ , excited by compression-decompression from new pressure,  $P$ , is,

$$\Delta n = n_0 - n = N\beta r_i \left[ 1 - \frac{r}{r_i} \right]. \quad (53)$$

For large compressions-decompressions,  $\Delta n$  is large, while for small compressions-decompressions,  $\Delta n$  is small. When  $\Delta n$  is folded over the gradient,  $G$ , in time, the product serves as a critical volume indicator and can be used as a limit point in the following way.

The rate at which gas inflates in tissue depends upon both the excess bubble number,  $\Delta n$ , and the gradient,  $G$ . The critical volume hypothesis requires that the integral of the product of the two must always remain less than some limit point,  $\alpha V$ , with  $\alpha$  a proportionality constant,

$$\int_0^\infty \Delta n G dt = \alpha V \quad (54)$$

for  $V$  the limiting gas volume. Assuming that gradients are constant during decompression,  $t_d$ , while decaying exponentially to zero afterwards, and taking the limiting condition of the equal sign, yields simply for a bounce dive, with  $\lambda$  the tissue constant,

$$\Delta n G (t_d + \lambda^{-1}) = \alpha V. \quad (55)$$

In terms of earlier parameters, one more constant,  $\delta$ , closes the set, defined by,

$$\delta = \frac{\gamma_c \alpha V}{\gamma \beta r_i N} = 7180 \text{ fsw min} \quad (56)$$

so that,

$$\left[1 - \frac{r}{r_i}\right] G (t_d + \lambda^{-1}) = \delta \frac{\gamma}{\gamma_c} = 500.8 \text{ fsw min.} \quad (57)$$

The five parameters,  $\gamma$ ,  $\gamma_c$ ,  $\delta$ ,  $\lambda_r$ ,  $r_i$ , are five of the six fundamental constants in the varying permeability model. The remaining parameter,  $\lambda_m$ , interpolating bounce and saturation exposures, represents the inverse time constant modulating multiding. Bubble growth experiments suggest that  $\lambda_m^{-1}$  is in the neighborhood of an hour. Discussion of  $\lambda_m$  follows in the next section (RGBM).

The depth at which a compartment controls an exposure, and the excitation radius as a function of half-time,  $\tau$ , in the range,  $12 \leq d \leq 220 \text{ fsw}$ , satisfy,

$$\frac{r}{r_i} = .9 - .43 \exp(-\zeta\tau) \quad (58)$$

with  $\zeta = .0559 \text{ min}^{-1}$ . The regeneration constant,  $\lambda_r$ , is on the order of inverse days, that is,  $\lambda_r = .0495 \text{ days}^{-1}$ . Characteristic halftimes,  $\tau_r$  and  $\tau_h$ , take the values  $\tau_r = 14 \text{ days}$  and  $\tau_h = 12.4 \text{ min}$ . For large  $\tau$ ,  $r$  is close to  $r_i$ , while for small  $\tau$ ,  $r$  is on the order of  $.5 r_i$ . At sea level,  $r_i = .8 \text{ microns}$  as discussed.

## 5. Reduced Gradient Bubble Algorithm

The phase integral for multiexposures is written,

$$\sum_{j=1}^J \left[ \Delta n G t_{d_j} + \int_0^{t_j} \Delta n G dt \right] \leq \alpha V \quad (59)$$

with the index  $j$  denoting each dive segment, up to a total of  $J$ , and  $t_j$  the surface interval after the  $j^{\text{th}}$  segment. For the inequality to hold, that is, for the sum of all growth rate terms to total less than  $\alpha V$ , obviously each term must be less than  $\alpha V$ . Assuming that  $t_J \rightarrow \infty$ , gives,

$$\sum_{j=1}^{J-1} [\Delta n G [t_{d_j} + \lambda^{-1} - \lambda^{-1} \exp(-\lambda t_j)]] + \Delta n G (t_{d_J} + \lambda^{-1}) \leq \alpha V. \quad (60)$$

Defining  $G_j$ ,

$$\Delta n G_j (t_{d_j} + \lambda^{-1}) = \Delta n G (t_{d_j} + \lambda^{-1}) - \Delta n G \lambda^{-1} \exp(-\lambda t_{j-1}) \quad (61)$$

for  $j = 2$  to  $J$ , and,

$$\Delta n G_1 = \Delta n G \quad (62)$$

for  $j = 1$ , it follows that

$$\sum_{j=1}^J \Delta n G_j (t_{d_j} + \lambda^{-1}) \leq \alpha V \quad (63)$$

with the important property,

$$G_j \leq G. \quad (64)$$

This implies we employ reduced gradients extracted from bounce gradients by writing,

$$G_j = \xi_j G \quad (65)$$

with  $\xi_j$  a *multidiving* fraction requisitely satisfying,

$$0 \leq \xi_j \leq 1 \quad (66)$$

so that, as needed,

$$\Delta n G_j \leq \Delta n G. \quad (67)$$

The fractions,  $\xi$ , applied to  $G$  always reduce them. As time and repetitive frequency increase, the body's ability to eliminate excess bubbles and nuclei decreases, so that we restrict the permissible bubble excess in time by writing,

$$\Delta n(t_{j-1}^{cum}) = N\beta r_i \left[ 1 - \frac{r(t_{j-1}^{cum})}{r_i} \right] = \Delta n \exp(-\lambda_r t_{j-1}^{cum}) \quad (68)$$

$$t_{j-1}^{cum} = \sum_{i=1}^{j-1} t_i \quad (69)$$

with  $t_{j-1}^{cum}$  cumulative dive time. A reduction factor,  $\eta_j^{reg}$ , accounting for creation of new micronuclei is taken to be the ratio of present excess over initial excess, written,

$$\eta_j^{reg} = \frac{\Delta n(t_{j-1}^{cum})}{\Delta n} = \exp(-\lambda_r t_{j-1}^{cum}) \quad (70)$$

For reverse profile diving, the gradient is restricted by the ratio (minimum value) of the bubble excess on the present segment to the bubble excess at the deepest point over segments. The gradient reduction,  $\eta_j^{exc}$ , is then written,

$$\eta_j^{exc} = \frac{(\Delta n)_{max}}{(\Delta n)_j} = \frac{(rd)_{max}}{(rd)_j} \quad (71)$$

with  $rd$  the product of the appropriate excitation radius and depth. Because bubble elimination periods are shortened over repetitive dives, compared to intervals for bounce dives, the gradient reduction,  $\eta_j^{rep}$ , is proportional to the difference between maximum and actual surface bubble inflation rate, that is,

$$\eta_j^{rep} = 1 - \left[ 1 - \frac{G^{min}}{G} \right] \exp(-\lambda_m t_{j-1}) \quad (72)$$

with  $t_{j-1}$  consecutive total dive time,  $\lambda_m^{-1}$  on the order of an hour, and  $G^{min}$  the smallest  $G_0$  in Table 2 (Part 2).

Finally, for multiding, the gradient reduction factor,  $\xi$ , is defined by the product of the three  $\eta$ ,

$$\xi_j = \eta_j^{exc} \eta_j^{rep} \eta_j^{reg} = \frac{(\Delta n)_{max}}{(\Delta n)_j} \left[ 1 - \left( 1 - \frac{G^{min}}{G} \right) \exp(-\lambda_m t_{j-1}) \right] \exp(-\lambda_r t_{j-1}^{cum}) \quad (73)$$

with  $t_{j-1}$  consecutive dive time, and  $t_{j-1}^{cum}$  cumulative dive time, as noted. Since bubble numbers increase with depth, reduction in permissible gradient is commensurate. Multiday diving is mostly impacted by  $\lambda_r$ , while repetitive diving mostly by  $\lambda_m$ . Obviously, the critical tension,  $M$ , takes the form,

$$M = \xi(G_0 + \Delta G d) + P. \quad (74)$$

## 6. Tissue Bubble Diffusion Algorithm

Bubbles shrink or grow according to a simple radial diffusion equation linking total gas tension,  $\Pi$ , ambient pressure,  $P$ , and surface tension,  $\gamma$ , to bubble radius,  $r$ ,

$$\frac{\partial r}{\partial t} = \frac{DS}{r} \left[ \Pi - P - \frac{2\gamma}{r} \right] \quad (75)$$

with  $D$  the gas diffusion coefficient, and  $S$  the gas solubility. Bubbles grow when the surrounding gas tension exceeds the sum of ambient plus surface tension pressure, and vice versa. Higher gas solubilities and diffusivities enhance the rate. Related bubble area,  $A$ , and volume,  $V$ , changes satisfy,

$$\frac{\partial A}{\partial t} = 8\pi r \frac{\partial r}{\partial t} \quad (76)$$

$$\frac{\partial V}{\partial t} = 4\pi r^2 \frac{\partial r}{\partial t} \quad (77)$$

Using Fick's law, a corresponding molar current,  $J$ , of gas into, or out of, the bubble is easily computed assuming an ideal gas,

$$J = -\frac{DS}{RT h} \left[ \Pi - P - \frac{2\gamma}{r} \right] \quad (78)$$

for  $R$  the ideal gas constant,  $T$  the temperature, and  $h$  an effective diffusion barrier thickness. And the molal flow rate is just the molal current times the interface area, that is,

$$\frac{\partial n}{\partial t} = JA \quad (79)$$

for  $n$  the number of moles of gas. The change in pressure and volume of the bubble, due to gas diffusion, follows simply from the ideal gas law,

$$\frac{\partial(PV + 2\gamma r^{-1}V)}{\partial t} = R \frac{\partial(nT)}{\partial t} \quad (80)$$

for  $V$  the bubble volume.

Obviously, the above constitute a coupled set of differential equations, solvable for a wide range of boundary and thermodynamic conditions connecting the state variables, namely,  $P$ ,  $V$ ,  $\Pi$ ,  $r$ ,  $n$ , and  $T$ .

A bubble dose, based on the hypothetical volume of an expanding test bubble, is linked to decompression data for the exposure. Maximum likelihood regression is used to correlate bubble dose with DCI risk, as seen in Figure 5 (Part 5).

### Exercises

1. Solve the perfusion rate equation for the tissue tension,  $p$ , as a function of time (Part 8)?
2. For a depth-time law of the form,  $dt_n^{1/2} = C$ , what is the nonstop time limit for compartment,  $\tau = 45$  min, and what is the depth,  $d$ , for  $C = 450$  fsw min<sup>1/2</sup> (Part 8)?
3. Average the diffusion limited tissue response over length,  $l$ , to eliminate spatial dependences (Part 8)?
4. Given temporal diffusion length,  $\zeta = l/D^{1/2} = 10$  sec<sup>1/2</sup>, what are short and long time values of the bulk diffusion response function (Part 8)?
5. In the VPM and RGBM, a normalized distribution of bubble seeds,  $n$ , in radii  $r$ , is assumed to be excited by compression-decompression, and takes the form,

$$n = N\beta \exp(-\beta r)$$

with  $N$  and  $\beta$  distribution constants. If the excess,  $\Delta n$ , excited into growth by compression-decompression is just the difference between the total number at  $r_0$  and the total number at  $r$ , with  $r$  and  $r_0$  linked by the magnitude of the pressure change,  $\Delta P$ , compute  $\Delta n$  for  $r$  and  $r_0$ , normalizing over all radii (Part 8)? For small argument,  $a$ , one has,  $\exp(-a) = 1 - a$ , so obtain a small argument expression for the bubble excess,  $\Delta n$ , (Part 8)?

6. Formally evaluate the phase volume integral, assuming constant gradients,  $G$ , during decompression, and exponentially decaying gradients afterwards, with tissue decay constant,  $\lambda$ , assuming  $\lambda t_d$  is small (Part 8)?
7. What is the minimum excitation gradient,  $G^{\min}$ , and saturation gradient,  $G^{\text{sat}}$ , for seeds of radius,  $r = .5$  microns, according to the VPM and RGBM (Part 8)? What is the corresponding pressure,  $P$ , for this saturation gradient (Part 8)?
8. Using the TBDM, couple the bubble volumetric growth rate to corresponding molal diffusion current, rate of pressure change for constant temperature (Part 8)?
9. In the TM, assuming  $J_0(a) \rightarrow 1$  and  $J_1(a) \rightarrow a$ , for small  $a$ , expand the tissue response function (Part 8)?

#### Related Reading

1. Hills B.A., 1977, *Decompression Sickness*, New York: John Wiley And Sons.
2. Johnson L.W. and Riess R.D., 1962, *Numerical Analysis*, Reading: Addison Wesley.
3. Kahaner D., Moler C., and Nash S., 1989, *Numerical Methods And Software*, Englewood Cliffs: Prentice Hall.
4. Leebaert D., 1991: *Technology 2001: The Future Of Computing And Communications*, Cambridge: Massachusetts Institute Of Technology Press.
5. Loyst K., Huggins K.E. and Steidley M., 1991, *Dive Computers*, San Diego: Watersports.
6. Mathews J. and Walker R.L., 1975, *Mathematical Methods Of Physics*, New York: W.A. Benjamin.
7. Parzen E., 1970, *Modern Probability Theory And Its Applications*, New York: John Wiley And Sons.
8. Press W., Teukolsky S., Vetterling W., and Flannery B., 1992, *Numerical Recipes In FORTRAN*, New York: Cambridge University Press.
9. Shreider Y.A., 1966, *The Monte Carlo Method*, New York: Pergamon Press.
10. Wienke B.R., 1998, *Physics, Physiology, And Decompression Theory For The Technical And Commercial Diver*, National Association Of Underwater Instructors Publication, Tampa.

## PART 9: DECOMPRESSION THEORY DIVING MALADIES AND DRUGS

### Maladies

Diving has its own brand of medical complications, linked to ambient pressure changes. For brief consideration, a few of the common medical problems associated with compression-decompression and diving follow. The bubble problem has been long discussed, but we can start off by summarizing a few consensus opinions concerning decompression sickness. A cursory discussion of some drugs then follows.

### Bends

Clinical manifestations of decompression sickness, or decompression illness (DCI), can be categorized as pulmonary, neurological, joint, and skin DCI, as summarized by Vann. All are linked to bubbles upon pressure reduction, with embolism also included in the categorization. Pulmonary DCI manifests itself as a sore throat with paroxysmal cough upon deep inspiration, followed by severe chest pain, and difficult respiration, a condition collectively called the *chokes*. Chokes is seen often in severe high altitude exposures. Neurological DCI affects the heart, brain, and spinal cord, through arterial gas emboli, venous gas emboli, shunted venous gas emboli (VGE that pass through the pulmonary circulation and enter the arterial circulation), and stationary, extravascular (*autochthonous*) bubbles. Joint DCI is a common form of mild bends, affecting the nervous (*neurogenic*), bone marrow (*medullar*), and joint (*articular*) assemblies. Neurogenic pain is localized at remote limb sites, usually without apparent cerebral or spinal involvement. Bubbles in the bone have been proposed as the cause of both dull aching pain and bone death. Expanding extravascular bubbles have been implicated in the mechanical distortion of sensory nerve endings. Skin DCI manifests itself as itching, rash, and a sense of localized heat. Skin DCI is not considered serious enough for hyperbaric treatment, but local pain can persist for a few days. Blotchy purple patching of the skin has been noted to precede serious DCI, especially the chokes.

Most believe that bends symptoms follow formation of bubbles, or the gas phase, after decompression. Yet, the biophysical evolution of the gas phase is incompletely understood. Doppler bubble and other detection technologies suggest that:

1. moving and stationary bubbles do occur following decompression;
2. the risk of decompression sickness increases with the magnitude of detected bubbles and emboli;
3. symptomless, or *silent*, bubbles are also common following decompression;
4. the variability in gas phase formation is likely less than the variability in symptom generation.

Gas phase formation is the single most important element in understanding decompression sickness, and is also a crucial element in preventative analysis.

Treatment of decompression sickness is an involved process, requiring a recompression chamber and various hyperbaric treatment schedules depending on severity of symptoms, location, and initiating circumstance. Recompression is usually performed in a double lock hyperbaric chamber, with the patient taken to a series of levels to mitigate pain, first, and then possibly as deep as 165 *fsw* for treatment. Depending on depth of treatment schedule, oxygen may, or may not, be administered to washout inert gas and facilitate breathing. Treatment of air embolism follows similar schedules.

### High Pressure Nervous Syndrome

Hydrostatic pressure changes, particularly in the several hundred *atm* range, are capable of affecting, though usually reversibly, central nervous system activity. Rapidly compressed divers, say 120 *fsw/min* to 600 *fsw*, breathing helium, experience coarse tremors and other neurological disorders termed *high pressure nervous syndrome* (HPNS). At greater depths, near 800 *fsw*,

cramps, dizziness, nausea, and vomiting often accompany the tremor. Although HPNS can be avoided by slowing the compression rate, the rate needs to be substantially reduced for compressions below 1,100 *fsw*.

While the underlying mechanisms of HPNS are not well understood, like so many other pressure related afflictions, the use of pharmacological agents, some nitrogen in the breathing mixture, staged compressions, alcohol, and warming have been useful in ameliorating HPNS in operational deep diving.

Gas induced osmosis has been implicated as partially causative in high pressure nervous syndrome. Water, the major constituent of the body, shifting between different tissue compartments, can cause a number of disorders. Mechanical disruption, plasma loss, hemoconcentration, and bubbles are some. Under rapid pressure changes, gas concentrations across blood and tissue interfaces may not have sufficient time to equilibrate, inducing balancing, but counter, fluid pressure gradients (osmotic gradients). The strength of the osmotic gradient is proportional to the absolute pressure change, temperature, and gas solubility.

#### Inert Gas Narcosis

It is well known that men and animals exposed to hyperbaric environments exhibit symptoms of intoxication, simply called *narcosis*. The narcosis was first noticed in subjects breathing compressed air as early as 1835. The effect, however, is not isolated to air mixtures (nitrogen and oxygen). Both helium and hydrogen, as well as the noble (rare) gases such as xenon, krypton, argon, and neon, cause the same signs and symptoms, though varying in their potency and threshold hyperbaric pressures. The signs and symptoms of inert gas narcosis have manifest similarity with alcohol, hypoxia (low oxygen tension), and anesthesia. Exposure to depths greater than 300 *fsw* may result in loss of consciousness, and at sufficiently great pressure, air has been used as an anesthetic. Individual susceptibility to narcosis varies widely from individual to individual. Other factors besides pressure potentiate symptoms, such as alcohol, work level, apprehension, and carbon dioxide levels. Frequent exposure to depth with a breathing mixture, as with DCS, affords some level of adaptation.

Many factors are thought contributory to narcosis. Combinations of elevated pressure, high oxygen tensions, high inert gas tensions, carbon dioxide retention, anesthesically blocked ion exchange at the cellular interface, reduced alveolar function, and reduced hemoglobin capacity have all been indicted as culprits. But, still today, the actual mechanism and underlying sequence is unknown.

The anesthetic aspects of narcosis are unquestioned in most medical circles. Anesthesia can be induced by a wide variety of chemically passive substances, ranging from inert gases to chloroform and ether. These substances depress central nervous system activity in a manner altogether different from centrally active drugs. Anesthetics have no real chemical structure associated with their potency, and act on all neural pathways, like a bulk phase. Physicochemical theories of anesthetics divide in two. One hypothesis envisions anesthetics interacting with hydrophobic surfaces and interfaces of lipid tissue. The other postulates anesthetic action in the aqueous phases of the central nervous system. The potency and latency of both relate to the stability of gas hydrates composing most anesthetics. The biochemistry of anesthetics and narcosis in divers has not, obviously, been unraveled.

#### Hyperoxia And Hypoxia

Elevated oxygen tensions (*hyperoxia*), similar to elevated inert gas tensions, can have a deleterious effect on divers, aviators, and those undergoing hyperbaric oxygen treatment. The condition is known as oxygen toxicity, and was first observed, in two forms, in the final quarter of the 1800s. Low pressure oxygen toxicity (Lorraine Smith effect) occurs when roughly a 50% oxygen mixture is breathed for many hours near 1 *atm*, producing lung irritation and inflammation. At higher partial pressures, convulsions develop in high pressure oxygen toxicity (Bert effect), with latency time inversely proportional to pressure above 1 *atm*. Factors contributing to the onset of symptoms are degree of exertion, amount of carbon dioxide retained and inspired, and individual susceptibility. Early symptoms of oxygen poisoning include muscular twitching (face and lips), nausea, tunnel vision, difficulty hearing and ringing, difficulty breathing and taking deep breaths, confusion, fatigue,

and coordination problems. Convulsions are the most serious manifestation of oxygen poisoning, followed ultimately by unconsciousness. Oxygen toxicity is not a problem whenever the oxygen partial pressures drop below  $.5 \text{ atm}$ .

Oxygen toxicity portends another very complex biochemical condition. Elevated oxygen levels interfere with the enzyme chemistry linked to cell metabolism, especially in the central nervous system. Reduced metabolic and electrolytic transport across neuronal membranes has been implicated as a causative mechanism. The role of carbon dioxide, while contributory to the chain of reactions according to measurements, is not understood, just as with inert gas narcosis. On the other hand, it has been noted that only small increases in brain carbon dioxide correlate with severe symptoms of oxygen toxicity. Carbon dioxide seems to play an important, though subtle, part in almost all compression-decompression afflictions.

Breathing air at atmospheric pressure after the onset of oxygen toxicity symptoms can restore balance, depending on severity of symptoms. Deep breathing and hyperventilation can also forestall convulsions if initiated at the earliest sign of symptoms.

When the tissues fail to receive enough oxygen, a tissue debt (*hypoxia*) develops, with varying impact and latency time on body tissue types. Hypoxia can result with any interruption of oxygen transport to the tissues. Although the nervous system itself represents less than 3% of body weight, it consumes some 20% of the oxygen inspired. When oxygen supply is cut, consciousness can be lost in 30 *seconds* or less, respiratory failure follows in about a *minute*, and irreparable damage to the brain and higher centers usually occurs in about 4 *minutes*. Obviously, the brain is impacted the most. The victim of hypoxia may be unaware of the problem, while euphoria, drowsiness, weakness, and unconsciousness progress. Blueness of the lips and skin results, as blood is unable to absorb enough oxygen to maintain its red color. When oxygen partial pressures drop below  $.10 \text{ atm}$ , unconsciousness is extremely rapid.

Hypoxia is a severe, life threatening condition. However, if fresh air is breathed, recovery is equally as rapid, providing breathing has not stopped. If breathing has stopped, but cardiac function continues, artificial respiration can stimulate the breathing control centers to functionality. Cardiopulmonary resuscitation can be equally successful when both breathing and heart action have ceased.

#### Hypercapnia And Hypocapnia

Tissue carbon dioxide excess (*hypercapnia*) can result from inadequate ventilation, excess in the breathing mixtures, or altered diver metabolic function. All tissues are affected by high levels of carbon dioxide, but the brain, again, is the most susceptible. The air we breathe contains only some .03% carbon dioxide. As partial pressures of carbon dioxide approach  $.10 \text{ atm}$ , symptoms of hypercapnia become severe, starting with confusion and drowsiness, followed by muscle spasms, rigidity, and unconsciousness. Carbon dioxide at  $.02 \text{ atm}$  pressure will increase breathing rate, and carbon dioxide at  $.05 \text{ atm}$  pressure induces an uncomfortable sensation of shortness of breath. Factors which increase the likelihood and severity of hypercapnia include corresponding high partial pressure of oxygen, high gas densities, breathing dead spaces, and high breathing resistance.

Any process which lowers carbon dioxide levels in the body below normal (*hypocapnia*), can produce weakness, faintness, headache, blurring of vision, and, in the extreme case, unconsciousness. Hypocapnia often results from hyperventilation. The respiratory system monitors both carbon dioxide and oxygen levels to stimulate breathing. Rising carbon dioxide tensions and falling oxygen tensions trigger the breathing response mechanism. Hyperventilation (rapid and deep breathing) lowers the carbon dioxide levels, leading to hypocapnia.

Extended breathholding after hyperventilation can lead to a condition known as shallow water blackout. Following hyperventilation and during a longer breathholding dive, oxygen tensions can fall to very low levels before a diver returns to the surface and resumes breathing. Oxygen levels are lowered because exertion causes oxygen to be used up faster, but also the sensitivity to carbon dioxide drops as oxygen tension drops, permitting oxygen levels to drop even further. Upon ascension, the

drop in the partial pressure of oxygen in the lungs may be sufficient to stop the uptake of oxygen completely, and, with the commensurate drop in carbon dioxide tension, the urge to breathe may also be suppressed.

While the short term effects of both hypercapnia and hypocapnia can be disastrous in the water, drowning if consciousness is lost, the long term effects following revival are inconsequential. Treatment in both cases is breathing standard air normally. Residual effects are minor, such as headache, dizziness, nausea, and sore chest muscles.

Carbon dioxide seems to be a factor in nearly every other compression-decompression malady, including decompression sickness, narcosis, hyperoxia, and hypoxia. It is a direct product of metabolic processes, with about 1 l of carbon dioxide produced for every 1 l of oxygen consumed. Carbon dioxide affects the metabolic rate, and many other associated biochemical reactions. The physical chemistry of carbon dioxide uptake and elimination is much more complex than that of inert gases, such as nitrogen and helium. Transfer of inert gases follows simple laws of solubility (Henry's law) in relation to partial pressures. Carbon dioxide transport depends on three factors, namely, gas solubility, chemical combination with alkaline buffers, and diffusion between the cellular and plasma systems. Only relatively small changes in partial pressures of carbon dioxide can induce chain reactions in the three mechanisms, and larger scale biological impact on gas exchange and related chemistry.

#### Barotrauma

With pressure decrease, air contained in body cavities expands. Usually, this expanding air vents freely and naturally, and there are no problems. If obstructions to air passage exist, or the expanding air is retained, overexpansion problems, collectively called barotrauma, can occur. One very serious overexpansion problem occurs in the lungs. The lungs can accommodate overexpansion to just a certain point, after which continued overpressurization produces progressive distention and then rupture of the alveoli (air exchange sacs). Problems with lung overexpansion can occur with pressure differentials as small as 5 *fsw*. This distention can be exacerbated by breathholding on ascent or inadequate ventilation, and partial obstruction of the bronchial passageways.

The most serious affliction of pulmonary overpressure is the dispersion of air from the alveoli into the pulmonary venous circulation (arterial embolism), thence, into the heart, systemic circulation, and possibly lodging in the coronary and cerebral arterioles. Continuing to expand with further decrease in pressure, these emboli (bubbles) can block blood flow to vital areas. Clinical features of arterial gas embolism develop rapidly, including dizziness, headache, and anxiety first, followed by unconsciousness, cyanosis, shock, and convulsions. Death can result from coronary or cerebral occlusion, inducing cardiac arrhythmia, shock, and circulatory and respiratory failure. The only treatment for air embolism is recompression in a hyperbaric chamber, with the intent of shrinking emboli in size, and driving the air out of the emboli into solution.

Gas from ruptured alveoli may pass into the membrane lining the chest, the parietal pleura, and also rupture the lining (*pneumothorax*). Trapped in the intrapleural lining, the gas may further expand on ascent, and push against the heart, lungs, and other organs. Often the lungs collapse under the pressure. Symptoms of pneumothorax include sudden chest pain, breathing difficulty, and coughing of frothy blood. Recompression is the indicated treatment for a concomitant condition, along with thoracentesis.

Gas trapped in the tissues about the heart and blood vessels, and the trachea (*mediastinal emphysema*), can adversely impact the circulation, particularly, the venous flow. Symptoms include pain in the sternum, shortness of breath, and sometimes fainting. The condition is exacerbated on ascent as gas trapped in tissues expands. In severe cases, hyperbaric treatment is utilized.

If the bubbles migrate to the tissues beneath the skin (*subcutaneous emphysema*), often a case accompanying mediastinal emphysema, their presence causes a swelling of neck tissue and enhanced local pressure. Feeling of fullness, and change of voice are associated with subcutaneous emphysema. Treatment consists of oxygen breathing, which accelerates tissue absorption of the air trapped in the

neck region.

Pressure increases and decreases can be tolerated by the body when they are distributed uniformly, that is, no local pressure differentials exist. When pressure differentials exist, outside pressure greater than inside pressure locally, and vice versa, distortion of the shape of the local site supporting the pressure difference is the outcome. Burst alveoli are one serious manifestation of the problem. Other areas may suffer similar damage, for instance, the ears, sinuses, teeth, confined skin under a wetsuit, and the intestines. Though such complications can be very painful, they are usually not life threatening. When local pressure differentials develop because of inside and outside pressure imbalances, blood vessels will rupture in attempt to equalize pressure. The amount of rupture and degree of bleeding is directly proportional to the pressure imbalance.

Pressures in air spaces in the sinuses, middle ear, and teeth fillings are often imbalanced during compression-decompression. To accommodate equalization when diving, air must have free access into and out of these spaces during descent and ascent. Failure to accommodate equalization on descent is termed a squeeze, with outside pressure greater than inside (air space) pressure, while failure to accommodate equalization on ascent is called a reverse block, with inside pressure (air space) greater than ambient pressure. In the case of the ear, it is the eustachian tube which does not permit air passage from the throat to the middle ear. The sinuses have very small openings which close under congestive circumstance, inhibiting air exchange. Similarly, small openings in and around teeth fillings complicate equalization of the air space under the filling (usually a bad filling). In all cases, slow descents and ascents are beneficial in ameliorating squeeze and reverse block problems.

#### Altitude Sickness

At altitudes greater than some 7,000 *ft*, decreased partial pressures of oxygen can cause arterial hypoxemia. Under hypoxic stimulation (low oxygen tension), hyperventilation occurs with secondary lowering of arterial carbon dioxide and production of alkalosis. Newcomers to high altitude typically experience dyspnea (shortness of breath), rapid heart rate, headache, insomnia, and malaise. Symptoms disappear within a week, and general graded exercise may hasten acclimatization.

Acclimatization is usually lost within a week at lower altitudes. Although increased oxygen at depth may be beneficial, the surface malaise often precludes diving until acclimatization. In itself, altitude sickness is not life threatening.

#### Pulmonary Edema

Pulmonary edema (fluid buildup in the lungs) can affect nonacclimatized individuals who travel within a day or two to elevations near, or above, 10,000 *ft*. Symptoms usually appear within 18 *hrs* after arrival, consisting of rasping cough, dyspnea, and possible pain in the chest. Treatment requires immediate removal to lower altitude, hospitalization with rest, oxygen, and diuretic therapy. Prevention includes adequate acclimatization and reduced levels of exertion. A month of graded exercise may be requisite. Again, increased oxygen partial pressures at depth are helpful, but diving rigors can precipitate pulmonary edema. Symptoms might resemble the chokes (decompression sickness).

Pulmonary edema can be a serious, even fatal, affliction, as noted by its yearly toll on mountain climbers. At altitude, evidence of cough, shortness of breath, or tightness serves as a warning. Rapid treatment, including lower altitude, hospitalization, and appropriate therapy, is recommended.

#### Hypothermia And Hyperthermia

Exposure to cold results in heat loss, called *hypothermia*, with the rate dependent upon body area, temperature difference, body fat, insulation properties of wet or dry suit, and physical activity. Exercise always increases heat loss. As core temperatures drop, symptoms progress from shivering, to weakness, to muscle rigidity, to coma, and then death. Rewarming at the earliest signs of hypothermia is prudent. While more of a cold water problem, hypothermia can also occur in relatively warm and even tropical waters. Severe hypothermia is a life threatening condition.

Shivering and a feeling of being very cold are first symptoms of hypothermia, and the situation

gets worse fast. Rewarming in dry clothing is standard and obvious treatment, as well as ingestion of balanced electrolytes. Exercise, caffeine, and alcohol are to be avoided. Care in the choice of protective suit to conserve body heat, attention to feelings of cold, and good physical condition help to minimize hypothermia.

Inadequate ventilation and body heat loss, called *hyperthermia*, usually in the presence of high environmental temperatures and low body fluid levels, lead to a progressive raising of temperatures in vital organs. As temperatures rise, symptoms progress from profuse sweating, to Replacement of body fluids and reduction of body temperature are necessary in effective treatment of hyperthermia. Cool water immersion is employed in severe cases, but the usual treatment consists of fluids, salt, and full body ventilation. Like hypothermia, severe hyperthermia is life threatening.

Hyperthermia can be avoided by proper attention to water intake and protection from environmental heat. Environmental temperatures above body temperature are potentially hazardous, especially with increasing levels of physical exertion.

#### Dysbaric Osteonecrosis

Bone rot (*dysbaric osteonecrosis*) is an insidious disease of the long bones associated with repeated high pressure and saturation exposures. Deep and saturation diving portend problems with temperature control in environmental suits, habitats, respiration and surface monitoring, compression and decompression, inert gas reactivity, communication, oxygen levels, and many others, all falling into an operational control category, that is, problems which can be ameliorated through suitable application of sets of established diving protocols. But aseptic bone necrosis is a chronic complication about which we know little.

Affecting the long bones as secondary arthritis or collapsed surface joints, lesions, detected as altered bone density upon radiography, are the suspected cause. Statistics compiled in the early 1980s by the US Navy, Royal Navy, Medical Research Council, and commercial diving industry suggest that some 8% of all divers exposed to pressures in the 300 *fsw* range exhibited bone damage, some 357 out of 4,463 examined divers. No lesions were seen in divers whose exposures were limited to 100 *fsw*. Some feel that very high partial pressures of oxygen for prolonged periods is the ultimate culprit for bone lesions, leading to fat cell enlargement in more closed regions of the bone core, a condition that reduces blood flow rate and probably increases local vulnerability to bubble growth. The facts, however, are still not clear. And commercial divers continue to be at higher risk of osteonecrosis.

#### Drugs

Very few studies have systematized the overall effects of drugs underwater. Drug utilization by divers is connected with medication used to ameliorate diving problems, medication used to treat illness, and recreational drugs. Recent studies suggest that drug effects are compounded at increasing depth, having been described as potentiating, antagonizing, and unpredictable as far as altered behavior with increasing pressure. Side effects can be subtle and also variable, possibly exacerbated by other risk factors such as cold water, oxygen, or nitrogen concentrations. Many different types of drugs are utilized.

Among the more common drugs used by divers are decongestants, taken for ear and sinus relief. These drug products are typically *antihistamines*, providing relief by constricting blood vessels, reducing tissue swelling, and opening passages between sinuses and middle ear for air exchange. Antihistamines often produce drowsiness and decreased mental acuity. Another decongestant, with trade name terfenadine, has no sedative effects. Drugs addressing motion sickness may lead to functional motor impairment. Antihistamines, particularly *meclizine* and *dimenhydrate* are often employed for motion sickness, additionally causing sedation. The skin patch drug, *scopolamine*, also possesses sedative properties, with some additional side effects of blurred vision and dry mouth. Individual reactions vary widely.

Sedative and pain agents also alter mental function. Anti-anxiety drugs, such as *valium*, *halcion*, and *dalmane*, are strong agents, producing significant changes in mental outlook. Muscle relaxants, such as *flexiril* and *robaxin*, induce drowsiness. Analgesics containing *propoxyphene*, *codein*,

*oxycodone*, or *hydrocodone* reduce mental and physical exercise capacity. Agents used in the treatment of depression or psychosis cause sedation, and have been noted to induce cardiac dysfunction. Tradename drugs in this category, *elavil*, *haldol*, and *sinequan*, impair cognitive abilities.

Hypertension drugs can limit diving performance. Diuretics, like *lasix* and *hydrochlorothiazide*, cause fluid loss, possibly compounding dehydration and electrolytic imbalance. Agents affecting heart rate and peripheral vasculature may cause drowsiness and reduce blood flow capacity. These drugs include *metoprolol*, *hytrin*, *tenez*, and others. Bronchodilators, used in the treatment of asthma, include *theophylline* and *steroids*. In the former category, tradename drugs, such as *theodur*, *uniphyl*, *metaprel*, and *ventolin* can cause cardiac dysrhythmias and CNS impairment. Gastrointestinal drugs containing histamines can also affect the central nervous system, causing drowsiness and headache. Antacids seem to have no noted adverse effects on divers.

According to the diving medical community at large, the bottom line on drugs underwater is caution, since little is known about many, particularly newer ones. Narcotics and hallucinogens, alcohol, and heavy doses of caffeine have been linked to reduced mental and physical acuity, sedation, vasodilatation, diuresis, and dehydration on the mild side, and extreme neurological, respiratory, and cardiovascular stress on the more severe side.

### *Exercises*

1. For the following set of conditions and/or symptoms, identify possible diving maladies (Part 9). Partial oxygen tension of 1.85 atm? Partial carbon dioxide tension of .10 atm, with muscle spasms? Rasping cough at an elevation of 14,000 ft? Intense shivering in a dry suit? Light-headedness on an air dive to 145 fsw? Weakness and headache following a hyperventilated skin dive? Pain in the sternum and coughing of blood? Pneumothorax Shortness of breath at 6,555 ft elevation? Lesions and cracks in the long bones of the leg? Paralysis of the lower legs? Partial oxygen tension of .09 atm? Chest pain and swelling of the neck? Profuse sweating and muscle cramps? Dull aching pain in the joints?
2. Match some of the following side effects to drugs possibly avoided when diving (Part 9)? Drowsiness? Motor impairment? Reduced blood flow capacity? Cardiac dysrhythmias? Blurred vision? Reduced cognitive functionality?

### *Related Reading*

1. Bennett P.B. and Elliot D.H., 1996, *The Physiology And Medicine Of Diving And Compressed Air Work*, London: Bailliere Tindall And Cassell.
2. Bookspan J., 1997, *Diving Physiology In Plain English*, Bethesda: Undersea And Hyperbaric Medical Society.
3. Bove A.A. and Davis J.C., 1990, *Diving Medicine*, Philadelphia: W.B. Saunders.
4. Buhlmann A.A., 1984, *Decompression/Decompression Sickness*, Berlin: Springer Verlag.
5. Edmonds C., Lowry C., And Pennefather J., 1994, *Diving And Subaquatic Medicine*, Portland: Book News.
6. Edmonds C., McKenzie B., and Thomas R., 1997, *Diving Medicine For Scuba Divers*, Sydney: Aquaquest Publications;
7. Hills B.A., 1977, *Decompression Sickness*, New York: John Wiley And Sons.
8. Somers L.H., 1991, *The University Of Michigan Diving Manual*, Ann Arbor: University Of Michigan Press.

PART 10: DECOMPRESSION THEORY  
BUBBLES AND BIOSYSTEMS

Doppler Effect

A change in the observed frequency of sound, light, and other waves, caused by relative source-observer motion, is known as the Doppler effect. One example is a change in train whistle pitch upon approach and retreat. The observed frequency,  $f'$ , is higher than the source frequency,  $f$ , as source and observer approach each other, and lower as source and observer retreat from each other.

For sound waves that propagate with characteristic velocity,  $u$ , in a medium (air, water, tissue), the Doppler shift depends on both source velocity,  $v_s$ , and observer velocity,  $v_o$ . The number of sound waves per second arriving at the observer can be estimated by simply counting the waves emitted per second by the source, and the change per second in the number of waves in flight from source to observer,

$$f' = f \frac{u - v_o}{u - v_s} \quad , \quad (1)$$

with source and observer velocities measured along the direction from source to observer (longitudinal component). If the observer is at rest, obviously,

$$\Delta f = f' - f = f \frac{v_s}{u - v_s} \quad , \quad (2)$$

as the usual case. If the observer is moving, and the source is at rest,

$$\Delta f = f' - f = -f \frac{v_o}{u} \quad . \quad (3)$$

A general definition of the sound speed,  $u$ , derives from the pressure derivative with respect to the density,

$$u^2 = \frac{dP}{d\rho} \quad , \quad (4)$$

which, in the adiabatic limit of no heat flow, reduces to,

$$u^2 = \frac{Y}{\rho} \quad , \quad (5)$$

$$Y = -V \frac{dP}{dV} \quad , \quad (6)$$

with  $Y$  the *bulk modulus* of the material. For ideal gases,  $Y = 5/3 P$ , but in solids and liquids, the bulk modulus must be determined.

A gas bubble will scatter sound waves in tissue by virtue of differences in bubble and tissue density,  $\rho$ , and bulk modulus,  $Y$ . First attempts to detect gas in tissues using ultrasound were designed to measure attenuation in fundamental frequency by scatter or reflection of the sound signal passed across the tissue region under investigation. Such techniques have the advantage that they can localize the gas region. However, both transmission and reflection techniques suffer from the heterogeneous nature of tissue, both in density and bulk modulus. Such an approach, called the pulse echo technique, has given way today to Doppler methods of detecting moving bubbles.

Moving Bubbles

Doppler devices used to monitor bubbles in the circulation, or trap speeders with radar detectors, are simple. High frequency waves, emitted by a sending crystal of a Doppler probe, easily travel through body tissue, with a portion reflected back towards a receiving crystal. Tissue moving toward or away from the sending unit will reflect part of the source signal with a frequency shift determined

by the velocity of the reflecting medium. Integrated Doppler systems discard the unshifted portion of the reflected signal, and only analyze the shifted portion. Shifted signals fall within the human audibility range. In the veins, bubbles reflect more of the signal than flowing blood, with chirps and pops superimposed on continuous flowing blood background sounds. Detected bubbles are graded from 0 to 4, roughly no bubbles to 1,000 or more per minute.

Doppler probes are inserted into leg and arm veins, pulmonary arteries (heart to lung), and even the heart ventricles. Bubbles detected in veins or ventricles are traveling from tissues to the lungs. They may, or may not, be associated with free phases at joints, or in the spinal column, causing DCS at these sites. Doppler prediction of DCS falls in the 10% to 15% success range, even for high grade bubbles (3-4 Doppler grade). While less than totally predictive, the preponderance of high Doppler grade bubbles for a dive profile renders the profile suspect at least. Following a typical nonstop dive to the limits, Doppler bubble levels tend to peak in an hour, or two. Recent studies by the Divers Alert Network (DAN) at Duke University reported that some 18% of recreational dives produced some level of Doppler bubbling, on tables or decompression meters.

Acoustical signals in the *megahertz* frequency range are typically employed in Doppler analysis. The size and velocity of reflecting bubbles in the flowing media are crucial factors in the reflected return signals. Where flow rates are the highest, the smallest bubbles can be detected with Doppler technology. Roughly, entrained bubbles in the 20 - 40  $\mu m$  diameter range are detectable in flows ranging 50 -60 *cm/sec*, as depicted in Figure 1, according to bubble flow experiments employing 5 *megahertz* acoustical signals.

#### Operational Protocols

The past ten years, or so, have witnessed a number of changes and additions to diving protocols and table procedures, such as shorter nonstop time limits, slower ascent rates, discretionary safety stops, ascending repetitive profiles, multilevel techniques, both faster and slower controlling repetitive tissue halftimes, lower critical tensions (*M*-values), longer flying-after-diving surface intervals, and others. Stimulated by by Doppler technology, decompression meter development, theory, statistics, or safer diving consensus, these modifications affect a gamut of activity, spanning bounce to multiday diving. As it turns out, there is good support for these protocols on operational, experimental, and theoretical grounds, and a comprehensive model addressing these concerns on firmer basis than earlier models is certainly possible, having been proposed by numbers of investigators.

Spencer pioneered the use of Doppler bubble counting to suggest reductions in the nonstop time limits of the standard US Navy Tables, on the order of a repetitive group or two at each depth in the Tables (1-4 *fsw* in critical tensions), basing recommendations on lowering bubble counts at shorter nonstop time limits. Others have also made similar recommendations over the past 15 years.

Smith and Stayton noted marked reductions in precordial bubbles when ascent rates were cut from 60 *fsw/min* to 30 *fsw/min*. In similar studies, Pilmanis witnessed an order of magnitude drop in venous gas emboli (VGE) counts in divers making short, shallow, safety stops following nominal bounce exposures at the 100 *fsw* level, while Neumann, Hall, and Linaweaver recorded comparable reductions in divers making short, but deeper, stops after excursions to 200 *fsw* for longer periods of time.

An American Academy Of Underwater Sciences (AAUS) workshop on repetitive diving, recorded by Lang and Vann, and Divers Alert Network (DAN) statistics suggest that present diving practices appear riskier under increasing exposure time and pressure loading, spawning development of ancillary safety measures for multiday diving. Dunford, Wachholz, Huggins, and Bennett noted persistent Doppler scores in divers performing repetitive, multiday diving, suggesting the presence of VGE in divers, all the time, under such loadings.

Ascent rates, safety stops, decompression computers, and altitude diving were also the subject of extensive discussion at workshops and technical forums sponsored by the American Academy of Underwater Sciences and the Undersea And Hyperbaric Medical Society (UHMS), as summarized by Lang and Hamilton, Lang and Egstrom, and Sheffield, Results of discussions culminated in a set of

recommendations, folded within standard Haldane table and meter procedures, even for exposures exceeding neither time limits nor critical tissue tensions.

The upshot of these studies, workshops, discussions, and tests are a set of discretionary protocols, not necessarily endorsed in all diving sectors, but which might be summarized as follows:

1. reduce nonstop time limits a repetitive group, or two, below the standard US Navy limits;
2. maintain ascent rates below 60 *fsw/min*, preferably slower, and requisitely slower at altitude;
3. limit repetitive dives to a maximum of three per day, not exceeding the 100 *fsw* level;
4. avoid multiday, multilevel, or repetitive dives to increasing depths;
5. wait 12 *hr* before flying after nominal diving, 24 *hr* after heavy diving (taxing, near decompression, or prolonged repetitive) activity, and 48 *hr* after decompression diving;
6. avoid multiple surface ascents and short repetitive dives (spikes) within surface intervals of 1 *hr*;
7. surface intervals of more than an hour are recommended for repetitive diving;
8. safety stops for 2-4 *min* in the 10-20 *fsw* zone are advisable for all diving, but particularly for deep (near 100 *fsw*), repetitive, and multiday exposures;
9. do not dive at altitudes above 10,000 *ft* using modified conventional tables, or linear extrapolations of sea level critical tensions;
10. in short, dive conservatively, remembering that tables and meters are not bends proof.

Procedures such as those above are prudent, theoretically sound, and safe diving protocols. Ultimately, they link to free phase and bubble mechanisms.

Validation is central to diving, and significant testing of nonstop and saturation diving schedules has transpired. In between, repetitive (more than one dive in a 12 hour period), multilevel (arbitrary depths throughout the course of a single dive), reverse profile (second repetitive dive deeper than first), and multiday (repetitive dives over days) diving cannot claim the same benefits, though some ongoing programs are breaking new ground. Application of (just) dissolved gas models in latter cases possibly has witnessed slightly higher decompression sickness (bends) incidence than in the former ones, as discussed in newsletters, workshops, and technical forums. Some hyperbaric specialists also suggest higher incidence of rash (skin bends) under repetitive loading. While statistics are not yet conclusive, they raise some concerns theoretically addressed by considering both dissolved and free phase gas buildup and elimination in broader based bubble models. Such models often focus on the amount of free phase precipitated by compression-decompression, and contain dissolved gas models as subset. In limiting the volume of free phase in time, they must also limit the growth rate.

#### Pulmonary And Circulatory Networks

The pulmonary and circulatory organs are connected gas transfer networks, as Figure 2 suggests. Lung blood absorbs oxygen from inspired air in the alveoli (lung air sacs), and releases carbon dioxide into the alveoli. The surface area for exchange is enormous, on the order of a few hundred square meters. Nearly constant values of alveolar partial pressures of oxygen and carbon dioxide are maintained by the respiratory centers, with ventilated alveolar volume near 4 *l* in adults. The partial pressure of inspired oxygen is usually higher than the partial pressure of tissue and blood oxygen, and the partial pressure of inspired carbon dioxide less, balancing metabolic requirements of the body.

Gas moves in direction of decreased concentration in any otherwise homogeneous medium with uniform solubility. If there exist regions of varying solubility, this is not necessarily true. For instance,

in the body there are two tissue types, one predominantly aqueous (watery) and the other (lipid), varying in solubility by a factor of five for nitrogen. That is, nitrogen is five times more soluble in lipid tissue than aqueous tissue. If aqueous and lipid tissue are in nitrogen equilibrium, then a gaseous phase exists in equilibrium with both. Both solutions are said to have a nitrogen tension equal to the partial pressure of the nitrogen in the gaseous phase, with the concentration of the dissolved gas in each species equal to the product of the solubility times the tension according to Henry's law. If two nitrogen solutions, one lipid and the other aqueous, are placed in contact, nitrogen will diffuse towards the solution with decreased nitrogen tension. The driving force for the transfer of any gas is the pressure gradient, whatever the phases involved, liquid-to-liquid, gas-to-liquid, or gas-to-gas. Tensions and partial pressures have the same dimensions. The volume of gas that diffuses under any gradient is a function of the interface area, solubility of the media, and distance traversed. The rate at which a gas diffuses is inversely proportional to the square root of its atomic weight. Following equalization, dissolved volumes of gases depend upon their individual solubilities in the media.

Lipid and aqueous tissues in the body exhibit inert gas solubilities differing by factors of roughly five, in addition to different uptake and elimination rates. Near standard temperature and pressure (32  $F^\circ$ , and 1  $atm$ ), roughly 65% of dissolved nitrogen gas will reside in aqueous tissues, and the remaining 35% in lipid tissues at equilibration, with the total weight of dissolved nitrogen about .0035  $lb$  for a 150  $lb$  human.

The circulatory system, consisting of the heart, arteries, veins, and lymphatics, convects blood throughout the body. Arterial blood leaves the left heart via the aorta (2.5  $cm$ ), with successive branching of arteries until it reaches arterioles (30  $\mu m$ ), and then systemic capillaries (8  $\mu m$ ) in peripheral tissues. These capillaries join to form venules (20  $\mu m$ ), which in turn connect with the vena cava (3  $cm$ ), which enters the right heart. During return, venous blood velocities increase from 0.5  $cm/sec$  to nearly 20  $cm/sec$ . Blood leaves the righthear through the pulmonary arteries on its way to the lungs. Upon oxygenation in the lungs, blood returns to the left heart through the pulmonary veins, beginning renewed arterial circulation. Flow patterns in lowest (still representative) order follow streamlines, for initial and final states,  $i$  and  $f$ ,

$$mv_f^2 + 2h_f + 2mgz_f = mv_i^2 + 2h_i + 2mgz_i = \gamma \quad (7)$$

with blood mass,  $m$ , velocity,  $v$ , enthalpy,  $h$ , position,  $z$ , and constant,  $\gamma$ , as the entrained blood routinely circulates. Obviously, as systemic vessels change size, branch, and recombine, blood coursing through them experiences speed changes according to mass flow conservation, that is, denoting mass flow rate,  $dm/dt$ ,

$$\frac{dm}{dt} = \rho_i A_i v_i = \rho_f A_f v_f \quad (8)$$

with  $A$  the cross sectional area of the blood vessel and more simply where,  $\rho_i = \rho_f$ , for incompressible fluids, like blood.

Blood has distinct components to accomplish many functions. Plasma is the liquid part, carrying nutrients, dissolved gases (excepting oxygen), and some chemicals, and makes up some 55% of blood by weight. Red blood cells (erythrocytes) carry the other 45% by weight, and through the protein, hemoglobin, transport oxygen to the tissues. Enzymes in red blood cells also participate in a chemical reaction transforming carbon dioxide to a bicarbonate in blood plasma. The average adult carries about 5  $l$  of blood, 30-35% in the arterial circulation (pulmonary veins, left heart, and systemic circulation), and 60-65% in the venous flow (veins and righthear). About 9.5  $ml$  of nitrogen are transported in each liter of blood. Arterial and venous tensions of metabolic gases, such as oxygen and carbon dioxide differ, while blood and tissue tensions of water vapor and nitrogen are the same. Oxygen tissue tensions are below both arterial and venous tensions, while carbon dioxide tissue tensions exceed both. Arterial tensions equilibrate with alveolar (inspired air) partial pressures in less than a minute. Such an arrangement of tensions in the tissues and circulatory system provides the

necessary pressure head between alveolar capillaries of the lungs and systemic capillaries pervading extracellular space.

Tissues and venous blood are typically unsaturated with respect to inspired air and arterial tensions, somewhere in the vicinity of 8-13% of ambient pressure. That is, summing up partial pressures of inspired gases in air, total venous and tissue tensions fall short in that percentage range. Carbon dioxide produced by metabolic processes is 25 times more soluble than oxygen consumed, and hence exerts a lower partial pressure by Henry's law. That tissue debt is called the *inherent unsaturation*, or *oxygen window*, in diving applications

#### Inherent Unsaturation

Inert gas transfer and coupled bubble growth are subtly influenced by metabolic oxygen consumption. Consumption of oxygen and production of carbon dioxide drops the tissue oxygen tension below its level in the lungs (alveoli), while carbon dioxide tension rises only slightly because carbon dioxide is 35 times more soluble than oxygen. Figure 3 compares the partial pressures (*fs<sub>w</sub>*) of oxygen, nitrogen, water vapor, and carbon dioxide in dry air, alveolar air, arterial blood, venous blood, and tissue (cells).

Arterial and venous blood, and tissue, are clearly unsaturated with respect to dry air at 1 *atm*. Water vapor content is constant, and carbon dioxide variations are slight, though sufficient to establish an outgradient between tissue and blood. Oxygen tensions in tissue and blood are considerably below lung oxygen partial pressure, establishing the necessary ingradient for oxygenation and metabolism. Experiments also suggest that the degree of unsaturation increases linearly with pressure for constant composition breathing mixture, and decreases linearly with mole fraction of inert gas in the inspired mix. A rough measure of the inherent unsaturation,  $\Delta_u$ , is given as a function of ambient pressure,  $P$ , and mole fraction,  $f_{N_2}$ , of nitrogen in the air mixture, in *fs<sub>w</sub>*

$$\Delta_u = (1 - f_{N_2})P - 2.04 f_{N_2} - 5.47 \quad . \quad (9)$$

Since the tissues are unsaturated with respect to ambient pressure at equilibrium, one might exploit this *window* in bringing divers to the surface. By scheduling the ascent strategically, so that nitrogen (or any other inert breathing gas) supersaturation just takes up this unsaturation, the total tissue tension can be kept equal to ambient pressure. This approach to staging is called the zero supersaturation ascent.

#### Surface Tension

Discontinuities in types of materials and/or densities at surfaces and interfaces give rise to interfacial forces, called *surface tension*. Discontinuities in density produce cohesive gradients tending to diminish density at the surface region. At the interfaces between immiscible materials, cohesive forces produce surface tension, but adhesional forces between dissimilar materials tend to offset (decrease) the interfacial tension. Surface and interfacial tension are readily observed in fluids, but less readily in solids. In solids, very little stretching of the surface region can occur if the solids are rigid. Upon heating rigid solids to higher temperature, surface tension becomes a discernible effect.

Any two phases in equilibrium are separated by a surface of contact, the existence of which also produces surface tension. The thin contact region is a transition layer, sometimes called the *film* layer. Phases can be solid, liquid, or vapor, with surface tension in each case different. The actual position, or displacement, of the phase boundary may alter the area of the phases on either side, leading to pressure differences in the phases. The difference between phase pressures is known as the surface, or film, pressure. The phase equilibration condition requires the temperatures and chemical potentials (Gibbs free energy) of phases be equal, but certainly not the pressures.

A simple description of measurable surface tension,  $\gamma$ , is linked to the magnitude of cohesive forces in materials  $a$  and  $b$ , denoted,  $\chi_a$  and  $\chi_b$ , wanting to pull the surfaces together, and the adhesional forces,  $\alpha_a$  and  $\alpha_b$ , wanting to draw the surfaces apart. The net surface tension,  $\gamma$ , is the

sum of cohesive forces minus adhesive forces, that is,

$$\gamma = \chi_a + \chi_b - \alpha_a - \alpha_b \quad . \quad (10)$$

Thermodynamically, surface tension contributes a differential work term,  $d\omega$ , to system balance equations given in terms of surface contact area,  $dA$ ,

$$d\omega = \gamma dA \quad , \quad (11)$$

Surface tension pressure,  $\tau$ , is surface tension force per unit area, that is, in terms of work function,  $\omega$ ,

$$\tau = - \left[ \frac{\partial \omega}{\partial V} \right]_{S,T} \quad , \quad (12)$$

at constant entropy,  $S$ , and temperature,  $T$ . Interfacial tension in liquids is measured by the pressure difference across surfaces, again denoted  $a$  and  $b$ ,

$$\tau = \gamma \left[ \frac{1}{r_a} + \frac{1}{r_b} \right] \quad , \quad (13)$$

given radii of curvature,  $r_a$  and  $r_b$ . For thin films, such as bubbles,  $r_a \approx r_b = r$ , and we see,

$$\tau_{bub} = \frac{2\gamma}{r} \quad , \quad (14)$$

deduced by Young and Laplace almost two centuries past. For water,  $\gamma = 50 \text{ dyne cm}$ , while for watery tissue,  $\gamma = 18 \text{ dyne cm}$ .

#### Adsorption

The surface of all solids and liquids adsorb foreign molecules from their surroundings. These adsorbed molecules change most of the chemical and physical properties of the underlying substrate. Adhesion, catalysis, corrosion, fracture, lubrication, and wear are affected by the topmost molecular layers on a surface. Understanding these changes involves close study of films themselves, as described.

The forces of attraction that cause adsorption are relatively weak and are the long range interactions existing between all atoms and molecules.

#### Surfactants

Water, gasoline, glycerin, and salad oil are clearly liquids. Pancake syrup, paster, eggwhite, silly putty, paint, glue, and soap are also liquids, that is, they flow on the application of stress, but border on classification otherwise. In mechanical response, the latter class differs from each other as much as they differ from solids. And the response is variable in time. Syrup becomes sticky as it dries. Dishwashing soap often dries into light flakes. Silly putty flows on tilt, but shatters on sudden impact. Airplane glue is springy and rubbery.

Substances in the latter category are called structured fluids, owing their distinctive and unusual properties to large polyatomic composites, many times the size of a water molecule. Fluids containing polyatomic structures manifest a wide variety of mechanical response and self organization. Body tissues and fluids host an uncountable variety of organic and inorganic matter, with many biochemical substances falling into structured fluid category. Among the structured fluids, a class of self assemblies, called surfactants, are very interesting, possessing properties which can stabilize microbubbles in various stages of evolution by offsetting surface tension.

A surfactant is a structured fluid which is *ambiphillic*, incorporating parts that assume preferential orientations at water-oil (immiscible) interfaces. A surfactant molecule usually consists of a bulky ion at one end, and a counter ion at the other. Isolated molecules cannot usually exist in one

media type, or the other, but instead orient themselves into *micelles*, configurations in which like parts clump together, that is head in one substance and tail in the other. Micelles typically possess diameters near  $10^{-3} \mu m$ , and render the interfaces unlike anything measured in the components. Lipid-aqueous tissue interfaces potentially present favorable environments for surfactants.

Under certain conditions, a surfactant can reduce interfacial surface tension, allowing the interface to grow and wrap around itself. The result is a microbundle full of alternating surfaces and interfaces, spherical in structure to minimize thermodynamic energy constraints. Many substances may be bound up in the microbundle. If small gas nuclei, but typically much larger than a micelle, are in contact with the interfaces, or surfactants directly, a spherical gas micronucleus-microemulsion can develop, varying in size and surfactant content. The assembly is stable when the effective surface tension is zero, when surfactant skin pressure just balances mechanical (Laplace) surface tension. If the effective surface tension of the microbubble,  $\gamma$ , is not zero, the collection will grow or contract until stable, or disassemble. In the case of gas microemulsions, the surfactant is thought to coat the inside boundary layer mostly, with free gas in the interior. The actual picture is probably more complex, but such a picture can be drawn for computational simplicity. Surfactant stabilized micronuclei may theoretically destabilize under compression-decompression processes in diving, perhaps spawning bubble growth fueled by high gas tension in surrounding media. Microbubbles may remain at the interfaces, but probably migrate. Sources of initial gas nuclei, surfactant composition, and tissue sites await description.

A full discussion of nucleation processes and coupled statistical mechanics is postponed until Part 11, but some general comments about micronuclei and phase mechanisms follow.

#### Micronuclei

Bubbles, which are unstable, are thought to grow from micron size, gas nuclei which resist collapse due to elastic skins of surface activated molecules (surfactants), or possibly reduction in surface tension at tissue interfaces or crevices. If families of these micronuclei persist, they vary in size and surfactant content. Large pressures (somewhere near  $10 \text{ atm}$ ) are necessary to crush them. Micronuclei are small enough to pass through the pulmonary filters, yet dense enough not to float to the surfaces of their environments, with which they are in both hydrostatic (pressure) and diffusion (gas flow) equilibrium. When nuclei are stabilized, and not activated to growth or contraction by external pressure changes, the skin (surfactant) tension offsets both the Laplacian (film) tension and any mechanical help from surrounding tissue. Then all pressures and gas tensions are equal. However, on decompression, the seed pockets are surrounded by dissolved gases at high tension and can subsequently grow (bubbles) as surrounding gas diffuses into them. The rate at which bubbles grow, or contract, depends directly on the difference between tissue tension and local ambient pressure, effectively the bubble pressure gradient, denoted  $G$ . At some point in time, a critical volume of bubbles, or separated gas, is established and bends symptoms become statistically more probable. On compression, the micronuclei are crunched down to smaller sizes across families, apparently stabilizing at new reduced size. Bubbles are also crunched by increasing pressure because of Boyle's law, and then additionally shrink if gas diffuses out of them. As bubbles get smaller and smaller, they probably restabilize as micronuclei.

Under compression-decompression, gas nuclei may grow as bubbles, depending on their effective bubble radius. Below a certain critical radius,  $r_c$ , listed in Table 1 below as a function of pressure according to a bubble model (varying permeability), as fitted to gel experiments, bubbles tend to collapse on themselves, while at larger equilibrium radius, they grow as gas diffuses into them. Stabilized nuclei evolve into unstable bubbles when their effective surface tension is greater than zero, or a sufficient diffusion gradient exists to drive gas into, or out of, the nucleus. At sea level, the model excitation radius is near  $.8 \mu m$ , smaller than living cells, having dimensions starting at a few microns.

Table 1. Micronuclei Excitation Radii.

pressure $P$ (fsw)	excitation radius $r_i$ ( $\mu m$ )	pressure $P$ (fsw)	excitation radius $r_i$ ( $\mu m$ )
13	.89	153	.49
33	.80	173	.46
53	.72	193	.44
73	.66	213	.41
93	.61	233	.39
113	.57	253	.37
133	.53	273	.36

Micronuclei can be broadly classified as *homogeneous* or *heterogeneous*, depending upon their composition and that of the surrounding media. If the composition of both micronuclei and parent media are essentially the same, the nucleation process is termed homogeneous. If the composition of micronuclei and parent media differ, the nucleation process is termed heterogeneous. Spontaneous bubble formation in pure supersaturated liquids under explosive decompression is mainly homogeneous, while bubble formation on dust particles in supersaturated fluids is mostly heterogeneous. Homogeneous nucleation and bubble formation usually require large decompressions (many tens of atmospheres), while heterogeneous nucleation and bubble formation processes transpire with very small decompressions (tenths of atmospheres). Homogeneous nucleation in body tissue under nominal and controlled conditions of decompression appears much less likely than heterogeneous nucleation, considering pressure change and host of organic and inorganic body substances.

Nucleation theory is consistent with a number of diving observations. Divers can significantly increase tolerance against bubble formation, and therefore bends, by following three simple practices:

1. make the first dive a deep, short (crush) dive, thereby constricting micronuclei down to smaller, safer size;
2. make succeeding dives progressively more shallow, thus diving within crush limits of the first dive and minimizing excitation of smaller micronuclei;
3. make frequent dives (like every other day), thus depleting the number of micronuclei available to form troublesome bubbles.

An underlying point can be made here. If nucleation sites are extinguished, reduced in number, or ill-disposed to excitation, bubble formation and risk are commensurately reduced. Regeneration times for classes of micronuclei are estimated to be near a week, underscoring physiological adaptation to recurring pressure environments. The mechanics of nucleation, stabilization, and bubble growth are fairly complex, with stabilization mechanisms only recently quantified. Source and generation mechanisms before stabilization are not well understood. Some candidates include cosmic radiation and charged particles, dissolved gases in fluids we drink, lymph draining tissues into veins, collisional coalescence, blood turbulence and vorticity, exercise, the stomach, and the thin air-blood endothelium in the lungs. Once formed, micronuclei must stabilize very rapidly with surfactant material. Passing through the pulmonary filters of the lungs, only sub-micron sizes might survive. If nuclei are persistent, it is not clear that they populate all tissue sites, nor possess the same size distributions. Some can argue that gel findings are not relevant because biological fluids are formed, and contained, in a sealed environment (the body), but the Strauss and Yount studies confirm the existence of preformed gas micronuclei in serum and egg albumin. Nuclei seem to pervade all manner of fluids.

Abandoning preformed nuclei, other methods of instantaneous bubble formation are certainly possible. Cavitation, produced by the rapid tearing, or moving apart, of tissue interfaces, is a candidate, as well as surface friction (tribonucleation). Crevices in tissues may form or trap gas phases, with

later potential for release. Vorticity in blood flow patterns might cause small microbubbles. Stable, or unstable, the copious presence of microbubbles in the venous circulation would impact dissolved gas elimination adversely, also possibly impairing the lungs or the arterial network. The presence of bubbles in the arterial circulation might result in embolism. Bubble clogging of the pulmonary circulation is thought to relate to the chokes, a serious form of decompression sickness, while cerebral decompression sickness is believed due to emboli. Microbubbles in the venous circulation would render gas uptake and elimination asymmetric, with uptake faster than elimination. Displacing blood, microbubbles would reduce the effective area and volume for tissue-blood gas exchange.

#### Free Phases

Henry's law tells us that a gas will tend to separate from solution (pass from the dissolved state to the free state) if the tension of the gas in the dissolved state exceeds its partial pressure in the adjacent free state. And the opposite holds true if the gradient is reversed. Phase separation can be delayed if some remnant of a free phase does not already exist in the liquid, providing a pathway for the dissolved gas to *dump* over into the free state, rendering the dissolved gas *metastable* during the delay. The challenge in tracking phase separation is the presence and quantification of free phase precursors, or seeds, that facilitate gas transfer in a process called *nucleation*.

#### Nucleation

Metastable states are unstable thermodynamic states lying close to stable configurations, that is, separated by relatively small energy differences. A substance in a metastable state will eventually transition into a stable state. For instance, a supercooled vapor will eventually condense into a liquid, a supercooled liquid will eventually become solid, and a superheated liquid will eventually evaporate into a gas. Bubble formation can be a process in which a gas, or vapor, phase is initially formed from a metastable liquid environment, one that is usually supersaturated with dissolved gas.

Metastable phase transitions deposit an unstable phase onto a stable phase, with aggregates in the stable phase serving as *nuclei* for the transition. Liquid drops in a supercooled vapor, if sufficiently large, become centers of condensation of the vapor, for example. Nuclei will form in both phases because of statistical fluctuations, but the nuclei in the metastable phase will disappear in time, while those in the stable phase will remain. Such nuclei form statistically as a result of thermal fluctuations in the interior of the media, with a certain (small) number reaching *critical* radius for growth. If large enough, nuclei in the stable phase seed the continuing process of phase transitions from the metastable state. For each metastable state, there is a minimum size which nuclei in the stable phase must possess to afford more stability than the metastable state. This size is called the critical radius,  $r_c$ . Nuclei smaller than the critical radius will not support phase transitions from the metastable state, and will also disappear in time. In assigning a critical radius to nuclei, spherical aggregate symmetry is assumed, and is requisite to minimize surface energy.

Homogeneous nucleation processes occur in single component systems, while heterogeneous nucleation processes involve more than one component. To describe nucleation, a heterogeneous model, ascribed to Plesset, containing the homogeneous case as a subset, has been useful in applications. A solid hydrophobic sphere, of radius  $r_0$ , is surrounded by a concentric layer of vapor, out to a radius  $r$ . The instantaneous (Boltzmann) probability,  $dw$ , for the state depends on the difference in free energy,  $\Delta G$ , associated with the vapor phase,

$$dw = \exp(-\Delta G/kT) dG \quad , \quad (15)$$

at temperature,  $T$ , for (Gibbs) free energy change,  $\Delta G$ ,

$$\Delta G = \frac{4}{3}\pi r^2 \gamma_{lv} + \frac{4}{3}\pi r_0^2 (\gamma_{vs} - \gamma_{ls}) \quad , \quad (16)$$

and  $\gamma_{lv}$ ,  $\gamma_{vs}$ , and  $\gamma_{ls}$  surface tensions associated with the liquid-vapor, vapor-solid, and liquid-solid interfaces. The homogeneous case corresponds to  $r_0 = 0$ , that is, no solid and only liquid-vapor nucleation.

Tensions, pulling parallel to their respective surfaces, at equilibrium have zero net component,

$$\gamma_{lv} \cos \theta = \gamma_{vs} - \gamma_{ls} \quad , \quad (17)$$

with liquid-vapor contact angle,  $\theta$ , measured through the liquid. Wetted (hydrophillic) solids exhibit acute contact angle, occurring when,

$$\gamma_{vs} - \gamma_{ls} > 0 \quad , \quad (18)$$

so that the meniscus of the liquid phase is concave. In this case, the solid has greater adhesion for the liquid than the liquid has cohesion for itself, the free energy required to maintain the vapor phase is large (because the solid surface tension term is positive), and the probability of nucleation is decreased by the solid impurity. For a nonwetting (hydrophobic) solid, the situation is reversed, that is, the contact angle is obtuse,

$$\gamma_{vs} - \gamma_{ls} < 0 \quad , \quad (19)$$

the meniscus is convex, the solid has less adhesion for the liquid than the liquid has cohesion for itself, the free energy is reduced because the solid surface tension term is negative, and the probability of formation is increased. In the limiting case,  $\cos \theta = -1$ , the free energy is given by,

$$\Delta G = \frac{4}{3} \pi \gamma_{lv} (r^2 - r_0^2) \quad , \quad (20)$$

which becomes small for cavity radius,  $r$ , near impurity radius,  $r_0$ .

While theories of heterogeneous and homogeneous nucleation work well for a number of liquids, the application of the heterogeneous model to water with impurities is not able to reduce the tensile strength to observable values. The homogeneous theory of nucleation predicts a tensile strength of water near 1,400 *atm*, the heterogeneous theory, with a variety of solid impurities, drops the tensile strength down to 1,000 *atm*, and the measured value for water is approximately 270 *atm*.

In any solution, gas nuclei can be deactivated (crushed) by the application of large hydrostatic pressures. The process of *crushing* is also termed *denucleation*. When denucleated solutions are decompressed in supersaturated states, much higher degrees of supersaturation are requisite to induce bubble formation. In diving, denucleation has been suggested as a mechanism for acclimatization. If denucleation is size selective, that is, greater hydrostatic pressures crush smaller and smaller nuclei, and if number distributions of nuclei increase with decreasing radius (suggested by some experiments), than a conservative deep dive, followed by sufficient surface interval, should in principle afford a margin of safety, by effectively crushing many nuclei and reducing the numbers of nuclei potentially excited into growth under compression-decompression.

The mechanisms of nucleation in the body are obscure. Though nucleation most probably is the precursor to bubble growth, formation and persistence time scales, sites, and size distributions of nuclei remain open questions. Given the complexity and number of substances maintained in tissues and blood, heterogeneous nucleation would appear a probable mechanism.

#### Cavitation

Simply, *cavitation* is the process of vapor phase formation of a liquid when pressure is reduced. A liquid cavitates when vapor bubbles are formed and observed to grow as consequence of pressure reduction. When the phase transition results from pressure change in hydrodynamic flow, a two phase stream consisting of vapor and liquid results, called a cavitating flow. The addition of heat, or heat transfer in a fluid, may also produce cavitation nuclei in the process called boiling. From the physico-chemical perspective, cavitation by pressure reduction and cavitation by heat addition represent the same phenomena, vapor formation and bubble growth in the presence of seed nuclei. Depending on the rate and magnitude of pressure reduction, a bubble may grow slowly or rapidly. A bubble that grows very rapidly (explosively) contains the vapor phase of the liquid mostly, because the diffusion time is too short for any significant increase in entrained gas volume. The process is

called vaporous cavitation, and depends on evaporation of liquid into the bubble. A bubble may also grow more slowly by diffusion of gas into the nucleus, and contain mostly a gas component. In this case, the liquid degasses in what is called gaseous cavitation, the mode observed in the application of ultrasound signals to the liquid. For vaporous cavitation to occur, pressure drops below vapor pressure are requisite. For gaseous cavitation to occur, pressure drops may be less than, or greater than, vapor pressure, depending on nuclei size and degree of liquid saturation. In supersaturated ocean surfaces, for instance, vaporous cavitation occurs very nearly vapor pressure, while gaseous cavitation occurs above vapor pressure.

In gaseous cavitation processes, the inception of growth in nuclei depends little on the duration of the pressure reduction, but the maximum size of the bubble produced does depend upon the time of pressure reduction. In most applications, the maximum size depends only slightly on the initial size of the seed nucleus. Under vaporous cavitation, the maximum size of the bubble produced is essentially independent of the dissolved gas content of the liquid. This obviously suggests different cavitation mechanisms for pressure (reduction) related bubble trauma in diving. Slowly developing bubble problems, such as limb bends many hours after exposure, might be linked to gaseous cavitation mechanisms, while rapid bubble problems, like central nervous system hits and embolism immediately after surfacing, might link to vaporous cavitation.

In a flowing fluid (or body moving through a stationary liquid), the cavitation number,  $\kappa$ , is an indication of the degree of cavitation, or the tendency to cavitate. Describing the similarity in the liquid-gas system, the cavitation number relates gas pressure,  $p$ , to absolute pressure,  $P$ , through,

$$\kappa = 2 \frac{P - p}{\rho u^2} \quad (21)$$

with  $\rho$  and  $u$  the fluid density and velocity. Cavitation and cavitating flows have long been of interest in shipbuilding and hydraulic machinery, underwater signal processing, propellor design, underwater detection, material damage, chemical processing, high pressure and temperature flows in nuclear reactors, volatility of rocket fuels, and bubble chambers for detection of high energy particles, to list a few. Cavitation processes in flowing blood and nearby tissue are also of considerable interest to decompression modelers and table designers.

Today we know that the inception of cavitation in liquids involves the growth of submicroscopic nuclei containing vapor, gas, or both, which are present within the liquid, in crevices, on suspended matter or impurities, or on bounding layers. The need for cavitating nuclei at vapor pressures is well established in the laboratory. There is some difficulty, however, in accounting for their presence and persistence. For a given difference between ambient and gas-vapor pressure, only one radius is stable. Changes in ambient, gas, or vapor pressures will cause the nuclei to either grow, or contract. But even if stable hydrostatically, bubbles and nuclei, because of constricting surface tension, will eventually collapse as gas and vapor diffuse out of the assembly. For instance, an air bubble of radius  $10^{-3}$  cm will dissolve in saturated water in about 6 sec, and even faster if the water is undersaturated or the bubble is smaller. In saturated solutions, bubbles will grow by diffusion, and then tend to be quickly lost at free surfaces as buoyant forces raise them up. A  $10^{-2}$  cm air bubble rises at the rate of 1.5 cm/sec in water. If nuclei are to persist in water, or for that matter, any liquid media, some mechanism must prevent their dissolution or buoyant exit.

A number of possibilities have been suggested to account for the presence of persistent, or stabilized, nuclei in undersaturated liquids, liquids that have been boiled, or denucleated. Crevices in the liquid, or surrounding boundary, may exert mechanical pressure on gas nuclei, holding them in place. Microscopic dust, or other impurities, on which gas and vapor are deposited, are stabilized already. Surface activated molecules, (such as hydrogen and hydroxyl ions in water), or surface activated skins formed from impurities may surround the nuclei and act as rigid spheres, offsetting constrictive surface tension, preventing diffusion of gas out of the nuclei and collapse. In all cases, the end result is a family, or group of families, of persistent nuclei. Time scales for stabilization and persistence of

nuclei would obviously equate to the strength and persistence of stabilizing mechanism. Experimentally, trying to differentiate stabilization modes is very difficult, because (eventual) growth patterns of nuclei are the same in all cases. The ultimate crumbling of surrounding shells, release of crevice mechanical pressure, removal of dust and impurity nucleation centers, and deactivation of surface chemicals leads to the onset of cavitation and bubble growth.

#### Bubble And Seed Pressure Response

Under changes in ambient pressure, bubbles will grow or contract, both due to diffusion (as discussed in Part 1) and Boyle's law. The change under Boyle's law is straightforward. Denoting initial and final pressures and volumes with subscripts,  $i$  and  $f$ , we have,

$$P_i V_i = P_f V_f \quad (22)$$

with bubble volume,

$$V = \frac{4}{3}\pi r^3 \quad (23)$$

for  $r$  the bubble radius. The above supposes totally flexible (probably permeable) bubble films or skins on the inside, certainly not unrealistic over small pressure changes (laboratory experiments). Similarly, if the response to pressure changes of the bubble skins is a smooth and slowly varying function, the above is also true in low order. Obviously, the relationship reduces to,

$$P_i r_i^3 = P_f r_f^3 \quad (24)$$

for a simple radial response to pressure change.

But in the case of structured, impermeable membranes, capable of offsetting constrictive surface tension, the response to Boyle's law is modified,

$$\xi_i P_i V_i = \xi_f P_f V_f \quad (25)$$

with  $\xi$  structure functions depending on pressure,  $P$ . For thin, permeable, and elastic bubble skins,  $\xi = 1$ . For all else,  $\xi \neq 1$ . For cases of gels studied in the laboratory, as an instance, surfactant stabilized micronuclei do not behave like ideal gas bubbles with thin elastic films. Instead under compression-decompression, their behavior is always less than ideal. That is to say, volume changes under compression or decompression are always less than computed by Boyle's law, similar to the response of a wetsuit described earlier. Full discussions follows in Part 12.

Such behavior is implicit in the varying permeability model (VPM), accounting for permeable and impermeable response under pressure changes. During a rapid compression from initial ambient pressure,  $P_i$ , to increased pressure,  $P$ , seeds and micronuclei are subjected to crushing compression which decreases radial size. This produces increased tolerance to supersaturation in blood and tissues since smaller nuclei form macroscopic (unstable) bubbles less readily than larger ones. The greater the crushing pressure,  $\Delta P = P - P_i$ , the greater the supersaturation required to excite a given number of bubbles in the body. A given distribution of nuclei in the body has, for each  $\Delta P$ , a critical radius,  $r_i$ , as seen earlier. Nuclei with radii less than  $r_i$  will not grow into bubbles, while nuclei with radii greater than  $r_i$  will be excited into growth. Said another way, all nuclei larger than  $r_i$  for any compression-decompression schedule,  $\Delta P$ , will evolve into macroscopic bubbles while the rest will not. But just how excited micronuclei grow requires a model for the behavior of effective surface tension under compression-decompression.

According to the VPM and RGBM (lab experiments), the corresponding change in critical radius,  $r$ , following compression,  $\Delta P$ , in the *permeable* region, satisfies the relationship,

$$\Delta P = 2(\gamma_{max} - \gamma) \left[ \frac{1}{r} - \frac{1}{r_i} \right] \quad (26)$$

with  $\gamma_{max}$  the maximum compressional strength of the surfactant skin,  $\gamma$  the surface tension, and  $r_i$  the critical radius at  $P_i$ . When  $P$  exceeds the structure breakpoint,  $P_{max}$ , an equation appropriate to the *impermeable* region must be used. Denoting the crushing pressure differential,  $\Delta P_{max} = P - P_{max}$ , the VPM requires,

$$\Delta P_{max} = 2(\gamma_{max} - \gamma) \left[ \frac{1}{r} - \frac{1}{r_{max}} \right] + P_{max} + 2P_i + P_i \left[ \frac{r_{max}}{r} \right]^3 \quad (27)$$

where,

$$r_{max} = \left[ \frac{P_{max} - P_i}{2(\gamma_{max} - \gamma)} + \frac{1}{r_i} \right]^{-1} \quad (28)$$

is the radius of the critical nucleus at the onset of impermeability, obtained by replacing  $P$  and  $r$  with  $P_{max}$  and  $r_{max}$  above.

The allowed tissue supersaturation,  $\Delta\Pi$ , is given by,

$$\Delta\Pi = 2 \frac{\gamma}{\gamma_{max} r} (\gamma_{max} - \gamma) \quad (29)$$

with, in the permeable region,

$$r = \left[ \frac{\Delta P}{2(\gamma_{max} - \gamma)} + \frac{1}{r_i} \right]^{-1} \quad (30)$$

and, in the impermeable region,

$$r^3 - 2(\gamma_{max} - \gamma)r^2 - \frac{P_i}{\zeta} r_{max}^3 = 0 \quad (31)$$

for,

$$\zeta = \Delta P_{max} - P_{max} + 2P_i + \frac{2(\gamma_{max} - \gamma)}{r_{max}} \quad (32)$$

Thus, allowed supersaturation is a function of three parameters,  $\gamma$ ,  $\gamma_{max}$ , and  $r_i$ . They can be fitted to exposures and lab data. Additionally, nuclei regenerate over times scales,  $\omega$ , such that,

$$r = r_0 + [1 - \exp(-\omega t)](r_i - r_0) \quad (33)$$

with  $r_0$ . the critical radius at initial time ( $t = 0$ ). The fourth parameter,  $\omega^{-1}$ , is on the order of many days (Part 2).

### Exercises

1. What is the (Doppler) frequency shift,  $\Delta f$ , of a boat horn,  $f = 32.5$  hertz, moving toward a stationary snorkeler at speed of  $v_s = 6$  knots (Part 10)?
2. In the adiabatic limit, what is the sound speed,  $u$ , in an ideal gas at atmospheric pressure,  $P = 1.009 \times 10^6$  dyne/cm<sup>2</sup> (Part 10, Table 2)?
3. What is the approximate bubble diameter,  $d$ , for audible bubbles moving with speed,  $u = 35$  cm/sec, in the pulmonary artery (Part 10, Figure 1)?
4. Blood is mainly incompressible water ( $\rho = 1$  g/cm<sup>3</sup>), and so, if blood moving at speed,  $u = 1.2$  cm/sec, through an artery of cross sectional area,  $A_i = .6$  cm, under pressure,  $p_i = 1.012$  atm, encounters a vessel constriction of cross section,  $A_f = .24$  cm, what is the blood speed at the constriction, assuming constant elevation and no external heat or work exchanged in flow (Part 10)? What is the mass flow rate,  $dm/dt$  (Part 10)? If a rupture develops in the artery, allowing blood to exit at atmospheric pressure,  $p_f = 1.0$  atm, what is the change in kinetic energy per unit mass,  $\Delta k = 1/2(v_f^2 - v_i^2)$ , at the rupture point (Parts 10, 1)?

5. What is the inherent unsaturation,  $\Delta_u$ , for an equilibrated diver at 33 fsw using 76/24 nitrox (Part 10)?
6. Laboratory bubble seed counts in gels and (some) living tissue suggest the seed size (radius),  $r$ , distribution,  $n$ , is exponential, decreasing in number as the seed radius increases, so that (differentially),

$$n_i = n_0 \exp(-\beta r_i)$$

with  $n_0$  and  $\beta$  constants. For small sample counts (microscope),  $n_1 = 9865$   $r_1 = .7$  microns and  $n_2 = 5743$ ,  $r_2 = 1.4$  microns, what are  $n_0$  and  $\beta$  (Parts 10, 1)? Assuming  $\beta$  is determined (given), how is the distribution function,  $n$ , normalized to the total seed count,  $N$ , across all sizes (Parts 10, 7)?

7. What is the work function,  $\omega$ , for thin film (Laplacian) bubbles of radius,  $r$ , at constant temperature and entropy (Part 10)?
8. What is the probability,  $dw$ , for purely homogeneous bubble nucleation in (watery) tissue, for any temperature,  $T$ , and radius,  $r$  (Parts 10, 7)? What happens to the nucleation probability as seed radii shrink, that is, as  $r \rightarrow 0$ ? How would this probability function be normalized over all bubble radii (Parts 10, 7)? What is the cumulative probability,  $\Pi$ , for nucleation in the range,  $r_{min} \leq r \leq r_{max}$  (Part 5)? Assuming  $(3kT/16\gamma)^{1/2} = 1 \mu\text{m}$ , evaluate the cumulative probability function (integral),  $\Pi$ , in the range,  $0.1 \leq r \leq 0.5 \mu\text{m}$ , using any convenient integration technique (analytic, approximate, numerical)?
9. What is the cavitation index,  $\kappa$ , for blood flowing through the pulmonary arteries at a speed,  $u = 5$  cm/sec, while saturated with metabolic and inert gases,  $p = .95$  atm, at depth,  $d = 45$  fsw (Part 10)?
10. A bubble of radius,  $r_i = 1.2 \mu\text{m}$ , in tissue interstice at 165 fsw will grow to what radius,  $r_f$ , if decompressed to sea level pressure (just Boyle's law expansion) (Parts 10, 1)?

#### Related Reading

1. Carslaw H.S. and Jaeger J.C., 1950, *Conduction Of Heat In Solids*, Oxford: Clarendon Press.
2. Frenkel J., 1946, *Kinetic Theory Of Liquids*, New York: Oxford University Press.
3. Hills B.A., 1977, *Decompression Sickness*, New York: John Wiley And Sons.
4. Hirschfelder J.O., Curtiss C.F., and Bird R.B., 1964, *Molecular Theory Of Gases And Liquids*, New York: John Wiley And Sons.
5. Huang K., 1973, *Statistical Mechanics*, New York: John Wiley And Sons.
6. Landau L.D. and Lifshitz E.M., 1985, *Fluid Mechanics*, Reading: Addison Wesley.
7. Sears F.W., 1969, *Thermodynamics*, Reading: Addison Wesley.
8. Shapiro A.H., 1958, *Dynamics And Thermodynamics Of Compressible Fluid Flow*, New York: Ronald.
9. Wienke B.R., 1998, *Physics, Physiology, And Decompression Theory For The Technical And Commercial Diver*, National Association Of Underwater Instructors Publication, Tampa.
10. Wienke B.R., 1994, *Basic Diving Physics And Application*, Flagstaff: Best.

PART 11: DECOMPRESSION THEORY  
NUCLEATION PROCESSES AND STATISTICAL MECHANICS

Quiescent Nucleation

Tribonucleation

Cavitation

Gas Turbulent Nucleation

Chemical Nucleation

Microscopic Mechanisms

Ensemble Theory

PART 12: DECOMPRESSION THEORY  
EQUATION OF STATE AND SEED PERSISTENCE

Gases

Solids

Structured Fluids

Unstructuree Fluids

Ensemble Averaging

Time Scales

## EPILOGUE

Gas exchange, bubble formation and elimination, and compression-decompression in blood and tissues are governed by many factors, such as diffusion, perfusion, phase separation and equilibration, nucleation and cavitation, local fluid shifts, and combinations thereof. Owing to the complexity of biological systems, multiplicity of tissues and media, diversity of interfaces and boundary conditions, and plethora of bubble impacting physical and chemical mechanisms, it is difficult to solve the decompression problem *in vivo*. Early decompression studies adopted the supersaturation viewpoint. Closer looks at the physics of phase separation and bubbles in the mid-1970s, and insights into gas transfer mechanisms, culminated in extended kinetics and dissolved-free phase theories. Integration of both approaches can proceed on the numerical side because calculational techniques can be made equivalent. Phase and bubble models are more general than supersaturation models, incorporating their predictive capabilities as subsets. Statistical models, developed mostly in the mid-1980s, are gray from mechanistic viewpoint, but offer the strongest correlations with actual experiments and exposures, possibly the best approach to table fabrication.

Computational models gain efficacy by their ability to track data, often independently of physical interpretation. In that sense, the bottom line for computational models is utility, operational reliability, and reproducibility. Correct models can achieve such ends, but almost any model with sufficient parameter latitude could achieve those same ends. It is fair to say that deterministic models admit varying degrees of computational license, that model parameters may not correlate as complete set with the real world, and that not all mechanisms are addressed optimally. That is, perhaps, one reason why we see representative diving sectors, such as sport, military, commercial, and research, employing different tables, meters, models, and algorithms. Yet, given this situation, phase models attempting to treat both free and dissolved gas exchange, bubbles and gas nuclei, and free phase trigger points appear preferable to other flags. Phase models have the right physical signatures, and thus the potential to extrapolate reasonably when confronting new applications and data. Expect to see their further refinement and development in the future.

Technical diving encompasses a wide spectrum of related disciplines, from geosciences to biosciences, atmospheric sciences to hydrodynamics, medical sciences to engineering sciences, and mathematical physics to statistical analysis. The scope is immense, and so any monograph need be selective, and probably not in depth as possible. And diving physics can be a tedious exercise for readers. Obviously, physiology is an even more complicated mix of physics, chemistry, and biology. Like comments apply to decompression theory, a combination of biophysics, physiology, and biochemistry in a much cloudier picture within perfused and metabolic tissue and blood. Biological systems are so complex, beyond even the fastest and biggest supercomputers for modeling analysis. The marine and geosciences are also beyond comprehensive treatment. Often, tedium relates to a proliferation of equations and deduced results without practical application.

So, selectivity with mathematical application was a direction taken here in narrative. Mathematical equations were kept at definitional level to facilitate description. The hope was to better encapsulate a large body of underlying physical principle in very readable form. Sample problems, with solutions, were included to enhance quantitative description and understanding. Topics were fundamental and chosen in their relevance to technical diving. Bibliographies offer full blown treatments of all principles detailed for diving. For highlight, Figures included some mathematical definitions for completeness, with intended purpose of extending discourse. Problems employed quantitative relationships detailed in the text, using data and information from Tables and Figures.

Thanks again to all of you who have provided impetus for this version. Hope it has met all of your particular needs. Please do contact me with any comments, questions, or concerns.

Safe and fun diving always.

## EXERCISES AND SOLUTIONS

### *Conventions And Units*

1. How many nautical miles to a kilometer?

$$1 \text{ nautical mile} = 1.85 \text{ km} \quad , \quad 1 \text{ km} = \frac{1}{1.85} \text{ nautical mile} = .54 \text{ nautical mile}$$

2. How many electrostatic units (esu) to a coulomb?

$$1 \text{ coul} = 2.99 \times 10^9 \text{ esu} \quad , \quad 1 \text{ esu} = \frac{1}{2.99 \times 10^9} \text{ coul} = 3.34 \times 10^{-10} \text{ coul}$$

3. How many light years to a mile?

$$1 \text{ light yr} = 5.88 \times 10^{12} \text{ mile} \quad , \quad 1 \text{ mile} = \frac{1}{5.88 \times 10^{12}} \text{ light yr} = 1.70 \times 10^{-13} \text{ light yr}$$

4. Convert depth,  $d = 38 \text{ fsw}$ , to ft in fresh water?

$$38 \text{ fsw} \times \frac{1 \text{ ft}}{.975 \text{ fsw}} = 38.9 \text{ ft}$$

5. Convert ascent rate,  $r = 60 \text{ fsw/min}$ , to  $\text{msw/sec}$ ?

$$r = 60 \text{ fsw/min} \times \frac{1 \text{ msw}}{3.28 \text{ fsw}} \times \frac{1 \text{ min}}{60 \text{ sec}} = .305 \text{ msw/sec}$$

6. Convert volume,  $V = 62 \text{ m}^3$ , to  $\text{ft}^3$ ?

$$V = 62 \text{ m}^3 \times \frac{3532 \text{ ft}^3}{\text{m}^3} = 2189 \text{ ft}^3$$

7. Convert pressure,  $P = 5.3 \text{ kg/m}^2$ , to  $\text{lb/in}^2$ ?

$$P = 5.3 \text{ kg/m}^2 \times \frac{.20 \text{ lb/ft}^2}{1 \text{ kg/m}^2} \times \frac{1 \text{ ft}^2}{144 \text{ in}^2} = .0074 \text{ lb/in}^2$$

8. Convert density,  $\rho = .06 \text{ lb/ft}^3$ , to  $\text{kg/m}^3$ ?

$$\rho = .06 \text{ lb/ft}^3 \times \frac{1 \text{ kg/m}^3}{.06 \text{ lb/ft}^3} = 1 \text{ kg/m}^3$$

9. Convert acceleration,  $g = 32 \text{ ft/sec}^2$ , to  $\text{m/sec}^2$ ?

$$g = 32 \text{ ft/sec}^2 \times \frac{1 \text{ m}}{3.28 \text{ ft}} = 9.8 \text{ m/sec}^2$$

Part 1: Gas, Fluid, And Phase Kinetics

1. A tank initially at standard temperature and pressure,  $P_i = 1 \text{ atm}$ , and,  $T_i = 273 \text{ K}^\circ$ , is heated to  $313 \text{ K}^\circ$  by the sun. What is the pressure,  $P$ , in the tank (Part 1)?

$$P = \frac{T}{T_i} P_i = \frac{313}{273} \times 1 \text{ atm} = 1.146 \text{ atm}$$

2. The air in a dry suit at ambient sea level pressure,  $P_0 = 33 \text{ fsw}$ , occupies volume,  $V_0 = .3 \text{ ft}^3$ , at temperature,  $T = 300 \text{ K}^\circ$ . What is volume,  $V$ , occupied at depth,  $P = 50 \text{ fsw}$ , and temperature,  $T = 280 \text{ K}^\circ$  (Part 1)?

$$\frac{P_0 V_0}{T_0} = \frac{PV}{T}$$

$$V = V_0 \frac{P_0 T}{P T_0} = .3 \times \frac{33 \times 280}{50 \times 300} \text{ ft}^3 = .185 \text{ ft}^3$$

3. What volume,  $V$ , does a gmole of an ideal gas occupy at standard temperature and pressure (Part 1)?

$$p = 10.1 \text{ nt/cm}^2 \quad , \quad T = 273 \text{ K}^\circ \quad , \quad R = 8.317 \text{ j/gmole K}^\circ$$

$$PV = nRT \quad , \quad V = \frac{nRT}{P}$$

$$V = \frac{8.317 \times 273}{.101} \text{ cm}^3 = 22.48 \times 10^3 \text{ cm}^3 = 22.48 \text{ l}$$

4. Convert  $37 \text{ C}^\circ$  to Fahrenheit ( $F^\circ$ ), and then to Rankine ( $R^\circ$ ) temperatures (Part 1)?

$$F^\circ = \frac{9}{5} C^\circ + 32 = \frac{9}{5} \times 37 + 32 = 98.6^\circ$$

$$R^\circ = F^\circ + 460 = 98.6 + 460 = 558.6^\circ$$

Convert  $80 \text{ F}^\circ$  to Centigrade ( $C^\circ$ ), and then to Kelvin ( $K^\circ$ ) temperatures (Part 1)?

$$C^\circ = \frac{5}{9} (F^\circ - 32) = \frac{5}{9} (80 - 32) = 26.6^\circ$$

$$K^\circ = C^\circ + 273 = 26.6 + 273 = 299.6^\circ$$

5. A skin diver with lung volume of  $6 \text{ qt}$  descends to a depth,  $d = 85 \text{ fsw}$ . Assuming his lung tissues are 40% air space, what is his compressed lung volume,  $V$  (Part 1)?

$$V_i = .4 \times 6 \text{ qt} = 2.4 \text{ qt} \quad , \quad V_{tis} = .6 \times 6 \text{ qt} = 3.6 \text{ qt}$$

$$P_i = 33 \text{ fsw} \quad , \quad P = 33 + d = 33 + 85 \text{ fsw} = 118 \text{ fsw}$$

$$P_i V_i = P V_f$$

$$V_f = V_i \frac{P_i}{P} = 2.4 \frac{33}{118} \text{ qt} = .67 \text{ qt}$$

$$V = V_f + V_{tis} = .67 + 3.6 \text{ qt} = 4.27 \text{ qt}$$

6. Compute the specific density,  $\eta$ , of mercury (Hg) with respect to seawater (Part 1)?

$$\rho_{Hg} = 13.55 \text{ g/cm}^3 \quad , \quad \rho_{seawater} = 1.026 \text{ gm/cm}^3$$

$$\eta = \frac{\rho_{Hg}}{\rho_{seawater}} = \frac{13.55}{1.026} = 13.21$$

7. What is the mass,  $m$ , of 1500 cm<sup>3</sup> of iron (Fe) (Part 1, Table 2)?

$$\rho_{Fe} = 7.86 \text{ g/cm}^3 \quad , \quad m = \rho_{Fe}V = 7.86 \times 1500 \text{ g} = 11.8 \text{ kg}$$

What volume,  $V$ , does 600 g of calcium (Ca) occupy (Part 1, Table 2)?

$$\rho_{Ca} = 1.55 \text{ g/cm}^3 \quad , \quad V = \frac{m}{\rho_{Ca}} = \frac{600}{1.55} \text{ cm}^3 = 387 \text{ cm}^3$$

What is the gram molecular weight,  $G$ , of osmium (Os), and density,  $\rho_{Os}$  (Part 1, Table 2)?

$$A_{Os} = 190.24 \quad , \quad G = A_{Os} \text{ g} = 190.24 \text{ g} \quad , \quad \rho_{Os} = 22.48 \text{ g/cm}^3$$

8. What is the pressure of a column of seawater,  $d = 33$  fsw, now assuming density,  $\rho = 64$  lbs/ft<sup>3</sup> (Part 1)?

$$P = \rho g d = 64 \times 33 \text{ lbs/ft}^2 = 2112 \text{ lbs/ft}^2 = 14.6 \text{ lbs/in}^2$$

What is the pressure of the same column of fresh water, assuming density,  $\rho = 62.4$  lbs/ft<sup>3</sup> (Part 1)?

$$P = \rho g d = 62.4 \times 33 \text{ lbs/ft}^2 = 2059 \text{ lbs/ft}^2 = 14.3 \text{ lbs/in}^2$$

9. A diver inflates his BC at depth,  $d = 10$  msw, to approximately .015 m<sup>3</sup>. How much work,  $dW$ , does the diver do (Part 1)?

$$dW = P dV$$

$$dW = 20.2 \times 10^4 \times .015 \text{ kg m}^2/\text{sec}^2 = 3.03 \times 10^3 \text{ j}$$

10. A 448 lb winch gear, displacing a volume,  $V = 2$  ft<sup>3</sup>, rests on a hard sea bottom at 99 fsw. What surface volume of air,  $V_{sur}$ , is needed to inflate lift bags to bring the gear to the surface (Parts 1, 3)?

$$d = 99 \text{ fsw} \quad , \quad \rho = 64 \text{ lbs/ft}^3 \quad , \quad w = 448 \text{ lbs}$$

$$V_{lift} = \frac{w}{\rho} = \frac{448}{64} \text{ ft}^3 = 7 \text{ ft}^3$$

$$V_{sur} = V_{lift} \left[ 1 + \frac{d}{33} \right] = 4 \times 7 \text{ ft}^3 = 28 \text{ ft}^3$$

11. A buoy weighing 48 lbs occupies,  $V = 3$  ft<sup>3</sup>. What fraction,  $\xi$ , of its volume will float above water (Parts 1, 3)?

$$V = 3 \text{ ft}^3 \quad , \quad \xi = \frac{V - V_{dis}}{V}$$

$$V_{dis} = \frac{w}{\rho} = \frac{48}{64} \text{ ft}^3 = .75 \text{ ft}^3$$

$$\xi = \frac{3 - .75}{3} = .75$$

12. What is the temperature,  $T$ , of a kgmole van der Waals gas at pressure,  $P = 500 \text{ nt/m}^2$ , and a specific volume,  $v = 2 \text{ m}^3/\text{kgmole}$ , taking the virial coefficients,  $a = 100 \text{ nt m/kgmole}$ , and  $b = .03 \text{ m}^3/\text{kgmole}$  (Part 1)?

$$RT = \left[ P + \frac{a}{v^2} \right] (v - b)$$

$$T = \left[ 500 + \frac{100}{4} \right] \times (2 - .03) \times \frac{1}{8.31 \times 10^{-3}} = 124.5 \times 10^3 \text{ K}^\circ$$

13. What is the relative buoyancy,  $\Delta B$ , of an empty 95 ft<sup>3</sup> steel tank, rated at 3300 lbs/in<sup>2</sup> (Part 1, Table 3)?

$$\Delta B = -6.11 \text{ lbs}$$

What is the approximate tank volume,  $V$  (Part 1, Table 3)?

$$r = \frac{d}{2}, \quad d = 7 \text{ in}, \quad l = 25 \text{ in}$$

$$V = \pi r^2 l = \frac{\pi d^2 l}{4} = \frac{3.14 \times 49 \times 25}{4} \text{ in}^3 = 962 \text{ in}^3 = .56 \text{ ft}^3$$

What does the tank weigh,  $w$ ?

$$V = .56 \text{ ft}^3, \quad \rho = 64 \text{ lbs}^3/\text{ft}, \quad \Delta B = -6.11 \text{ lbs}$$

$$w = \rho g V - \Delta B = 64 \times .56 + 6.11 \text{ lbs} = 42.5 \text{ lbs}$$

14. A mole of air in a tank at 300 K<sup>o</sup> is released to the atmosphere and registers an average temperature drop of 30 K<sup>o</sup>. What is the mean square speed change,  $v dv$ , of the exiting gas (Part 1)?

$$\frac{dv}{dT} = \frac{1}{v} \frac{R\gamma}{1-\gamma}$$

$$\gamma = \frac{5}{3}, \quad R = 8.317 \text{ j/gmole K}^\circ, \quad dT = -30 \text{ K}^\circ$$

$$v dv = \left[ \frac{R\gamma}{1-\gamma} \right] dT = \left[ \frac{8.317 \times 5/3}{2/3} \right] \times 30 \text{ m}^2/\text{sec}^2 = 623.7 \text{ m}^2/\text{sec}^2$$

If the mean square speed change is roughly half the velocity squared of the exiting gas, what is the average velocity,  $v$  (Part 1)?

$$\frac{v^2}{2} = v dv = 623.7 \text{ m}^2/\text{sec}^2$$

$$v = (2v dv)^{1/2} = (2 \times 623.7)^{1/2} \text{ m/sec} = 35.3 \text{ m/sec}$$

15. What is the inspired oxygen fraction,  $i_{O_2}$ , for a rebreather delivering 7.6 l/min of 50/50 nitrox to a Navy SEAL needing 1 l/min oxygen for metabolic consumption off the coast of Kuwait (Part 1)?

$$i_{O_2} = \frac{f_{O_2} F - m}{F - m}$$

$$f_{O_2} = .50, \quad F = 7.6 \text{ l/min}, \quad m = 1.0 \text{ l/min}$$

$$i_{O_2} = \frac{.5 \times 7.6 - 1.0}{7.6 - 1.0} = \frac{2.8}{6.6} = .42$$

If ambient pressure doubles, what is the nozzle flow,  $F_d$ , and inspired oxygen fraction,  $i_{O_2}$  (Part 1)?

$$F_d = F \frac{P}{2P} = \frac{7.6}{2} \text{ l/min} = 3.8 \text{ l/min}$$

$$i_{O_2} = \frac{.5 \times 3.8 - 1.0}{3.8 - 1.0} = \frac{.9}{2.8} = .32$$

16. What is the total pressure,  $P_t$ , inside a bubble lodged in an arteriole of diameter,  $2r = 10 \mu\text{m}$ , if ambient pressure,  $P = 45 \text{ fsw}$ , and assuming a watery surface tension,  $\gamma = 50 \text{ dyne/cm}$  (Part 1)?

$$P = \frac{45}{33} \times 10.1 \text{ nt/cm}^2 = 13.77 \text{ nt/cm}^2$$

$$\frac{2\gamma}{r} = \frac{100}{5 \times 10^{-6}} \text{ dyne/cm}^2 = 2 \text{ nt/cm}^2$$

$$P_t = P + \frac{2\gamma}{r} = 13.77 + 2 \text{ nt/cm}^2 = 15.77 \text{ nt/cm}^2$$

For ambient pressure,  $P = 28 \text{ fsw}$ , what is the watery critical bubble radius,  $r_c$ , at total tissue tension,  $p_t = 20 \text{ nt/cm}^2$  (Part 1)?

$$2\gamma = 1.0 \times 10^{-3} \text{ nt/cm}^2$$

$$p_t = 20 \text{ nt/cm}^2 \quad , \quad P = \frac{28}{33} \times 10.1 \text{ nt/cm}^2 = 8.56 \text{ nt/cm}^2$$

$$r_c = \frac{2\gamma}{p_t - P} = \frac{1.0 \times 10^{-3}}{20 - 8.56} \text{ cm} = 1.14 \mu\text{m}$$

17. After 6 halftimes,  $t = 6\tau$ , what is the ratio,  $\omega$ , of tissue saturation gradient,  $(p - p_a)$ , to initial tissue saturation gradient,  $(p - p_i)$  (Part 1)?

$$\omega = \frac{p - p_a}{p_i - p_a} = \exp(-\lambda t) = \exp(-.693 \times 6) = .016$$

#### Part 2: Critical Tensions And Phase Volumes

1. What is the USN critical tension,  $M$ , in the 80 min tissue compartment at a depth,  $d = 80 \text{ fsw}$  (Part 2, Figure 1)?

$$M_0 = 52 \text{ fsw} \quad , \quad \Delta M = 1.26$$

$$M = M_0 + \Delta M d$$

$$M = 52 + 1.26 \times 80 \text{ fsw} = 152.8 \text{ fsw}$$

What is the critical ratio,  $R$  (Parts 2, 5)?

$$R = \frac{M}{P} \quad , \quad P = 80 + 33 \text{ fsw} = 113 \text{ fsw}$$

$$R = \frac{152.8}{113} = 1.35$$

What is the critical gradient,  $G$  (Parts 2, 5)?

$$G = M - P = 152.8 - 113 \text{ fsw} = 39.8 \text{ fsw}$$

2. What is the critical tension,  $M$ , at depth,  $d = 34$  fsw, for the nitrogen tissue compartment,  $\tau = 7.56$  min (Part 2)?

$$M = 152.7\tau^{-1/4} + 3.25\tau^{-1/4}d$$

$$M = 152.7 \times .603 + 3.25 \times .603 \times 34 \text{ fsw} = 158.7 \text{ fsw}$$

3. What is the instantaneous nitrogen pressure,  $p$ , in the 15 min tissue compartment of a Maine scallop diver at 67 fsw for 38 min, assuming initial sea level equilibration (Parts 2, 1)?

$$\tau = 15 \text{ min} \quad , \quad f_{N_2} = .79$$

$$p_i = 33 \times .79 \text{ fsw} = 26.1 \text{ fsw}$$

$$p_a = f_{N_2}(P_0 + d) = (33 + 67) \times .79 \text{ fsw} = 79 \text{ fsw}$$

$$\lambda = \frac{.693}{15} \text{ min}^{-1} = .046 \text{ min}^{-1}$$

$$p = p_a + (p_i - p_a) \exp(-\lambda t)$$

$$p = 79 + (26.1 - 79) \times .174 \text{ fsw} = 69.7 \text{ fsw}$$

What is the tension in the 240 min compartment (Parts 2, 1)?

$$\lambda = \frac{.693}{240} \text{ min}^{-1} = .0029 \text{ min}^{-1}$$

$$p = 79 + (26.1 - 79) \times .896 \text{ fsw} = 31.6 \text{ fsw}$$

4. What is the critical tension,  $M$ , at a nominal depth of 10 fsw for the 15 min tissue compartment (Parts 2, 5)?

$$M = 152.7\tau^{-1/4} + 3.25\tau^{-1/4}d$$

$$M = 152.7 \times .51 + 3.25 \times .51 \times 10 \text{ fsw} = 94.4 \text{ fsw}$$

What is the corresponding critical ratio,  $R$ , (Parts 2, 5)?

$$R = \frac{M}{P} = \frac{94.4}{43} = 2.19$$

5. How long does it take for the 80 min tissue compartment to approach its critical surfacing tension,  $M = M_0 = 52$  fsw, at a depth of 140 fsw, assuming initial nitrogen tension of 45 fsw (Parts 2, 1)?

$$p_i = 45 \text{ fsw} \quad , \quad p_a = f_{N_2}(33 + d)$$

$$p_a = .79 \times (33 + 140) \text{ fsw} = 136.6 \text{ fsw}$$

$$\lambda = \frac{.693}{80} \text{ min}^{-1} = .0087 \text{ min}^{-1} \quad , \quad M = 52 \text{ fsw}$$

$$t_n = \frac{1}{\lambda} \ln \left[ \frac{p_i - p_a}{M - p_a} \right] = 114.9 \times \ln \left[ \frac{91.6}{84.6} \right] \text{ min} = 9.1 \text{ min}$$

What is the nonstop limit,  $t_n$ , for the 80 min tissue at this depth (Parts 2, 1)?

$$t_n = 9.1 \text{ min}$$

6. If the nonstop time limit at depth,  $d = 90$  fsw, is,  $t_n = 22$  min, what is the surfacing critical tension,  $M_0$ , assuming that the 5 min compartment controls the exposure (has largest computed tissue tension at this depth) (Parts 2, 1)?

$$\lambda = \frac{.693}{5} \text{ min}^{-1} = .1386 \text{ min}^{-1}$$

$$p_i = .79 \times 33 \text{ fsw} = 26.1 \text{ fsw}$$

$$p_a = .79 \times (33 + 90) = 97.1 \text{ fsw}$$

$$M_0 = p_a + (p_i - p_a) \exp(-\lambda t_n)$$

$$M_0 = 97.1 - 78.2 \exp(-.1386 \times 22) \text{ fsw} = 94 \text{ fsw}$$

7. An oil rig diver is saturated at a depth of 300 fsw in the North Sea on heliox. For critical helium gradient (absolute),  $G = M - P = 40$  fsw, what is the minimum depth (ceiling),  $d$ , accessible to the platform diver (Parts 2, 5)?

$$M = 333 \text{ fsw} \quad , \quad P = M - G = (333 - 40) \text{ fsw} = 293 \text{ fsw}$$

$$d = (P - 33) \text{ fsw} = (293 - 33) \text{ fsw} = 260 \text{ fsw}$$

8. For a compression-decompression,  $\Delta P = 120$  fsw, at an ambient pressure,  $P = 13$  fsw, what is the seed excitation radius,  $r$  (Part 2, Part 10, Table 1)?

$$\frac{1}{r} = \frac{1}{r_i} + \frac{\Delta P}{\zeta} \quad , \quad \zeta = 158 \mu\text{m fsw} \quad , \quad r_i = .89 \mu\text{m}$$

$$r = \frac{\zeta r_i}{\zeta + \Delta P r_i} = \frac{158 \times .89}{158 + 120 \times .89} \mu\text{m} = .47 \mu\text{m}$$

9. What is the reduction factor,  $\xi$ , for a repetitive dive, after 40 min surface interval, to a depth of 80 fsw, if a first dive was to 40 fsw following 6 consecutive days of diving, using the multiday regeneration timescale of 21 days for the compartment,  $\tau = 40$  min (Part 2, Figures 5, 6, 7)?

$$\xi = \eta^{reg} \eta^{ep} \eta^{exc}$$

$$\omega^{-1} = 21 \text{ days} \quad , \quad \eta^{reg} = .74 \text{ (7 days cumulative)}$$

$$\eta^{ep} = .70 \text{ (40 min surface interval, } \tau = 40 \text{ min)}$$

$$\eta^{exc} = .52 \text{ (} d_{prev} = 40 \text{ fsw, } d_{pres} = 80 \text{ fsw)}$$

$$\xi = .74 \times .70 \times .52 = .29$$

What is the bounding reduction factor,  $\xi^{bd}$ , for this compartment and exposure (Part 2)?

$$\tau = 40 \text{ min} \quad , \quad \lambda_{bd} = .0559 \text{ min}^{-1}$$

$$\xi^{bd} = \frac{.12 + .18 \exp(-480\lambda_{bd})}{.12 + .18 \exp(-\tau\lambda_{bd})}$$

$$\xi^{bd} = \frac{.12 + .18 \times 10^{-12}}{.12 + .18 \times .12} = .83$$

At depth,  $d = 80$  fsw, what is the critical gradient,  $\bar{G}$ , same exposure and tissue compartment (Part 2, Table 2)?

$$\bar{G} = \xi G \quad , \quad \xi = \xi^{bd} = .83 \quad , \quad d = 80 \text{ fsw}$$

$$G = G_0 + \Delta G d \quad , \quad G_0 = 36 \text{ fsw} \quad , \quad \Delta G = .468$$

$$\bar{G} = \xi(G_0 + \Delta G d) = .83 \times (36 + .468 \times 80) \text{ fsw} = 60.9 \text{ fsw}$$

10. Which tissues are affected most by slow ascent rates and safety stops (Part 2, Tables 3, 4)?

*Slow Tissue Compartments*

*Part 3: Altitude Similarity And Procedures*

1. What is ambient pressure,  $P_h$ , at an elevation of 6,500 ft (Part 3)?

$$P_h = P_0 \exp(-0.038h) \quad , \quad P_0 = 33 \text{ fsw} \quad , \quad h = 6.5$$

$$P_{6.5} = 33 \exp(-0.038 \times 6.5) \text{ fsw} = 33 \times .78 \text{ fsw} = 25.7 \text{ fsw}$$

What is the altitude scaling factor,  $\alpha$ , for depth, and what is the equivalent sea level depth,  $\delta$ , for actual depth,  $d = 78 \text{ ft}$  (Part 3)?

$$\alpha = \exp(0.038h) = \exp(0.038 \times 6.5) = 1.28$$

$$\delta = \eta \alpha d = .975 \times 1.28 \times 78 \text{ fsw} = 97.5 \text{ fsw}$$

2. If a decompression stop is required at 20 fsw according to the USN Tables, what is the actual depth,  $d$ , of the stop at 6,500 ft elevation (Part 3)?

$$\delta = 20 \text{ fsw} \quad , \quad d = \frac{\delta}{\eta \alpha} = \frac{20}{.975 \times 1.28} \text{ ft} = 16 \text{ ft}$$

3. Construct a set of critical surfacing ratios,  $R_7$ , at 7,000 ft elevation using the standard USN set,  $R_0$ , at sea level, and altitude similarity (downscaling) through the correction factor,  $\alpha$  (Parts 3, 7)?

$$\alpha = \exp(0.0381h) \quad , \quad h = 7$$

$$R_h = \frac{R_0}{\alpha} = R_0 \exp(-0.0381h)$$

$$R_0 = (3.15, 2.67, 2.18, 1.76, 1.58, 1.55)$$

$$R_7 = R_0 \exp(-0.0381 \times 7) = .77 R_0$$

$$R_7 = (2.43, 2.05, 1.67, 1.35, 1.20, 1.19)$$

4. At an altitude,  $z = 10,000 \text{ ft}$ , what is the approximate nonstop limit,  $t_n$ , for an exposure at 60 fsw (Part 3, Figure 3)?

$$t_n \approx 17 \text{ min}$$

Using the similarity method, what is the nonstop time limit (Part 3, Part 7, Figure 1)?

$$\alpha = \exp(0.038h) \quad , \quad h = 10$$

$$\alpha = \exp(.38) = 1.462 \quad , \quad d = 1.462 \times 60 \text{ fsw} = 87.7 \text{ fsw}$$

$$t_n \approx 25 \text{ min}$$

5. A 75 kg diver journeys to a mountain lake at 1,830 m. What is the surface wetsuit buoyancy,  $\Delta w$ , increase (Part 3)?

$$\Delta w = .0029wh \quad , \quad h = \frac{1830}{1000} \times 3.28 = 6 \quad , \quad w = mg$$

$$\Delta w = .0029 \times 75 \times 9.8 \times 6 \text{ nt} = 12.7 \text{ nt}$$

6. What is the salt water to fresh water buoyancy loss,  $\Delta W$ , for a salvage diver plus gear of mass,  $m = 90 \text{ kg}$  (Part 3)?

$$W = mg$$

$$\Delta W = -.025 W = -.025 \times 90 \times 9.8 \text{ nt} = -22.5 \text{ nt}$$

7. A fully inflated BC displaces,  $V = .78 \text{ ft}^3$ , of sea water. What is the lift,  $B$ , provided by the BC (Parts 3,2)?

$$B = \rho g V$$

$$B = 64 \times .78 \text{ lb} = 49.9 \text{ lb}$$

8. A pearl diver displaces,  $V = 3.5 \text{ ft}^3$ , of fresh water. What is the buoyant force,  $B$ , on diver and gear (Parts 3,2)?

$$B = \rho g V$$

$$B = 62.4 \times 3.5 \text{ lb} = 218 \text{ lb}$$

If diver plus gear weigh,  $W = 200 \text{ lb}$ , how much add additional weigh,  $\Delta W$ , must be added to the belt for neutral buoyancy (Parts 3,2)?

$$\Delta W = B - W = (218 - 200) \text{ lb} = 18 \text{ lb}$$

9. The air pressure in a scuba tank drops from  $2475 \text{ lbs/in}^2$  to  $1500 \text{ lbs/in}^2$  in 8 min. What is the air consumption rate,  $\chi$  (Part 3)?

$$\chi = \frac{2475 - 1500}{8} \text{ lbs/in}^2 \text{ min} = 121.9 \text{ lbs/in}^2 \text{ min}$$

If the tank is rated at  $72 \text{ ft}^3$ , what is the consumption rate,  $\chi$ , in  $\text{ft}^3/\text{min}$  (Part 3)?

$$121.9 \text{ lbs/in}^2 \text{ min} \times \frac{72 \text{ ft}^3}{2475 \text{ lbs/in}^2} = 3.5 \text{ ft}^3/\text{min}$$

10. How long,  $t$ , will a tank containing,  $V = 34 \text{ ft}^3$ , of air last at 33 fsw for an EOD specialist swimming against a 6 knot very cold current in the ocean (Part 3, Table 5)?

$$P_0 = 33 \text{ fsw} \quad , \quad \chi_0 = 2 \text{ ft}^3/\text{min} \quad , \quad \chi = \chi_0 \left[ 1 + \frac{d}{P_0} \right]$$

$$\chi = 2 \times \left[ 1 + \frac{33}{33} \right] \text{ ft}^3/\text{min} = 4 \text{ ft}^3/\text{min}$$

$$t = \frac{V}{\chi} = \frac{34}{4} \text{ min} = 8.5 \text{ min}$$

11. What is the air consumption rate,  $\chi$ , at depth,  $d = 46 \text{ ft}$ , and elevation,  $z = 6,500 \text{ ft}$ , for sea level surface consumption rate,  $\chi_0 = .95 \text{ ft}^3/\text{min}$ , in fresh water (Part 3)?

$$\chi = \frac{\chi_0}{\alpha} \left[ 1 + \frac{d\eta\alpha}{P_0} \right]$$

$$\chi = \frac{.95}{1.28} \times \left[ 1 + \frac{46 \times .975 \times 1.28}{33} \right] \text{ ft}^3/\text{min} = 2.03 \text{ ft}^3/\text{min}$$

12. If a hookah unit pumps a surface rate,  $\chi_0 = 5 \text{ ft}^3/\text{min}$ , of air, what rate,  $\chi$ , will it deliver at depth,  $d = 20 \text{ fsw}$ , on a reef (Part 3)?

$$\chi = \chi_0 \frac{P_0}{P_0 + d} = 5 \times \frac{33}{53} \text{ ft}^3/\text{min} = 3.13 \text{ ft}^3/\text{min}$$

13. What fill rate at 9,000 ft elevation will a high speed compressor deliver if its rated output is 10  $\text{ft}^3/\text{min}$  at sea level (Part 3)?

$$\chi_0 = 10 \text{ ft}^3/\text{min} \quad , \quad h = 9$$

$$\alpha = \exp(-0.038 \times 9) = 1.41$$

$$\chi = \frac{\chi_0}{\alpha} = \frac{10}{1.41} \text{ ft}^3/\text{min} = 7.09 \text{ ft}^3/\text{min}$$

14. At an altitude,  $z = 1,300 \text{ m}$ , what reading,  $\delta$ , will a capillary gauge register at actual depth,  $d = 18 \text{ m}$ , in fresh water (Part 3)?

$$\delta = \alpha \eta d \quad , \quad h = \frac{1300}{1000} \times 3.28 = 4.26$$

$$\alpha = \exp(-0.038 \times 4.26) = 1.19 \quad , \quad \delta = 1.19 \times .975 \times 18 \text{ msw} = 20.3 \text{ msw}$$

What does a bourdon (oil filled) gauge read,  $\delta$  (Part 3)?

$$P_0 = 10 \text{ msw} \quad , \quad P_{4.26} = 8.4 \text{ msw}$$

$$\delta = \eta d + P_h - P_0 = .975 \times 18 + 8.4 - 10 \text{ msw} = 15.9 \text{ msw}$$

15. A tank rated 80  $\text{ft}^3$  at 3000  $\text{lb}/\text{in}^2$ , registers a pressure,  $P = 1420 \text{ lb}/\text{in}^2$  on a sub gauge. What is the remaining air volume,  $V$  (Part 3)?

$$V = V_r \frac{P}{P_r}$$

$$V = 80 \times \frac{1420}{3000} \text{ ft}^3 = 37.8 \text{ ft}^3$$

What is the tank constant,  $\kappa$  (Part 3)?

$$\kappa = \frac{P_r}{V_r} = \frac{3000}{80} \text{ lb}/\text{in}^2 \text{ ft}^3 = 37.5 \text{ lb}/\text{in}^2 \text{ ft}^3$$

#### Part 4: Mixed Gases And Decompression

1. At elevation,  $z = 3,800 \text{ m}$ , what are the working depths,  $d_{max}$  and  $d_{min}$ , for a 74/26 nitrox mixture, assuming 1.6 atm and .16 atm as the upper and lower oxygen partial pressure limits (Parts 4, 3)?

$$f_{N_2} = .74$$

$$h = 3800 \times \frac{3.28}{1000} = 12.46 \quad , \quad P_{12.46} = 33 \times \exp(-.038 \times 12.46) \text{ fsw} = 20.55 \text{ fsw}$$

$$\eta d_{max} = \frac{52.8}{f_{O_2}} - P_h \text{ fsw} \quad , \quad \eta d_{min} = \frac{5.3}{f_{O_2}} - P_h \text{ fsw}$$

$$\eta d_{max} = \frac{52.8}{.26} - 20.55 \text{ fsw} = 182.5 \text{ fsw}$$

$$d_{max} = \frac{182.5}{\eta} \text{ ft} = 187.2 \text{ ft}$$

$$\eta d_{min} = \frac{5.3}{.26} - 20.55 \text{ fsw} = -.2 \text{ fsw} \text{ (means surface is OK)}$$

$$d_{min} = -\frac{.2}{\eta} \text{ ft} = -.21 \text{ ft}$$

2. What is the equivalent air depth,  $\delta$ , at ocean depth,  $d = 98 \text{ fsw}$ , for enriched 74/26 nitrox (Part 4)?

$$f_{N_2} = .74$$

$$\delta = \frac{f_{N_2}}{.79} (33 + d) - 33 = \frac{.74}{.79} \times (33 + 98) - 33 \text{ fsw} = 89.7 \text{ fsw}$$

3. What is the nitrogen fraction,  $f_{N_2}$ , for an equivalent air depth,  $\delta = 110 \text{ fsw}$ , at ocean depth,  $d = 125 \text{ fsw}$  (Part 4)?

$$f_{N_2} = \frac{.79(\delta + 33)}{(d + 33)} = \frac{.79 \times 143}{158} = .72$$

What is the corresponding oxygen floor,  $d_{max}$  (Part 4)?

$$f_{O_2} = .28 \text{ , } P_0 = 33 \text{ fsw}$$

$$d_{max} = \frac{52.8}{f_{O_2}} - P_0 \text{ fsw} = \frac{52.8}{.28} - 33 = 156 \text{ fsw}$$

4. What is the relative concentration,  $c$ , of neon dissolved in oil at a partial pressure  $p = 9.8 \text{ atm}$  (Part 4, Table 2)?

$$c = Sp = .009 \times 9.8 = .0882$$

What is the ratio,  $\zeta$ , of relative solubilities of neon in water and oil (Part 4, Table 2)?

$$\zeta = \frac{S_{water}}{S_{oil}} = \frac{.009}{.021} = .43$$

How much more,  $\xi$ , is nitrogen soluble in oil versus water (Part 4, Table 2)?

$$\xi = \frac{S_{oil}}{S_{water}} = \frac{.067}{.012} = 5.6$$

5. According to Graham, what roughly is the ratio,  $\psi$ , of molecular diffusion speeds of hydrogen to oxygen (Part 4)?

$$\psi = \left[ \frac{A_{O_2}}{A_{H_2}} \right]^{1/2} = \left[ \frac{32}{2} \right]^{1/2} = 4$$

6. A commercial diving operation is constructing a set of helium proprietary tables using the popular DCIEM nitrogen tables as a basis before testing. If the spectrum of tissues,  $\tau$ , in the DCIEM nitrogen tables is ( 2.5, 5, 10, 20, 40, 80, 160, 320 min), what are the corresponding set for the helium tables, assuming the same critical tensions,  $M$ , as the nitrogen tables (Parts 4,7)?

$$\tau_{He} = \left[ \frac{A_{He}}{A_{N_2}} \right]^{1/2} \tau_{N_2} = \left[ \frac{4}{28} \right]^{1/2} \tau_{N_2} = .38 \times \tau_{N_2}$$

$$\tau_{He} = (.94, 1.89, 3.78, 7.56, 15.12, 30.24, 60.48, 120.96) \text{ min}$$

7. What is the ratio,  $\zeta$ , of narcotic potency of helium to argon (Part 4, Table 2)?

$$\zeta = \frac{\nu_{He}}{\nu_{Ar}} = \frac{4.26}{.43} = 9.9$$

Which is the least potent (Part 4, Table 2)?

*Least Potent Gas = Helium*

8. What is the surface oxygen partial pressure,  $p_0$ , for a normoxic breathing mixture at 450 fsw (Part 4)?

$$p = .21 \text{ atm (normoxic)} , P_0 = 33 \text{ fsw} , P = 450 + 33 \text{ fsw} = 483 \text{ fsw}$$

$$p_0 = \frac{P_0}{P} p = \frac{33}{483} \times .2 \text{ atm} = .0137 \text{ atm}$$

What can you say about such a mixture at the surface (Parts 4, 11)?

$$p_0 \leq .16 \text{ atm}$$

*Mixture Is Hypoxic (Very Hypoxic)*

9. Assuming surface equilibration on air, what is the total tissue tension,  $\Pi$ , in the,  $\tau = 20$  min, compartment after 10 min at depth,  $d = 90$  fsw, of a salvage diver breathing 60/25/15 trimix ( $f_{He} = .60, f_{N_2} = .25, f_{O_2} = .15$ ) (Parts 4, 1)?

$$\Pi = p_{He} + p_{N_2} , d = 90 \text{ fsw} , \tau_{N_2} = 20 \text{ min} , \tau_{He} = \frac{20}{2.65} = 7.55 \text{ min}$$

$$\lambda_{N_2} = \frac{.693}{\tau_{N_2}} = \frac{.693}{20} \text{ min}^{-1} = .0347 \text{ min}^{-1}$$

$$\lambda_{He} = \frac{.693}{\tau_{He}} = \frac{.693}{7.55} \text{ min}^{-1} = .0918 \text{ min}^{-1}$$

$$p_{aN_2} = f_{N_2} p_a = f_{N_2} (33 + d) \text{ fsw} , p_{iN_2} = .79 P_0$$

$$p_{aHe} = f_{He} p_a = f_{He} (33 + d) \text{ fsw} , p_{iHe} = 0.0$$

$$p_{N_2} = p_{aN_2} + (p_{iN_2} - p_{aN_2}) \exp(-\lambda_{N_2} t)$$

$$p_{iN_2} = .79 \times 33 \text{ fsw} = 26.01 \text{ fsw} , p_{aN_2} = f_{N_2} p_a = .25 \times 123 = 30.7 \text{ fsw}$$

$$p_{N_2} = 30.7 + (26.1 - 30.7) \exp(-.0347 \times 10) \text{ fsw} = 27.4 \text{ fsw}$$

$$p_{iHe} = 0.00 \text{ fsw} , p_{aHe} = f_{He} p_a = .60 \times 123 \text{ fsw} = 73.8 \text{ fsw}$$

$$p_{He} = 73.8 - 73.8 \exp(-.0918 \times 10) \text{ fsw} = 44.3 \text{ fsw}$$

$$\Pi = 27.4 + 44.3 \text{ fsw} = 71.7 \text{ fsw}$$

What is the critical surfacing tension,  $M_0$ , for the 20 min compartment (Part 2)?

$$M_0 = 72 \text{ fsw}$$

Should this diver ascend to the surface on his trimix?

*Probably - But Slowly*

10. What is the critical tension,  $M$ , at depth,  $d = 34$  fsw, in the helium tissue compartment,  $\tau = 15$  min, using the air fit to critical tensions (Parts 4, 2)?

$$\tau = 2.65\tau_{He} = 2.65 \times 15 \text{ min} = 39.8 \text{ min} \quad , \quad d = 34 \text{ fsw}$$

$$M = 152.7 \times 39.8^{-1/4} + 3.25 \times 39.8^{-1/4} \times 34 \text{ fsw} = 104.7 \text{ fsw}$$

11. If an oil rig diver on 80/20 heliox saturated at  $P_i = 6$  atm, switches to 80/20 nitrox at  $P_a = 4$  atm on ascent, how long after the switch,  $t_m$ , does isobaric counterdiffusion produce a minima in total gas tension,  $\Pi$ , in the  $\tau_{N_2} = 54$  min compartment (Part 4)?

$$\tau_{N_2} = 54 \text{ min} \quad , \quad \lambda_{N_2} = \frac{.693}{54} \text{ min}^{-1} = .0128 \text{ min}^{-1}$$

$$\tau_{He} = \frac{\tau_{N_2}}{2.7} = \frac{54}{2.7} \text{ min} = 20 \text{ min} \quad , \quad \lambda_{He} = \frac{.693}{20} \text{ min}^{-1} = .0347 \text{ min}^{-1}$$

$$p_{iHe} = f_{He}P_i = .8 \times 6 \text{ atm} = 4.8 \text{ atm} \quad , \quad p_{aHe} = f_{He}P_a = .8 \times 4 \text{ atm} = 3.2 \text{ atm}$$

$$p_{iN_2} = 0 \text{ atm} \quad , \quad p_{aN_2} = f_{N_2}P_a = .8 \times 4 \text{ atm} = 3.2 \text{ atm}$$

$$t_m = \frac{1}{\lambda_{He} - \lambda_{N_2}} \ln \left[ \frac{\lambda_{He}(p_{iHe} - p_{aHe})}{\lambda_{N_2}(p_{aN_2} - p_{iN_2})} \right]$$

$$t_m = \frac{1}{(.0347 - .0128)} \times \ln \left[ \frac{.0347 \times (4.8 - 3.2)}{.0128 \times (3.2 - 0)} \right] \text{ min} = 13.9 \text{ min}$$

If the gas switch is 80/20 nitrox to 80/20 heliox, how long after the switch (all else the same),  $t_m$ , does isobaric counterdiffusion produce a maxima in total gas tension,  $\Pi$ , in the same compartment (Part 4)?

$$p_{iN_2} = 4.8 \text{ atm} \quad , \quad p_{aN_2} = 3.2 \text{ atm} \quad , \quad p_{iHe} = 0 \text{ atm} \quad , \quad p_{aHe} = 3.2 \text{ atm}$$

$$t_m = \frac{1}{\lambda_{N_2} - \lambda_{He}} \ln \left[ \frac{\lambda_{N_2}(p_{iN_2} - p_{aN_2})}{\lambda_{He}(p_{aHe} - p_{iHe})} \right]$$

$$t_m = \frac{1}{(.0128 - .0347)} \times \ln \left[ \frac{.0128 \times (4.8 - 3.2)}{.0347 \times (3.2 - 0)} \right] \text{ min} = 77.1 \text{ min}$$

12. How many OTUs does a 14/50 trimix (14% oxygen, 50% helium) diver register at 230 fsw for 45 min (Part 4)?

$$d = 230 \text{ fsw} \quad , \quad P_{sur} = 33 \text{ fsw} \quad , \quad f_{O_2} = .14$$

$$p_{O_2} = f_{O_2} \frac{P_{sur} + d}{33} = .14 \times \frac{33 + 230}{33} \text{ atm} = 1.12 \text{ atm}$$

$$\Upsilon = \left[ \frac{p_{O_2} - 0.5}{0.5} \right]^{0.83} t$$

$$\Upsilon = \left[ \frac{1.12 - 0.5}{0.5} \right]^{0.83} \times 45 \text{ min} = 53.8 \text{ min}$$

What is the toxic limit,  $t_x$ , on this mixture at this depth (Part 4)?

$$t_x = 4160 \exp(-2.77p_{O_2}) = 4160 \exp(-2.77 \times 1.12) \text{ min} = 186.9 \text{ min}$$

*Part 5: Decompression Tables, Meters, And Models*

1. According to the Wienke-Yount bulk diffusion law, what is the nonstop time limit,  $t_n$ , at a depth of 155 fsw (Part 5)?

$$dt_n^{1/2} = C \quad , \quad C = 400 \text{ fsw min}^{1/2}$$

$$t_n = \left[ \frac{C}{d} \right]^2 = \left[ \frac{400}{155} \right]^2 = 6.4 \text{ min}$$

2. According to USN Tables (modified), what is the surfacing Group for a photographer at 67, fsw for 35 min, assuming the ascent rate is standard,  $r = 60 \text{ fsw/min}$  (Part 5, Figure 1)?

$$\text{Group} = G$$

If 68 min are spent on the surface, what is the new Group (Part 5, Figure 1)?

$$\text{Group} = F$$

On the next dive to 46 fsw, what is the penalty time,  $t$  (Part 5, Figure 1)?

$$\text{Penalty Time} = t = 47 \text{ min}$$

If bottom time at 46 fsw is 15 min, what is the new surfacing Group (Part 5, Figure 1)?

$$\text{Group} = I$$

3. A Group F diver sustains what overpressure,  $\Delta P$ , in nitrogen loading (absolute) in the 120 min compartment (Part 5)?

$$\Delta P = 6 \times 2 \text{ fsw} = 12 \text{ fsw}$$

What is the nitrogen tension,  $p$ , in the 120 min compartment of that (surface) F diver after 160 min (Parts 5, 1)?

$$\Delta P = 12 \text{ fsw} \quad , \quad p_i - p_a = f_{N_2} \Delta P = .79 \times 12 \text{ fsw} = 9.48 \text{ fsw}$$

$$\lambda = \frac{.693}{120} \text{ min}^{-1} = .0058 \text{ min}^{-1}$$

$$p = p_a + (p_i - p_a) \exp(-\lambda t)$$

$$p = 26.1 + 9.48 \times \exp(-.0058 \times 160) \text{ fsw} = 29.8 \text{ fsw}$$

Into what Group does the diver now fall (Parts 1, 7)?

$$\Delta P = \frac{(p - p_a)}{f_{N_2}} = \frac{(29.8 - 26.1)}{.79} \text{ fsw} = 4.68 \text{ fsw}$$

$$\text{Group} = C$$

4. A reef ecologist at depth,  $d = 35 \text{ fsw}$ , on a dive computer registers a spectrum of nitrogen tensions,  $p = (50, 48, 43, 41, 40, 42, 44) \text{ fsw}$ , in tissues,  $\tau = (5, 10, 20, 40, 80, 120, 240) \text{ min}$ . What are the corresponding tissue gradients,  $g = p - p_a$  (Parts 5, 1)?

$$g = p - p_a \quad , \quad P = 33 + 35 \text{ fsw} = 68 \text{ fsw} \quad , \quad p_a = .79 P = 53.7 \text{ fsw}$$

$$g = (-3.7, -5.7, -10.7, -12.7, -13.7, -11.7, -9.7) \text{ fsw}$$

Since tissue gradients are inward (all negative), what is the implication for the present dive (Parts 5, 1)?

*Present Dive Has Been Short And Shallow*

What might higher tissue tensions in the two slowest compartments, relative to faster middle compartments, suggest (Parts 5, 1)?

*Repetitive Diving Within 12 – 24 hrs*

5. If a Park Ranger lugs his dive gear to Lake Catherine above Santa Fe (New Mexico) at an elevation of 9,560 ft and plans a dive to 40 ft, what is the altitude correction factor,  $\beta$ , and what is the sea level equivalent depth,  $\delta$ , for the dive (Parts 5, 3)?

$$\beta = \eta \exp(0.038h) = .975 \times \exp(0.038 \times 9.65) = 1.40$$

$$\delta = \beta d = 1.40 \times 40 \text{ fsw} = 56.2 \text{ fsw}$$

If the ascent rate,  $r_0$ , in the Tables at sea level is 60 fsw/min, what is the altitude rate,  $r$  (Parts 5, 3)?

$$r = \frac{r_0}{\beta} = \frac{60}{1.4} \text{ ft/min} = 42.8 \text{ ft/min}$$

If the excursion to Lake Catherine is launched from Santa Fe, elevation 6,860 ft, taking 15 min, what Group should the Ranger diver assign to the start of the dive (Part 3, Table 1)?

$$\Delta z = 9650 - 6860 \text{ ft} = 2790 \text{ ft}$$

*Altitude Group = B*

If the dive lasts 20 min, in what group does the diver surface (Part 5, Figure 1)?

$$\text{Group B Penalty Time (60 fsw)} = 11 \text{ min}$$

$$\text{Total Dive Time} = 20 + 11 \text{ min} = 31 \text{ min}$$

*Surfacing Group = G*

As a Group G diver, what is the maximum change in altitude permitted (Part 3, Table 1)?

$$\text{Permitted Altitude Change} = 6,000 \text{ ft}$$

How long before a mountain Group G diver drops into Group A (Part 5, Figure 1)?

$$\text{Surface Interval Time} = 7.6 \text{ hr}$$

How long before a Group G diver can ascend 7,000 ft in elevation, according to the 24 hr rule (Part 3, Table 2)?

$$\text{Surface Interval Time} = 3.7 \text{ hr}$$

6. According to the USN Tables at sea level, the nonstop limit at 100 fsw is 22 min. What is the nonstop limit,  $t_n$ , at elevation of 5,600 ft, using the similarity method (Parts 5, 3 Figure 1)?

$$\beta = \eta \exp(0.038h) = .975 \times \exp(0.038 \times 5.6)$$

$$\beta = .975 \times 1.23 = 1.20$$

$$\delta = 100 \times 1.20 \text{ fsw} = 120 \text{ fsw}$$

$$t_n = 12 \text{ min}$$

7. If the surfacing critical tension for the  $\tau = 90$  min compartment is,  $M_0 = 55$  fsw, what is the compartment limit,  $t_n$ , for 79/21 nitrox (air) at,  $d = 50$  fsw (Parts 5, 2, 4)?

$$f_{N_2} = .79 \quad , \quad p_i = f_{N_2} \times 33 \text{ fsw} = .79 \times 33 \text{ fsw} = 26.1 \text{ fsw}$$

$$p_a = f_{N_2}(33 + 50) \text{ fsw} = .79 \times 83 \text{ fsw} = 65.6 \text{ fsw}$$

$$\lambda = \frac{.693}{90} = .0077 \text{ min}^{-1} \quad , \quad t_n = \frac{1}{\lambda} \ln \left[ \frac{p_i - p_a}{M_0 - p_a} \right]$$

$$t_n = \frac{1}{.0077} \times \ln \left[ \frac{26.1 - 65.6}{55 - 65.6} \right] \text{ min} = 121.6 \text{ min}$$

What is the compartment limit,  $t_n$ , for 79/21 heliox at,  $d = 50$  fsw (Parts 5, 2, 4)?

$$\lambda = \frac{.693}{90/2.65} \text{ min}^{-1} = .0204 \text{ min}^{-1}$$

$$t_n = \frac{1}{.0204} \times \ln \left[ \frac{26.1 - 65.6}{55 - 65.6} \right] \text{ min} = 45.8 \text{ min}$$

8. Match model features to the BDM, MTM, TM, VPM, RGBM, and TBDM (Parts 5, 8)?  
Dissolved gas phase treatment only?

MTM, BDM

Many perfusion tissue compartments?

MTM, TM, VPM, RGBM, TBDM

Single bulk tissue compartment?

BDM

Exponential distributions of bubble seeds?

VPM, RGBM

Critical tension, ratio, or gradient limit points?

BDM, MTM

Critical separated phase volume or dose limit points?

TM, VPM, RGBM, TBDM

Pain thresholds?

TM

Multidiving limitations?

RGBM

Commercial meter implementations?

MTM, RGBM

Seed regeneration?

VPM, RGBM

Dissolved and free gas phase treatment?

TM, VPM, RGBM, TBDM

*Part 6: Comparative Profiles And Operational Diving*

1. Match the following problematic profiles to model issues addressed by the BDM, MTM, TM, VPM, RGBM, or TBDM (Parts 6, 5)?

*Deepest dive not first?*

*Additional bubble seed excitation*

*Yo, yo diving?*

*Rapid bubble growth*

*Multiple inert gas switches during dive?*

*Isobaric counterdiffusion*

*Multilevel diving?*

*Bubble growth and gas elimination*

*Rapid ascents?*

*VGE elimination*

*Short interval repetitive diving?*

*Bubble growth and gas elimination*

*Multiday diving?*

*Seed regeneration*

*Saturation exposures?*

*Very slow tissue compartments*

*Altitude diving?*

*Larger bubble seed excitation radii*

2. Link the MTM, BDM, TM, VPM, RGBM, and TBDM to the 5 overlapping steps leading to bubble trouble (Parts 6, 5)?

*Nucleation and stabilization?*

*VPM and RGBM*

*Supersaturation?*

*MTM, BDM, TM, VPM, RGBM, and TBDM*

*Bubble excitation and growth?*

*TM, VPM, RGBM, and TBDM*

*Coalescence?*

*TM, VPM, and RGBM*

*Tissue deformation and occlusion?*

*TM*

*Part 7: Decompression Risk And Statistics*

1. What is the probability,  $P(3)$ , for 3 DCI cases in 100 dives, given an underlying incidence rate of 5% (Part 7)?

$$P(n) = \frac{N!}{n! m!} p^n q^m, \quad N = 100, \quad n = 3, \quad m = 97$$

$$p = .05, \quad q = .95$$

$$P(3) = \left[ \frac{100!}{3! 97!} \right] (.05)^3 (.95)^{97} = \left[ \frac{100 \times 99 \times 98}{1 \times 2 \times 3} \right] (.0001)(.0069) = .111$$

What is the probability,  $Q(97)$ , for 97 cases for no DCI in the same sample (Part 7)?

$$Q(97) = 1 - P(3) = 1 - .111 = .899$$

2. What is the probability,  $P(1)$ , for one hit (DCI) in 20 dives with underlying incidence,  $p = .01$  (Part 7, Table 1)?

$$P(1) = .16$$

What is the probability,  $P_{>}(2)$ , for two or more hits in 20 dives for the same underlying incidence (Part 7, Table 1)?

$$P_{>}(2) = .02$$

3. What is the survivor fraction,  $1 - \chi$ , for decompression of saturated air divers across,  $G = 35$  fsw (Part 7)?

$$1 - \chi = \exp \left[ - \left( \frac{G - 14.3}{25.1} \right)^{4.73} \right]$$

$$1 - \chi = \exp \left[ - \left( \frac{21.7}{25.1} \right)^{4.73} \right] = \exp (-.46) = .63$$

What is the cumulative DCI incidence rate,  $\chi$  (Part 7)?

$$\chi = 1 - .63 = .37$$

4. What can you say about the DCI relative incidence,  $p$ , for a nonstop exposure at 80 fsw for 40 min (Part 8, Table 2)?

$$0.01 < p < 0.05$$

What can you say about the (old) USN nonstop limit of 200 min at 40 fsw (Part 7, Table 2)?

$$p > 0.05$$

5. A table modeler wants to use maximum likelihood in fitting the data to a DCI risk function,  $\phi$ , of the temporal form,  $\phi = \exp(-qt)$ , for 1000 trial dives with some 200 cases of DCI. What are the risk forms,  $\rho$  and  $\sigma$  (probabilities) (Part 7)?

$$\rho(t) = 1 - \exp \left[ - \int_0^t \phi(t') dt' \right] = 1 - \exp [-(\exp(-qt) - 1)/q]$$

$$\sigma(t) = \exp \left[ - \int_0^t \phi(t') dt' \right] = \exp [-(\exp(-qt) - 1)/q]$$

What are the asymptotic limits,  $\rho(\infty)$  and  $\sigma(\infty)$ ?

$$\rho(\infty) \rightarrow 1 - \exp(-1/q)$$

$$\sigma(\infty) \rightarrow \exp(-1/q)$$

What is the value of  $q$  for the asymptotic forms (Part 7)?

$$\Psi = 200 \ln [1 - \exp(-1/q)] + 800 \ln [\exp(-1/q)]$$

$$\frac{\partial \Psi}{\partial q} = \left[ \frac{-200}{1 - \exp(-1/q)} \right] \left[ \frac{\exp(-1/q)}{q^2} \right] + \left[ \frac{800}{\exp(-1/q)} \right] \left[ \frac{\exp(-1/q)}{q^2} \right] = 0$$

$$\exp(-1/q) = .800 \quad , \quad - \left[ \frac{1}{q} \right] = \ln .8$$

$$q = - \left[ \frac{1}{\ln .8} \right] = 4.48$$

### Part 8: Computing And Decompression Algorithms

1. Solve the perfusion rate equation for the tissue tension,  $p$ , as a function of time (Part 8)?

$$\frac{\partial p}{\partial t} = -\lambda(p - p_a)$$

$$y = p - p_a \quad , \quad dy = dp$$

$$\frac{dy}{y} = -\lambda dt$$

$$\ln y = -\lambda t + c \quad (c \text{ is integration constant})$$

$$y = c \exp(-\lambda t) \quad , \quad t = 0 \quad , \quad p = p_i \quad , \quad y = p_i - p_a = c$$

$$p - p_a = (p_i - p_a) \exp(-\lambda t)$$

2. For a depth-time law of the form,  $dt_n^{1/2} = C$ , what is the nonstop time limit for compartment,  $\tau = 45$  min, and what is the depth,  $d$ , for  $C = 450$  fsw min<sup>1/2</sup> (Part 8)?

$$\lambda t_n = 1.25 \quad , \quad \tau = 45 \text{ min}$$

$$t_n = \frac{1.25}{\lambda} = \frac{1.25 \tau}{.693} = \frac{1.25 \times 45}{.693} \text{ min} = 81.2 \text{ min}$$

$$dt_n^{1/2} = C = 450 \text{ fsw min}^{1/2}$$

$$d = \frac{C}{t_n^{1/2}} = \frac{450}{81.2^{1/2}} \text{ fsw} = 49.9 \text{ fsw}$$

3. Average the diffusion limited tissue response over length,  $l$ , to eliminate spatial dependences (Part 8)?

$$p - p_a = (p_i - p_a) \sum_{n=1}^{\infty} W_n \frac{1}{l} \int_0^l \sin(\omega_n x) dx \exp(-\omega_n^2 Dt)$$

$$p - p_a = (p_i - p_a) \sum_{n=1}^{\infty} \frac{2W_n}{\omega_n} \exp(-\omega_n^2 Dt)$$

$$p - p_a = (p_i - p_a) \sum_{n=1}^{\infty} \frac{8}{(2n-1)^2 \pi^2} \exp(-\omega_{2n-1}^2 Dt)$$

4. Given temporal diffusion length,  $\zeta = l/D^{1/2} = 10 \text{ sec}^{1/2}$ , what are short and long time values of the bulk diffusion response function (Part 8)?

$$p - p_a = (p_i - p_a) \left[ 1 - \frac{(4Dt)^{1/2}}{l\pi^{1/2}} \right] \quad (\text{short})$$

$$p - p_a = (p_i - p_a) \left[ 1 - \frac{.4t^{1/2}}{\pi^{1/2}} \right]$$

$$p - p_a = (p_i - p_a) \frac{l}{(4\pi Dt)^{1/2}} \quad (\text{long})$$

$$p - p_a = (p_i - p_a) \frac{10}{(4\pi t)^{1/2}}$$

5. In the VPM and RGBM, a normalized distribution of bubble seeds,  $n$ , in radii  $r$ , is assumed to be excited by compression-decompression, and takes the form,

$$n = N\beta \exp(-\beta r)$$

with  $N$  and  $\beta$  distribution constants. If the excess,  $\Delta n$ , excited into growth by compression-decompression is just the difference between the total number at  $r_0$  and the total number at  $r$ , with  $r$  and  $r_0$  linked by the magnitude of the pressure change,  $\Delta P$ , compute  $\Delta n$  for  $r$  and  $r_0$ , normalizing over all radii (Part 8)?

$$\Delta n = \int_r^\infty n dr - \int_{r_0}^\infty n dr = N \left[ \int_r^\infty \exp(-\beta r) dr - \int_{r_0}^\infty \exp(-\beta r) dr \right]$$

$$\Delta n = N [\exp(-\beta r) - \exp(-\beta r_0)]$$

For small argument,  $a$ , one has,  $\exp(-a) = 1 - a$ , so obtain a small argument expression for the bubble excess,  $\Delta n$ , (Part 8)?

$$\Delta n = N [1 - \beta r - 1 + \beta r_0] = N [\beta r_0 - \beta r]$$

6. Formally evaluate the phase volume integral, assuming constant gradients,  $G$ , during decompression, and exponentially decaying gradients afterwards, with tissue decay constant,  $\lambda$ , assuming  $\lambda t_d$  is small (Part 8)?

$$G \rightarrow G \quad 0 \leq t \leq t_d \quad , \quad G \rightarrow G \exp(-\lambda t) \quad t_d < t$$

$$\int_0^\infty \Delta n G dt = \int_0^{t_d} \Delta n G dt + \int_{t_d}^\infty \Delta n G dt = \alpha V$$

$$\int_0^\infty \Delta n G dt = \Delta n G \int_0^{t_d} dt + \Delta n G \int_{t_d}^\infty \exp(-\lambda t) dt = \Delta n G t_d + \lambda^{-1} \Delta n G \exp(-\lambda t_d)$$

$$\int_0^\infty \Delta n G dt = \Delta n G [t_d + \lambda^{-1} \exp(-\lambda t_d)]$$

$$\exp(-\lambda t_d) \rightarrow 1 \quad , \quad \lambda t_d \ll 1$$

$$\int_0^\infty \Delta n G dt \rightarrow \Delta n G [t_d + \lambda^{-1}] \rightarrow \alpha V$$

7. What is the minimum excitation gradient,  $G^{min}$ , and saturation gradient,  $G^{sat}$ , for seeds of radius,  $r = .5$  microns, according to the VPM and RGBM (Part 8)?

$$G^{min} = \frac{11.01}{r}, \quad G^{sat} = \frac{58.6}{r} - 49.9$$

$$G^{min} = \frac{11.01}{.5} fsw = 22.02 fsw$$

$$G^{sat} = \frac{58.6}{.5} - 49.9 fsw = 67.3 fsw$$

What is the corresponding pressure,  $P$ , for this saturation gradient (Part 8)?

$$G^{sat} = .372P + 11.01$$

$$P = \frac{G^{sat}}{.372} + 26.6 = \frac{67.3}{.372} + 26.6 fsw = 207.5 fsw$$

8. Using the TBDM, couple the bubble volumetric growth rate to corresponding molal diffusion current, rate of pressure change for constant temperature (Part 8)?

$$\frac{\partial(PV + 2\gamma r^{-1})}{\partial t} = R \frac{\partial(nT)}{\partial t}$$

$$V \frac{\partial P}{\partial t} + P \frac{\partial V}{\partial t} + \frac{2\gamma}{r} \frac{\partial V}{\partial t} - \frac{2V\gamma}{r^2} \frac{\partial r}{\partial t} = TR \frac{\partial n}{\partial t}$$

$$\frac{\partial r}{\partial t} = \frac{1}{4\pi r^2} \frac{\partial V}{\partial t}$$

9. In the TM, assuming  $J_0(a) \rightarrow 1$  and  $J_1(a) \rightarrow a$ , for small  $a$ , expand the tissue response function (Part 8)?

$$p - p_v = (p_i - p_v) \frac{16}{b^2 - 4a^2} \sum_{n=1}^{\infty} \frac{1}{\epsilon_n^2} \frac{J_1^2(\epsilon_n b/2)}{J_0^2(\epsilon_n a) - J_1^2(\epsilon_n b/2)} \exp(-\epsilon_n^2 Dt)$$

$$p - p_v = (p_i - p_a) \frac{16}{b^2 - 4a^2} \sum_{n=1}^{\infty} \frac{1}{\epsilon_n^2} \frac{(\epsilon_n b/2)^2}{1 - (\epsilon_n b/2)^2} \exp(-\epsilon_n^2 Dt)$$

$$p - p_v = (p_i - p_v) \sum_{n=1}^{\infty} \left[ \frac{16}{(\epsilon_n b)^2 - (2\epsilon_n a)^2} \right] \left[ \frac{(\epsilon_n b)^2}{4 - (\epsilon_n b)^2} \right] \exp(-\epsilon_n^2 Dt)$$

#### Part 9: Diving Maladies And Drugs

1. For the following set of conditions and/or symptoms, identify possible diving maladies (Part 9).

Partial oxygen tension of 1.85 atm?

*Hyperoxia*

Partial carbon dioxide tension of .10 atm, with muscle spasms?

*Hypercapnia (Severe)*

Rasping cough at an elevation of 14,000 ft?

*Pulmonary Edema*

*Intense shivering in a dry suit?*

*Hypothermia*

*Light-headedness on an air dive to 145 fsw?*

*Nitrogen Narcosis*

*Weakness and headache following a hyperventilated skin dive?*

*Hypocapnia*

*Pain in the sternum and coughing of blood?*

*Pneumothorax*

*Shortness of breath at 6,555 ft elevation?*

*Altitude Sickness*

*Lesions and cracks in the long bones of the leg?*

*Dysbaric Osteonecrosis*

*Paralysis of the lower legs?*

*DCI (Neurological)*

*Partial oxygen tension of .09 atm?*

*Hypoxia (Moderate)*

*Chest pain and swelling of the neck?*

*Subcutaneous Emphysema*

*Profuse sweating and muscle cramps?*

*Hyperthermia*

*Dull aching pain in the joints?*

*DCI (Articular)*

2. Match some of the following side effects to drugs possibly avoided when diving (Part 9)?

*Drowsiness?*

*Scopolamine, Flexiril, Robaxin, Elavil, Haldol, Sinequan*

*Motor impairment?*

*Meclizine, Dimenhydrate, Propoxyphene, Codein, Oxycodone, Hydrocodone*

*Reduced blood flow capacity?*

*Metoprolol, Hytrin, Tenex, Theophylline*

*Cardiac dysrhythmias?*

*Theodur, Metaprel, Uniphyl, Ventolin*

*Blurred vision?*

*Scopolamine*

*Reduced cognitive functionality?*

*Valium, Halcion, Dalmane, Elavil, Haldol, Sinequan*

Part 10: Bubbles And Biosystems

1. What is the (Doppler) frequency shift,  $\Delta f$ , of a boat horn,  $f = 32.5$  hertz, moving toward a stationary snorkeler at speed of  $v_s = 6$  knots (Part 10)?

$$\Delta f = f \frac{v_s}{u - v_s}$$

$$u = 333 \text{ m/sec} \quad , \quad v_s = 6 \times .514 \text{ m/sec} = 3.08 \text{ m/sec}$$

$$\Delta f = 32.5 \times \frac{3.08}{333 + 3.08} \text{ hertz} = .0314 \text{ hertz}$$

2. In the adiabatic limit, what is the sound speed,  $u$ , in an ideal gas at atmospheric pressure,  $P = 1.009 \times 10^6$  dyne/cm<sup>2</sup> (Part 10, Table 2)?

$$u^2 = \frac{Y}{\rho} \quad , \quad Y = 5/3P \quad , \quad \rho = .00024 \text{ g/cm}^3$$

$$u = \left[ \frac{5/3P}{\rho} \right]^{1/2} = \left[ \frac{5/3 \times 1.009 \times 10^6}{.00024} \right]^{1/2} \text{ cm/sec} = 837.2 \text{ m/sec}$$

3. What is the approximate bubble diameter,  $d$ , for audible bubbles moving with speed,  $u = 35$  cm/sec, in the pulmonary artery (Part 10, Figure 1)?

$$d = 78 \text{ } \mu\text{m}$$

4. Blood is mainly incompressible water ( $\rho = 1 \text{ g/cm}^3$ ), and so, if blood moving at speed,  $u = 1.2$  cm/sec, through an artery of cross sectional area,  $A_i = .6$  cm, under pressure,  $p_i = 1.012$  atm, encounters a vessel constriction of cross section,  $A_f = .24$  cm, what is the blood speed at the constriction, assuming constant elevation and no external heat or work exchanged in flow (Part 10)?

$$p_i = 1.012 \text{ atm} = 1.012 \times 1.013 \times 10^6 \text{ dyne/cm}^2 = 1.0252 \times 10^6 \text{ dyne/cm}^2$$

$$\rho_i = \frac{m}{V_i} = \rho_f = \frac{m}{V_f} = \rho = 1.0 \text{ g/cm}^3 \quad , \quad v_i = u$$

$$\rho_i v_i A_i = \rho_f v_f A_f$$

$$v_f = \frac{\rho_i A_i}{\rho_f A_f} v_i = \frac{A_i}{A_f} v_i = \frac{.6}{.24} \times 1.2 \text{ cm/sec} = 3.0 \text{ cm/sec}$$

What is the mass flow rate,  $dm/dt$  (Part 10)?

$$\frac{dm}{dt} = \rho A_i v_i = \rho A_f v_f = 1.0 \times .6 \times 1.2 \text{ g/sec} = 1.0 \times .24 \times 3 \text{ g/sec} = .72 \text{ g/sec}$$

If a rupture develops in the artery, allowing blood to exit at atmospheric pressure,  $p_f = 1.0$  atm, what is the change in kinetic energy per unit mass,  $\Delta k = 1/2(v_f^2 - v_i^2)$ , at the rupture point (Parts 10, 1)?

$$\Delta k = \frac{1}{2}(v_f^2 - v_i^2) = \frac{(p_i - p_f)}{\rho}$$

$$\Delta k = \frac{.012 \times 1.013 \times 10^6}{1.0} \text{ ergs/g} = 12.2 \times 10^3 \text{ ergs/g}$$

5. What is the inherent unsaturation,  $\Delta_u$ , for an equilibrated diver at 33 fsw using 76/24 nitrox (Part 10)?

$$\begin{aligned}\Delta_u &= (1 - f_{N_2})P - 2.04f_{N_2} - 5.47 \text{ fsw} \\ f_{N_2} &= .76 \quad , \quad P = P_0 + d = 33 + 33 \text{ fsw} = 66 \text{ fsw} \\ \Delta_u &= .24 \times 66 - 2.04 \times .76 - 5.47 \text{ fsw} = 8.82 \text{ fsw}\end{aligned}$$

6. Laboratory bubble seed counts in gels and (some) living tissue suggest the seed size (radius),  $r$ , distribution,  $n$ , is exponential, decreasing in number as the seed radius increases, so that (differentially),

$$n_i = n_0 \exp(-\beta r_i)$$

with  $n_0$  and  $\beta$  constants. For small sample counts (microscope),  $n_1 = 9865$   $r_1 = .7$  microns and  $n_2 = 5743$ ,  $r_2 = 1.4$  microns, what are  $n_0$  and  $\beta$  (Parts 10, 1)?

$$\begin{aligned}n_i &= n_0 \exp(-\beta r_i) \quad , \quad \ln(n_1/n_2) = -\beta(r_1 - r_2) \\ \beta &= \frac{1}{r_2 - r_1} \ln(n_1/n_2) = \frac{1}{.7} \times \ln(9865/5743) \mu m^{-1} = .773 \mu m^{-1} \\ n_0 &= n_i \exp(\beta r_i) = n_1 \exp(\beta r_1) = 9865 \exp(.773 \times .7) = 16947\end{aligned}$$

Assuming  $\beta$  is determined (given), how is the distribution function,  $n$ , normalized to the total seed count,  $N$ , across all sizes (Parts 10, 7)?

$$\begin{aligned}n_0 \int_0^{\infty} \exp(-\beta r) dr &= \frac{n_0}{\beta} = N \\ n_0 &= \beta N\end{aligned}$$

7. What is the work function,  $\omega$ , for thin film (Laplacian) bubbles of radius,  $r$ , at constant temperature and entropy (Part 10)?

$$\begin{aligned}\frac{\partial \omega}{\partial V} &= -\tau = -\frac{2\gamma}{r} \\ V &= \frac{4}{3}\pi r^3 \\ \frac{\partial \omega}{\partial V} &= \frac{\partial \omega}{\partial r} \frac{\partial r}{\partial V} = \frac{1}{4\pi r^2} \frac{\partial \omega}{\partial r} \\ \frac{\partial \omega}{\partial r} &= -4\pi r^2 \frac{2\gamma}{r} = -8\pi\gamma r \\ \omega &= \int -8\pi\gamma r dr = -4\pi\gamma r^2\end{aligned}$$

8. What is the probability,  $dw$ , for purely homogeneous bubble nucleation in (watery) tissue, for any temperature,  $T$ , and radius,  $r$  (Parts 10, 7)?

$$dw = \exp(-\Delta G/kT) \quad , \quad \Delta G = \frac{4}{3}\pi\gamma r^2 \quad , \quad \gamma = 18 \text{ dyne/cm}$$

What happens to the nucleation probability as seed radii shrink, that is, as  $r \rightarrow 0$ ?

$$\lim_{r \rightarrow 0} dw = \lim_{r \rightarrow 0} \exp(-4\pi\gamma r^2/3kT) \rightarrow \exp(0) \rightarrow 1$$

How would this probability function be normalized over all bubble radii (Parts 10, 7)?

$$\Gamma = \int_0^{\infty} \exp(-4\pi\gamma r^2/3kT) dr = \left[ \frac{3kT}{16\gamma} \right]^{1/2}$$

$$dw = \Gamma^{-1} \exp(-4\pi\gamma r^2/3kT) dr$$

What is the cumulative probability,  $\Pi$ , for nucleation in the range,  $r_{min} \leq r \leq r_{max}$  (Part 5)?

$$\Pi = \Gamma^{-1} \int_{r_{min}}^{r_{max}} \exp(-4\pi\gamma r^2/3kT) dr$$

Assuming  $(3kT/16\gamma)^{1/2} = 1 \mu m$ , evaluate the cumulative probability function (integral),  $\Pi$ , in the range,  $0.1 \leq r \leq 0.5 \mu m$ , using any convenient integration technique (analytic, approximate, numerical)?

$$\Gamma = \left[ \frac{3kT}{16\gamma} \right]^{1/2} = 1 \mu m$$

$$\Pi = \Gamma^{-1} \int_{0.1}^{0.5} \exp(-4\pi\gamma r^2/3kT) dr$$

$$\Pi = \Gamma^{-1} \int_{0.1}^{0.5} \exp(-\pi r^2/4\Gamma^2) dr = .3673$$

9. What is the cavitation index,  $\kappa$ , for blood flowing through the pulmonary arteries at a speed,  $u = 5 \text{ cm/sec}$ , while saturated with metabolic and inert gases,  $p = .95 \text{ atm}$ , at depth,  $d = 45 \text{ fsw}$  (Part 10)?

$$\kappa = 2 \frac{P - p}{\rho u^2}, \quad \rho = 1.04 \text{ gm/cm}^3$$

$$p = .95 \times 1.013 \times 10^6 \text{ dyne/cm}^2 = .962 \times 10^6 \text{ dyne/cm}^2$$

$$P = (1 + 45/33) \times 1.013 \times 10^6 \text{ dyne/cm}^2 = 2.394 \times 10^6 \text{ dyne/cm}^2$$

$$\kappa = 2 \times \frac{1.41 \times 10^6}{1.04 \times 25} = 73.3 \times 10^6$$

10. A bubble of radius,  $r_i = 1.2 \mu m$ , in tissue interstice at 165 fsw will grow to what radius,  $r_f$ , if decompressed to sea level pressure (just Boyle's law expansion) (Parts 10, 1)?

$$P_i r_i^3 = P_f r_f^3, \quad P_i = 198 \text{ fsw}, \quad P_f = 33 \text{ fsw}, \quad r_i = 1.2 \mu m$$

$$r_f = \left[ \frac{P_i}{P_f} \right]^{1/3} r_i = \left[ \frac{198}{33} \right]^{1/3} \times 1.2 \mu m = 1.80 \times 1.2 \mu m = 2.17 \mu m$$

## BIBLIOGRAPHY

References span a wide spectra of technical diving material and details, broaching historical to modern developments. Entries are alphabetically and chronologically listed, completing or extending related reading at the end of each Part.

1. Abramowitz M. and Stegun I.A., 1972, *Handbook Of Mathematical Functions*, New York: Dover Publications.

2. Adamson A.W., 1976, *The Physical Chemistry Of Surfaces*, New York: John Wiley And Sons.
3. Albano G., Griscuoli P.M., and Ciulla C., 1962, *La Sindrome Neuropsichica Di Profundita*, *Lav. Um.* 14, 351-358.
4. Atkins C.E., Lehner C.E., Beck K.A., Dubielzig R.R., Nordheim E.V. and Lanphier E.H., 1988, *Experimental Respiratory Decompression Sickness In Sheep*, *J. Appl. Physiol.* 65, 1163-1171.
5. Bassett B.E., 1979, *And Yet Another Approach To The Problems Of Altitude Diving And Flying After Diving, Decompression In Depth Proceedings, Professional Association Of Diving Instructors, Santa Ana.*
6. Batchelor G.K., 1953, *Theory Of Homogeneous Turbulence*, New York: Cambridge University Press.
7. Bateman J.B. and Lang J., 1945, *Formation And Growth Of Bubbles In Aqueous Solutions*, *Canad. J. Res.* E23, 22-31.
8. Beckwith B., 1969, *Mechanical Measurement*, Reading: Addison Wesley.
9. Bell R.L. and Borgwardt R.E., 1976, *The Theory Of High Altitude Corrections To The US Navy Standard Decompression Tables*, *Undersea Biomed. Res.* 3, 1-23.
10. Behnke A.R., 1971, *Decompression Sickness: Advances And Interpretations*, *Aerospace Med.* 42, 255-267.
11. Behnke A.R., 1967, *The Isobaric (Oxygen Window) Principle Of Decompression*, *Trans. Third Annual Conf. Marine Tech, Soc.* 1, 213-228.
12. Behnke A.R., 1945, *Decompression Sickness Incident To Deep Sea Diving And High Altitude*, *Medicine* 24, 381-402.
13. Bennett P.B. and Elliot D.H., 1996, *The Physiology And Medicine Of Diving And Compressed Air Work*, London: Bailliere Tindall And Cassell.
14. Bennett P.B. and Hayward A.J., 1968, *Relative Decompression Sickness In Rats Of Neon And Other Inert Gases*, *Aerospace Med.* 39, 301-302.
15. Berghage T.E. and Durman D., 1980, *US Navy Air Recompression Schedule Risk Analysis*, *Nav. Med. Res. Bull.* 1, 1-22.
16. Bert P., 1878, *La Pression Barometrique*, Paris: Masson.
17. Boni M., Schibli R., Nussberger P. and Buhlmann A. A., 1976, *Diving At Diminished Atmospheric Pressure: Air Decompression Tables For Different Altitudes*, *Undersea Biomed. Res.* 3, 189-204.
18. Bookspan J., 1997, *Diving Physiology In Plain English*, Bethesda: Undersea And Hyperbaric Medical Society.
19. Bove A.A. and Davis J.C., 1990, *Diving Medicine*, Philadelphia: W.B. Saunders.
20. Bowker A.H. and Lieberman G.J., 1964, *Engineering Statistics*, Engelwood Cliffs: Prentice-Hall.

21. Boycott A.E., Damant G.C.C., and Haldane J.S., 1908, *The Prevention Of Compressed Air Illness*, *J. Hyg.* 8, 342-443.
22. Brereton R.G., 1974, *US Navy SEAL Combat Manual*, Memphis: Naval Technical Training.
23. Buckles R.G., 1968, *The Physics Of Bubble Formation And Growth*, *Aerospace Med.* 39, 1062-1069.
24. Buhlmann A.A., 1984, *Decompression/Decompression Sickness*, Berlin: Springer Verlag.
25. Buhlmann A.A., 1966, *Saturation And Desaturation With N<sub>2</sub> And He At 4 Atmospheres*, *J. Appl. Physiol.* 23, 458-462.
26. Carslaw H.S. and Jaeger J.C., 1950, *Conduction Of Heat In Solids*, Oxford: Clarendon Press.
27. Carter L.L. and Cashwell E.D., 1975, *Particle Transport Simulations With The Monte Carlo Method*, Oak Ridge: United States Energy And Research Development Administration.
28. Case K.M. and Zweifel P.F., 1977, *Linear Transport Theory*, Reading: Addison Wesley.
29. Conkin J. and Van Liew H.D., 1991, *Failure Of The Straight Line Boundary Between Safe And Unsafe Decompressions When Extrapolated To The Hypobaric Regime*, *Undersea Biomed. Res.* 18, 16.
30. Crocker W.E. and Taylor H.J., 1952, *A Method Of Calculating Decompression Stages And The Formulation Of New Diving Tables*, *Investigation Into The Decompression Tables*, Medical Research Council Report, UPS 131, London.
31. Cross E.R., 1970, *High Altitude Decompression*, *Skin Diver Magazine* 19, 17-18.
32. Davidson W.M., Sutton B.M., and Taylor H.J., 1950, *Decompression Ratio For Goats Following Long Exposure And Return To Atmospheric Pressure Without Stoppage*, Medical Research Council Report, UPS 110, London.
33. Des Granges M., 1957, *Repetitive Diving Decompression Tables*, USN Experimental Diving Unit Report, NEDU 6-57, Washington DC.
34. Duffner G.J., Synder J.F., and Smith L.L., 1959, *Adaptation Of Helium-Oxygen To Mixed Gas Scuba*, USN Experimental Diving Unit Report, NEDU 3-59, Washington, DC
35. Dwyer J.V., 1956, *Calculation Of Repetitive Diving Decompression Tables*, USN Experimental Diving Unit Report, NEDU 1-57, Washington DC.
36. Eckenhoff R.G., Olstad C.E. and Carrod G.E., 1990, *Human Dose Response Relationship For Decompression And Endogenous Bubble Formation*, *J. Appl. Physiol.* 69, 914-918.
37. Eckenhoff R.G., Olstad C.E., Parker S.F. and Bondi K.R., 1986, *Direct Ascent From Shallow Air Saturation Exposures*, *Undersea Biomed. Res.* 13, 305-316.
38. Eckenhoff R.G., 1985, *Doppler Bubble Detection*, *Undersea Biomed. Res.* 12, 485-489.
39. Edmonds C., Lowry C., and Pennefather J., 1994, *Diving And Subaquatic Medicine*, Portland: Book News.
40. Edmonds C, McKenzie B., and Thomas R., 1997, *Diving Medicine For Scuba Divers*, Sydney: Aquaquest Publications.

41. Eisenberg P., 1953, *Progress On The Mechanics Of Cavitation, David Taylor Model Basin Rept. 842.*
42. Epstein P.S. and Plesset M.S., 1950, *On The Stability Of Gas Bubbles In Liquid-Gas Solutions, J. Chm. Phys. 18, 1505-1509.*
43. Evans A. and Walder D.N., 1969, *Significance Of Gas Macronuclei In The Aetiology Of Decompression Sickness, Nature London 222, 251-252.*
44. Farm F.P., Hayashi E.M., and Beckman E.L., 1986, *Diving And Decompression Sickness Treatment Practices Among Hawaii's Diving Fisherman, University of Hawaii Sea Grant Report, UNIHI-SEAGRANT-TP-86-01, Honolulu.*
45. Feynman R.P., Leighton R.B., and Sands M., 1975, *The Feynman Lectures On Physics I, II, III, Reading: Addison Wesley.*
46. Fisher J.C., 1948, *The Fracture Of Liquids, J. Appl. Phys. 19, 1062-1067.*
47. Fleagle R.G. and Businger J.A., 1963, *Introduction To Atmospheric Physics, New York: Academic Press.*
48. Frenkel J., 1946, *Kinetic Theory Of Liquids, New York: Oxford University Press.*
49. Gernhardt M.L., Lambertsen C.J., Miller R.G., and Hopkins E., 1990, *Evaluation Of A Theoretical Model Of Tissue Gas Phase Growth And Resolution During Decompression From Air Diving, Undersea Biomed. Res. 17, 95.*
50. Gernhardt M.L., 1985, *Tissue Gas Bubble Dynamics During Hypobaric Exposures, Society Of Automotive Engineers Report, SAE-851337, Warrendale.*
51. Gilliam B., Webb D. and von Maier R., 1995, *Deep Diving, San Diego: Watersports.*
52. Golding F.C., Griffiths P.D., Paton W.D.M., Walder D.N., and Hempleman H.V., 1960, *Decompression Sickness During Construction Of The Dartford Tunnel, Brit. J. Ind. Med. 17, 167-180.*
53. Goldstein H., 1969, *Mechanics, Reading: Addison Wesley.*
54. Gradshteyn I.S. and Ryzhik I.M., 1965, *Table Of Integrals, Series, And Products, New York: Academic Press.*
55. Gray J.S., Masland R.L., and Mahady S.C., 1945, *The Effects Of Breathing Carbon Dioxide On Altitude Decompression Sickness, US Air Force School Of Aviation Medicine Report, Project 409, Randolph Field.*
56. Groen P., 1967, *The Waters Of The Sea, University Park: Pennsylvania State University Press.*
57. Guillen M., 1995, *Five Equations That Changed The World, New York: Hyperion.*
58. Hamilton R.W., 1975, *Development Of Decompression Procedures For Depths In Excess Of 400 Feet, Undersea And Hyperbaric Medical Society Report, WS: 2-28-76, Bethesda.*
59. Harvey E.N., 1945, *Decompression Sickness And Bubble Formation In Blood And Tissue, Bull. N.Y. Acad. Med. 21, 505-536.*

60. Harvey E.N., Barnes D.K., McElroy W.D., Whiteley A.H., Pease D.C., and Cooper K.W., 1944, *Bubble Formation In Animals. I. Physical Factors*, *J. Cell. Comp. Physiol.* 24, 1-22.
61. Harvey E.N., Whiteley A.H., McElroy W.D., Pease D.C., and Barnes D.K., 1944, *Bubble Formation In Animals. II. Gas Nuclei And Their Distribution In Blood And Tissues*, *J. Cell Comp. Physiol.* 24, 23-24.
62. Harvey E.N., McElroy W.D., Whiteley A.H., Warren G.H., and Pease D.C., 1944, *Bubble Formation In Animals. III. An Analysis Of Gas Tension And Hydrostatic Pressure In Cats*, *J. Cell. Comp. Physiol.* 24, 117-132.
63. Hawkins J.A., Shilling C.W., and Hansen R.A., 1935, *A Suggested Change In Calculating Decompression Tables For Diving*, *USN Med. Bull.* 33, 327-338.
64. Hempleman H.V., 1957, *Further Basic Facts On Decompression Sickness, Investigation Into The Decompression Tables*, *Medical Research Council Report, UPS 168*, London.
65. Hempleman H.V., 1952, *A New Theoretical Basis For The Calculation Of Decompression Tables*, *Medical research Council Report, UPS 131*, London.
66. Heine J., 1991, *Cold Water Diving*, Flagstaff: Best.
67. Hennessy T.R. and Hempleman H.V., 1977, *An Examination Of The Critical Released Gas Concept In Decompression Sickness*, *Proc. Royal Soc. London B197*, 299-313.
68. Hennessy T.R., 1974, *The Interaction Of Diffusion And Perfusion In Homogeneous Tissue*, *Bull. Math. Biol.* 36, 505-527.
69. Hills B.A., 1977, *Decompression Sickness*, New York: John Wiley And Sons.
70. Hills B.A., 1976, *Supersaturation By Counterdiffusion And Diffusion Of Gases*, *J. Appl. Physiol.* 43, 56-69.
71. Hills B.A., 1969, *Radial Bulk Diffusion Into Heterogeneous Tissue*, *Bull. Math. Biophys.* 31, 25-34.
72. Hills B.A., 1968, *Linear Bulk Diffusion Into Heterogeneous Tissue*, *Bull. Math. Biophys.* 30, 47-59.
73. Hills B.A., 1968, *Variation In Susceptibility To Decompression Sickness*, *Int. J. Biometeor.* 12, 343-349.
74. Hills B.A., 1968, *Relevant Phase Conditions For Predicting The Occurrence Of Decompression Sickness*, *J. Appl. Physiol.* 25, 310-315.
75. Hirschfelder J.O., Curtiss C.F., and Bird R.B., 1964, *Molecular Theory Of Gases And Liquids*, New York: John Wiley And Sons.
76. Huang K., 1973, *Statistical Mechanics*, New York: John Wiley And Sons.
77. Huggins K.E., 1987, *Multiprocessor Applications To Multilevel Air Decompression Problems*, *Michigan Sea Grant Publication, MICHU-SG-87-201*, Ann Arbor.
78. Irving J. and Mullineux N., 1972, *Mathematics In Physics And Engineering*, London: Academic Press.
79. Johnson L.W. and Riess R.D., 1962, *Numerical Analysis*, Reading: Addison Wesley.

80. Kahaner D., Moler C., and Nash S., 1989, *Numerical Methods And Software*, Englewood Cliffs: Prentice Hall.
81. Keller H. and Buhlmann A.A., 1965, *Deep Diving And Short Decompression By Breathing Mixed Gases*, *J. Appl. Physiol.* 20, 1267.
82. Kunkle T.D. and Beckman E.L., 1983, *Bubble Dissolution Physics And The Treatment Of Decompression Sickness*, *Med. Phys.* 10, 184-190.
83. Lambertsen J.L. and Bornmann R.C., 1979, *Isobaric Inert Gas Counterdiffusion*, *Undersea And Hyperbaric Medical Society Publication 54WS(IC)1-11-82*, Bethesda.
84. Lambertsen C.J. and Bardin H., 1973, *Decompression From Acute And Chronic Exposure To High Pressure Nitrogen*, *Aerospace Med.* 44, 834-836.
85. Landau L.D. and Lifshitz E.M., 1985, *Fluid Mechanics*, Reading: Addison Wesley.
86. Landau L.D. and Lifshitz E.M., 1980, *Mechanics*, Reading: Addison Wesley.
87. Lang M.A. and Vann R.D., 1992, *Proceedings Of The American Academy Of Underwater Sciences Repetitive Diving Workshop*, AAUS Safety Publication AAUSDSP-RDW-02-92, Costa Mesa.
88. Lang M.A. and Egstrom G.H., 1990, *Proceedings Of The American Academy Of Underwater Sciences Biomechanics Of Safe Ascents Workshop*, American Academy Of Underwater Sciences Diving Safety Publication, AAUSDSP-BSA-01-90, Costa Mesa.
89. Lang M.A. and Hamilton R.W., 1989, *Proceedings Of The American Academy Of Underwater Sciences Dive Computer Workshop*, University Of Southern California Sea Grant Publication, USCSG-TR-01-89, Los Angeles.
90. Leebaert D., 1991: *Technology 2001: The Future Of Computing And Communications*, Cambridge: Massachusetts Institute Of Technology Press.
91. Lehner C.E., Hei D.J., Palta M., Lightfoot E.N., and Lanphier E.H., 1988, *Accelerated Onset Of Decompression Sickness In Sheep After Short Deep Dives*, University Of Wisconsin Sea Grant College Program Report, WIS-SG-88-843, Madison.
92. Leitch D.R. and Barnard E.E.P., 1982, *Observations On No Stop And Repetitive Air And Oxyntrogen Diving*, *Undersea Biomed. Res.* 9, 113-129.
93. Le Messurier D.H. and Hills B.A., 1965, *Decompression Sickness: A Study Of Diving Techniques In The Torres Strait*, *Hvaldradets Skrifter* 48, 54-84.
94. Loyst K., Huggins K.E. and Steidley M., 1991, *Dive Computers*, San Diego: Watersports.
95. Mathews J. and Walker R.L., 1975, *Mathematical Methods Of Physics*, New York: W.A. Benjamin.
96. Mount T. and Gilliam B., 1991, *Mixed Gas Diving*, San Diego: Watersport.
97. Neal J.G., O'Leary T.R. and Wienke B.R., 1999, *Trimix Diving*, Fort Lauderdale: Underwater Dynamics Incorporated.
98. Neuman T.S., Hall D.A. and Linaweaver P.G., 1976, *Gas Phase Separation During Decompression In Man*, *Undersea Biomed. Res.* 7, 107-112.

99. Nishi R.Y., Eatock B.C., Buckingham I.P. and Ridgewell B.A., 1982, *Assessment Of Decompression Profiles By Ultrasonic Monitoring: No Decompression Dives*, Defense And Civil Institute Of Environmental Medicine Report, D.C.IEM 82-R-38, Toronto.
100. Parzen E., 1970, *Modern Probability Theory And Its Applications*, New York: John Wiley And Sons.
101. Paton W.D.M. and Walder D.N., 1954, *Compressed Air Illness*, Medical Research Council Report, HMSO 281, London.
102. Pease D.C. and Blinks L.R., 1947, *Cavitation From Solid Surfaces In The Absence Of Gas Nuclei*, J. Phys. Coll. Chem. 51, 556-567.
103. Pilmanis A.A., 1976, *Intravenous Gas Emboli In Man After Compressed Air Ocean Diving*, Office Of Naval Research Contract Report, N00014-67-A-0269-0026, Washington, DC
104. Powell R.P. and Rogers R.E., 1989, *Doppler Ultrasound Monitoring Of Gas Phase Formation And Resolution In Repetitive Diving*, Undersea Biomed. Res. 16, 69.
105. Powell C.F., 1928, *Condensation Phenomena At Different Temperatures*, Proc. Royal Soc. London A119, 553-577.
106. Press W., Teukolsky S., Vetterling W., and Flannery B., 1992, *Numerical Recipes In FORTRAN*, New York: Cambridge University Press.
107. Rashbass C., 1955, *New Tables, Investigation Into The Decompression Tables*, 243 Medical Research Council Report, UPS 151, London.
108. Rogers R.E. and Powell M.R., 1989, *Controlled Hyperbaric Chamber Tests Of Multiday Repetitive Dives*, Undersea Biomed. Res. 16, 68.
109. Roughton F.J.W., 1952, *Diffusion And Chemical Reaction Velocity In Cylindrical And Spherical Systems Of Physiological Interest*, Proc. Royal Soc. B140, 203-221.
110. Rutkowski D., 1989, *Nitrox Manual*, San Diego: International Association of Nitrox Divers (IAND).
111. Sagan H., 1971, *Boundary And Eigenvalue Problems In Mathematical Physics*, New York: John Wiley And Sons.
112. Sawatzky K.D. and Nishi R.Y., 1990, *Intravascular Doppler Detected Bubbles And Decompression Sickness*, Undersea Biomed. Res. 17, 34-39.
113. Schreiner H.R. and Hamilton R.W., 1987, *Validation Of Decompression Tables*, Undersea And Hyperbaric Medical Society Publication 74 (VAL), Bethesda.
114. Sears F.W., 1969, *Thermodynamics*, Reading: Addison Wesley.
115. Shapiro A.H., 1958, *Dynamics And Thermodynamics Of Compressible Fluid Flow*, New York: Ronald.
116. Sheffield P.J., 1990, *Flying After Diving*, Undersea And Hyperbaric Medical Society Publication 77 (FLYDIV), Bethesda.
117. Shreider Y.A., 1966, *The Monte Carlo Method*, New York: Pergamon Press.

118. Smith K.H. and Stayton L., 1978, *Hyperbaric Decompression By Means Of Bubble Detection*, Office Of Naval Research Report, N0001-469-C-0402, Washington DC
119. Smith C.L., 1975, *Altitude Procedures For The Ocean Diver*, National Association Of Underwater Instructors Technical Publication 5, Colton.
120. Somers L.H., 1991, *The University Of Michigan Diving Manual*, Ann Arbor: University Of Michigan Press.
121. Spencer M.P., 1976, *Decompression Limits For Compressed Air Determined By Ultrasonically Detected Blood Bubbles*, *J. Appl. Physiol.* 40, 229-235
122. Spencer M.P. and Campbell S.D., 1968, *The Development Of Bubbles In The Venous And Arterial Blood During Hyperbaric Decompression*, *Bull. Mason Cli.* 22, 26-32.
123. Strauss R.H., 1974, *Bubble Formation In Gelatin: Implications For Prevention Of Decompression Sickness*, *Undersea Biomed. Res.* 1, 169-174.
124. Strauss R.H. and Kunkle T.D., 1974, *Isobaric Bubble Growth: Consequence Of Altering Atmospheric Gas*, *Science* 186, 443-444.
125. Thompson A.M., Cavert H.M., and Lifson N., 1958, *Kinetics Of D<sub>2</sub>O And Antipyrine In Isolated Perfused Rat Liver*, *Amer. J. Physiol.* 192, 531-537.
126. Tikuisis P., 1986, *Modeling The Observations Of In Vivo Bubble Formation With Hydrophobic Crevices*, *Undersea Biomed. Res* 13, 165-180.
127. Tikuisis P., Ward C.A. and Venter R.D., 1983, *Bubble Evolution In A Stirred Volume Of Liquid Closed To Mass Transport*, *J. Appl. Phys.* 54, 1-9.
128. Van Liew H.D. and Hlastala M.P., 1969, *Influence Of Bubble Size And Blood Perfusion On Absorption Of Gas Bubbles In Tissues*, *Resp. Physiol.* 24, 111-121.
129. Van Liew H.D., Bishop B, Walder P.D., and Rahn H., 1975, *Bubble Growth And Mechanical Properties Of Tissue In Decompression*, *Undersea Biomed. Res.* 2, 185-194.
130. Vann R.D., Dovenbarger J., Wachholz C., and Bennett P.B., 1989, *Decompression Sickness In Dive Computer And Table Use*, *DAN Newsletter* 3-6.
131. Vann R.D., Grimstad J., and Nielsen C.H., 1980, *Evidence For Gas Nuclei In Decompressed Rats*, *Undersea Biomed. Res.* 7, 107-112.
132. Vann R.D. and Clark H.G., 1975, *Bubble Growth And Mechanical Properties Of Tissue In Decompression*, *Undersea Biomed. Res.* 2, 185-194.
133. Walder D.N., Evans A., and Hempleman H.V., 1968, *Ultrasonic Monitoring Of Decompression*, *Lancet.* 1, 897-898.
134. Walder D.N., 1968, *Adaptation To Decompression Sickness In Caisson Work*, *Biometeor.* 11, 350-359.
135. Wallace D., 1975, *NOAA Diving Manual*, Washington DC: US Government Printing Office.
136. Weathersby P.K., Survanshi S. and Homer L.D., 1985, *Statistically Based Decompression Tables: Analysis Of Standard Air Dives, 1950-1970*, Naval Medical Research Institute report, NMRI 85-16, Bethesda.

137. Weathersby P.K., Homer L.D., and Flynn E.T., 1984, *On The Likelihood Of Decompression Sickness*, *J. Appl. Physiol.* 57, 815-825.
138. Wienke B.R., 1998, *Physics, Physiology, And Decompression Theory For The Technical And Commercial Diver*, National Association Of Underwater Instructors Publication, Tampa.
139. Wienke B.R., 1993, *Diving Above Sea Level*, Flagstaff: Best.
140. Wienke B.R., 1994, *Basic Diving Physics And Application*, Flagstaff: Best.
141. Wienke B.R., 1992, *Numerical Phase Algorithm For Decompression Computers And Application*, *Comp. Biol. Med.* 22, 389-406.
142. Wienke B.R., 1991, *Basic Decompression Theory And Application*, Flagstaff: Best.
143. Wienke B.R., 1991, *Bubble Number Saturation Curve And Asymptotics Of Hypobaric And Hyperbaric Exposures*, *Int. J. Biomed. Comp.* 29, 215-225.
144. Wienke B.R., 1991, *High Altitude Diving*, National Association Of Underwater Instructors Technical Publication, Montclair.
145. Wienke B.R., 1990, *Reduced Gradient Bubble Model*, *Int. J. Biomed. Comp.* 26, 237-256.
146. Wienke B.R., 1990, *Modeling Dissolved And Free Phase Gas Dynamics Under Decompression*, *Int. J. BioMed. Comp.* 25, 193-205.
147. Wienke B.R., 1989, *Equivalent Multitissue And Thermodynamic Decompression Algorithms*, *Int. J. BioMed. Comp.* 24, 227-245.
148. Wienke B.R., 1989, *Tissue Gas Exchange Models And Decompression Computations: A Review*, *Undersea Biomed. Res.* 16, 53-89.
149. Wienke B.R., 1989, *N<sub>2</sub> Transfer And Critical Pressures In Tissue Compartments*, *Math. Comp. Model.* 12, 1-15.
150. Wienke B.R., 1987, *Computational Decompression Models*, *Int. J. BioMed. Comp.* 21, 205-221.
151. Wienke B.R., 1986, *DECOMP: Computational Package For Nitrogen Transport Modeling In Tissues*, *Comp. Phys. Comm.* 40, 327-336.
152. Wienke B.R., 1986, *Phenomenological Models For Nitrogen Transport In Tissues*, *Il Nuovo Cimento* 8D, 417-435.
153. Wilkes M.V., 1959, *Oscillations Of The Earth's Atmosphere*, London: Cambridge University Press.
154. Wittenborn A.F., 1963, *An Analytic Development Of A Decompression Computer*, *Proc. Second Symp. Underwater Physiol.*, Washington, DC: National Academy Of Science 1, 82-90.
155. Workman R.D., 1965, *Calculation Of Decompression Schedules For Nitrogen-Oxygen And Helium-Oxygen Dives*, *USN Experimental Diving Unit Report, NEDU 6-65*, Washington DC
156. Yang W.J., 1971, *Dynamics Of Gas Bubbles In Whole Blood And Plasma*, *J. Biomech.* 4, 119-125.
157. Yarborough O.D., 1937, *Calculations Of Decompression Tables*, *USN Experimental Diving Unit Report, EDU 12-37*, Washington DC

158. Yount D.E. and Hoffman DC, 1986, *On The Use Of A Bubble Formation Model To Calculate Diving Tables*, *Aviat. Space Environ. Med.* 57, 149-156.
159. Yount D.E., Gillary E.W., and Hoffman DC, 1984, *A Microscopic Investigation Of Bubble Formation Nuclei*, *J. Acoust. Soc. Am.* 76, 1511-1521.
160. Yount D.E., 1982, *On The Evolution, Generation, And Regeneration Of Gas Cavitation Nuclei*, *J. Acoust. Soc. Am.* 71, 1473-1481.
161. Yount D.E., 1979, *Skins Of Varying Permeability: A Stabilization Mechanism For Gas Cavitation Nuclei*, *J. Acoust. Soc. Am.* 65, 1431-1439.
162. Yount D.E., Yeung C.M., and Ingle F.W., 1979, *Determination Of The Radii Of Gas Cavitation Nuclei By Filtering Gelatin*, *J. Acoust. Soc. Am.* 65, 1440-1450.
163. Yount D.E. and Strauss R.H., 1976, *Bubble Formation In Gelatin: A Model For Decompression Sickness*, *J. Appl. Phys.* 47, 5081-5089.
164. Zhang J., Fife C.E., Currie M.S., Moon R.E., Pintadosi C.A. and Vann R.D., 1991, *Venous Gas Emboli And Complement Activation After Deep Air Diving*, *Undersea Biomed. Res.* 18, 293-302.